Title
Synthesis of Sequence-Defined Degradable Polymers through Ring-Opening Polymerization

Author
Deng, Shijie

Publication Date
2023

Peer reviewed|Thesis/dissertation

UNIVERSITY OF CALIFORNIA

Los Angeles

Synthesis of Sequence-Defined Degradable Polymers through Ring-Opening Polymerization

A dissertation submitted in partial satisfaction of the requirements for the degree Doctor of Philosophy in Chemistry

by

Shijie Deng

2023

ABSTRACT OF THE DISSERTATION

Synthesis of Sequence-Defined Degradable Polymers

through Ring-Opening Polymerization

by

Shijie Deng

Doctor of Philosophy in Chemistry

University of California, Los Angeles, 2023

Professor Paula Loredana Diaconescu, Chair

Ring-opening polymerization is an essential form of chain-growth polymerization that facilitates precise control over the polymerization process. Our research delved into the realm of redox-switchable catalysis and its application in synthesizing polyesters, ethers, and carbonates through ring-opening polymerization. To broaden the range of available monomers, we also explored the ring-opening polymerization of aromatic N-carboxyanhydrides with six-membered rings, resulting in the creation of aromatic polyamides. Leveraging the potential of biodegradable polymers crafted from ring-opening polymerizations, we investigated how the stereocomplexation of block copolymers could enhance the shear viscosity of the polymer solutions in brine.

The dissertation of Shijie Deng is approved.

Chong Liu

Hosea M. Nelson

Jeffrey I. Zink

Paula Loredana Diaconescu, Committee Chair

University of California, Los Angeles

2023

This thesis is dedicated to my beloved grandma and grandpa.

TABLE OF CONTENTS

LIST OF TABLES AND FIGURES

Chapter 1: Introduction

Chapter 2: Redox-switchable dimeric yttrium compound and its activity in ring-opening polymerization

Chapter 3: Ring-opening polymerization of six-membered ring N-carboxyanhydride toward aromatic polyamide synthesis

Chapter 4: Stereocomplex-enhanced shear viscosity of PLA-PEG-PLA amphiphilic triblock copolymers

ACKNOWLEDGEMENTS

For this thesis and throughout my five-year Ph.D. journey, I wish to extend my sincere gratitude to my advisor, Prof. Paula Diaconescu. Looking at the first manuscript I penned and those I just completed, the journey unfolds before me. In retrospect, my decision to enter graduate school was driven by curiosity about polymers. While crafting the chapters, I realized the progress I made in gaining a deeper understanding of polymers and polymerization processes. It's not just the knowledge and skills gained but also the mindset and methodologies. None of these would have been attainable without Paula's guidance and the opportunities she provided. Beyond research, Paula has stood as a role model. Actions speak louder than words; the tenacity and perseverance she displayed in the face of challenges, akin to that of a warrior, have always inspired me and will continue to do so.

I also wish to express my gratitude to my fellow group members: Ruxi, Amy, Zach, Yi, George (Yin-Pok), Shiyun, Hootan, Joon, and Ramzi. Their help spans from the first word I learned in the lab, ‘spatula’, to the art of glovebox maintenance. Those encouraging and entertaining discussions, encompassing both on scientific and nonscientific topics, greatly alleviated the despair of failed reactions. Special thanks to the MIC staff scientists — Dr. Ignacio Martini, Dr. Gregory Khitrov, and Dr. Ta-Chung Ong — for their invaluable assistance in dealing with the tantrums of the instruments. I am also greatly indebted to my collaborators: Prof. Loi Do, Dr. Matthew Thompson, and the late Prof. Jeffery Byers. Their insights and support have been pivotal in shaping this thesis.

My appreciation extends to my friends and family for their unwavering emotional support during those difficult days. Amidst my struggles with flasks and pumps in the lab, I scarcely

realized how swiftly time flew by. We have gone through different stages of our lives, and despite physical distances, we share a common sentiment that transcends time zones.

Though arduous, laden with both losses and gains, this is a journey I never regret embarking upon. Just as the saying goes, 'Fear not the infinity of truth, for every inch forward comes with an inch of joy', armed with strength and determination, I am ready to reel in that giant marlin fish.

Specific acknowledgements for this work:

Chapter 1 is a version of Deng, S., Jolly, B.J., Wilkes, J.R., Mu, Y., Byers, J.A., Do, L.H., Miller, A.J., Wang, D., Liu, C. and Diaconescu, P.L., Spatiotemporal Control for Integrated Catalysis. *Nat. Rev. Methods Primers* 2023 *3*, 28.

Chapter 2 is a version of Deng, S. and Diaconescu, P. L. A Switchable Dimeric Yttrium Complex and its Three Catalytic States in Ring Opening Polymerization. *Inorg. Chem. Front.* 2021, *8,* 2088-2096.

Chapter 3 is a version of a submitted manuscript Deng, S., Shen, Y., Chantranuwathana, V., Nguyen, H. D., Tran, T. V., Vasquez, K., Byers, J.A., Do, L.H., and Diaconescu, P.L., ortho-Aromatic Polyamides by Ring-opening Polymerization of N-carboxyanhydrides. *Manuscript submitted*.

Chapter 4 is a version of a manuscript in preparation Deng, S., Roshandel, H., Gallin, C. F., Li, Y., Aften, C., Vasquez, K., Byers, J.A., and Diaconescu, P.L., Stereocomplex-enhanced Shear Viscosity of PLA-PEG-PLA Amphiphilic Triblock Copolymers.

VITA

Education

B.S., Chemistry, Nankai University-Tianjin, China (2014)

Award

UCLA Evelyn Pan Dissertation Award (2023)

UCLA John Alan Walker Excellence in Research Award (2022)

Publications

1. **Deng, S.**, Roshandel, H., Gallin, C. F., Li, Y., Aften, C., Vasquez, K., Byers, J.A., and Diaconescu, P.L, Stereocomplex-enhanced Shear Viscosity of PLA-PEG-PLA Amphiphilic Triblock Copolymers., *manuscript in preparation.*

2. **Deng, S.**, Shen, Y., Chantranuwathana, V., Nguyen, H. D., Tran, T. V., Vasquez, K., Byers, J.A., Do, L.H., and Diaconescu, P.L., ortho-Aromatic Polyamides by Ring-opening Polymerization of N-carboxyanhydrides, *manuscript submitted.*

3. Dai, R., Valloppilly, S., Watuthanthrige, N. D. A., Chakma, P., **Deng, S.**, Konkolewicz, D., and Diaconescu, P. L., Synthesis and Self-assembly of Limonene Oxide-Lactide Block Copolymers. **2023** *Preprint at https://doi.org/10.48550/arXiv.2006.07038.*

4. Dai, R., **Deng, S.**, Peng, Z., Pei, Q., and Diaconescu, P.L., Post-functionalization and Mechanical Properties of Poly (lactide-cyclohexadiene oxide) Block Copolymers. **2023** *Preprint at https://doi.org/10.26434/chemrxiv-2023-81ng7.*

5. **Deng, S.**, Jolly, B.J., Wilkes, J.R., Mu, Y., Byers, J.A., Do, L.H., Miller, A.J., Wang, D., Liu, C. and Diaconescu, P.L., Spatiotemporal Control for Integrated Catalysis. *Nat. Rev. Methods Primers* **2023** *3*, 28.

6. Tran, T.V., Shen, Y., Nguyen, H.D., **Deng, S.**, Roshandel, H., Cooper, M.M., Watson, J.R., Byers, J.A., Diaconescu, P.L. and Do, L.H., N-Carboxyanhydrides Directly from Amino Acids and Carbon Dioxide and Their Tandem Reactions to Therapeutic Alkaloids. *Green Chem.* **2022,** *23*, 9245-9252.

7. **Deng, S.** and Diaconescu, P. L. A Switchable Dimeric Yttrium Complex and its Three Catalytic States in Ring Opening Polymerization. *Inorg. Chem. Front.* **2021**, *8,* 2088-2096.

Chapter 1: Introduction

1.1. Sustainable polymers

Polymers are an indispensable category of materials, the global production of which seconds only that of steel and cement. We use polymers for all kinds of applications ranging from packaging, textiles, electronics to healthcare. In 2018, global plastic production was 454 million metric tons. Of this, polymers with C-C backbone such as polyethylene (PE), polypropylene (PP), polystyrene (PS), polyvinylchloride (PVC) accounted for nearly 77%, while polymers with degradable backbones, such as polyethylene terephthalate (PET), polyurethane (PUR), and polyester, polyamide, and acrylic (PP&A), and others accounted for only 33%.[1, 2]

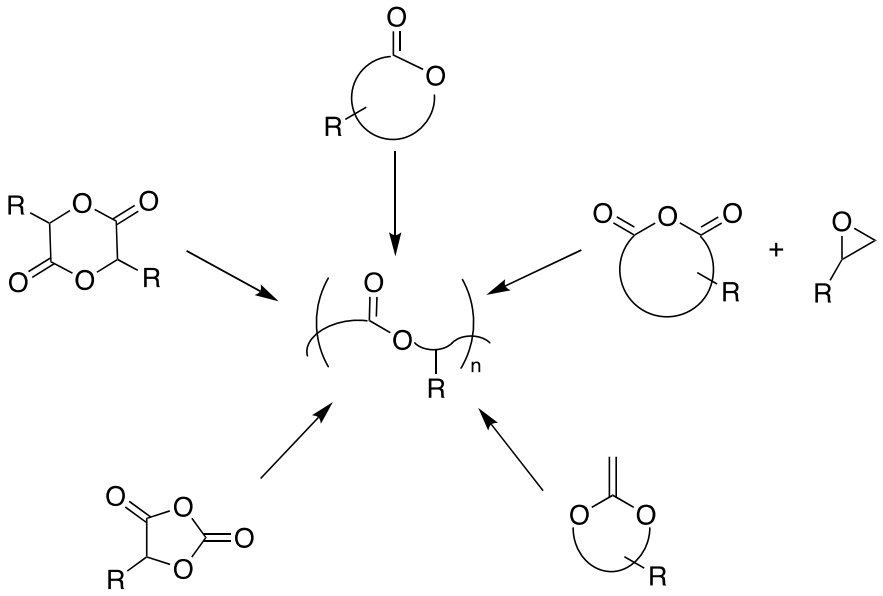

Figure 1-1. Ring opening polymerization of different types of monomers toward polyesters synthesis.

The non-degradable polymer waste accumulating in the natural environment has posed a great threat to marine wildlife and the global ecosystem.[3] Therefore, it's imperative for us to optimize

our polymer design, taking into consideration both the polymer performance and end-of-life treatment. To achieve that, precise control over the polymer synthesis is required. In the synthesis of polyesters and polyamides, polycondensation reactions play a crucial role. These reactions involve the repeated condensation of monomers with the elimination of small molecules, such as water or alcohol, as byproducts. While step-growth polymerization, i.e., polycondensation, is a versatile method for polymer synthesis, it can lead to challenges in controlling the molecular weight and dispersity of the resulting polymers. An alternative route is chain-growth polymerization, which has gained an increasing interest over the years for its controlled nature. For polyester synthesis, different types of monomers can be employed in such chain-growth polymerization *e.g.*, ring opening polymerization of lactide and derivatives, lactones, and O-carboxyanhydrides; radical ring opening polymerization of cyclic ketene acetals; ring opening copolymerization of epoxides and cyclic anhydrides (Figure 1-1).

In addition to homopolymers, block copolymers offer great opportunities to enrich our polymer library for different properties and applications. Even if they currently have a limited monomer scope, we can easily modify the block length, block sequence, number of blocks, polymer architecture, polymer topology to attain a plethora of polymers with various properties[4]. By tailoring polymer sequence and structure, we can leverage the self-assembled morphology of block copolymer to fine-tune the polymer properties for diverse applications such as membrane[5], nanoparticle[6] and thermoplastic elastomer[7].

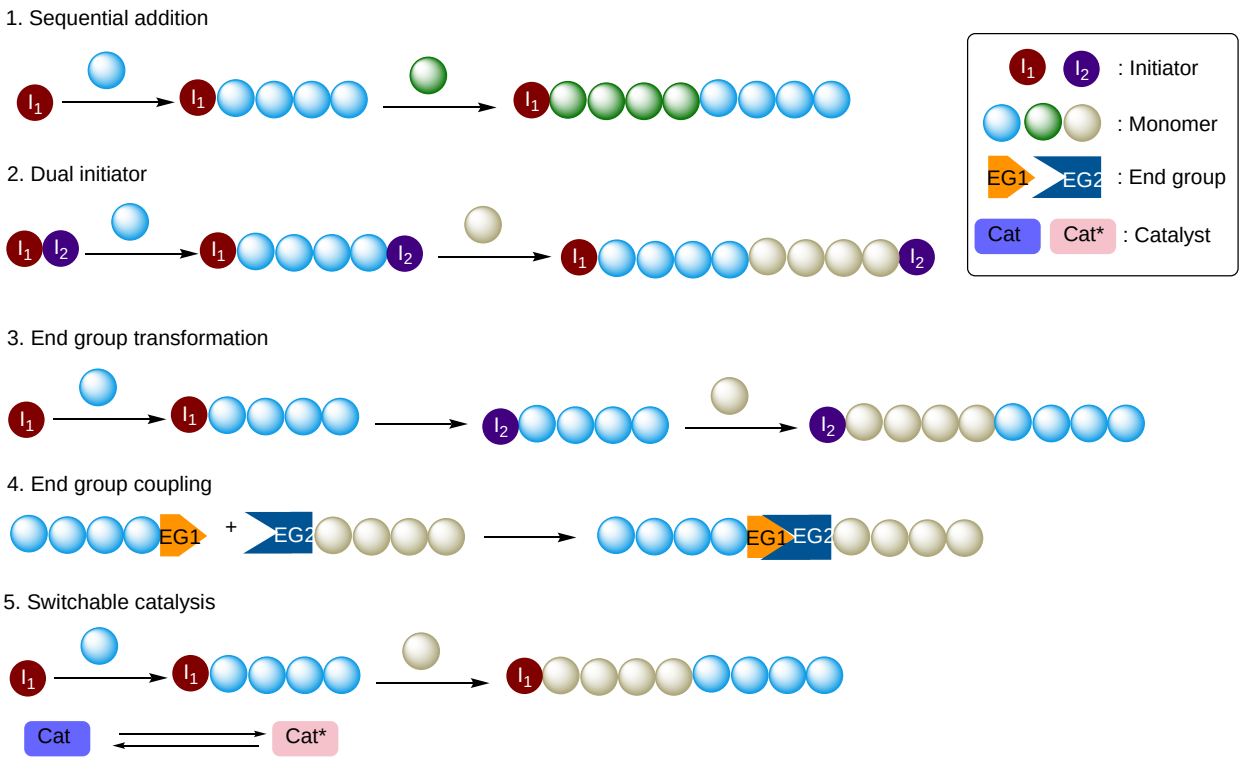

Figure 1-2. Different approaches for block copolymer synthesis.

To synthesize block copolymers, various approaches can be employed (Figure 1-2). The first approach involves the sequential addition of different monomers. In this method, the chain end of the first block should be capable of initiating the polymerization of the second monomer. Therefore, sequential addition typically works only for the same type of monomer. The second approach involves the use of a dual initiator, which consists of two functionalities, each capable of initiating a specific type of polymerization. A similar strategy involves transforming the chain end of a homopolymer to make it capable of initiating another type of polymerization. Coupling the end groups of two homopolymer serves as another approach. In addition to these approaches, switchable catalysis has emerged as an important method for block copolymer synthesis. In switchable catalysis, the catalyst can oscillate between different states in response to external

stimuli. In each state, the catalyst can catalyze different types of polymerization reactions. Switchable catalysis obviates the tedious workup processes, making it possible to make block copolymers with well-defined sequence and structure in one pot.

1.2. Spatial-temporally controlled catalysis

In nature, living organisms have the ability to respond to environmental factors, causing them to behave differently or take on different forms. At the microscopic level, external stimuli regulate feedback loops and modulate enzymatic reactions within cells to effect biological changes. Taking inspiration from nature, scientists have been working on artificial catalytic systems that could be tuned reversibly by external stimuli. In such switchable systems, a catalyst could be toggled on/off or may oscillate between different catalytic states to achieve orthogonal reactivity (Figure 1-3). Depending on the application and reaction conditions, different external stimuli can be used to implement a switchable behavior. In this section, redox, chemo-, and photo-switching will be discussed, with a focus on the switching mechanisms and general catalyst design concepts. Several comprehensive reviews have been published on temporally switchable catalysis.[8-12]

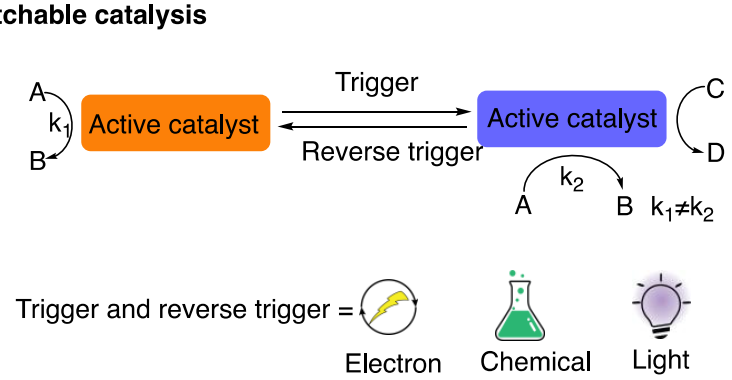

Figure 1-3. Switchable catalysis using different external stimuli.

A challenge associated with achieving switchable catalysis is designing a system that has two (or more) different reactive states that can be accessed through application of external stimuli. Since redox reactions change the electronic configuration of a compound, which is intimately associated with its reactivity, an attractive option for switchable catalysts is through iterative addition of oxidants or reductants. A common way to carry out redox-switchable catalysis is to design redox-active ancillary ligands[13-15] that are coordinated to a redox-inactive metal, which serves as the site for catalysis. This strategy was employed in the first example of redox-switchable catalysis,[16] when a rhodium complex supported by a cobaltocene bis(phosphine) was used for the hydrogenation and isomerization of alkenes. Despite this first example being applied to catalysis involving small molecules, the utility of redox-switchable catalysis has been exploited with more success in polymerization. For example, a titanium complex containing two redox-active ferrocene moieties appended to a salen ancillary ligand (Figure 1-4)[17] demonstrated redox modulation when used for the polymerization of lactide, with the reduced species being more active than the oxidized form of the catalyst. Since this report, several groups have utilized the ferrocene moiety for redox-switchable polymerization.[18-23] For example, using chelating ligands to position the ferrocene moiety in close proximity to the redox-inactive site for catalysis results in a greater difference in the reaction rate of the oxidized and reduced states of a catalyst (Figure 1-4). For example, while both forms of the above titanium complex demonstrated some activity for lactide polymerization, an yttrium complex showed complete on/off activity for lactide polymerization.[24]

An alternative method for redox-switchable catalysis is to use redox-active metals that serve as the redox-switching moiety and the site for catalysis (Figure 1-4). Catalysts based on several different redox-active metals have been explored using this strategy, with the most notable examples being

ring-opening polymerization catalysts using cerium salfen[25] and iron bis(imino)pyridine complexes.[26] These catalysts show similar behavior as that of polymerization catalysts utilizing redox-active ancillary ligands, demonstrating that it is not necessary to separate the redox-switching entity from the catalytically active entity.

One challenge associated with redox-switchable catalysis is the need to add oxidants and reductants to the reaction. When chemical redox reagents are used, purification of the product is required to remove the byproducts from the redox-switch. Moreover, adding chemical redox reagents to reactions that require gaseous reagents at elevated pressures requires specialized equipment. To address these limitations, an electrochemical potential can be used instead of chemical redox reagents for redox switching (Figure 1-4). Such electrochemical potential can be achieved by employing bis(imino)pyridine iron complexes whose redox-active site is also the site for catalysis,[27] or catalysts that contain redox-switchable moieties installed in the ancillary ligand.[28]

While there are now many redox-switchable catalysts, a mechanistic understanding of how these systems perform redox switching is not well established. The oxidation state of the active catalyst and the efficiency of the redox switch are dependent on many factors. In addition to the proximity of the redox-switching moiety to the catalytically active site, another important factor is the identity of the metal center. For example, while the yttrium complex is active for lactide polymerization in its reduced state, the indium complex that contains the same ancillary ligand is active for lactide polymerization in its oxidized form.[24] The interaction between the metal center and the redox switchable moiety can be intricate; as revealed by the combination of computational and experimental studies[29, 30], the oxidation state of redox active group can alter the Lewis acidity of the metal center, as well as change the energetic profile of the catalyst-substrate intermediate.[31]

Another factor is the identity of the reactant; different some reactants may display orthogonal reactivity with respect to the oxidation state of the catalyst and some may not. For example, the iron complex shown in Figure 1-4,[32] as well as other redox switchable catalysts,[20, 22, 24, 29, 33, 34] is capable of polymerizing selectively lactide in its reduced form and epoxide in its oxidized form, but less selectivity is observed for lactones or cyclic carbonates.[30, 33, 35-37] Selectivity shown by each state of the system or orthogonal reactivity behavior is important in being able to combine multiple catalytic cycles without interference from the reaction that is turned off, for example. While more work is needed to understand these and other effects that have been observed, two related factors appear to be important in polymerization catalysis: the propensity of the monomer to bind to the catalytically active site and the electrophilicity/nucleophilicity of reactive intermediates.[30, 36, 38] Both factors are altered by changing the oxidation state of the catalysts, and the relative importance of each is related to the nature of each reaction, including the identity of the metal centers and the monomers employed.

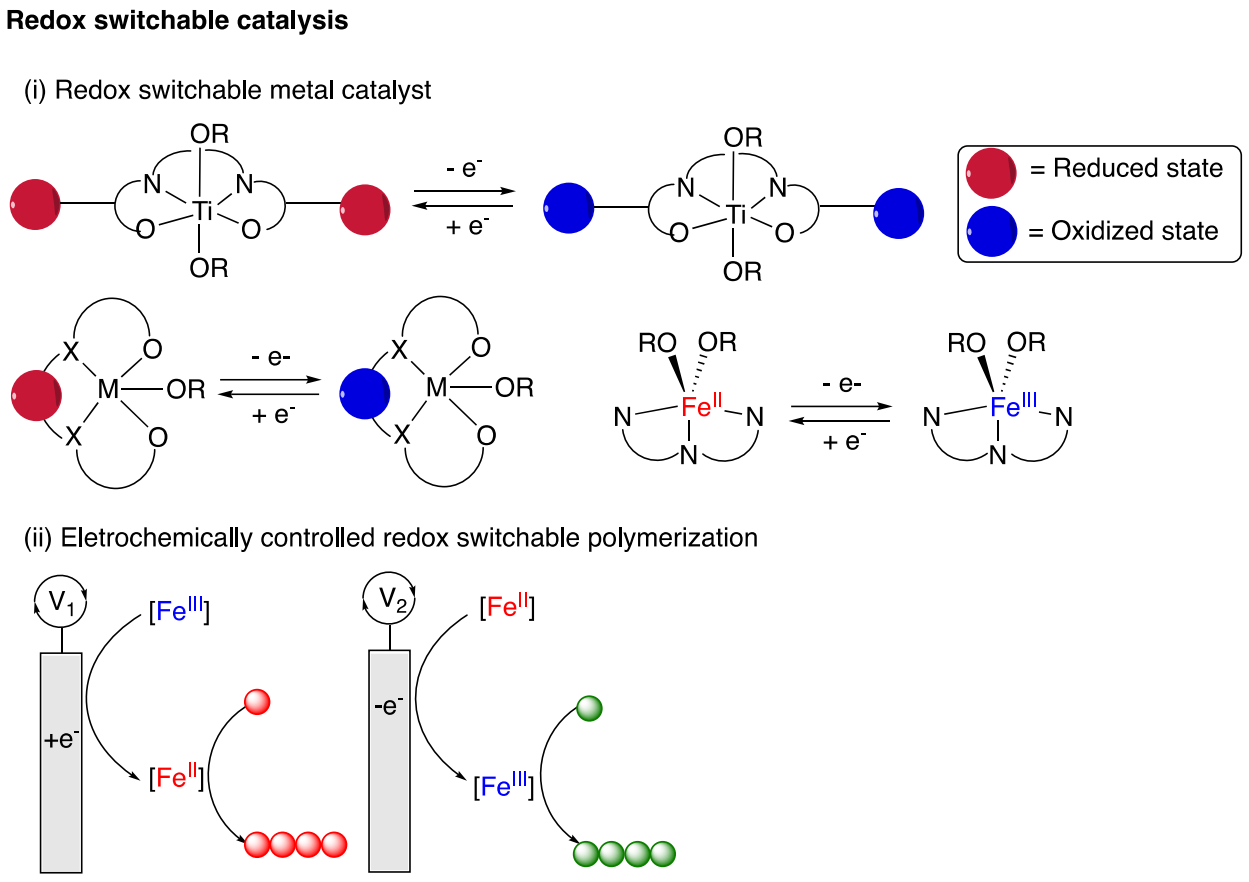

Figure 1-4. Redox-switchable catalysis. Design of a redox-switchable metal catalyst (i). Redox-switchable polymerization using electrochemical setup (ii).

Chemoswitchable catalysts are compounds that are responsive to the presence of external chemical additives. Unlike redox-switchable catalysis, chemoselective catalysis does not involve alterations to the catalyst that leads to changes in their formal oxidation state. Because chemical reagents have a wide range of properties, they can trigger molecular events via various modes of action. For example, cations can bind Lewis basic sites, whereas anions can bind Lewis acidic sites. Such interactions could turn a catalyst on or off, or modulate their reaction rates. Alternatively, chemical

reagents could covalently modify a catalyst to produce another active species capable of achieving orthogonal reactivity.

The key design challenge in chemoswitchable catalysis is to enable a catalyst to change its structure and function by interacting with a chemical additive. One effective strategy for chemoswitchable reactivity involves regulating catalysis using anion coordination/dissociation to alter the metal complex geometry or block/unblock catalytically active sites. For instance, a supramolecular triple layer catalyst, comprising an aluminum salen complex flanked by two rhodium nodes equipped with biaryl blocking groups, was used for the chemoswitchable polymerization of lactones (Figure 1-5). In the closed form, the rhodium centers are ligated by the amino donor of the supporting ligand, which positions the biaryl units above and below the aluminum active site.[39] Because aluminum is inaccessible due to the steric bulk of the amino arms, the catalyst cannot react with substrates. In the open form, chloride anions are bound to rhodium so that the amino groups are forced away from aluminum, opening up access to incoming monomers. When chloride salts are added, the triple layer catalyst reaches an open state that is active for the ring-opening polymerization of e-caprolactone; when sodium salts are added, the chloride is abstracted from the rhodium centers, re-forming the closed catalyst state and almost completely stopping the polymerization. Remarkably, the molecular weight of the polymer increased linearly with conversion even as the catalyst was activated, deactivated, and reactivated, indicating an excellent control over catalysis.

Another strategy for chemoselective switching is to regulate catalysis using cations. By installing crown ether moieties in ancillary ligands, alkali metal cations can interact with the crown ether moiety to tune the electron density of the catalytically active site. This type of cation switching has been well-demonstrated in small molecule activation (Figure 1-5).[40] For example, an iridium

PCN-pincer complex was prepared containing an aza-crown ether macrocycle, which serves as a hemilabile ligand and cation receptor. When sodium or lithium tetrararylborate salts were added to a CD_2Cl_2/Et_2O solution of the compound, the free energy of aza-crown ether dissociation from iridium is lowered due to the favorable interaction of the alkali metal ion with the macrocycle. In the presence of these alkali metal cations, binding of dihydrogen becomes possible, and the cation-activated iridium species catalyzed H/D exchange with D_2 is significantly faster than the unactivated complex. This concept can be extended to a three-state (off/slow/fast) catalyst system, such as the positional olefin isomerization.[41] For example, iridium chloride complex is inactive for isomerization of allylbenzene; removal of the chloride produces a cationic species with hemilabile Ir–O interactions resulting in a slow catalyst. Addition of Li^+ salts to this cationic catalyst enhances the isomerization rate over 1,000-fold. The rate enhancement is attributed to cation–crown interactions making olefin binding more favorable, and increasing the amount of iridium that is actively engaged in catalysis. Another example of cation-switchable system was used to achieve regioselectivity in positional isomerization: without salts added, alkenes were isomerized from the 1- to the 2-position; under the same conditions but with added Na^+ salts, 3-alkenes were observed instead.[42]

The cation coordination strategy of a catalyst can be used to tune not only the reaction rates but also the architecture of a polymer product.[43] For example, a family of nickel phenoxyimine complexes bearing polyethylene glycol (PEG) chains can coordinate secondary metals (Figure 1-5); the addition of M^+ (where $M^+ = Li^+$, Na^+, or K^+) can produce 1:1 and 2:1 nickel: alkali species. The association constants between Ni and M^+ correlated with the size match between the ionic radius of M^+ and the chain length of the PEG chelator (larger cations require longer PEG chains and vice versa). Combining Na^+ or K^+ with the nickel catalysts featuring tri- or tetra-ethylene

glycol chains increased the ethylene polymerization activity and gave polymers with higher molecular weight and branching density than the nickel catalysts alone. Cation-tuning was also applied to other olefin polymerization platforms and catalyst nuclearity was controlled through suitable ligand design.[44-47]

Small gas molecules can also be utilized as chemoselective switches by serving either as a trigger or a substrate for a reaction. For example, CO_2 can be used to oscillate a catalytic system between ring opening polymerization (ROP) of a lactone and ring opening copolymerization (ROCOP) of epoxides and CO_2 (Figure 1-5).[48, 49] Another example of a small gas molecule switch is O_2. Although more well-known as a radical scavenger, O_2 can also be used in chemical transformations to generate radical species that can initiate radical polymerization.[50, 51] Small gas molecules have the advantage of being easy to remove, however, a pressure reactor might be needed to accommodate the reaction.

Such examples demonstrate that chemical switching can be a useful strategy for regulating many different catalytic processes. Chemical switching can also take advantage of solution equilibria to tune reaction rates in a dynamic fashion. In cation tuning, different amounts or types of metal salts can be used to achieve different effects without requiring tedious synthetic modifications of the catalyst. Ideally, the chemical switch is only needed in catalytic amounts relative to the substrate (for example, in cation switching) or is incorporated into the reaction product (such as in CHO and CO_2 ROCOP). Some possible disadvantages of chemical switching are that the chemical reagents used are not traceless so they may need to be removed from the final product or they might not be compatible with subsequent steps in one-pot tandem or cascade reactions. Another potential limitation in cation switching is that the catalyst must be amenable to installation of secondary

metal binding groups to achieve high cation responsiveness since Lewis acid additives are relatively commonly used to enhance activity.[52]

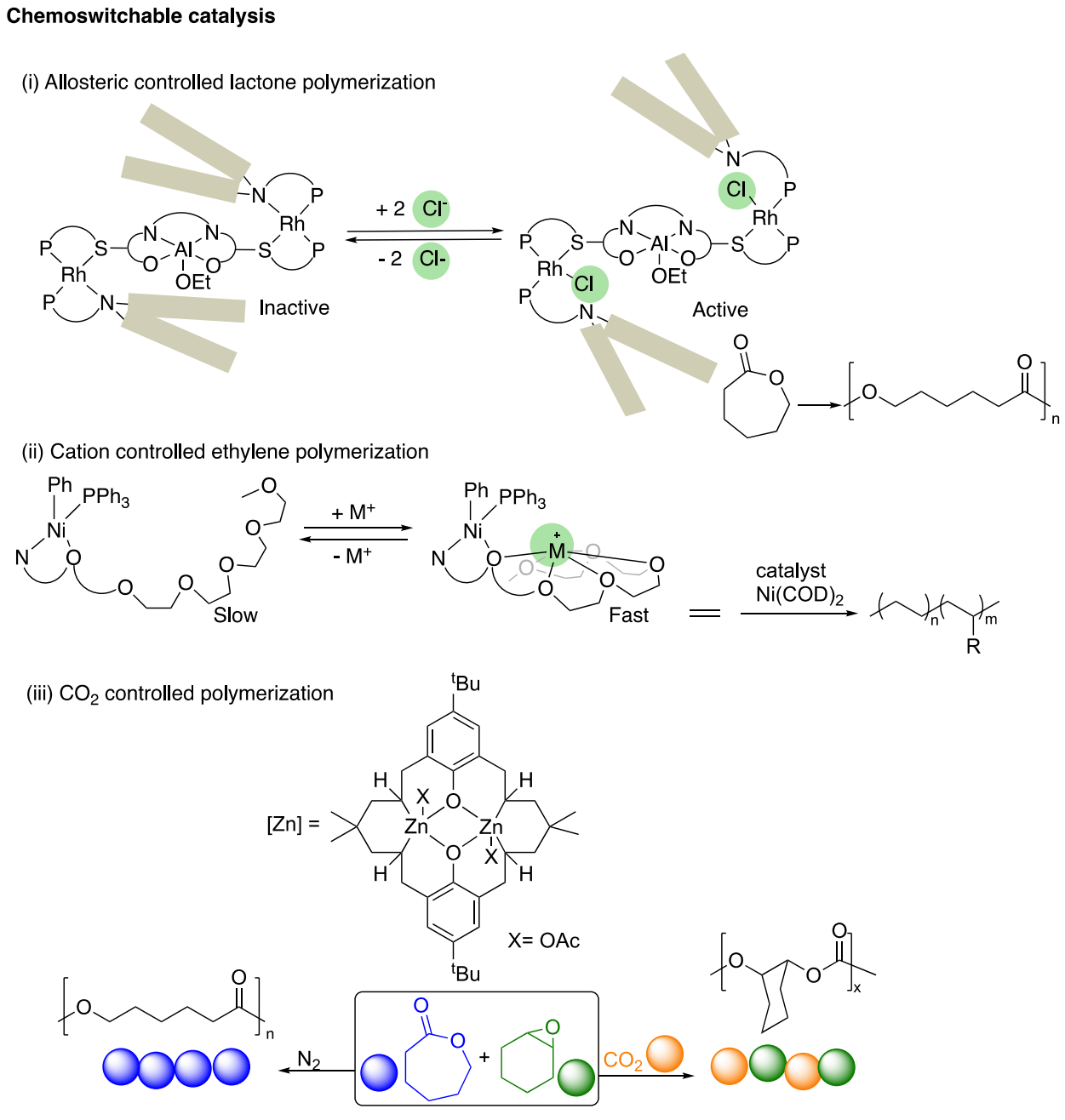

Figure 1-5. Chemoswitchable catalysis. Anion coordination leads to allosteric change which unblocks the catalytic active center for the ring opening polymerization of e-caprolactone (i). Metal cation coordination onto the hemilabile crown ether moiety promotes the hydrogen

activation reaction (ii). Metal cation coordination to the oligomeric ethylene glycol chain increases ethylene polymerization activity (iii). Presence of CO_2 stagnates the polymerization of e-caprolactone and initiates the ring opening copolymerization of CO_2 and cyclohexene oxide (iv).

Photoresponsive processes are ubiquitous in nature and in artificial synthesis and catalysis. Photoswitchable catalysis involves a catalytically active species that can undergo a reversible photochemical transformation, which consequently changes its intrinsic catalytic properties.[53] In photoswitchable catalysis, photochromic functionalities such as azobenzenes, which can undergo an E-Z isomerization, and diarylethenes, which can undergo a photo-induced ring closing, are commonly employed.

The photoinduced E-Z isomerization of diarylethenes and stilbenes can lead to a change in the steric environment of the active site, which can block or unblock substrate access or bring substrates closer together or further apart, thus changing the catalytic activity.[54] Such azobenzene photochromic functionality has been used to control the rate of an amidation reaction (Figure 1-6).[55] For example, for the amidation between aminoadenosine and adenosine-derived *p*-nitrophenol ester, a template molecule that contains two adenine receptors linked by an azobenzene spacer was designed. When the template molecule is in the E configuration, substrates bound to each receptor are far apart, resulting in a slow coupling rate. Upon UV irradiation (λ_{ex} = 366 nm), the template molecule undergoes a photo-induced isomerization, resulting in a photostationary state ratio of E:Z = 1:1. The *Z* configuration brings the two substrates in close proximity, thereby accelerating the reaction.

The photoinduced ring opening or ring closing of photochromic functionalities, such as spiropyrans[56, 57] and diarylethenes,[58] results in steric and electronic changes that have been used to

alter rates of lactone polymerization. For example, in a diarylethene-based system (Figure 1-6),[59] the ring-opened phenol catalyst uses the exposed -OH group to activate lactide, which leads to a high polymerization rate. Upon UV irradiation (λ_{ex} = 300 nm), a photostationary state is reached, leading to 98% of the ring-closed ketone isomer, which shows a diminished polymerization rate. The system can be turned back on to the active state by irradiation with visible light. The different rates of the opened and closed forms toward valerolactone and trimethylenecarbonate (TMC) polymerization can also be harnessed to control the microstructure of the polymers. The ring-opened phenol catalyst, incorporates more valerolactone than TMC to synthesize copolymers with higher valerolactone content, while the ring-closed ketone isomer leads to a polymer with higher TMC than valerolactone content.

Unlike most redox-switchable and chemoswitchable catalysts, photoswitchable catalysis provides a non-invasive method to achieve temporal control since light is the only reagent required for switching. Consequently, product purification does not require removing excess reagents. Additionally, switching can be fast and not limited by mass transport.[60,61,62] A combination of different polymerization mechanisms can also be achieved by changing the wavelengths of light. For example, by using photocatalysts and a thiocarbonate chain transfer agent, cationic polymerization could be initiated by green light, while radical polymerization could be commenced by blue light (Figure 1-6).[63] In terms of experimental setup, light-emitting diodes are typically used as a source of light with specific and narrow wavelength. Although photoswitchable catalysis shows many advantages in temporal control, it also needs to overcome several hurdles such as obtaining a high photostationary state isomer ratio with a short irradiation time, finding isomers with orthogonal reactivity, and using UV light, which limits compatibility with some organic substrates or metal catalysts.

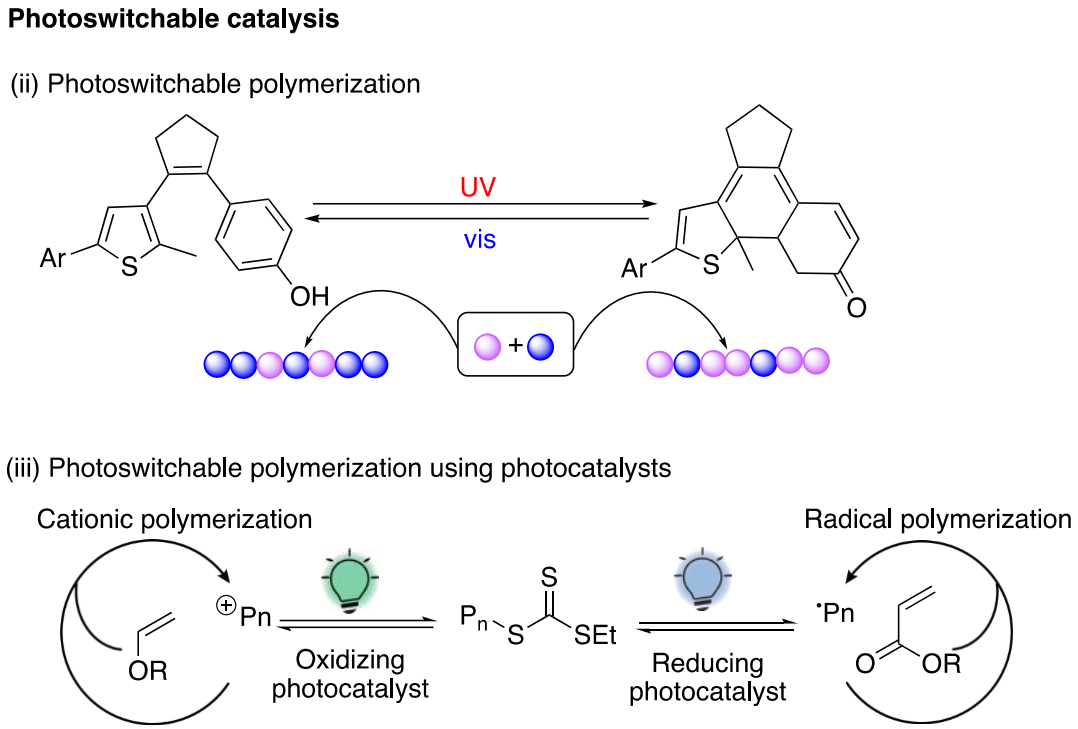

Figure 1-6. Photoswitchable catalysis. The catalyst can bind the substrates via hydrogen bonds; in the E form it can bring the substrates closer and accelerate the amidation process, while the Z form separates the substrates apart and thus slows down the amidation (i). The diarylethene-type catalyst with a phenol moiety in the ring-opened phenol form incorporates more valerolactone while the ring-closed ketone form incorporates more trimethylene carbonate in the copolymerization process (ii). By using different photocatalysts and changing the wavelength of light, the polymerization mechanism can switch between radical and cationic polymerization (iii).

1.3. Thesis Summary

Ring-opening polymerization plays a crucial role in chain-growth polymerization, enabling precise control over the process. In summary, our study focused on redox-switchable catalysis and its application in synthesizing polyesters, ethers, and carbonates via ring-opening polymerization.

Additionally, we expanded the monomer variety by investigating the polymerization of aromatic N-carboxyanhydrides, yielding aromatic polyamides with six-membered rings. Through the utilization of biodegradable polymers produced by ring-opening polymerization, we explored how the stereocomplexation of block copolymers can enhance the shear viscosities of polymer solutions when subjected to brine environments.

1.4. References

(1) Geyer, R.; Jambeck, J. R.; Law, K. L. Production, use, and fate of all plastics ever made. *Science Advances* **2017**, *3* (7), e1700782.

(2) Law, K. L.; Narayan, R. Reducing environmental plastic pollution by designing polymer materials for managed end-of-life. *Nature Reviews Materials* **2022**, *7* (2), 104-116.

(3) MacLeod, M.; Arp, H. P. H.; Tekman, M. B.; Jahnke, A. The global threat from plastic pollution. *Science* **2021**, *373* (6550), 61-65.

(4) Bates, F. S.; Hillmyer, M. A.; Lodge, T. P.; Bates, C. M.; Delaney, K. T.; Fredrickson, G. H. Multiblock polymers: Panacea or Pandora's box? *Science* **2012**, *336* (6080), 434-440.

(5) Nunes, S. P. Block Copolymer Membranes for Aqueous Solution Applications. *Macromolecules* **2016**, *49* (8), 2905-2916.

(6) Cabral, H.; Miyata, K.; Osada, K.; Kataoka, K. Block Copolymer Micelles in Nanomedicine Applications. *Chemical Reviews* **2018**, *118* (14), 6844-6892.

(7) You, I.; Kong, M.; Jeong, U. Block Copolymer Elastomers for Stretchable Electronics. *Accounts of Chemical Research* **2019**, *52* (1), 63-72.

(8) Teator, A. J.; Lastovickova, D. N.; Bielawski, C. W. Switchable polymerization catalysts. *Chem. Rev.* **2016**, *116* (4), 1969-1992, Review.

(9) Blanco, V.; Leigh, D. A.; Marcos, V. Artificial switchable catalysts. *Chem. Soc. Rev.* **2015**, *44* (15), 5341-5370.

(10) Choudhury, J. Recent developments on artificial switchable catalysis. *Tetrahedron Lett.* **2018**, *59* (6), 487-495.

(11) Kaler, S.; Jones, M. D. Recent advances in externally controlled ring-opening polymerisations. *Dalton Trans.* **2022**, *51* (4), 1241-1256.

(12) Doerr, A. M.; Burroughs, J. M.; Gitter, S. R.; Yang, X. J.; Boydston, A. J.; Long, B. K. Advances in polymerizations modulated by external stimuli. *ACS Catal.* **2020**, *10* (24), 14457-14515.

(13) Lastovickova, D. N.; Shao, H. L.; Lu, G.; Liu, P.; Bielawski, C. W. A ring-opening metathesis polymerization catalyst that exhibits redox-switchable monomer selectivities. *Chem. A Eur. J.* **2017**, *23* (25), 5994-6000.

(14) Zou, W. P.; Pang, W. M.; Chen, C. L. Redox control in palladium catalyzed norbornene and alkyne polymerization. *Inorg. Chem. Front.* **2017**, *4* (5), 795-800.

(15) Anderson, W. C.; Rhinehart, J. L.; Tennyson, A. G.; Long, B. K. Redox-active ligands: an advanced tool to modulate polyethylene microstructure. *J. Am. Chem. Soc.* **2016**, *138* (3), 774-777.

(16) Lorkovic, I. M.; Duff, R. R.; Wrighton, M. S. Use of the redox-active ligand 1, 1'-bis (diphenylphosphino) cobaltocene to reversibly alter the rate of the rhodium (I)-catalyzed reduction and isomerization of ketones and alkenes. *J. Am. Chem. Soc.* **1995**, *117* (12), 3617-3618.

(17) Gregson, C. K. A.; Gibson, V. C.; Long, N. J.; Marshall, E. L.; Oxford, P. J.; White, A. J. P. Redox control within single-site polymerization catalysts. *J. Am. Chem. Soc.* **2006**, *128* (23), 7410-7411.

(18) Zhao, M. H.; Chen, C. L. Accessing multiple catalytically active states in redox-controlled olefin polymerization. *ACS Catal.* **2017**, *7* (11), 7490-7494.

(19) Varnado, C. D.; Rosen, E. L.; Collins, M. S.; Lynch, V. M.; Bielawski, C. W. Synthesis and study of olefin metathesis catalysts supported by redox-switchable diaminocarbene [3] ferrocenophanes. *Dalton Trans.* **2013**, *42* (36), 13251-13264.

(20) Doerr, A. M.; Burroughs, J. M.; Legaux, N. M.; Long, B. K. Redox-switchable ring-opening polymerization by tridentate ONN-type titanium and zirconium catalysts. *Catal. Sci. Technol.* **2020**, *10* (19), 6501-6510.

(21) Anderson, W. C.; Park, S. H.; Brown, L. A.; Kaiser, J. M.; Long, B. K. Accessing multiple polyethylene grades via a single redox-active olefin polymerization catalyst. *Inorg. Chem. Front.* **2017**, *4* (7), 1108-1112.

(22) Brown, L. A.; Rhinehart, J. L.; Long, B. K. Effects of ferrocenyl proximity and monomer presence during oxidation for the redox-switchable polymerization of l-lactide. *ACS Catal.* **2015**, *5* (10), 6057-6060.

(23) Wei, J. N.; Diaconescu, P. L. Redox-switchable ring-opening polymerization with ferrocene derivatives. *Acc. Chem. Res.* **2019**, *52* (2), 415-424.

(24) Broderick, E. M.; Guo, N.; Vogel, C. S.; Xu, C. L.; Sutter, J.; Miller, J. T.; Meyer, K.; Mehrkhodavandi, P.; Diaconescu, P. L. Redox control of a ring-opening polymerization catalyst. *J. Am. Chem. Soc.* **2011**, *133* (24), 9278-9281.

(25) Broderick, E. M.; Diaconescu, P. L. Cerium(IV) catalysts for the ring-opening polymerization of lactide. *Inorg. Chem.* **2009**, *48* (11), 4701-4706.

(26) Biernesser, A. B.; Li, B.; Byers, J. A. Redox-controlled polymerization of lactide catalyzed by bis(imino)pyridine iron bis(alkoxide) complexes. *J. Am. Chem. Soc.* **2013**, *135* (44), 16553-16560.

(27) Qi, M.; Dong, Q.; Wang, D.; Byers, J. A. Electrochemically switchable ring-opening polymerization of lactide and cyclohexene oxide. *J. Am. Chem. Soc.* **2018**, *140* (17), 5686-5690.

(28) Hern, Z. C.; Quan, S. M.; Dai, R.; Lai, A.; Wang, Y.; Liu, C.; Diaconescu, P. L. ABC and ABAB block copolymers by electrochemically controlled ring-opening polymerization. *J. Am. Chem. Soc.* **2021**, *143* (47), 19802-19808.

(29) Quan, S. M.; Wang, X.; Zhang, R.; Diaconescu, P. L. Redox switchable copolymerization of cyclic esters and epoxides by a zirconium complex. *Macromolecules* **2016**, *49* (18), 6768-6778.

(30) Wei, J. N.; Riffel, M. N.; Diaconescu, P. L. Redox control of aluminum ring-opening polymerization: A combined experimental and DFT investigation. *Macromolecules* **2017**, *50* (5), 1847-1861.

(31) Xu, X.; Luo, G.; Hou, Z.; Diaconescu, P. L.; Luo, Y. Theoretical insight into the redox-switchable activity of group 4 metal complexes for the ring-opening polymerization of ε-caprolactone. *Inorg. Chem. Front.* **2020**, *7* (4), 961-971.

(32) Biernesser, A. B.; Chiaie, K. R.; Curley, J. B.; Byers, J. A. Block copolymerization of lactide and an epoxide facilitated by a redox switchable iron-based catalyst. *Angew. Chem. Int. Ed.* **2016**, *55* (17), 5251-5254.

(33) Lai, A.; Hern, Z. C.; Diaconescu, P. L. Switchable Ring-Opening Polymerization by a Ferrocene Supported Aluminum Complex. *ChemCatChem* **2019**, *11* (16), 4210-4218.

(34) Wang, X.; Thevenon, A.; Brosmer, J. L.; Yu, I.; Khan, S. I.; Mehrkhodavandi, P.; Diaconescu, P. L. Redox control of group 4 metal ring-opening polymerization activity toward l-lactide and ε-caprolactone. *J. Am. Chem. Soc.* **2014**, *136* (32), 11264-11267.

(35) Abubekerov, M.; Vlček, V.; Wei, J.; Miehlich, M. E.; Quan, S. M.; Meyer, K.; Neuhauser, D.; Diaconescu, P. L. Exploring oxidation state-dependent selectivity in polymerization of cyclic esters and carbonates with zinc (II) complexes. *Iscience* **2018**, *7*, 120-131.

(36) Lowe, M. Y.; Shu, S. S.; Quan, S. M.; Diaconescu, P. L. Investigation of redox switchable titanium and zirconium catalysts for the ring opening polymerization of cyclic esters and epoxides. *Inorg. Chem. Front.* **2017**, *4* (11), 1798-1805.

(37) Deng, S.; Diaconescu, P. L. A switchable dimeric yttrium complex and its three catalytic states in ring opening polymerization. *Inorg. Chem. Front.* **2021**, *8* (8), 2088-2096, 10.1039/D0QI01479F.

(38) Ortuno, M. A.; Dereli, B.; Delle Chiaie, K. R.; Biernesser, A. B.; Qi, M.; Byers, J. A.; Cramer, C. J. The role of alkoxide initiator, spin state, and oxidation state in ring-opening polymerization of epsilon-caprolactone catalyzed by iron bis(imino)pyridine complexes. *Inorg. Chem.* **2018**, *57* (4), 2064-2071.

(39) Yoon, H. J.; Kuwabara, J.; Kim, J. H.; Mirkin, C. A. Allosteric supramolecular triple-layer catalysts. *Science* **2010**, *330* (6000), 66-69.

(40) Kita, M. R.; Miller, A. J. M. Cation-modulated reactivity of iridium hydride pincer-crown ether complexes. *J. Am. Chem. Soc.* **2014**, *136* (41), 14519-14529.

(41) Kita, M. R.; Miller, A. J. M. An ion-responsive pincer-crown ether catalyst system for rapid and switchable olefin isomerization. *Angew. Chem. Int. Ed.* **2017**, *56* (20), 5498-5502.

(42) Camp, A. M.; Kita, M. R.; Blackburn, P. T.; Dodge, H. M.; Chen, C. H.; Miller, A. J. M. Selecting double bond positions with a single cation-responsive iridium olefin isomerization catalyst. *J. Am. Chem. Soc.* **2021**, *143* (7), 2792-2800.

(43) Cai, Z. Z.; Xiao, D. W.; Do, L. H. Fine-tuning nickel phenoxyimine olefin polymerization catalysts: performance boosting by alkali cations. *J. Am. Chem. Soc.* **2015**, *137* (49), 15501-15510.

(44) Cai, Z. Z.; Do, L. H. Thermally robust heterobimetallic palladium-alkali catalysts for ethylene and alkyl acrylate copolymerization. *Organometallics* **2018**, *37* (21), 3874-3882.

(45) Tran, T. V.; Karas, L. J.; Wu, J. I.; Do, L. H. Elucidating secondary metal cation effects on nickel olefin polymerization catalysts. *ACS Catal.* **2020**, *10* (18), 10760-10772.

(46) Tran, T. V.; Nguyen, Y. H.; Do, L. H. Development of highly productive nickel-sodium phenoxyphosphine ethylene polymerization catalysts and their reaction temperature profiles. *Polym. Chem.* **2019**, *10* (27), 3718-3721.

(47) Tran, T. V.; Lee, E.; Nguyen, Y. H.; Nguyen, H. D.; Do, L. H. Customizing polymers by controlling cation switching dynamics in non-living polymerization. *J. Am. Chem. Soc.* **2022**, *144* (37), 17129-17139.

(48) Romain, C.; Williams, C. K. Chemoselective polymerization control: from mixed-monomer feedstock to copolymers. *Angew. Chem. Int. Ed.* **2014**, *53* (6), 1607-1610.

(49) Coulembier, O.; Moins, S.; Todd, R.; Dubois, P. External and Reversible CO2 Regulation of Ring-Opening Polymerizations Based on a Primary Alcohol Propagating Species. *Macromolecules* **2014**, *47* (2), 486-491.

(50) Lv, C. N.; He, C. Z.; Pan, X. C. Oxygen-initiated and regulated controlled radical polymerization under ambient conditions. *Angew. Chem. Int. Ed.* **2018**, *57* (30), 9430-9433.

(51) Zhang, B. H.; Wang, X. J.; Zhu, A. Q.; Ma, K.; Lv, Y.; Wang, X.; An, Z. S. Enzyme-Initiated Reversible Addition-Fragmentation Chain Transfer Polymerization. *Macromolecules* **2015**, *48* (21), 7792-7802.

(52) Sha, S.-C.; Tcyrulnikov, S.; Li, M.; Hu, B.; Fu, Y.; Kozlowski, M. C.; Walsh, P. J. Cation−π Interactions in the Benzylic Arylation of Toluenes with Bimetallic Catalysts. *J. Am. Chem. Soc.* **2018**, *140* (39), 12415-12423.

(53) Neilson, B. M.; Bielawski, C. W. Illuminating photoswitchable catalysis. *ACS Catal.* **2013**, *3* (8), 1874-1885.

(54) Dorel, R.; Feringa, B. Photoswitchable catalysis based on the isomerisation of double bonds. *Chem. Commun.* **2019**, *55* (46), 6477-6486.

(55) Wurthner, F.; Rebek, J. Light-switchable catalysis in synthetic receptors. *Angew. Chem. Int. Ed.* **1995**, *34* (4), 446-448.

(56) Fu, C. K.; Xu, J. T.; Boyer, C. Photoacid-mediated ring opening polymerization driven by visible light. *Chem. Commun.* **2016**, *52* (44), 7126-7129.

(57) Berkovic, G.; Krongauz, V.; Weiss, V. Spiropyrans and spirooxazines for memories and switches. *Chem. Rev.* **2000**, *100* (5), 1741-1753.

(58) Majee, D.; Presolski, S. Dithienylethene-based photoswitchable catalysts: state of the art and future perspectives. *ACS Catal.* **2021**, *11* (4), 2244-2252.

(59) Eisenreich, F.; Kathan, M.; Dallmann, A.; Ihrig, S. P.; Schwaar, T.; Schmidt, B. M.; Hecht, S. A photoswitchable catalyst system for remote-controlled (co)polymerization in situ. *Nat. Catal.* **2018**, *1* (7), 516-522.

(60) Corrigan, N.; Jung, K.; Moad, G.; Hawker, C. J.; Matyjaszewski, K.; Boyer, C. Reversible-deactivation radical polymerization (controlled/living radical polymerization): from discovery to materials design and applications. *Prog. Polym. Sci.* **2020**, *111*.

(61) Leibfarth, F. A.; Mattson, K. M.; Fors, B. P.; Collins, H. A.; Hawker, C. J. External regulation of controlled polymerizations. *Angew. Chem. Int. Ed.* **2013**, *52* (1), 199-210.

(62) Xu, J. T.; Jung, K.; Atme, A.; Shanmugam, S.; Boyer, C. A robust and versatile photoinduced living polymerization of conjugated and unconjugated monomers and its oxygen tolerance. *J. Am. Chem. Soc.* **2014**, *136* (14), 5508-5519.

(63) Kottisch, V.; Michaudel, Q.; Fors, B. P. Photocontrolled interconversion of cationic and radical polymerizations. *J. Am. Chem. Soc.* **2017**, *139* (31), 10665-10668.

Chapter 2: Redox-switchable dimeric yttrium compound and its activity in ring-opening polymerization

2.1. Introduction

Redox-switchable catalysis has emerged as a powerful tool to modulate polymerization reactions. By changing the electron density either at the metal center or at the ligand scaffold, the catalytic activity and selectivity of a catalyst can be altered.[1-5] In 2006, Long and coworkers reported a titanium Schiff base complex bearing two peripheral ferrocene units that displayed a different activity toward *rac*-lactide polymerization in the two different oxidation states9/1/2023 6:46:00 AM.[6] Since then, redox-switchable polymerization has been applied to the ring opening polymerization of cyclic ester and ethers,[5, 7-27] the coordination insertion polymerization of olefins,[28-36] olefin metathesis,[37-41] and controlled radical polymerization.[42-44]

In all aforementioned cases, only two oxidation states were available, systems addressing multiple catalytic oxidation states remaining scarce. In 2016, Chen and coworkers reported an α-diimine palladium compound, **Pd-CN** (Chart 2-1), which was the first example of catalytic system that was amenable to two stepwise oxidations.[45] The three oxidation states not only had different catalytic activities toward ethylene polymerization but also produced polyethylene with different molar masses and different topologies. Another example was recently reported by Hey-Hawkins and coworkers, who showed that a trinuclear gold(I) complex supported by a tris(ferrocenyl)arene-based tris-phosphine, **[Au]$_3$** (Chart 2-1) had four accessible oxidation states, making it possible to tune in a stepwise fashion the rate of catalytic ring-closing isomerisation of *N*-(2-propyn-1-yl)benzamide.[46] However, to the best of our knowledge, a system with multiple catalytic oxidation states has not been investigated and exploited for the ring opening polymerization of cyclic esters and ethers.

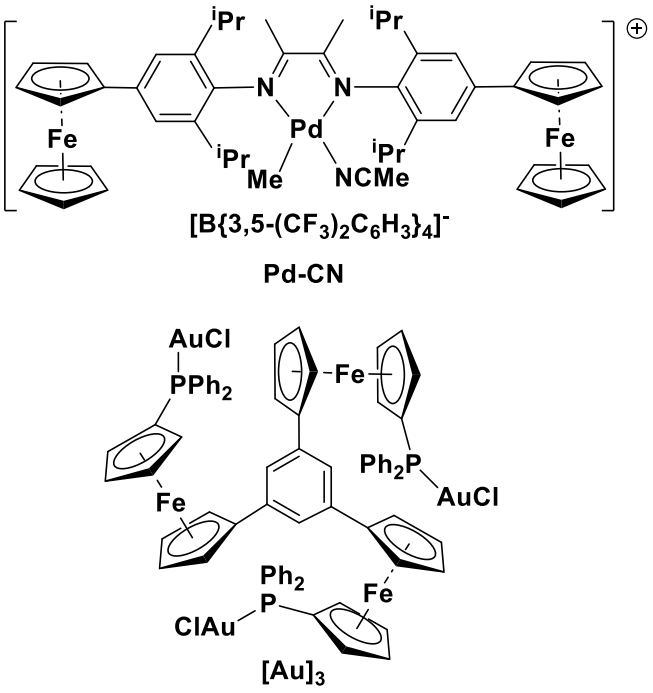

Chart 2-1. Previously reported representative ferrocene-based metal complexes.

Our group has been developing redox switchable catalytic systems for ring opening polymerization in order to synthesize biodegradable polymers. In 2011, we reported the first and only redox-switchable yttrium complex, (phosfen)Y(O^{t}Bu) (phosfen = 1,1'-di(2-*tert*-butyl-6-diphenylphosphinimino-phenoxy)ferrocene, Chart 1), which is active toward lactide and trimethyl carbonate ring opening polymerization in the reduced state while inactive when oxidized.[47] Although many efforts have been exerted to developing ligand-based redox-switchable metal complexes for the ring opening polymerization of cyclic esters and ethers by us[16, 19-21, 26, 48] and others,[49-51] most of them reported so far are based on group 4 metals.[18, 22-25] On the other hand, group 3 metal complexes remaining mostly unexplored despite their high activity in ring opening polymerization.[52-56] In this contribution, we report the synthesis and characterization of a redox-

switchable dimeric yttrium compound, [(salfen)Y(OPh)]$_2$ (salfen = N,N'-bis(2,4-di-*tert*-butylphenoxy)- 1,1'-ferrocenediimine), which can switch between three different oxidation states, and its application in redox-switchable ring opening polymerization.

2.2. Results and Discussion

Synthesis of [(salfen)Y(OPh)]$_2$

A salt metathesis reaction between (salfen)YCl(THF) and KOPh in toluene at ambient temperature led to the formation of the phenoxide compound [(salfen)Y(OPh)]$_2$ (Scheme 2-1). The ^{1}H NMR spectrum showed a set of major peaks and a set of minor peaks, with a ratio of 5:1. We also attempted another synthetic route by reacting (salfen)YCl(THF) with LiN(SiMe$_3$)$_2$ to generate an yttrium amide intermediate, to which phenol was then added added (Scheme 2-1). However, the same product with an identical ^{1}H NMR spectrum was obtained. Similar results were reported by Williams et al.: it was suggested that the minor peaks belong to an isomer resulting from a different ligand conformation or yttrium coordination geometry.[57, 58] Therefore, a variable temperature ^{1}H NMR experiment was performed and showed that the two sets of peaks showed coalesced at 95 °C.

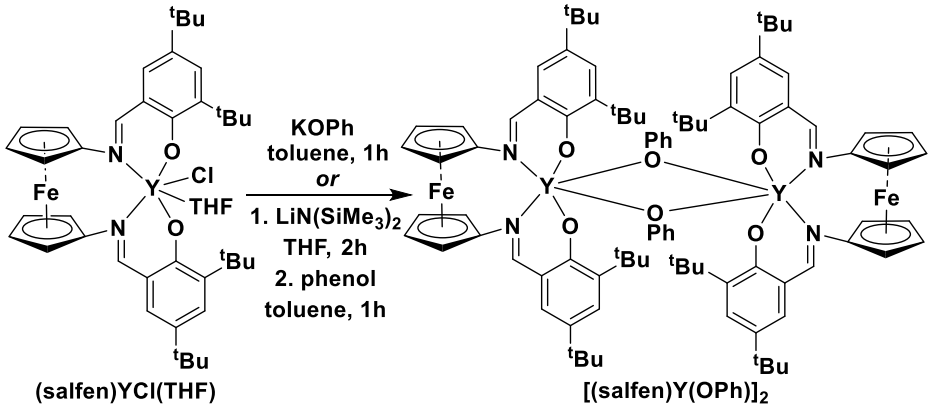

Scheme 2-1. Synthetic routes to $[(salfen)Y(OPh)]_2$.

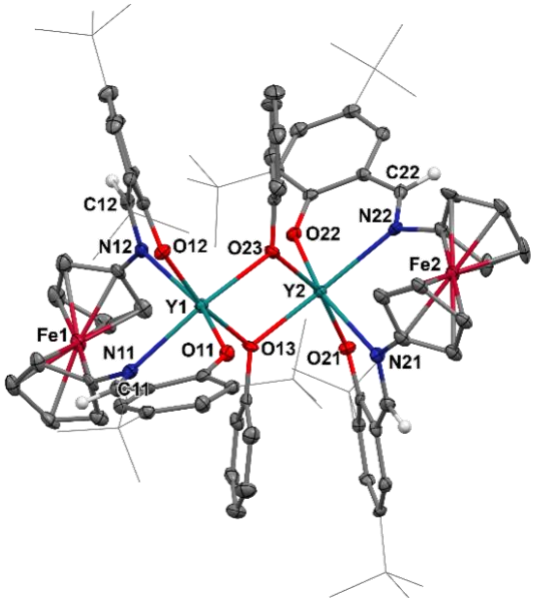

Figure 2-1. Thermal ellipsoid (50% probability) representation of $[(salfen)Y(OPh)]_2$. Hydrogen atoms were omitted and phenolic *t*-butyl groups were represented as sticks for clarity.

Single crystals suitable for X-ray crystallography analysis were grown from a dilute hexanes solution at ambient temperature. The solid-state molecular structure of $[(salfen)Y(OPh)]_2$ (Figure 2-1) shows a dimeric species, in which two yttrium centres are bridged by two phenoxide groups. Diffusion ordered spectroscopy (DOSY) NMR experiments were conducted to determine whether the dimeric structure was maintained in solution. The solution hydrodynamic radius r_H was calculated to be 8.2 Å, while the solid-state value $r_{x\text{-}ray}$ was determined to be 7.8 Å using X-ray crystallographic data (Figure A10), indicating that the compound exists as a dimer in solution as well.

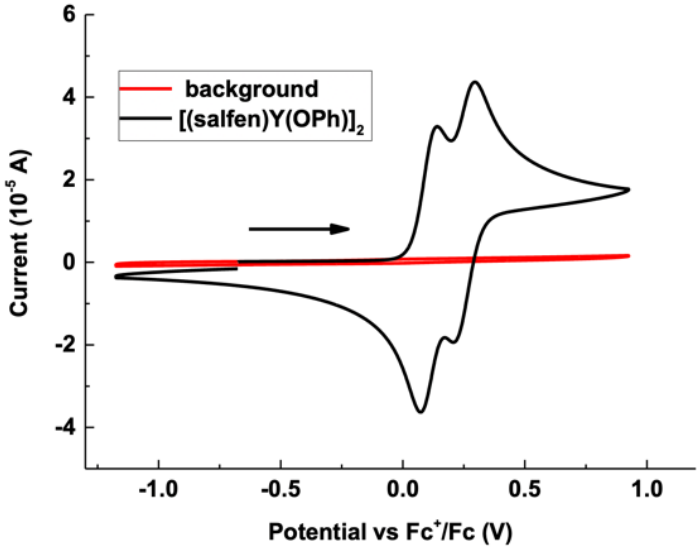

Figure 2-2. Cyclic voltammogram of 5 mM [(salfen)Y(OPh)]$_2$ recorded at a glassy carbon electrode at a scan rate of 100 mV/s.1,2-difluorobenzene was used as a solvent and 100 mM TPABAr^F was used as the electrolyte.

Redox properties of [(salfen)Y(OPh)]$_2$

In order to gain insight into the redox properties of [(salfen)Y(OPh)]$_2$, an electrochemical study, as well as chemical redox experiments were performed. According to the reported electrochemical studies of the previously mentioned **Pd-CN**, the half potentials of the electron transfer events were close to each other ($E_{1/2}$ vs Ag/AgCl for **Pd-CN**: 0.50 V; for [**Pd-CN**]$^+$: 0.47 V; for [**Pd-CN**]$^{2+}$: 0.46 V).[45] However, in our case, the cyclic voltammogram of [(salfen)Y(OPh)]$_2$ (Figure 2) clearly shows two reversible electron transfer events with half potentials of 0.16 V and 0.32 V versus Fc/Fc$^+$, suggesting that [(salfen)Y(OPh)]$_2$ can be reversibly oxidized in a stepwise fashion. Chemical redox experiments were also conducted using ^{Ac}FcBAr^F as an oxidant and $CoCp_2$ as a reductant. ^{1}H NMR spectra showed that the addition of 1 or 2 equivalents of ^{Ac}FcBAr^F resulted in the

disappearance of the [(salfen)Y(OPh)]$_2$ signals and the formation of broad paramagnetic peaks, likely corresponding to [(salfen)Y(OPh)]$_2^+$ and [(salfen)Y(OPh)]$_2^{2+}$, respectively, while the addition of $CoCp_2$ led to the reappearance of [(salfen)Y(OPh)]$_2$ peaks. Byers and coworkers recently reported a technique using DOSY NMR spectroscopy to characterize heterobimetallic compounds where one of the metals was a paramagnetic first-row transition metal;[59] this technique might be a useful tool to characterize and elucidate the structure of the oxidized species. When we applied it, we found that the doubly oxidized species [(salfen)Y(OPh)]$_2^{2+}$ showed a single peak in the diffusion spectrum that indicated that the dimeric structure was maintained; the mono-oxidized [(salfen)Y(OPh)]$_2^+$ was more complicated, but the majority of the signals were also attributed to a dimeric form. Crossover experiment was also performed by adding 1 equivalent of [(salfen)Y(OPh)]$_2$ into doubly oxidized [(salfen)Y(OPh)]$_2^{2+}$, the ^{1}H NMR and DOSY NMR spectra matched with those of the mono-oxidized species [(salfen)Y(OPh)]$_2^+$. Furthermore, stability tests revealed that all three oxidation states were robust, no decomposition was observed at 80 °C after 24 hours (Figures S7-9).

Scheme 2-2. Redox switch between the three oxidation states of [(salfen)Y(OPh)]$_2$.

Homopolymerization reactions

The catalytic activity of the reduced state and of the two *in situ* generated oxidized states was studied toward the ring opening polymerization of cyclic esters, carbonate, and ethers.

In LLA (L-lactide) polymerization, the reduced state compound, $[(salfen)Y(OPh)]_2$, showed the highest activity, where 200 equivalents of monomer were polymerized to 73% conversion in 0.5 hours at ambient temperature (Table 2-1, entry 1). To gain insight of the catalytically active species, DOSY NMR experiements were performed on PLLA obtained from 60 equivalents of LLA polymerized by the reduced state $[(salfen)Y(OPh)]_2$, before and after quenching with H_2O. Despite a more complicated diffusion pattern, the active polymer chain showed a diffusion coefficient of 2.7×10^{-11} m^2/s which agreed with quenched free polymer chain which showed a diffusion coefficient of 2.9×10^{-11} m^2/s, indicating that the active species is more likely to be mono-nuclear during the polymerization. The mono-oxidized state demonstrated a slower polymerization rate but produced polymer with a narrower dispersity, and the molar mass of the resulting polymer revealed that only one of the two phenoxide groups initiated the polymerization (Table 2-1, entry 2). The doubly oxidized compound had the lowest activity, only 23% conversion was reached after 24 hours, and the polymer molar mass also suggested a single phenoxide initiation (Table 2-1, entry 3). A similar trend was observed in CL (ε-caprolactone) and VL (δ-valerolactone) polymerizations, where the reduced compound showed the highest rate and the activity decrease along with oxidation (Table 2-1, entries 4-9). However, unlike LLA polymerization, which was well-controlled, lactone polymerizations were poorly regulated, leading to high polymer molar masses compared to theoretical values. In TMC (1,3-trimethylene carbonate) polymerization, the reduced state showed the highest activity but the molar mass of the resulting polymer was much higher than expected, probably due to transesterification[21] or catalyst deactivation. The mono-oxidized compound showed a

slower polymerization rate but better controlled molar mass in comparison to the reduced state (Table 2-1, entries 10-12).

Ring opening polymerization of epoxides showed an opposite trend, where the activity of the yttrium compound increases as the oxidation state increases. For example, the reduced compound was inactive toward the polymerization of CHO (cyclohexene oxide), while both the mono-oxidized and doubly oxidized compounds reached full conversion in 5 minutes. Such a high activity of the oxidized states caused a broad dispersity and uncontrolled molar mass of the polymer (Table 2-1, entries 13-15). This behavior was also observed for some other ferrocene-based metal complexes. We previously reported a combination of experimental results and DFT calculations to elucidate the CHO polymerization mechanism by the oxidized compound, which manifests that coordination insertion pathway is more feasible than cationic polymerization pathway. Another epoxide, PO (propylene oxide), was also tested as a monomer, and the same trend as for CHO was observed (Table 2-1, entries 10-12). The reduced state compound didn't polymerize PO even when the temperature was elevated to 80 °C. However, both the mono-oxidized and doubly oxidized compounds which were inactive at ambient temperature, reached certain conversion when heated to 80 °C for 48 hours (Table 2-1, entry 16-18). Since $^{Ac}FcBAr^{F}$ can act as catalyst in CHO polymerization, a control experiment of PO polymerization with the oxidant was performed, and it turned out that $^{Ac}FcBAr^{F}$ can polymerize PO at 25 °C and 81% conversion was reached after 2 hours.

Table 2-1. Homopolymerization with $[(salfen)Y(OPh)]_2$, $[(salfen)Y(OPh)]_2^+$, and $[(salfen)Y(OPh)]_2^{2+}$ toward different monomers.[a]

Entry	Monomer[b]	Cat.[c]	Time	Conv. (%)	$M_{n,calc}$[d] (kDa)	$M_{n,exp}$[e] (kDa)	Đ
1	LLA	red	0.5 h	73	11	10	1.51
2	LLA	ox^+	6 h	83	12	23	1.25
3	LLA	ox^{2+}	24 h	23	3.3	6.9	1.11
4	CL	red	21 h	81	8.3	59	1.47
5	CL	ox^+	24 h	3	N/A		
6	CL	ox^{2+}	24 h	0	N/A		
7	VL	red	10 h	82	8.2	65	1.23
8	VL	ox^+	24 h	20	2.2	13	1.20
9	VL	ox^{2+}	24 h	7	0.7	13	1.02
10	TMC	red	24 h	96	9.8	158	1.24
11	TMC	ox^+	72 h	84	8.6	10.2	1.11
12	TMC	ox^{2+}	72 h	38	2.9	21	1.13
13	CHO	red	24 h	0	N/A		
14	CHO	ox^+	5 min	98	9.6	23	3.3
15	CHO	ox^{2+}	5 min	100	9.8	66	3.5
16[f]	PO	red	24 h	0	N/A		
17[f]	PO	ox^+	48 h	16	0.9	291	1.23
18[f]	PO	ox^{2+}	48 h	65	3.8	380	1.18

[a] All polymerization reactions were performed with 2.5 μmol precatalyst, 0.6 mL of C_6D_6 as the solvent, 200 equivalents of monomer, at ambient temperature unless otherwise mentioned; conversions were determined by ^1H NMR spectroscopy. Each polymerization experiment was performed at least twice, and one of the trials is listed.[b] LLA stands for L-lactide, CL stands for ε-caprolactone, VL stands for δ-valerolactone, TMC stands for 1,3-trimethylene carbonate, CHO stands for cyclohexene oxide, and PO stands for propylene oxide. [c] "red" represents $[(salfen)Y(OPh)]_2$, "ox^+" represents *in situ* generated $[(salfen)Y(OPh)]_2^+$, and "ox^{2+}" represents *in situ* generated $[(salfen)Y(OPh)]_2^{2+}$. [d] $M_{n,calc}$ is calculated based on initiation from both phenoxide groups, $M_{n,calc} = M_{monomer} \times 100 \times$ conversion. [e] $M_{n,exp}$ were determined by SEC measurements. [f] Polymerization was conducted at 80 °C.

Copolymerization reactions

Based on the homopolymerization results, copolymerization experiments were performed. We first tried copolymerization of LLA and TMC. Only a few examples[48, 60, 61] reported before are capable of polymerizing TMC after LLA because, after the insertion of LLA, a five-membered ring intermediate would make the energy barrier for insertion too high for the next lactide and even harder for TMC incorporation. In 2018, we reported a dimeric zinc compound that can polymerize TMC after LLA and thus synthesize multiblock copolymers; DFT studies indicated that the dimeric structure lowers the overall activation barrier making the propagation possible after the insertion of LLA.[48] Therefore, we first attempted a one-pot copolymerization of LLA and TMC with $[(salfen)Y(OPh)]_2$ (Table 2, entry 1). Real time ^1H NMR spectroscopy was used to monitor the conversion of both monomers, and indicated that a tapered copolymer was generated. The linkages were confirmed by the $^{13}C\{^1H\}$ NMR spectrum of the isolated polymer. However, due to the uncontrolled nature of TMC polymerization, the polymer molar mass did not agree with the theoretical value.

Table 1-2. Copolymerization studies.[a]

Entry	Monomer[b]	Cat.[c]	Time [g]	Conv.[h] (%)	$M_{n,calc}$[d] (kDa)	$M_{n,exp}$[e] (kDa)	Đ
1[f]	LLA-TMC	red	17 h	100 - 82	23	52	1.51
2	LLA-TMC	red-ox$^+$	15 min - 24 h	100 - 53	21	29	1.31

3	LLA-CHO	red-ox^{2+}	15 min - 5 min	46 - 100	4.4	7.9	1.32
4	LLA-CHO-LLA	red-ox^{2+}-red	15 min - 5min - 25 min	55 - 100 - 100	N/A		
5	LLA-CHO-LLA	ox^{+}-ox^{2+}-ox^{+}	5 h - 5 min - 1 h	55 - 80 - 73	N/A		
6	LLA-TMC-CHO	red-ox^{+}-ox^{2+}	15 min - 24 h - 6 h	100 - 63 - 0	N/A		

[a] All polymerization reactions were performed with 2.5 μmol precatalyst, 0.6 mL of C_6D_6 as the solvent, 200 equivalents of monomer, at ambient temperature unless otherwise mentioned; conversions were determined by ^{1}H NMR spectroscopy. [b] LLA stands for L-lactide, TMC stands for 1,3-trimethylene carbonate, and CHO stands for cyclohexene oxide. [c] "red" represents $[(salfen)Y(OPh)]_2$, "ox^{+}" represents *in situ* generated $[(salfen)Y(OPh)]_2^{+}$, and "ox^{2+}" represents *in situ* generated $[(salfen)Y(OPh)]_2^{2+}$. [d] $M_{n,calc}$ is calculated based on initiation from both phoxide groups, $M_{n,calc} = M_{monomer} \times 100 \times$ conversion [e] $M_{n,exp}$ were determined by SEC measurements. [f] Polymerization was conducted in one pot. [g] Each number represents the polymerization time catalyzed by each oxidation state, which starts with the addition of monomer and ends with the addition of next redox reagents. [h] Entry 1,2,3,6, each number represents the monomer conversion at the end of polymerization. Entry 4 and 5, the first number represents the conversion after the first time period, the other two conversion numbers represent the conversion at the end of the polymerization.

To synthesize a better regulated block copolymer, we then carried out the redox controlled copolymerization of LLA and TMC by sequentially adding the monomers (Table 2-2, entry 2). 55% conversion of LLA was reached after 15 min with $[(salfen)Y(OPh)]_2$. Subsequently, 1 equivalent of $^{Ac}FcBAr^{F}$ was added to oxidize the catalyst to the mono-oxidized state, followed by the addition of the second monomer, TMC. After another 24 h

of polymerization, LLA was depleted while TMC reached 53% conversion. ^{1}H NMR monitoring of the polymerization, as well as the ^{13}C{^{1}H} NMR spectrum of the isolated polymer, indicated that LLA and TMC were still polymerized in a tapered fashion when they coexisted in the system. We also characterized our copolymers with thermogravimetric analysis, and it turned out that, unlike pure PLLA or PTMC which can endure higher temperature, the PLLA-PTMC copolymer we obtained started thermal decomposition at 50°C which could be attributed to the alternating segment in the polymer (Figure A64-65). DOSY of the isolated polymer showed a single diffusion peak which confirmed that a diblock copolymer was synthesized.

We also performed a LLA and CHO copolymerization utilizing a redox switch (Table 2-2, entry 3). We first polymerized LLA with the reduced state; 2 equivalents of ^{Ac}FcBAr^{F} was added to oxidize the catalyst to the doubly oxidized state, halting the LLA polymerization. Then, 200 equivalents of CHO was added subsequently and a full conversion was reached after 5 minutes according to real time ^{1}H NMR monitoring. However, the ^{1}H NMR spectrum of the isolated polymer showed only 27% PCHO incorporation; the PCHO homopolymer was probably removed during the polymer purification process. To determine whether the catalytic activity toward LLA polymerization can be restored after the CHO polymerization, a triblock copolymerization was attempted (Table 2-2, entry 4). Aliquots were taken to characterize the polymer at each stage, and, according to the SEC traces, the PLLA-PCHO peak shifted from the PLLA homopolymer peak, however, the PLLA-PCHO-PLLA peak was on top of the PLLA-PCHO peak implying that the triblock copolymer synthesis was unsuccessful. When we initiated the LLA polymerization with the

mono-oxidized state (Table 2-2, entry 5), a 55% conversion was reached after 5 hours; 1 equivalent of $^{Ac}FcBAr^{F}$ was then added to halt LLA polymerization and generate the doubly oxidized species that would start the CHO polymerization. After the subsequent addition of 1 equivalent of $CoCp_2$ to switch back to the mono-oxidized state, another 200 equiv of LLA was added. After the polymerization of CHO, LLA polymerization rate with the regenerated mono-oxidized compound was much faster, an overall 73% conversion was reached within 1 hour. This behaviour agreed with results from our previous study, which investigated in depth on how one monomer influences the polymerization rate of another monomer, where LLA is polymerized more quickly after CHO with a ferrocene-based zirconium compound.[49] SEC traces also indicated that homopolymers instead of a targeted triblock copolymer were obtained. We also tried to polymerize CHO after the copolymerization of LLA and TMC (Table 2-2, entry 6); however, after adding 1 equivalent of $^{Ac}FcBAr^{F}$ and 200 equivalents of CHO, no CHO polymerization was observed after 6 hours. We postulate that the failure to synthesize a triblock copolymer could be ascribed to the different redox behaviour when a substrate was present.[62]

2.3. Conclusions

We synthesized the dimeric yttrium compound $[(salfen)Y(OPh)]_2$ that can be oxidized twice in a stepwise fashion. ^{1}H and DOSY NMR spectroscopy were employed to characterize the three oxidation states. The catalytic activity toward ring opening polymerization of LLA, CL, VL, and TMC decreased along with oxidation. In TMC and LLA polymerization,

2.4. Experimental Section

General considerations

All experiments were performed under a dry nitrogen atmosphere in an MBraun glovebox or using standard Schlenk techniques. Solvents were purified with a two-state solid-state purification system by the method of Grubbs[63] and transferred into a glovebox without exposure to air. NMR solvents were purchased from Cambridge Isotope Laboratories, degassed, and stored over activated molecular sieves prior to use. ^{1}H NMR spectra were recorded on Bruker AV-300, Bruker AV-500, or Bruker DRX-500 spectrometers at room temperature. Chemical shifts are reported with respect to the residual solvent peaks, 7.16 ppm (C_6D_6), 7.26 ppm ($CDCl_3$) for ^{1}H NMR spectra. Liquid monomers and 1,2-difluorobenzene were distilled over CaH_2 and brought into the glovebox without exposure to air. Solid monomers were recrystallized from toluene at least twice before use. *n*-BuLi, 2,4-di-*tert*-butylphenol and $CoCp_2$ were purchased from Sigma-Aldrich and used as received. ^{Ac}FcBAr^{F} (^{Ac}Fc = acetylferrocene, BAr^{F} = tetrakis(3,5-bis(trifluoromethyl)-phenyl)borate),[64] KOPh, and (salfen)YCl(THF)[65] were synthesized following previously published procedures. Molar masses of polymers were determined by size exclusion chromatography using a SEC-MALS instrument at UCLA. SEC-MALS uses a Shimazu Prominence-i LC 2030C 3D equipped with an autosampler, two MZ Analysentechnik MZ-Gel SDplus LS 5 μm, 300 × 8 mm linear columns, a Wyatt DAWN HELEOS-II, and a Wyatt Optilab T-rEX. The column temperature was set at 40 °C. A flow rate of 0.70 mL/min was used and samples were dissolved in THF. The number average molar mass and dispersity values were determined using the dn/dc values which were calculated by 100% mass recovery method from the RI signal. CHN analyses were performed on an Exeter

Analytical, Inc. CE-440 Elemental Analyzer. Thermal gravimetric analysis was performed using a PerkinElmer Pyris Diamond TG/DTA Instruments under argon. The program used was to increase the temperature from 50 to 500 °C at 5 °C/min.

Synthesis of [(salfen)Y(OPh)]$_2$. (salfen)YCl(THF) (261.2 mg, 0.4 mmol) was dissolved in 10 mL of toluene; then, a KOPh (113 mg, 0.4 mmol) slurry in toluene was added to it. The mixture was stirred for 1 hour at room temperature. Volatiles were removed under a reduced pressure. The residue was dissolved in hexanes, concentrated, and kept at -30 °C overnight. An orange powder was collected after filtration. Yield: 0.115g, 80%. X-ray quality single crystals of [(salfen)Y(OPh)]$_2$ was grown from a dilute hexanes solution at room temperature. ^{1}H NMR (500 MHz, C_6D_6, 25 °C), δ (ppm): 7.91 (s, 2H, N=C*H*), 7.56 (d, 2H, Ar*H*), 7.29 (d, 2H, Ar*H*), 6.78 (d, 2H, Ar*H*), 6.69 (t, 2H, Ar*H*), 6.45 (t, 1H, Ar*H*), 4.81 (s, 2H, fc-*H*), 3.72-4.03 (s,s and s, 6H, fc-*H*), 1.58 (s, 18H, C(C*H*$_3$)$_3$), 1.27 (s, 18H, C(C*H*$_3$)$_3$). ^{13}C {^{1}H} NMR (125 MHz, C_6D_6, 25 °C), δ(ppm): 164.8 (N=*C*), 158.8 (m-O*C*$_6$H$_2$), 138.8 (m-O*C*$_6$H$_2$), 136.6 (m-O*C*$_6$H$_2$), 130.1 (m-O*C*$_6$H$_5$), 129.7 (m-O*C*$_6$H$_5$), 128.3 (m-O*C*$_6$H$_2$), 122.7 (m-O*C*$_6$H$_2$), 121.4(m-O*C*$_6$H$_2$), 119.3 (m-O*C*$_6$H$_5$), 109.2 (m-O*C*$_6$H$_5$), 61.8-68.3(*C*$_5$H$_4$), 34.5 (*C*(CH$_3$)$_3$), 33.6 (C(*C*H$_3$)$_3$), 31.3 (C(*C*H$_3$)$_3$), 30.5 (C(*C*H$_3$)$_3$). Elemental analysis for $C_{47}H_{62}FeN_2O_3Y$, Calcd: C, 66.90%, H, 6.93%, N, 3.32%; Found: C, 67.22%, H, 7.37%, N, 3.41%.

Isolation of [(salfen)Y(OPh)]$_2$[BAr^F]. [(salfen)Y(OPh)]$_2$ (20 mg, 0.025 mmol) and ^{Ac}FcBAr^F (13.2 mg, 0.012 mmol) were each dissolved in 1,2-difluorobenzene. ^{Ac}FcBAr^F was added to [(salfen)Y(OPh)]$_2$ dropwise. The mixture was stirred at room temperature for 0.5 h and solvent was then removed under reduced pressure. The resulting dark red oil was washed with 2 mL of cold hexanes for 3 times and then resolved in benzene. After removing volatiles, a dark red powder was generated. Yield: 25 mg (83%). ^{1}H NMR (300 MHz, 25°C,

C_6D_6), δ (ppm): 8.14 (s, 8H, BAr^F, *o*-Ar*H*), 8.03 (d, 2H, Ar*H*), 7.70 (d, 2H, Ar*H*), 7.49 (s, 4H, BAr^F, *p*-Ar*H*), 4.03-4.29 (m, 8H, Cp-*H*), 3.61 (s, 9H, $C(CH_3)_3$), 1.69 (s, 9H, $C(CH_3)_3$), 1.34 (br, 9H, $C(CH_3)_3$), 1.24 (s, 9H, $C(CH_3)_3$).

Isolation of $[(salfen)Y(OPh)]_2[BAr^F]_2$. $[(salfen)Y(OPh)]_2$ (15 mg, 0.02 mmol) and $^{Ac}FcBAr^F$ (19.9 mg, 0.01 mmol) were each dissolved in 5 mL diethyl ether. $^{Ac}FcBAr^F$ was added to $[(salfen)Y(OPh)]_2$ dropwise. The mixture was stirred at room temperature for 0.5 h and solvent was then removed under reduced pressure. The resulting dark red oil was washed with 2 mL of cold hexanes for 3 times and then resolved in benzene. After removing volatiles, a dark red powder was generated. Yield: 28 mg (92%). ^1H NMR (300 MHz, 25°C, C_6D_6), δ (ppm): 8.41 (s, 8H, BAr^F, *o*-Ar*H*), 8.09 (d, 2H, Ar*H*), 7.71 (d, 2H, Ar*H*), 7.56 (s, 4H, BAr^F, *p*-Ar*H*), 4.09-4.25 (m, 8H, Ar*H*), 3.63 (br, 9H, $C(CH_3)_3$), 1.69 (s, 9H, $C(CH_3)_3$), 1.25 (s, 9H, $C(CH_3)_3$), 0.03 (s, 24H, Cp-*H*), -0.95 (s, 4H, Cp-*H*).

Homopolymerizations with $[(salfen)Y(OPh)]_2$. Under an inert atmosphere, $[(salfen)Y(OPh)]_2$ (2.5 μmol), C_6D_6 (0.6 mL), and the monomer were added to a J-Young NMR tube. The reaction mixture was shaken occasionally. The tube was sealed and brought out of the glovebox and placed in an oil bath when a higher than ambient temperature was needed. The NMR tube was taken out of the oil bath and the monomer conversion was monitored by ^1H NMR spectroscopy. When the reaction reached the desired conversion, CH_2Cl_2 was added to dissolve the polymer and the resulting solution was poured into 10 mL of cold methanol to precipitate the polymer; the mixture was centrifuged for 5 minutes, and the supernatant was decanted. This process was repeated twice to remove the catalyst and unreacted monomer. The obtained polymer was dried under a reduced pressure before characterization.

Homopolymerizations with *in situ* generated $[(salfen)Y(OPh)]_2^+$ and $[(salfen)Y(OPh)]_2^{2+}$. Under an inert atmosphere, $[(salfen)Y(OPh)]_2$ (2.5 μmol), $^{Ac}FcBAr^F$ solution (0.05/0.1 mL, 50 μM in 1,2-difluorobenzene) and C_6D_6 (0.6 mL) were added to a J-Young NMR tube. The reaction mixture was left at room temperature for 15 minutes while being shaken occasionally. Then, the monomer was added. The tube was sealed and brought out of the glovebox and placed in an oil bath when a higher than ambient temperature was needed. The NMR tube was taken out of the oil bath and the monomer conversion was monitored by ^1H NMR spectroscopy. When the reaction reached the desired conversion, CH_2Cl_2 was added to dissolve the polymer and the resulting solution was poured into 10 mL of cold methanol to precipitate the polymer; the mixture was centrifuged for 5 minutes, and the supernatant was decanted. This process was repeated twice to remove the catalyst and unreacted monomer. The obtained polymer was dried under a reduced pressure before characterization.

General procedure for copolymerization. Under an inert atmosphere, $[(salfen)Y(OPh)]_2$ (2.5 μmol), an internal standard (hexamethylbenzene), C_6D_6 (0.6 mL), and the monomer were added to a J-Young NMR tube. The reaction mixture was left at room temperature for 15 minutes while being shaken occasionally. The tube was sealed and brought out of the glovebox and the monomer conversion was monitored by ^1H NMR spectroscopy. When a desired conversion was reached, the NMR tube was brought back into the glovebox, and $^{Ac}FcBAr^F$ (0.05/0.1 mL, 50 μM in 1,2-difluorobenzene) or $CoCp_2$ (0.05/0.1 mL, 50 μM in 1,2-difluorobenzene) was added. The reaction mixture was shaken occasionally for 15 minutes before the next monomer was added. When the reaction reached the desired conversion, CH_2Cl_2 was added to dissolve the polymer and the resulting solution was

poured into 10 mL of cold methanol to precipitate the polymer; the mixture was centrifuged for 5 minutes, and the supernatant was decanted. This process was repeated twice to remove the catalyst and unreacted monomer. The obtained polymer was dried under a reduced pressure before characterization.

Cyclic voltammetry study of [(salfen)Y(OPh)]$_2$. Cyclic voltammetry was performed in a 100 mM solution of TPABAr^F (TPA = tetra-*n*-propylammonium, BAr^F = tetrakis(3,5-bis(trifluoro-methyl)-phenyl)borate)) in 1,2-difluorobenzene. 1 mM of [(salfen)Y(OPh)]$_2$ was added. The experiment setup used a glassy carbon working electrode, a platinum counter electrode, and an Ag/Ag$^+$ pseudo reference electrode. The working and auxiliary electrodes were polished with an aqueous suspension of 1.00 μm, 0.30 μm, and 0.05 μm alumina successively on a Microcloth polishing pad before each cyclic voltammogram was recorded. Cyclic voltammograms were acquired with a CH Instruments CHI630D potentiostat and recorded with CH Instruments software (version 13.04). Data was processed using Origin 9.2 and all potentials are given with respect to the ferrocene-ferrocenium couple.

2.5. Appendix

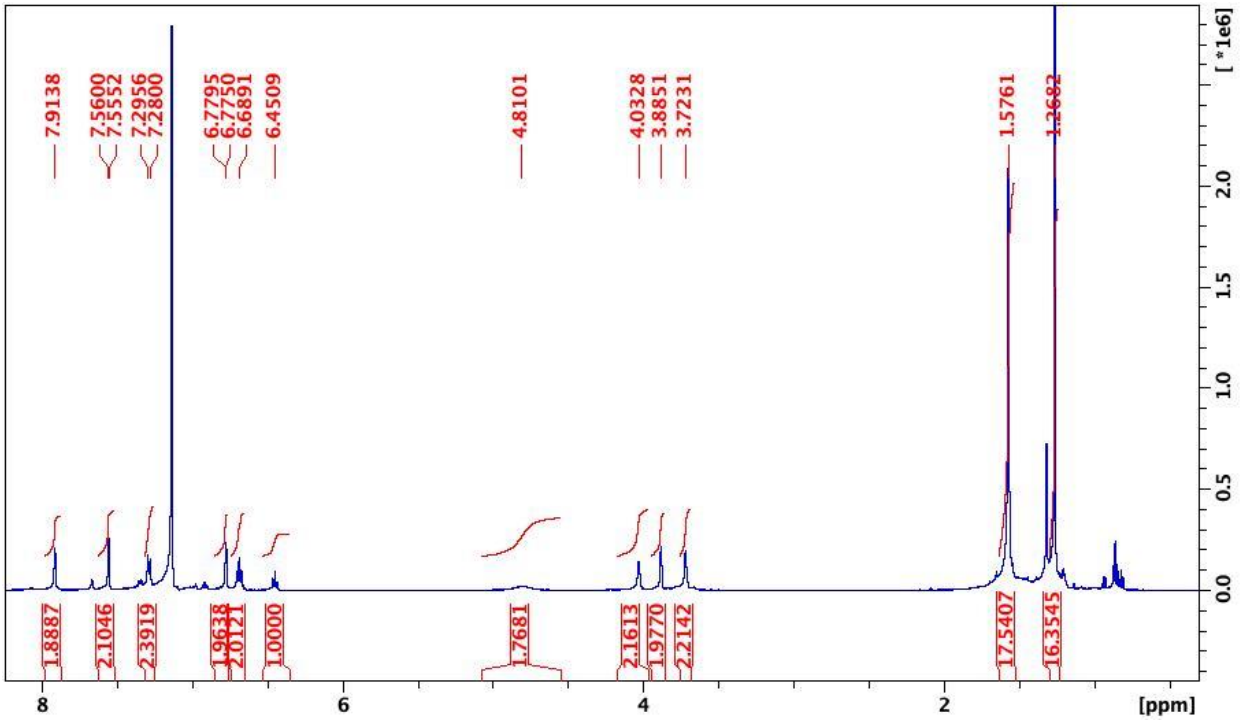

Figure A1. ^{1}H NMR (C_6D_6, 500 MHz, 298 K) spectrum of [(salfen)Y(OPh)]$_2$ δ (ppm): 7.91 (s, 2H, N=C*H*), 7.56 (d, 2H, Ar*H*), 7.29 (d, 2H, Ar*H*), 6.78 (d, 2H, Ar*H*), 6.69 (t, 2H, Ar*H*), 6.45 (t, 1H, Ar*H*), 4.81 (s, 2H, fc-*H*), 3.72-4.03 (s, s and s, 6H, fc-*H*), 1.58 (s, 18H, C(C*H*$_3$)$_3$), 1.27 (s, 18H, C(C*H*$_3$)$_3$).

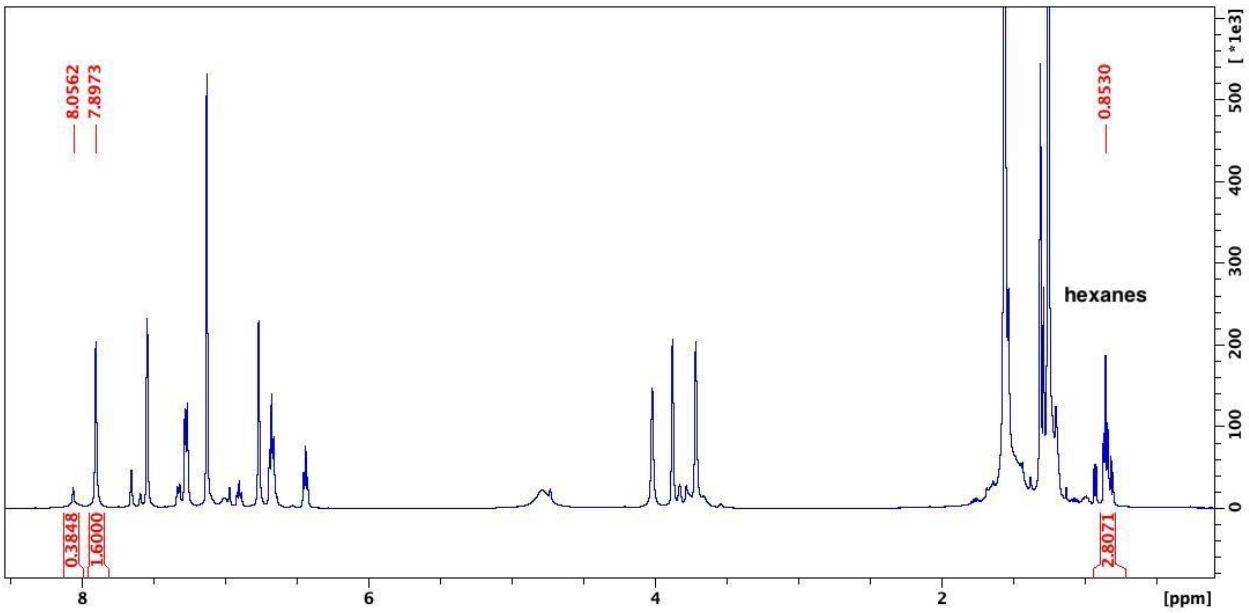

Figure A2. ^{1}H NMR (C_6D_6, 500 MHz, 298 K) spectrum of $[(salfen)Y(OPh)]_2$. The peaks at 8.05 ppm and 8.04 ppm represent 2 H atom together. The peak at 0.85 ppm, which represents hexanes in remaining in the sample, integrates as 2.80. The integration indicates that the formula of the sample is $[(salfen)Y(OPh)]_2 \bullet (C_6H_{14})_{0.2}$.

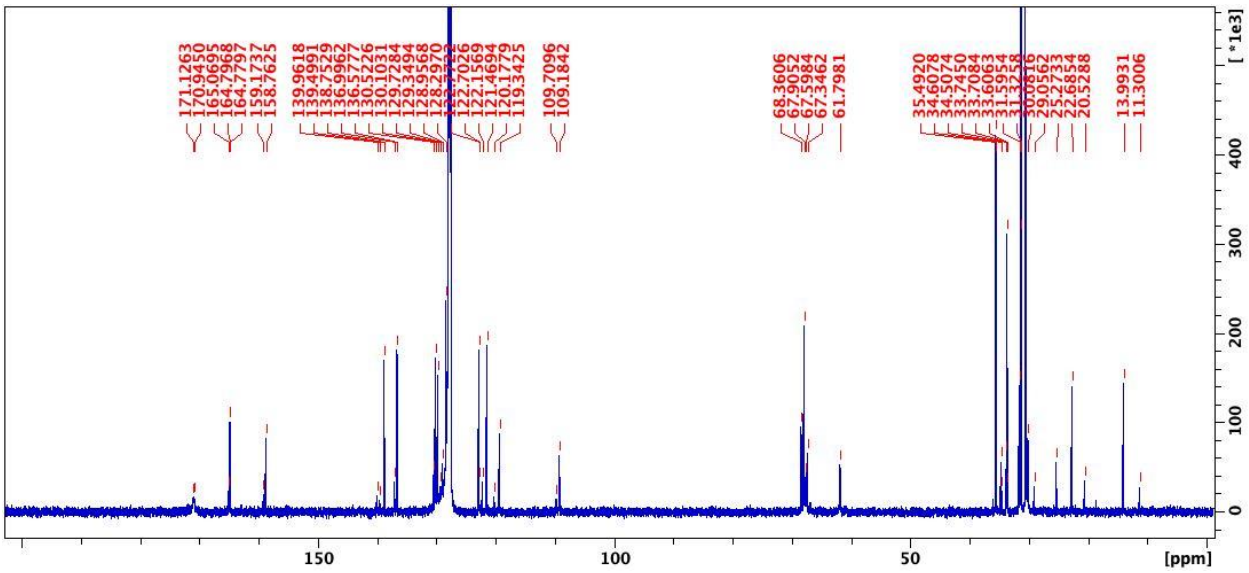

Figure A3. $^{13}C\{^{1}H\}$ NMR (C_6D_6, 125 MHz, 298 K) spectrum of [(salfen)Y(OPh)]$_2$ δ (ppm): 164.8 (N=*C*), 158.8 (m-O*C*$_6$H$_2$), 138.8 (m-O*C*$_6$H$_2$), 136.6 (m-O*C*$_6$H$_2$), 130.1 (m-O*C*$_6$H$_5$), 129.7 (m-O*C*$_6$H$_5$), 128.3 (m-O*C*$_6$H$_2$), 122.7 (m-O*C*$_6$H$_2$), 121.4(m-O*C*$_6$H$_2$), 119.3 (m-O*C*$_6$H$_5$), 109.2 (m-O*C*$_6$H$_5$), 61.8-68.3(*C*$_5$H$_4$), 34.5 (*C*(CH$_3$)$_3$), 33.6 (C(*C*H$_3$)$_3$), 31.3 (C(*C*H$_3$)$_3$), 30.5 (C(*C*H$_3$)$_3$).

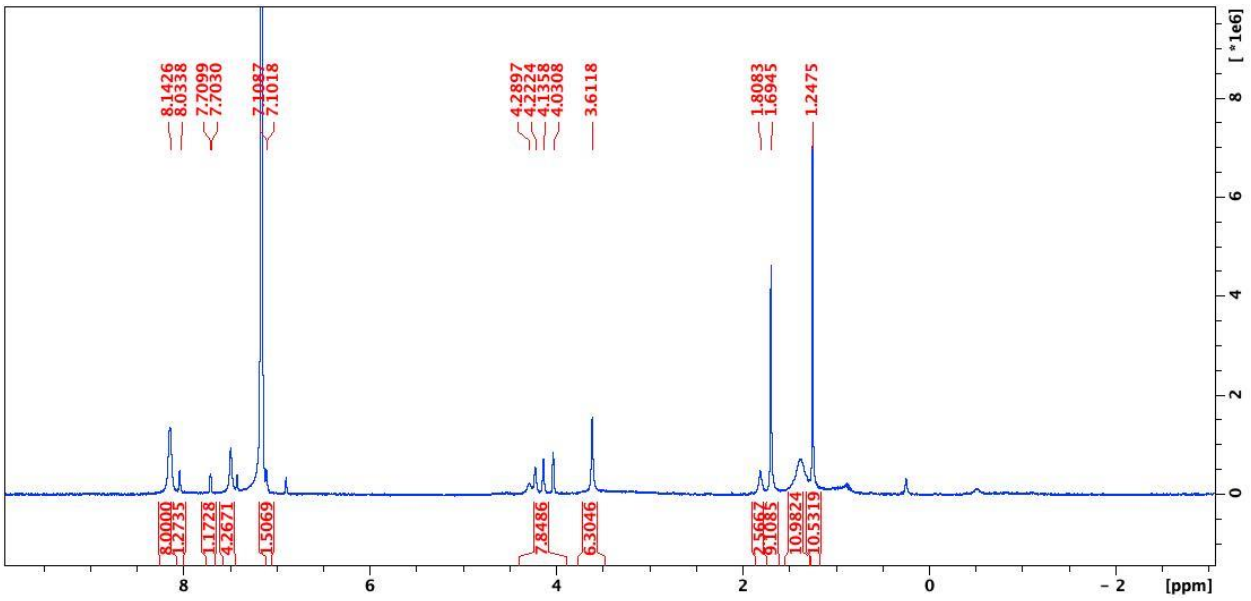

Figure A4. ^{1}H NMR (C_6D_6, 300 MHz, 298 K) spectrum of [(salfen)Y(OPh)]$_2$[BAr^F] δ (ppm): 8.14 (s, 8H, BAr^F, *o*-Ar*H*), 8.03 (d, 2H, Ar*H*), 7.70 (d, 2H, Ar*H*), 7.49 (s, 4H, BAr^F, *p*-Ar*H*), 4.03-4.29 (m, 8H, Cp-*H*), 3.61 (s, 9H, C(C*H*$_3$)$_3$), 1.69 (s, 9H, C(C*H*$_3$)$_3$), 1.34 (br, 9H, C(C*H*$_3$)$_3$), 1.24 (s, 9H, C(C*H*$_3$)$_3$). Other ^{1}H NMR peaks were not observed due to the paramagnetic nature of this compound.

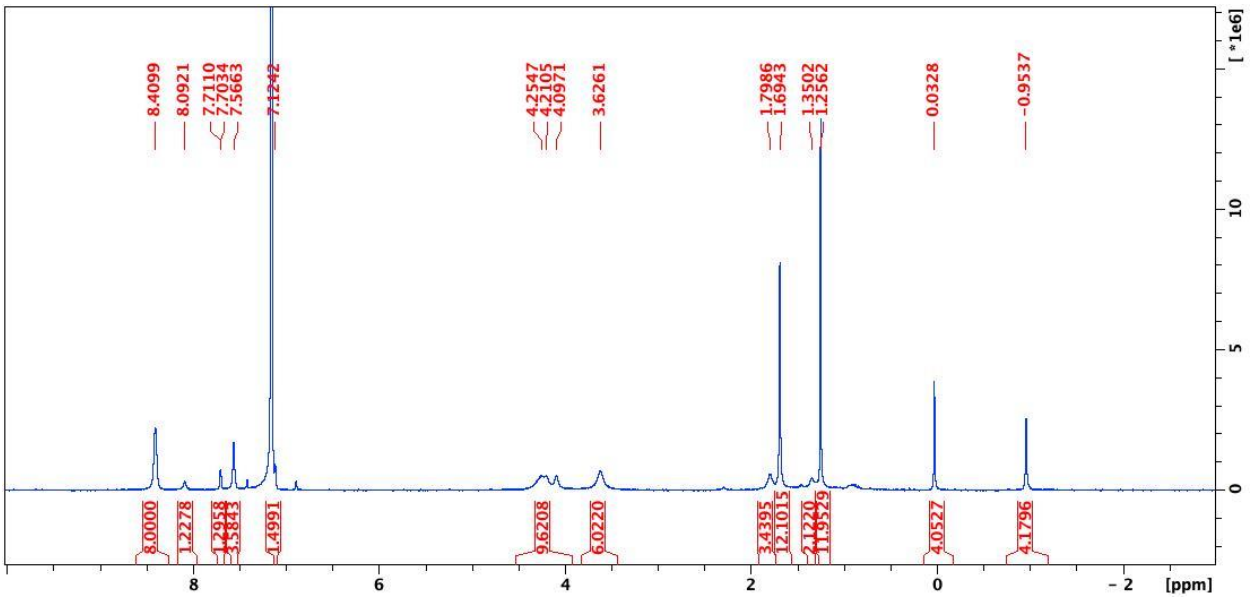

Figure A5. ^{1}H NMR (C_6D_6, 300 MHz, 298 K) spectrum of [(salfen)Y(OPh)]$_2$[BAr^F]$_2$ δ (ppm): 8.41 (s, 8H, BAr^F, *o*-Ar*H*), 8.09 (d, 2H, Ar*H*), 7.71 (d, 2H, Ar*H*), 7.56 (s, 4H, BAr^F, *p*-Ar*H*), 4.09-4.25 (m, 8H, Ar*H*), 3.63 (br, 9H, C(C*H*$_3$)$_3$), 1.69 (s, 9H, C(C*H*$_3$)$_3$), 1.25 (s, 9H, C(C*H*$_3$)$_3$), 0.03 (s, 24H, Cp-*H*), -0.95 (s, 4H, Cp-*H*). Other ^{1}H NMR peaks were not observed due to the paramagnetic nature of this compound.

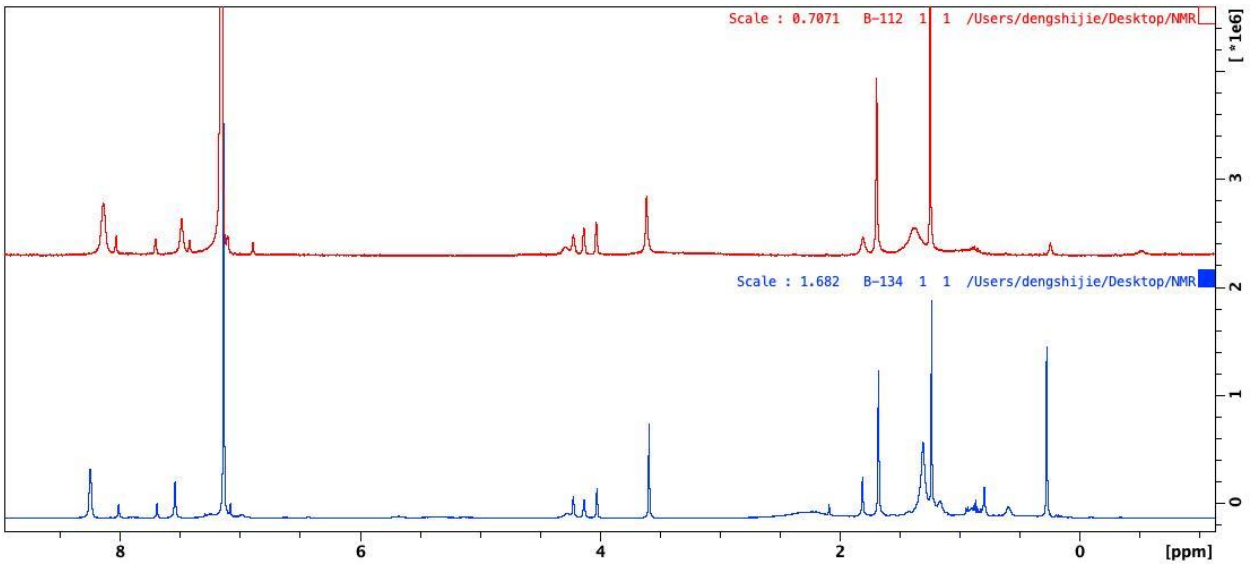

Figure A6. ^{1}H NMR (C_6D_6, 300 MHz, 298 K) spectrum of $[(salfen)Y(OPh)]_2[BAr^F]$ (top) and $[(salfen)Y(OPh)]_2$ +1 equivalent of $[(salfen)Y(OPh)]_2[BAr^F]_2$ (bottom).

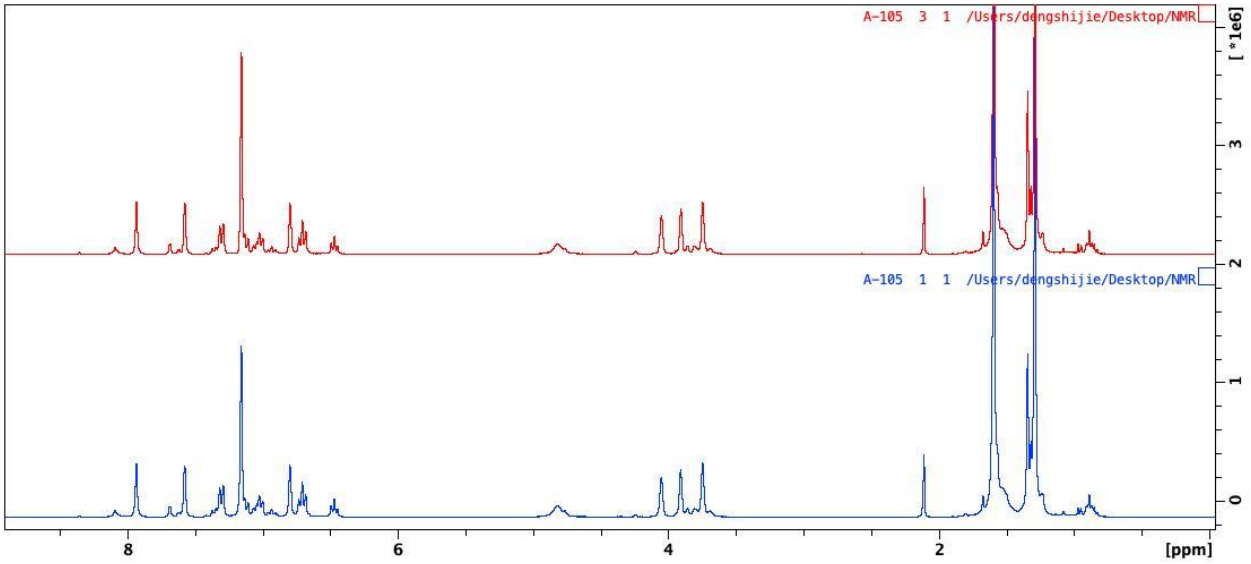

Figure A7. Thermal decomposition study (C_6D_6, 300 MHz, 298 K) of $[(salfen)Y(OPh)]_2$. $[(salfen)Y(OPh)]_2$ before heating (bottom) and after heating at 80°C for 24 h (top).

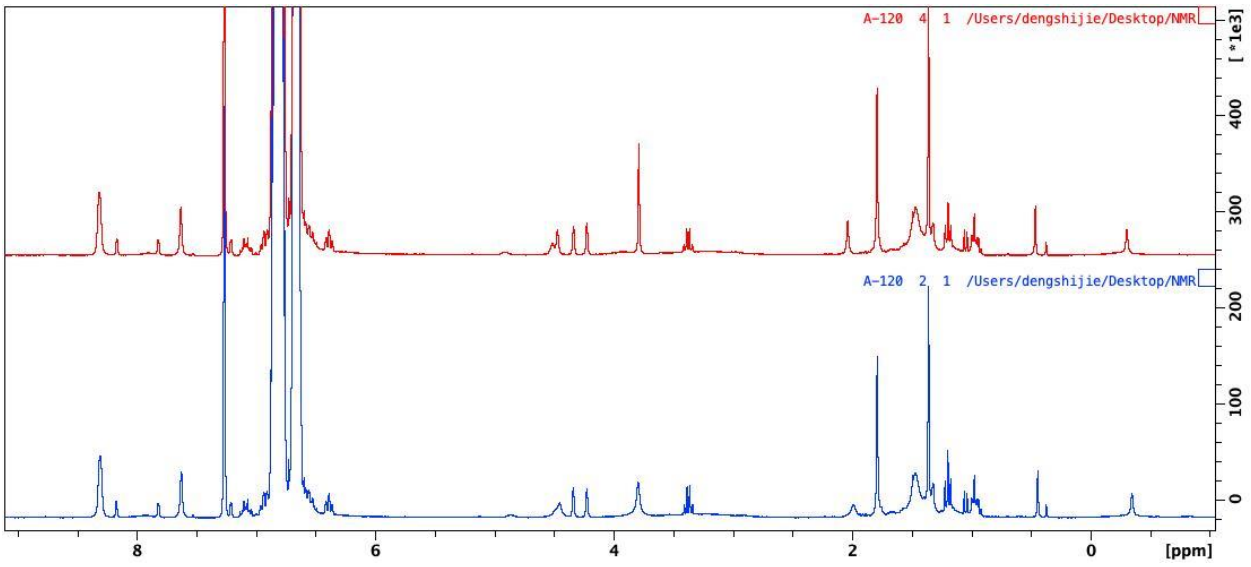

Figure A8. Thermal decomposition study (C_6D_6, 300 MHz, 298 K) of $[(salfen)Y(OPh)]_2[BAr^F]$. $[(salfen)Y(OPh)]_2[BAr^F]$ generated *in situ* before heating (bottom) and after heating at 80°C for 24 h (top).

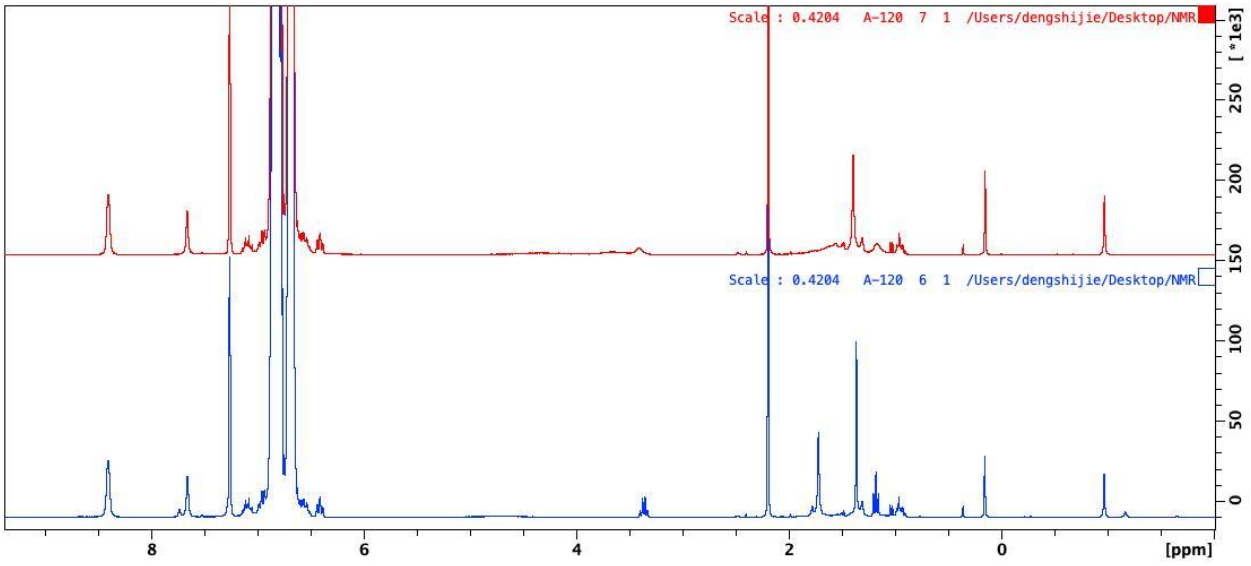

Figure A9. Thermal decomposition study (C_6D_6, 300 MHz, 298 K) of $[(salfen)Y(OPh)]_2[BAr^F]_2$. $[(salfen)Y(OPh)]_2[BAr^F]_2$ generated *in situ* before heating (bottom) and after heating at 80°C for 24 h (top).

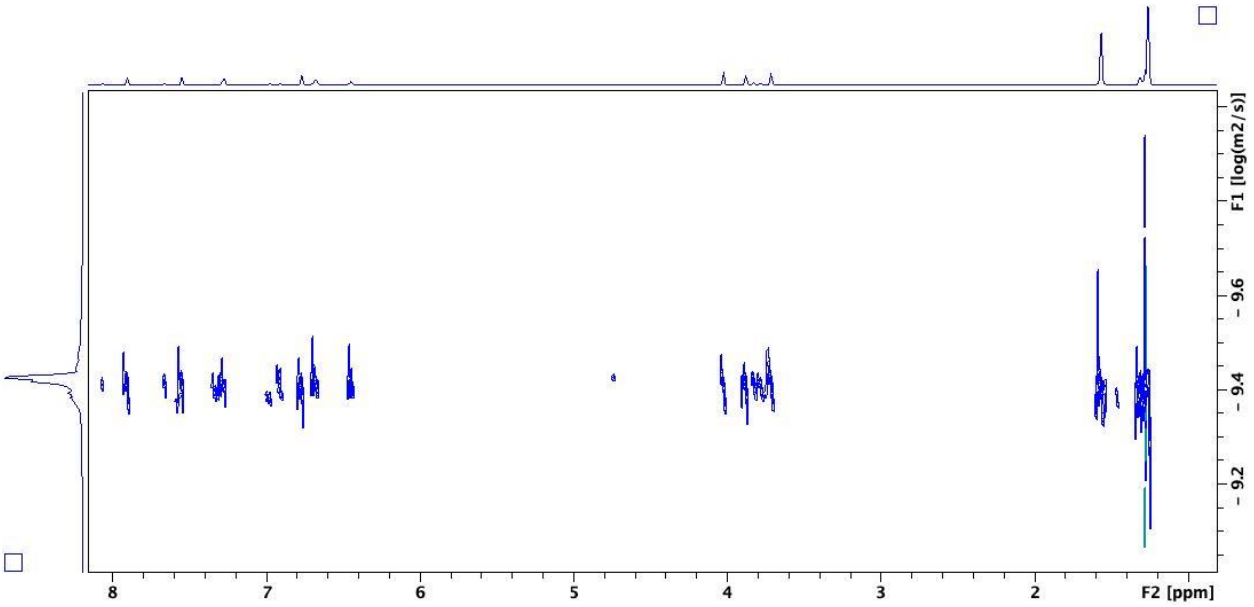

Figure A10. DOSY (C_6D_6, 500 MHz, 298 K) of $[(salfen)Y(OPh)]_2$.

Radius in benzene r_H: Stoke-Einstein equation $D = (kT)/(6\pi\eta r_H)$ was used to calculated hydrodynamic radius in solution, D was obtained from DOSY NMR spectrum.

Radius in solid state $r_{X\text{-}ray}$: The molecular volume was obtained from Olex2.[66] The molecule was assumed to be a sphere and the solid-state radius was calculated using the sphere volume equation.

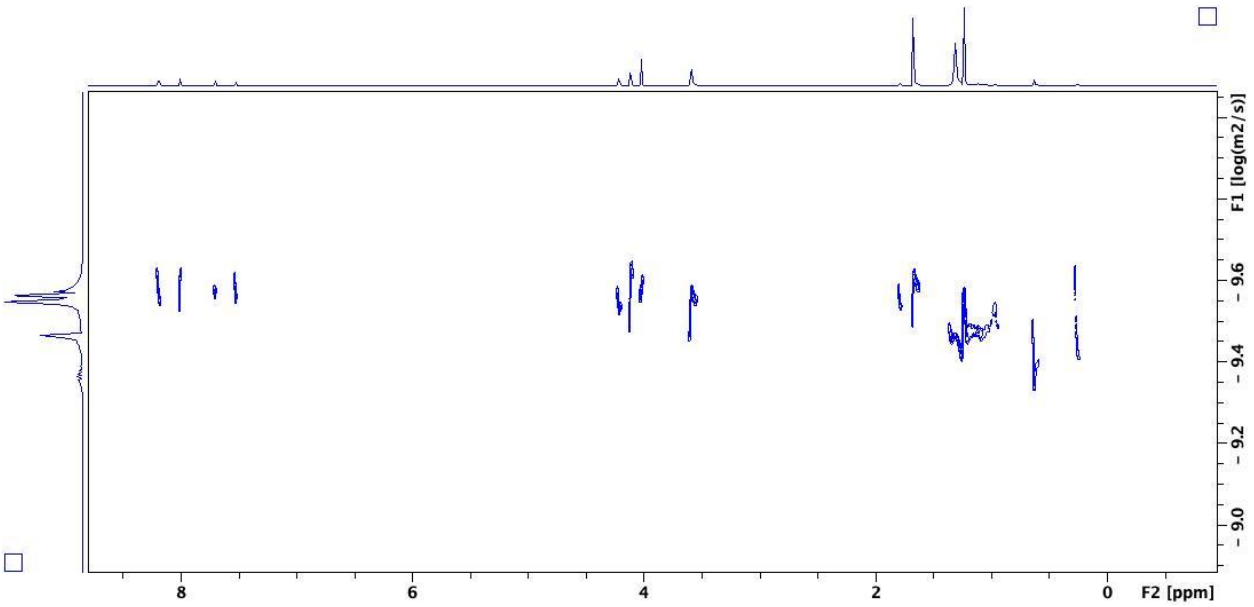

Figure A11. DOSY (C_6D_6, 500 MHz, 298 K) of $[(salfen)Y(OPh)]_2[BAr^F]$.

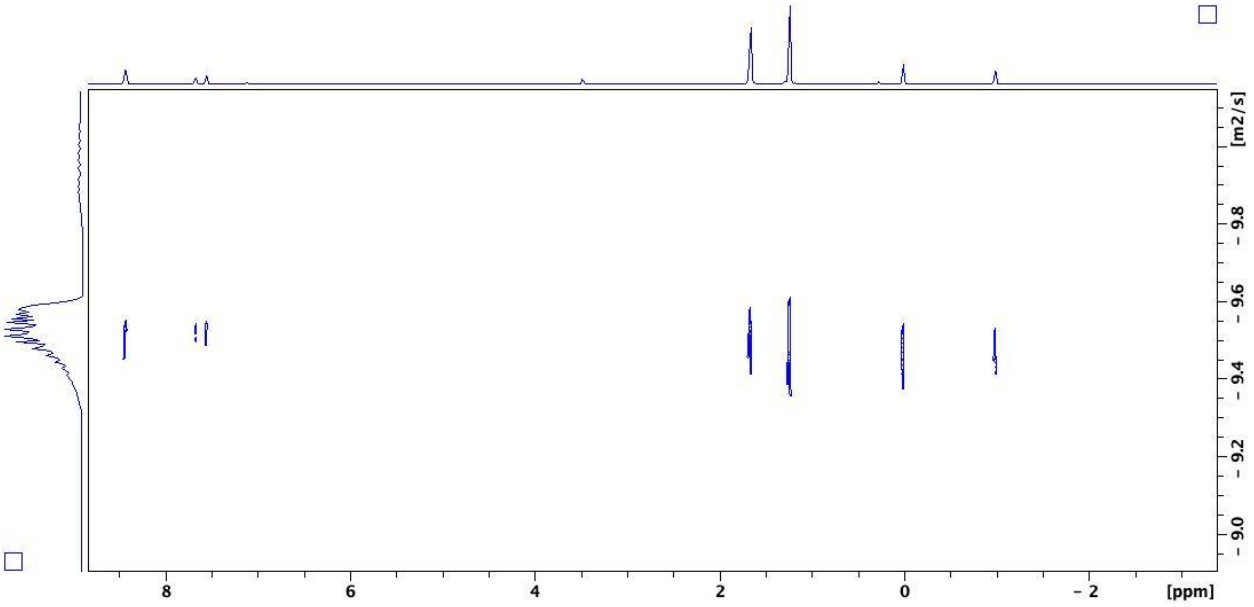

Figure A12. DOSY (C_6D_6, 500 MHz, 298 K) of $[(salfen)Y(OPh)]_2[BAr^F]_2$.

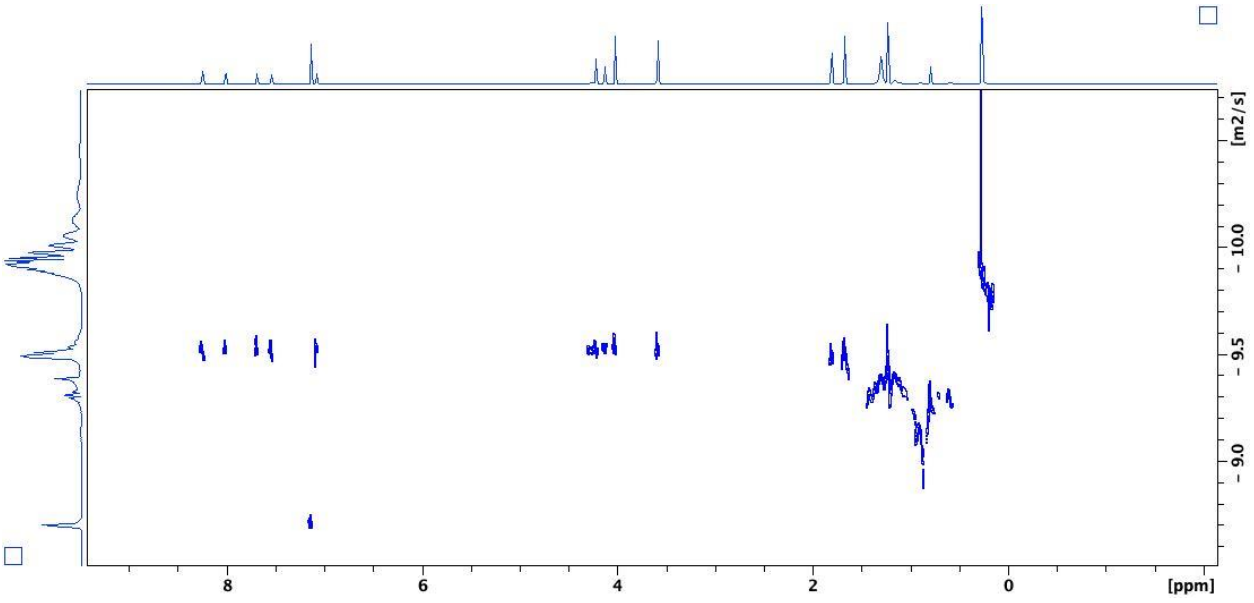

Figure A13. DOSY (C_6D_6, 500 MHz, 298 K) of $[(salfen)Y(OPh)]_2$ + 1 equivalent of $[(salfen)Y(OPh)]_2[BAr^F]_2$.

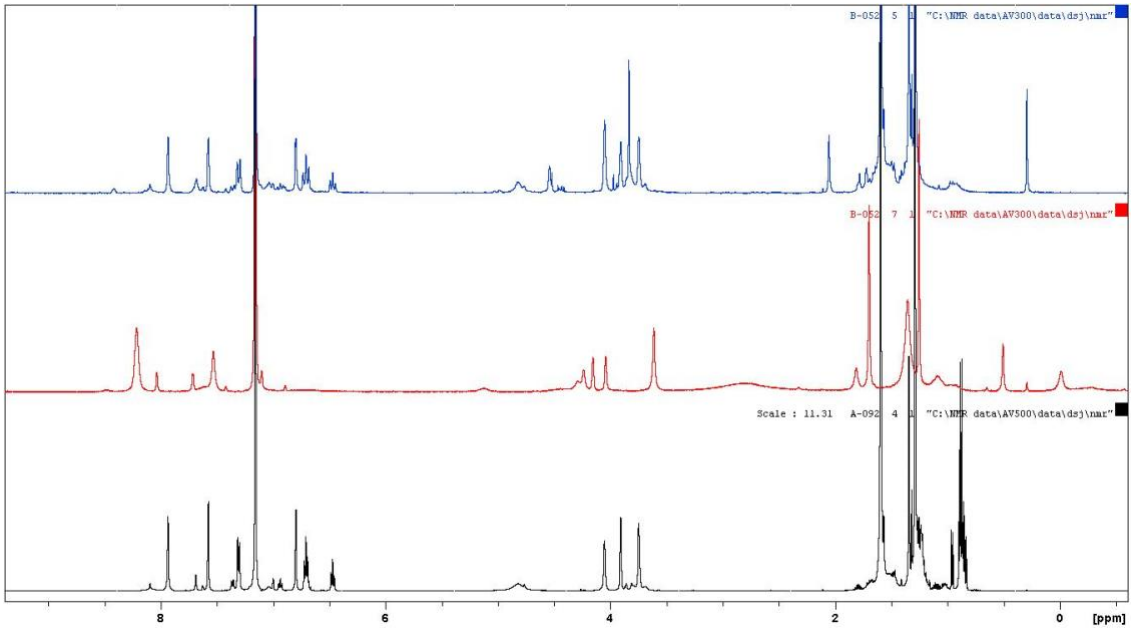

Figure A14. ^1H NMR (C_6D_6, 300 MHz, 298 K) spectrum of $[(salfen)Y(OPh)]_2$ (bottom), $[(salfen)Y(OPh)]_2[BAr^F]$ generated in situ (middle), and $[(salfen)Y(OPh)]_2$ generated from $[(salfen)Y(OPh)]_2[BAr^F]$ (top). All the peaks in the top spectrum match those in the bottom spectrum. The extra peaks in the bottom spectrum belong to ^{Ac}Fc and $CoCp_2[BAr^F]$.

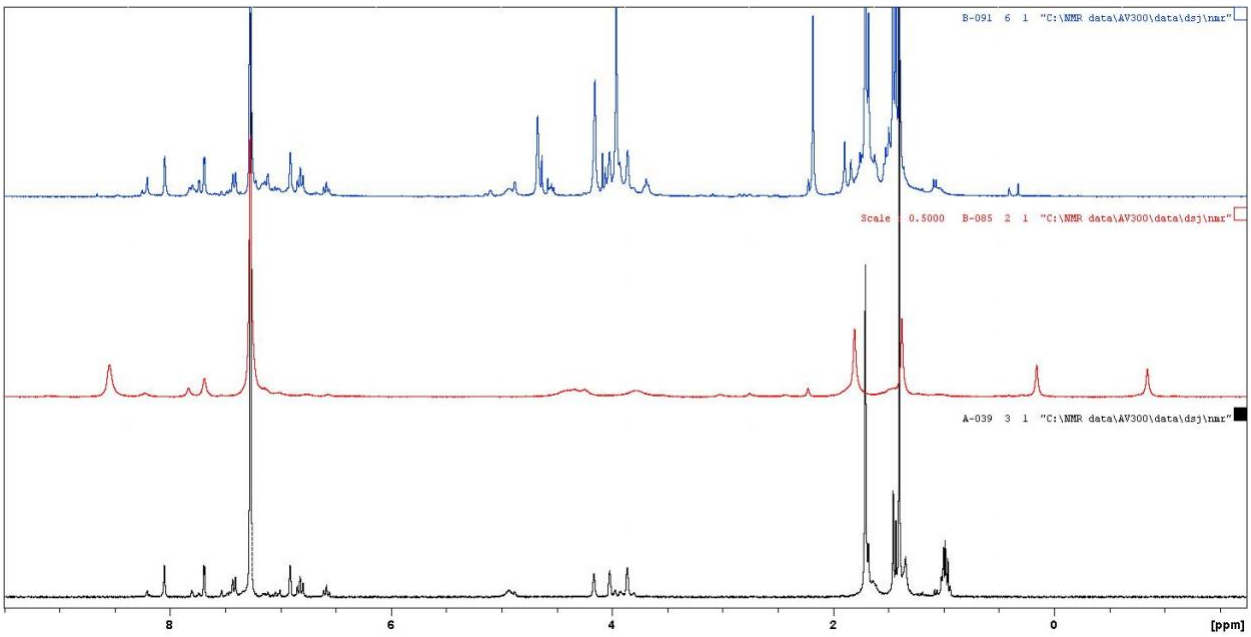

Figure A15. ^{1}H NMR (C_6D_6, 300 MHz, 298 K) spectrum of $[(salfen)Y(OPh)]_2$ (bottom), $[(salfen)Y(OPh)]_2[BAr^F]_2$ generated in situ (middle), and $[(salfen)Y(OPh)]_2$ generated from $[(salfen)Y(OPh)]_2[BAr^F]_2$ (top). All the peaks in the top spectrum match those in the bottom spectrum. The extra peaks in the bottom spectrum belong to AcFc and $CoCp_2[BAr^F]$.

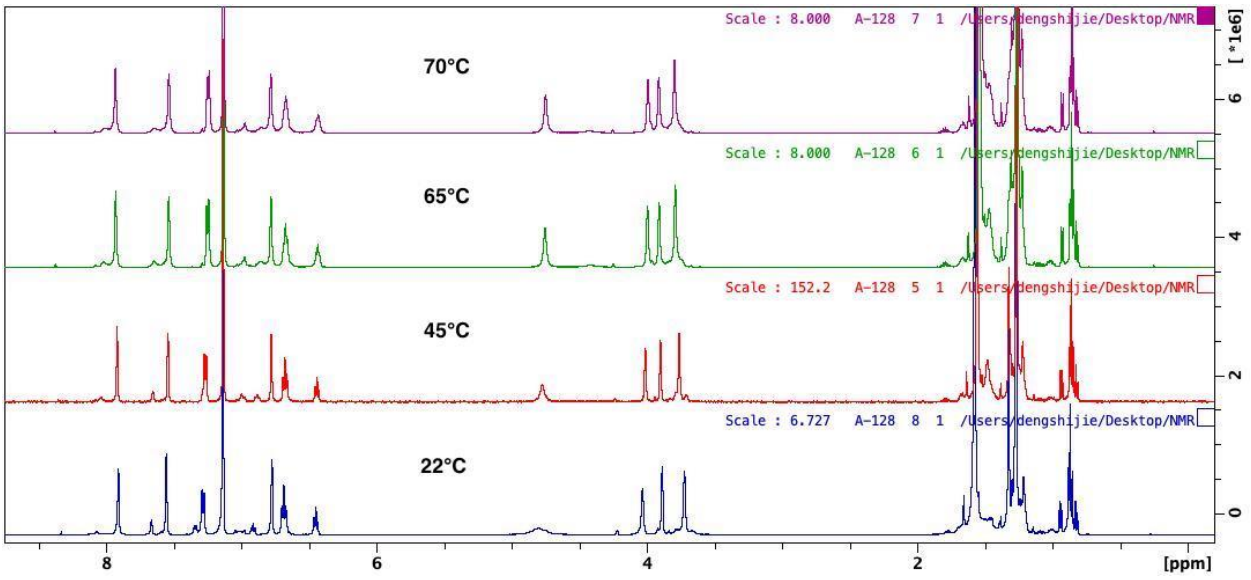

Figure A16. Variable temperature ^{1}H NMR (C_6D_6, 500 MHz) study of $[(salfen)Y(OPh)]_2$.

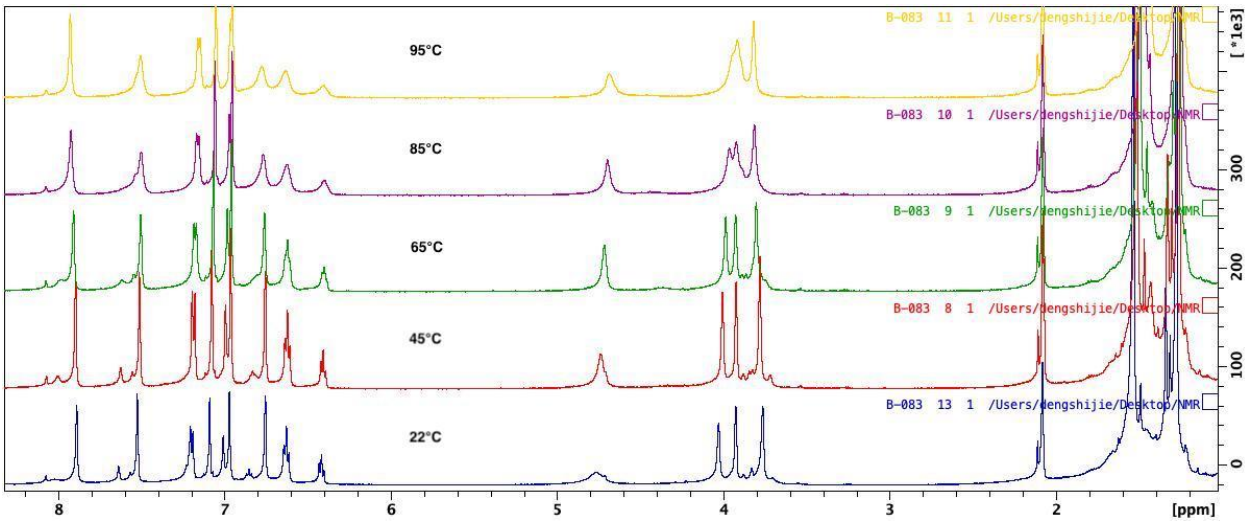

Figure A17. Variable temperature ^{1}H NMR (toluene-d_8, 500 MHz) study of [(salfen)Y(OPh)]$_2$.

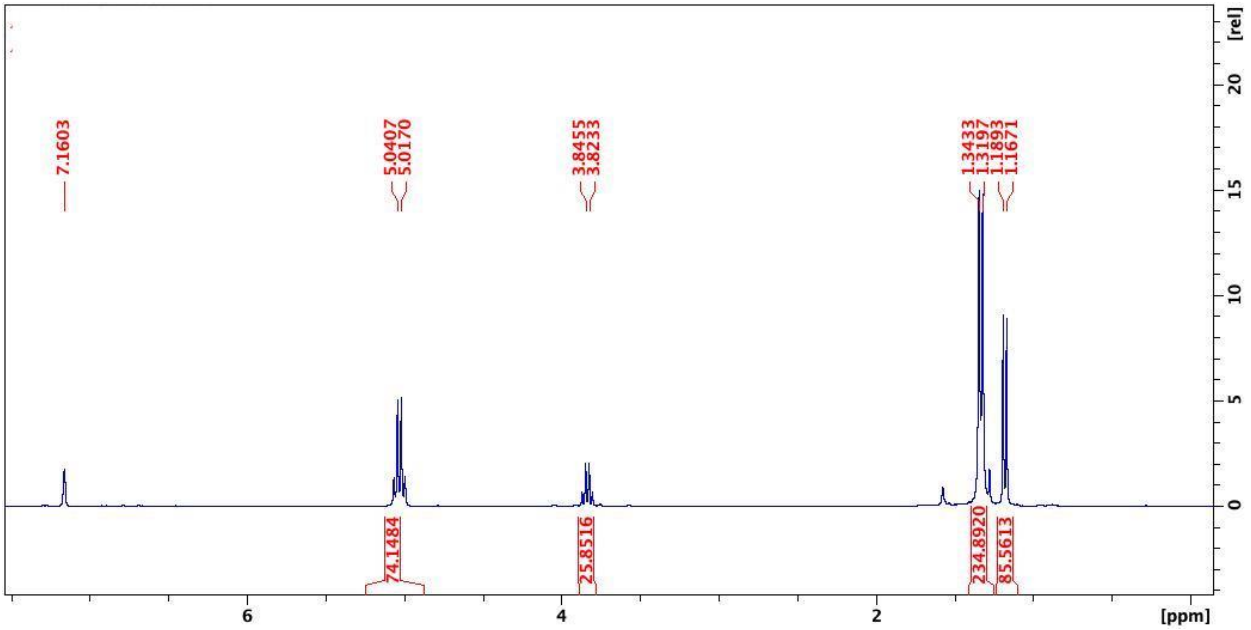

Figure A18. ^{1}H NMR (C_6D_6, 300 MHz, 298 K) spectrum of 200 equivalents of L-lactide polymerization by [(salfen)Y(OPh)]$_2$ (Table 2-1, entry 1). δ (ppm): 5.04 (q, 1H, C*H*(CH$_3$)COO, PLA), 3.83 (t, 1H, C*H*(CH$_3$)COO, LA), 1.34 (d, 3H, CH(C*H*$_3$)COO, PLA), 1.19 (d, 3H, CH(C*H*$_3$)COO, LA).

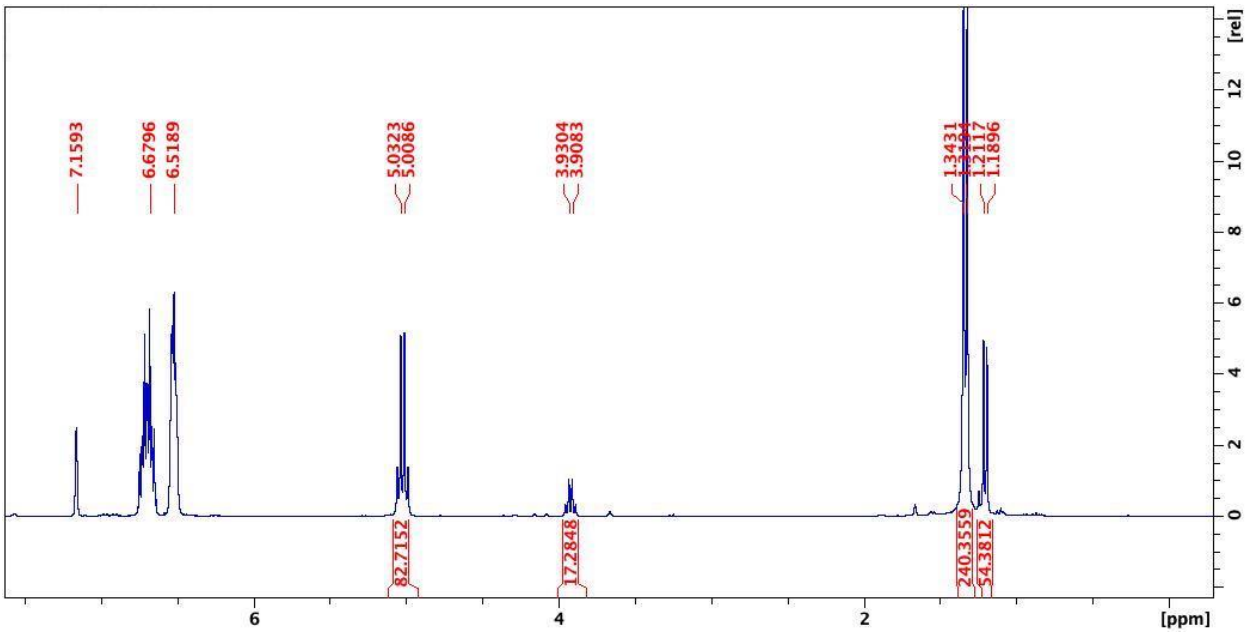

Figure A19. ^{1}H NMR (C_6D_6, 300 MHz, 298 K) spectrum of 200 equivalents of L-lactide polymerization by *in situ* generated $[(salfen)Y(OPh)]_2^+$ (Table 2-1, entry 2). δ (ppm): 5.03 (q, 1H, C*H*(CH_3)COO, PLA), 3.93 (t, 1H, C*H*(CH_3)COO, LA), 1.34 (d, 3H, CH(C*H*$_3$)COO, PLA), 1.21 (d, 3H, CH(C*H*$_3$)COO, LA).

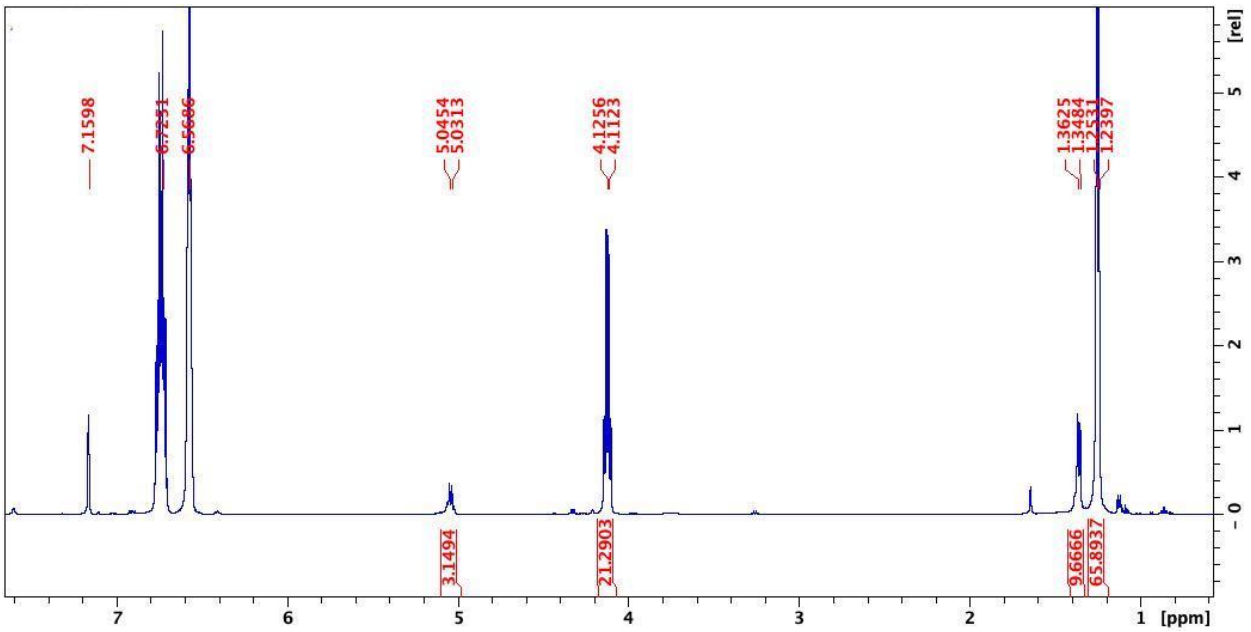

Figure A20. ^{1}H NMR (C_6D_6, 300 MHz, 298 K) spectrum of 200 equivalents of L-lactide polymerization by *in situ* generated $[(salfen)Y(OPh)]_2^{2+}$ (Table 2-1, entry 3). δ (ppm): 5.03 (q, 1H, C*H*(CH_3)COO, PLA), 4.12 (t, 1H, C*H*(CH_3)COO, LA), 1.36 (d, 3H, CH(C*H*$_3$)COO, PLA), 1.24 (d, 3H, CH(C*H*$_3$)COO, LA).

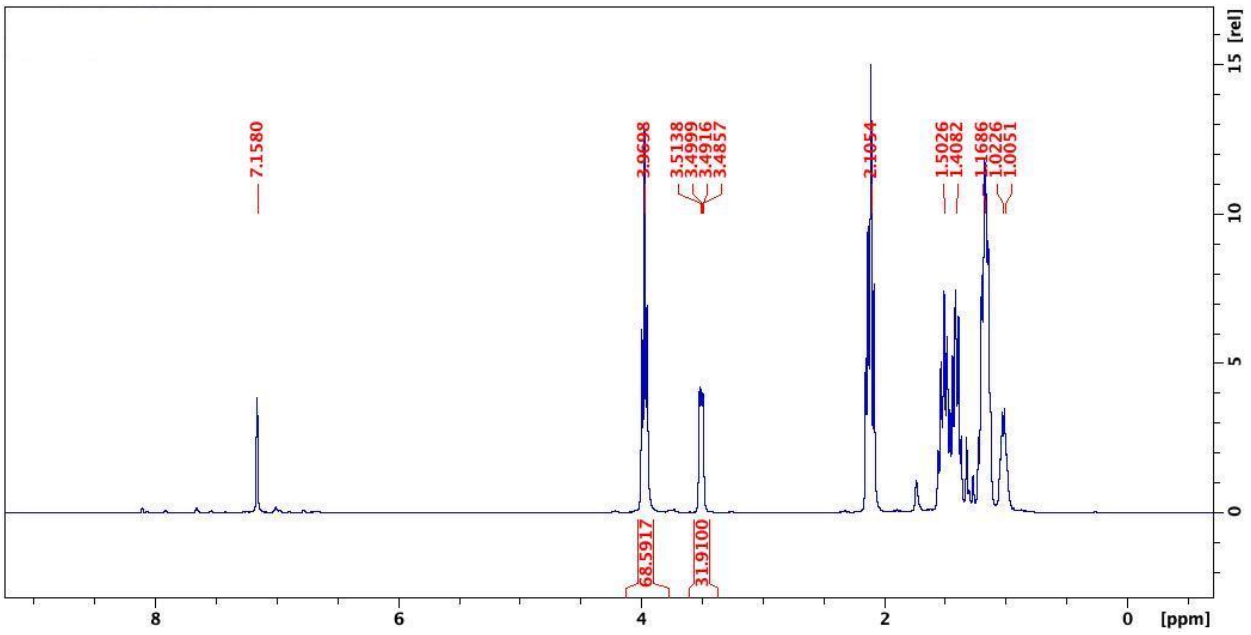

Figure A21. ^{1}H NMR (C_6D_6, 300 MHz, 298 K) spectrum of 200 equivalents of ε-caprolactone polymerization by [(salfen)Y(OPh)]$_2$ (Table 2-1, entry 4). δ (ppm): 3.97 (t, 2H, COOC*H*$_2$, PCL), 3.50 (t, 2H, COOC*H*$_2$, CL), 2.10 (t, 2H, C*H*$_2$COO, PCL). 1.50 (m, 2H, COOCH$_2$C*H*$_2$, PCL) 1.40 (m, 2H, COOCH$_2$CH$_2$C*H*$_2$, PCL), 1.16 (m, 2H, COOCH$_2$CH$_2$CH$_2$C*H*$_2$, PCL), 1.02. (m, 2H, COOCH$_2$CH$_2$CH$_2$C*H*$_2$, CL).

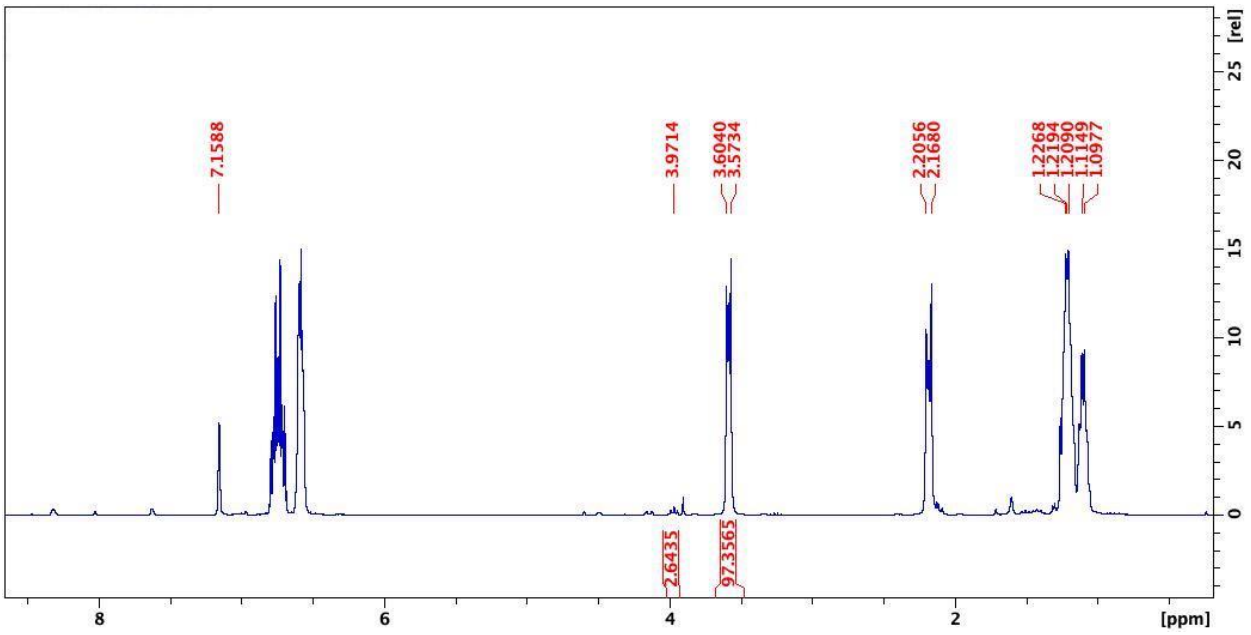

Figure A22. ^{1}H NMR (C_6D_6, 300 MHz, 298 K) spectrum of 200 equivalents of ε-caprolactone polymerization by *in situ* generated $[(salfen)Y(OPh)]_2^+$ (Table 2-1, entry 5). δ (ppm): 3.97 (t, 2H, COOCH_2, PCL), 3.60 (t, 2H, COOCH_2, CL), 2.20 (t, 2H, CH_2COO, PCL). 1.50 (m, 2H, $COOCH_2CH_2$, PCL) 1.40 (m, 2H, $COOCH_2CH_2CH_2$, PCL), 1.16 (m, 2H, $COOCH_2CH_2CH_2CH_2$, PCL), 1.10. (m, 2H, $COOCH_2CH_2CH_2CH_2$, CL).

Figure A23.

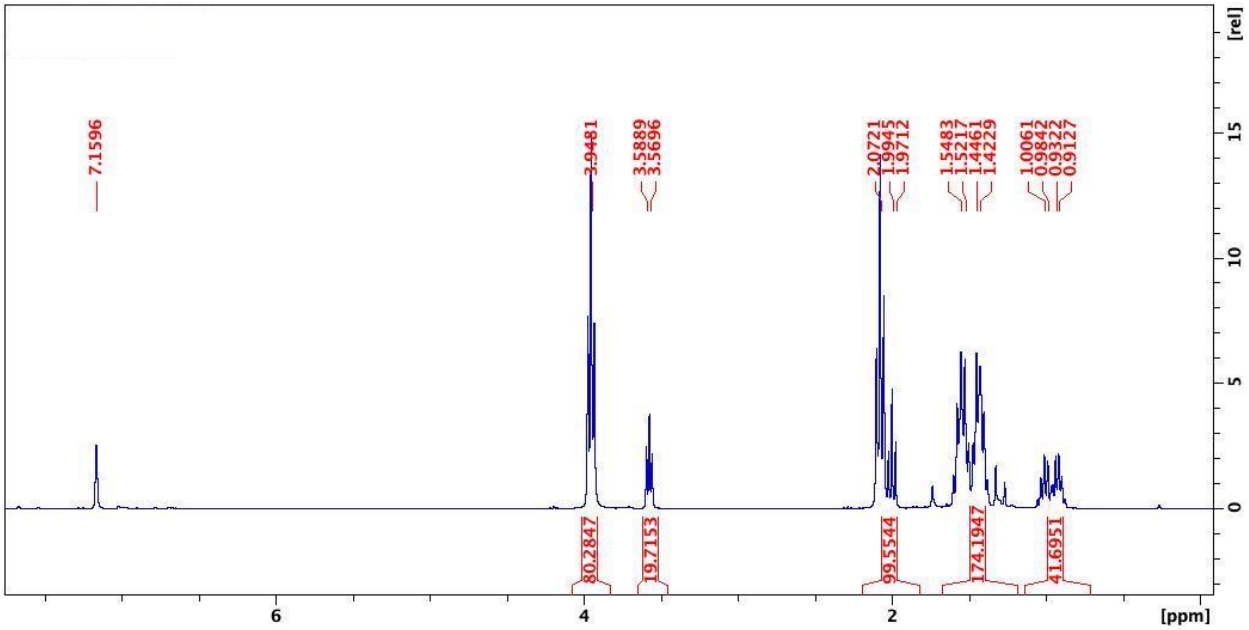

Figure A24. ^{1}H NMR (C_6D_6, 300 MHz, 298 K) spectrum of 200 equivalents of δ-valerolactone polymerization by [(salfen)Y(OPh)]$_2$ (Table 2-1, entry 7). δ (ppm): 3.95 (t, 2H, COOC*H*$_2$, PVL), 3.57 (t, 2H, COOC*H*$_2$, VL), 2.07 (t, 2H, C*H*$_2$COO, PVL), 1.99 (t, 2H, C*H*$_2$COO, VL), 1.54 (m, 4H, C*H*$_2$C*H*$_2$CH$_2$COO, PVL), 0.96 (m, 4H, C*H*$_2$C*H*$_2$CH$_2$COO, VL).

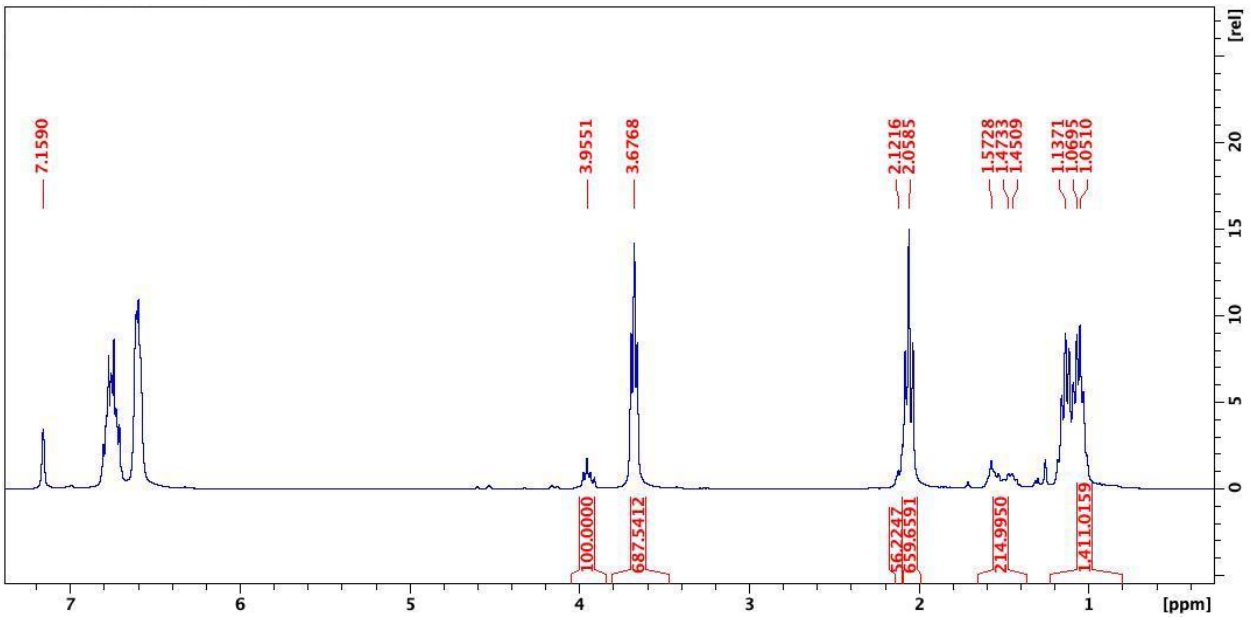

Figure A25. ^{1}H NMR (C_6D_6, 300 MHz, 298 K) spectrum of 200 equivalents of δ-valerolactone polymerization by *in situ* generated $[(salfen)Y(OPh)]_2^+$ (Table 2-1, entry 8). δ (ppm): 3.95 (t, 2H, COOC*H*$_2$, PVL), 3.57 (t, 2H, COOC*H*$_2$, VL), 2.07 (t, 2H, C*H*$_2$COO, PVL), 1.99 (t, 2H, C*H*$_2$COO, VL), 1.54 (m, 4H, C*H*$_2$C*H*$_2$CH$_2$COO, PVL), 0.96 (m, 4H, C*H*$_2$C*H*$_2$CH$_2$COO, VL).

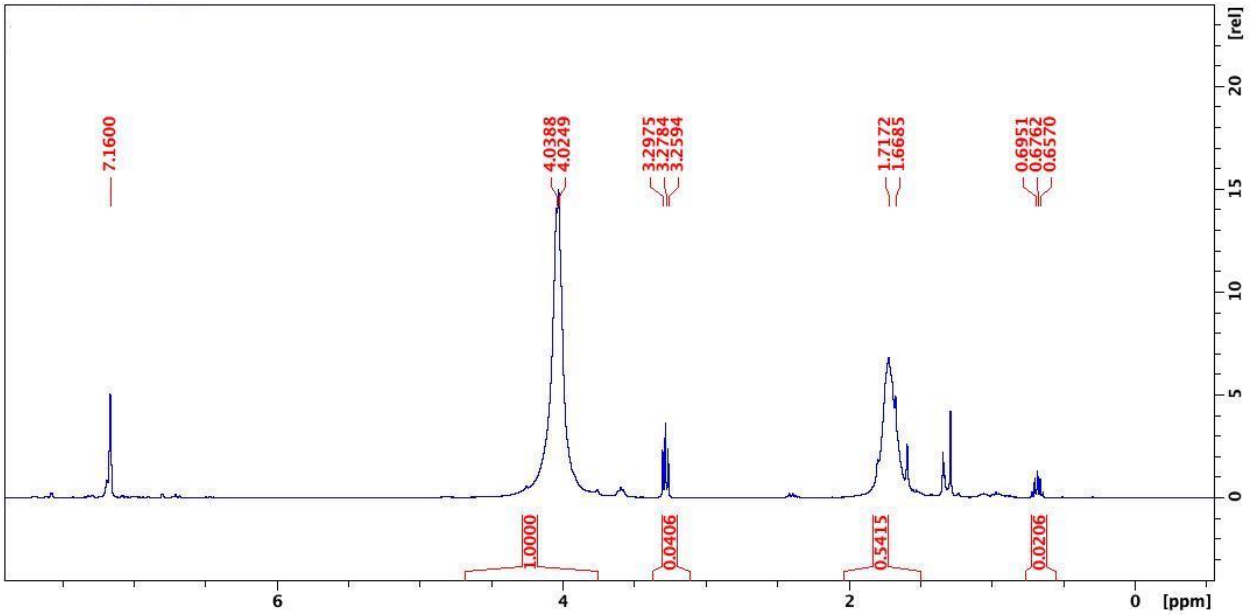

Figure A26. ^{1}H NMR (C_6D_6, 300 MHz, 298 K) spectrum of 200 equivalents of trimethylene carbonate polymerization by $[(salfen)Y(OPh)]_2$ (Table 2-1, entry 10). δ (ppm): 4.03 (s, 4H,

OC*H*$_2$CH$_2$C*H*$_2$O, PTMC), 3.28 (t, 4H, OC*H*$_2$CH$_2$C*H*$_2$O, TMC), 1.71 (br, 2H, OCH$_2$C*H*$_2$CH$_2$O, PTMC), 0.70 (m, 2H, OCH$_2$C*H*$_2$CH$_2$O, TMC).

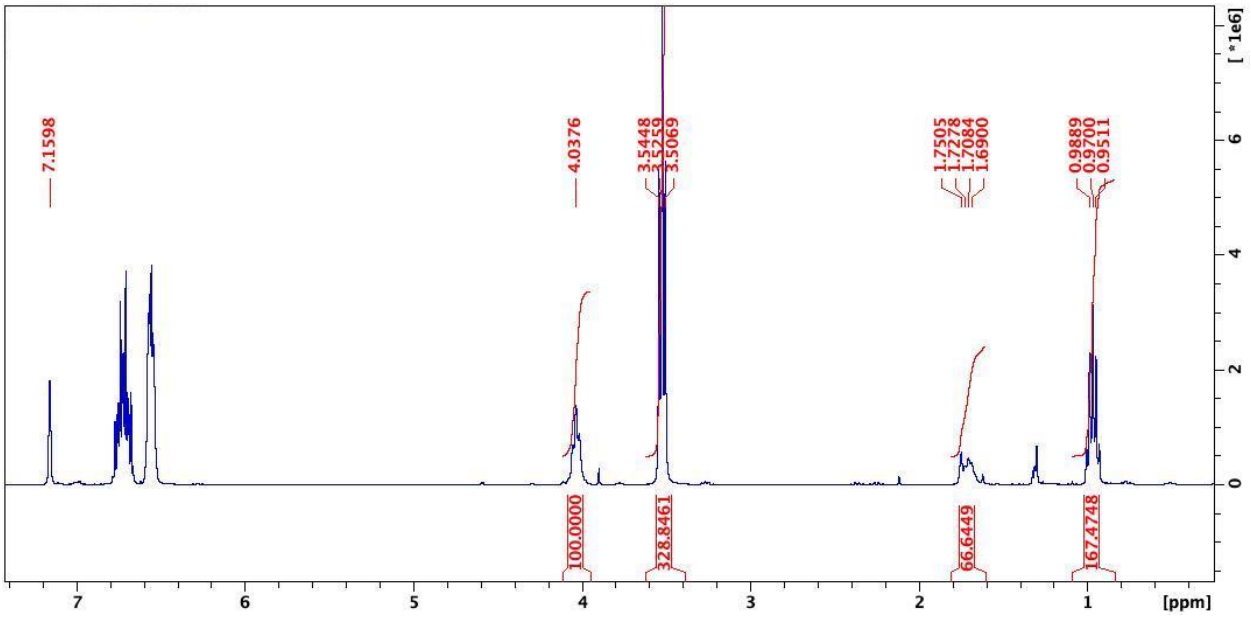

Figure A27. ^{1}H NMR (C_6D_6, 300 MHz, 298 K) spectrum of 200 equivalents of trimethylene carbonate polymerization by *in situ* generated [(salfen)Y(OPh)]$_2^+$ (Table 2-1, entry 11). δ (ppm): 4.04 (s, 4H, OC*H*$_2$CH$_2$C*H*$_2$O, PTMC), 3.53 (t, 4H, OC*H*$_2$CH$_2$C*H*$_2$O, TMC), 1.73 (br, 2H, OCH$_2$C*H*$_2$CH$_2$O, PTMC), 0.97 (m, 2H, OCH$_2$C*H*$_2$CH$_2$O, TMC).

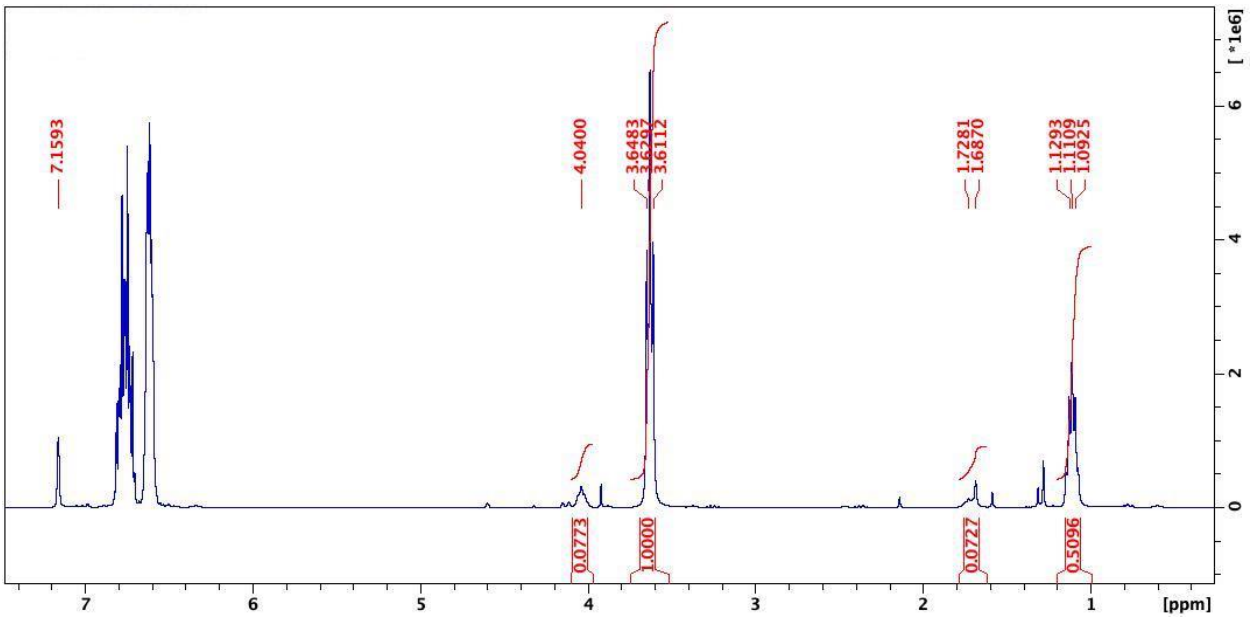

Figure A28. ^{1}H NMR (C_6D_6, 300 MHz, 298 K) spectrum of 200 equivalents of trimethylene carbonate polymerization by *in situ* generated $[(salfen)Y(OPh)]_2^{2+}$ (Table 2-1, entry 12). δ (ppm): 4.04 (s, 4H, OC*H*$_2$CH$_2$C*H*$_2$O, PTMC), 3.63 (t, 4H, OC*H*$_2$CH$_2$C*H*$_2$O, TMC), 1.73 (br, 2H, OCH$_2$C*H*$_2$CH$_2$O, PTMC), 1.11 (m, 2H, OCH$_2$C*H*$_2$CH$_2$O, TMC).

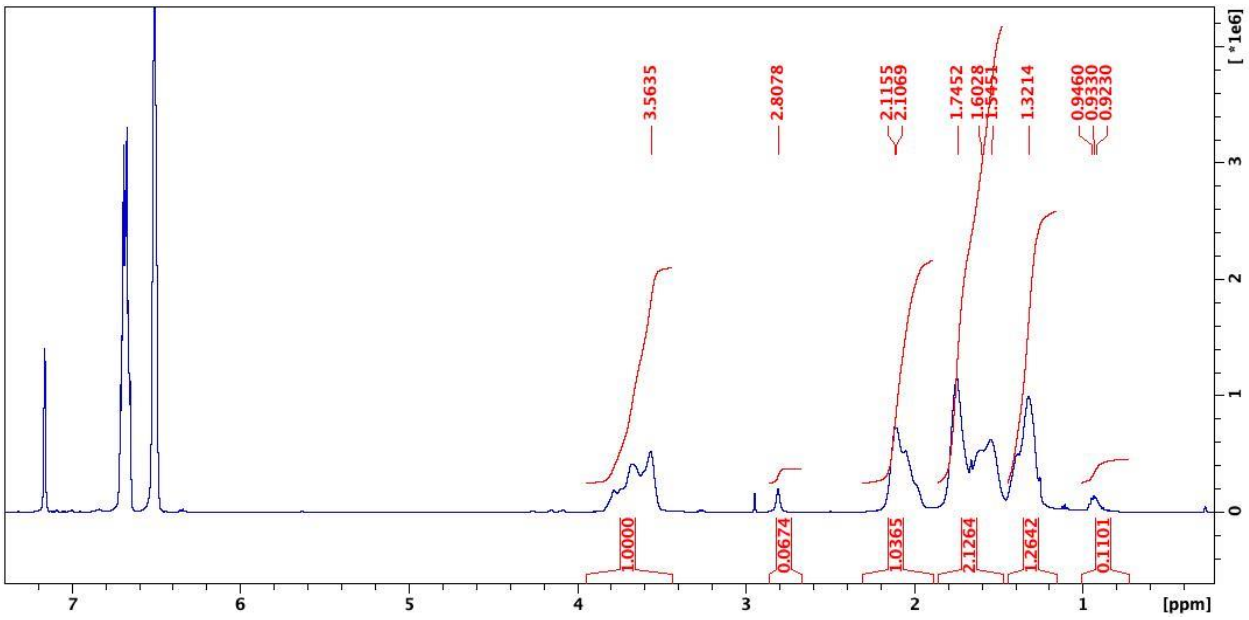

Figure A29. ^{1}H NMR (C_6D_6, 300 MHz, 298 K) spectrum of 200 equivalents of cyclohexene oxide polymerization by *in situ* generated $[(salfen)Y(OPh)]_2^+$ (Table 2-1, entry 14). δ (ppm): 3.56 (br, 2H, CH_2CH_2CH(O), PCHO), 2.80 (br, 2*H*, CH_2CH_2CH(O), CHO), 2.11 (br, 2H, CH_2CH_2CH(O), PCHO), 1.74 (br, 2H, CH_2CH_2CH(O), PCHO), 1.54 (br, 2H, CH_2CH_2CH(O), PCHO), 1.32 (br, 2H, CH_2CH_2CH(O), PCHO), 0.94 (br, 2H, CH_2CH_2CH(O), CHO).

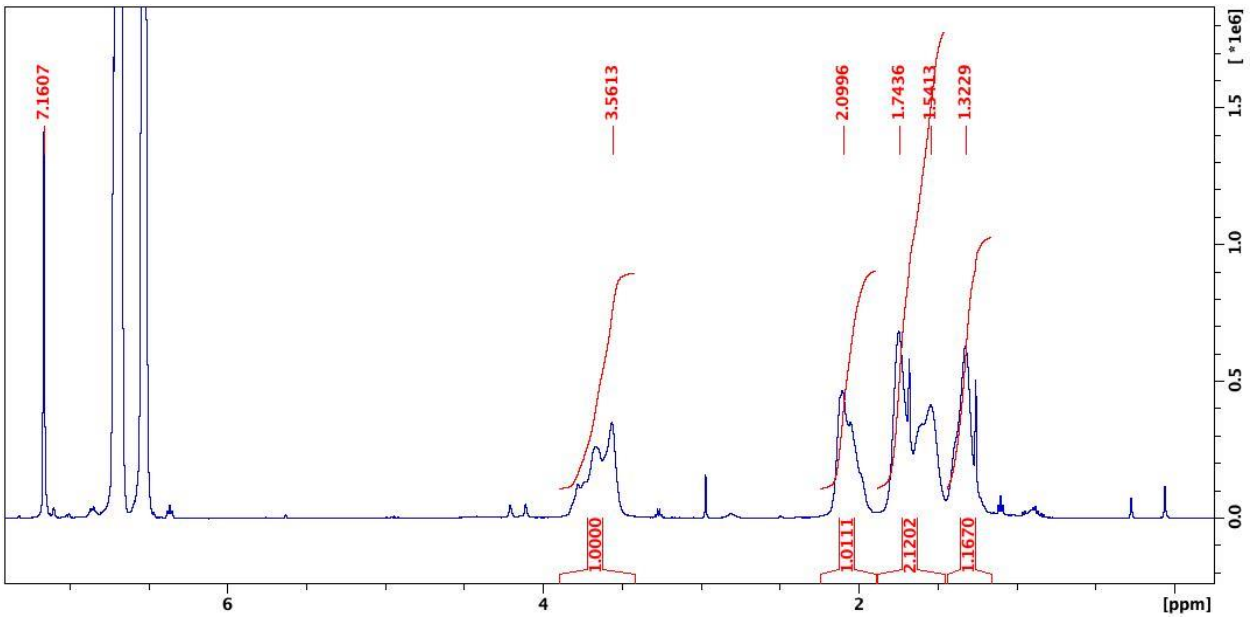

Figure A30. ^{1}H NMR (C_6D_6, 300 MHz, 298 K) spectrum of 200 equivalents of cyclohexene oxide polymerization by *in situ* generated $[(salfen)Y(OPh)]_2^{2+}$ (Table 2-1, entry 15). δ (ppm): 3.56 (br, 2H, CH_2CH_2CH(O), PCHO), 2.10 (br, 2H, CH_2CH_2CH(O), PCHO), 1.74 (br, 2H, $CH_2CH_2CH_2$CH(O), PCHO), 1.54 (br, 2H, CH_2CH_2CH(O), PCHO), 1.32 (br, 2H, CH_2CH_2CH(O), PCHO).

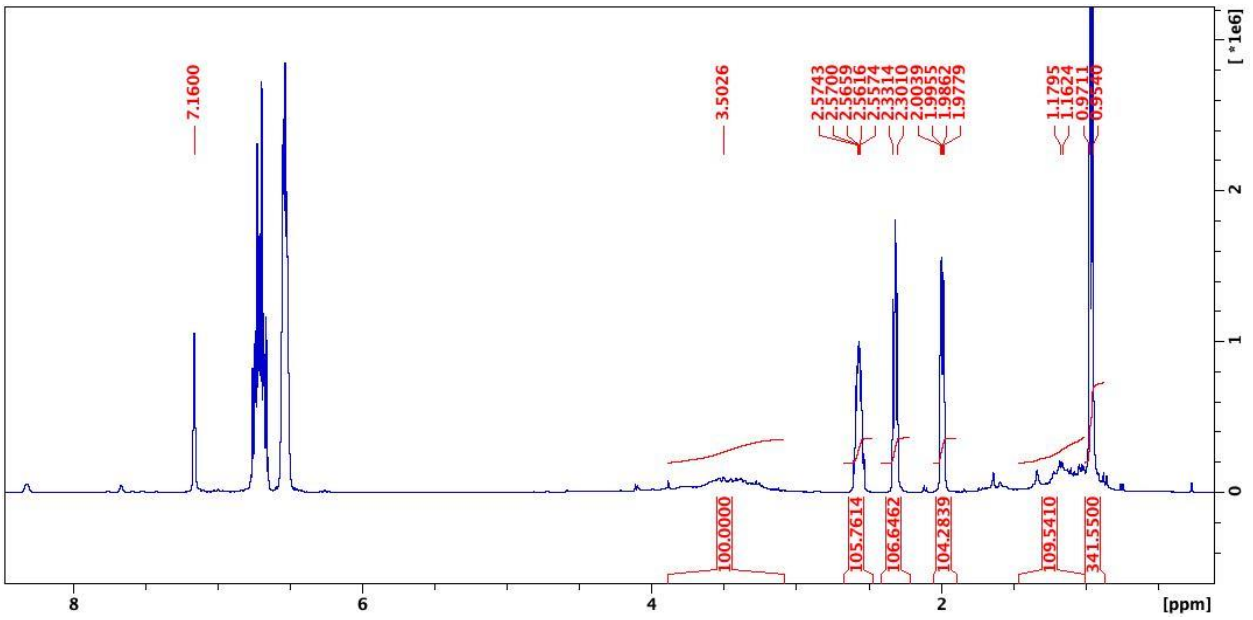

Figure A31. ^{1}H NMR (C_6D_6, 300 MHz, 298 K) spectrum of 200 equivalents of propylene oxide polymerization by *in situ* generated $[(salfen)Y(OPh)]_2^+$ (Table 2-1, entry 17). δ (ppm): 3.50 (br, 3H, OC*H*(CH_3)C*H*$_2$O, PPO), 2.57(m, 1H, OC*H*(CH_3)CH_2O, PO), 2.32(t, 1H, OCH(CH_3)C*H*$_2$O, PO), 2.00(m, 1H, OCH(CH_3)C*H*$_2$O, PO), 1.17 (br, 3H, OCH(C*H*$_3$)CH_2O, PPO), 0.97(d, 3H, OCH(C*H*$_3$)CH_2O, PO).

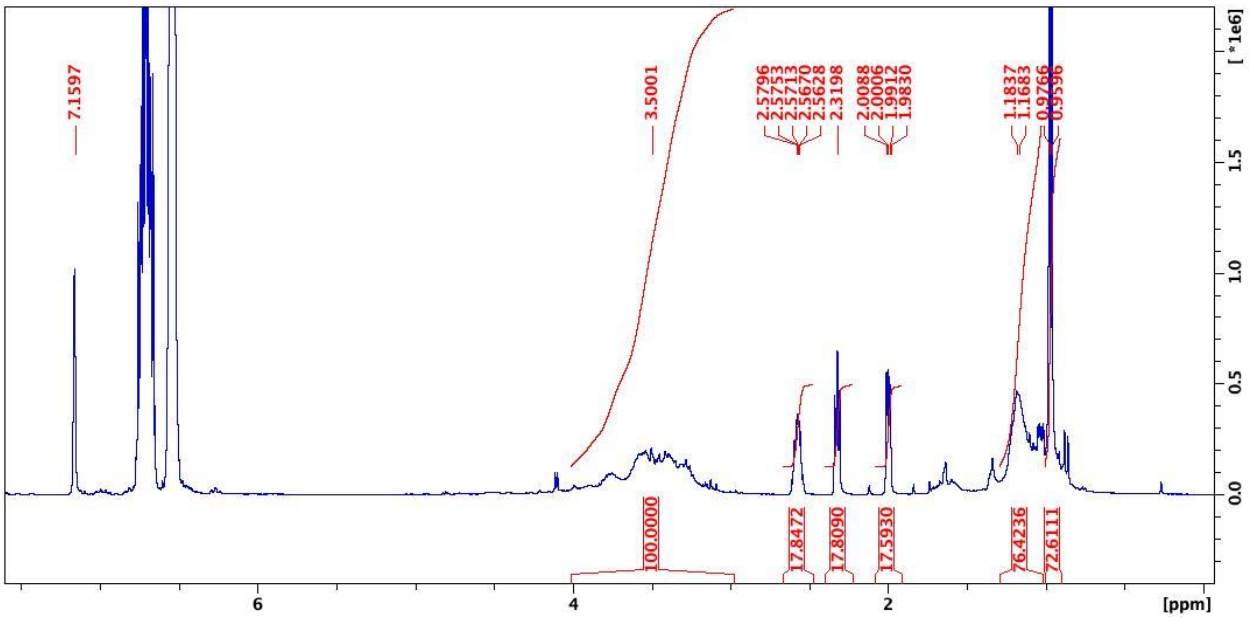

Figure A32. ^{1}H NMR (C_6D_6, 300 MHz, 298 K) spectrum of 200 equivalents of propylene oxide polymerization by *in situ* generated $[(salfen)Y(OPh)]_2^{2+}$ (Table 2-1, entry 18). δ (ppm): 3.50 (br, 3H, OC*H*(CH_3)C*H*$_2$O, PPO), 2.57(m, 1H, OC*H*(CH_3)CH_2O, PO), 2.32(t, 1H, OCH(CH_3)C*H*$_2$O, PO), 2.00(m, 1H, OCH(CH_3)C*H*$_2$O, PO), 1.18 (br, 3H, OCH(C*H*$_3$)CH_2O, PPO), 0.97(d, 3H, OCH(C*H*$_3$)CH_2O, PO).

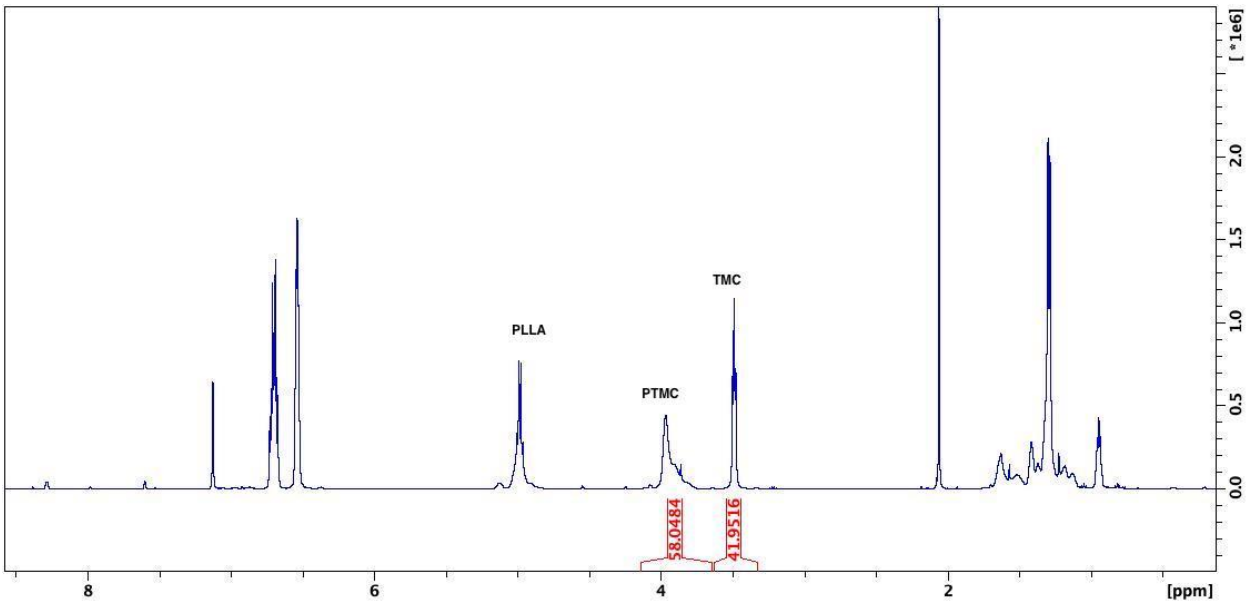

Figure A33. ^{1}H NMR (C_6D_6, 300 MHz, 298 K) spectrum of 200 equivalents of LLA and 200 equivalents of TMC copolymerization (Table 2-2, entry 2).

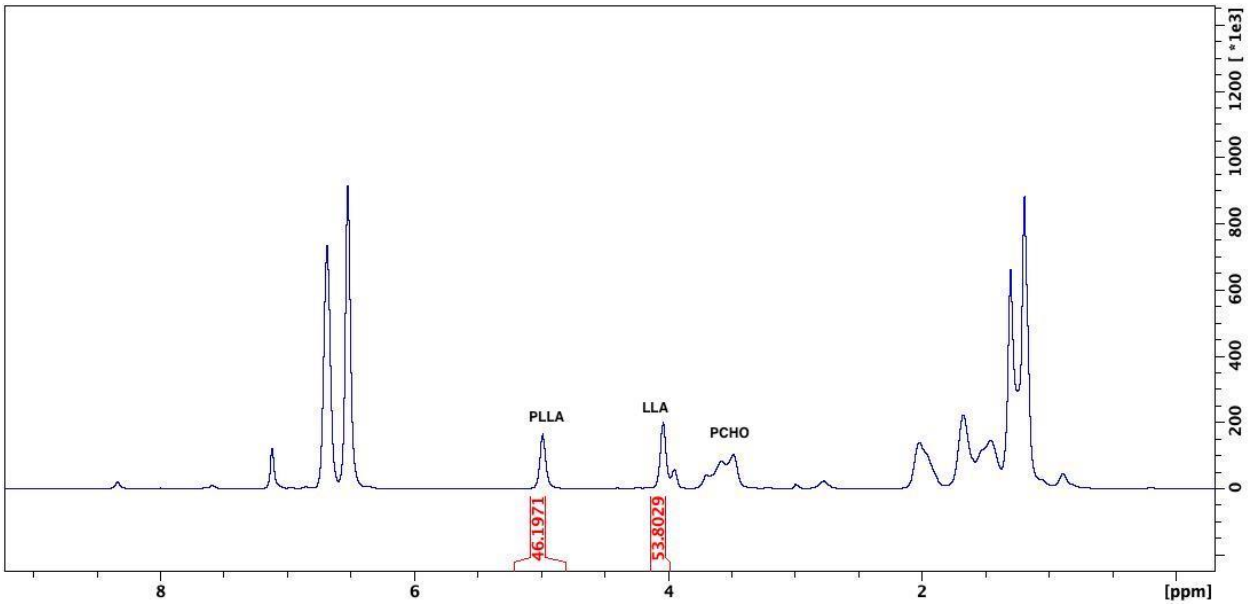

Figure A34. ^{1}H NMR (C_6D_6, 300 MHz, 298 K) spectrum of 200 equivalents of LLA and 200 equivalents of CHO copolymerization (Table 2-2, entry 3).

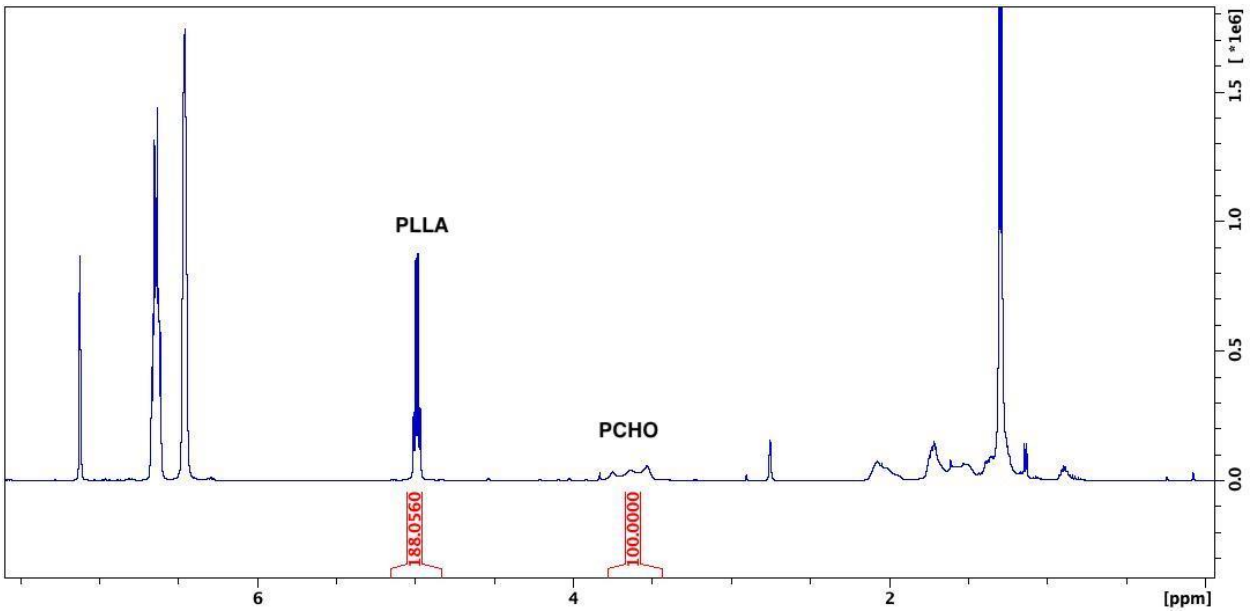

Figure A35. ^{1}H NMR (C_6D_6, 300 MHz, 298 K) spectrum of 200 equivalents of LLA and 200 equivalents of CHO and another 200 equivalents of LLA copolymerization (Table 2-2, entry 4).

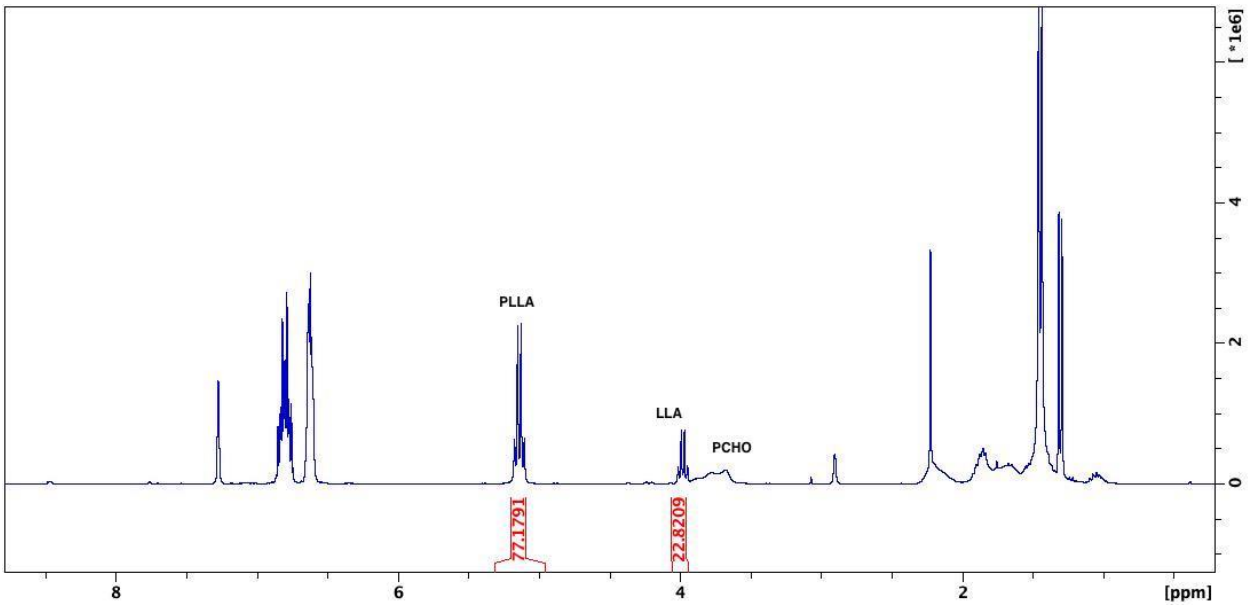

Figure A36. ^{1}H NMR (C_6D_6, 300 MHz, 298 K) spectrum of 200 equivalents of LLA ,200 equivalents of CHO, and another 200 equivalents of LLA copolymerization (Table 2-2, entry 5).

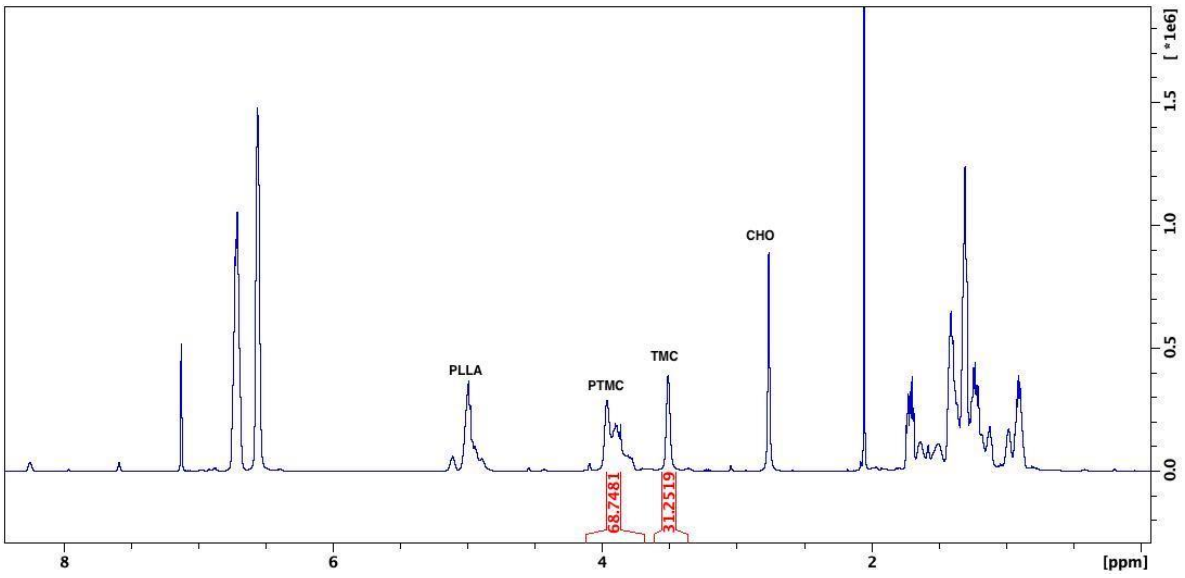

Figure A37. ^{1}H NMR (C_6D_6, 300 MHz, 298 K) spectrum of 200 equivalents of LLA, 200 equivalents of TMC and 200 equivalents of CHO copolymerization (Table 2-2, entry 6).

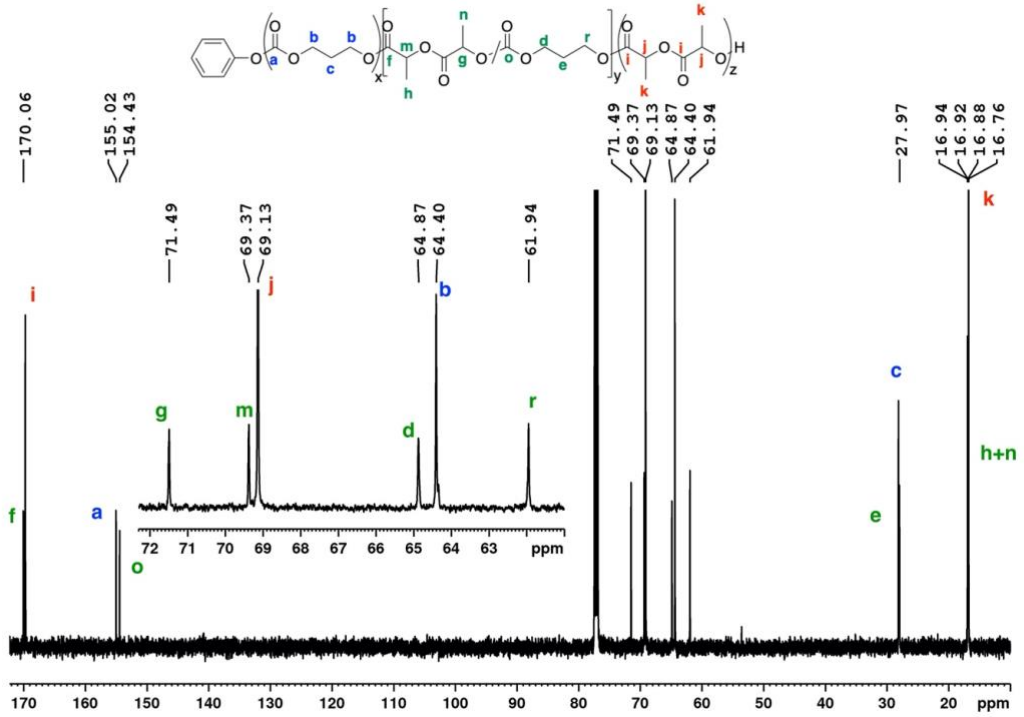

Figure A38. $^{13}C\{^{1}H\}$ NMR ($CDCl_3$, 125 MHz, 298 K) spectrum of 200 equivalents of LLA, 200 equivalents of TMC copolymerization (Table 2-2, entry 1).

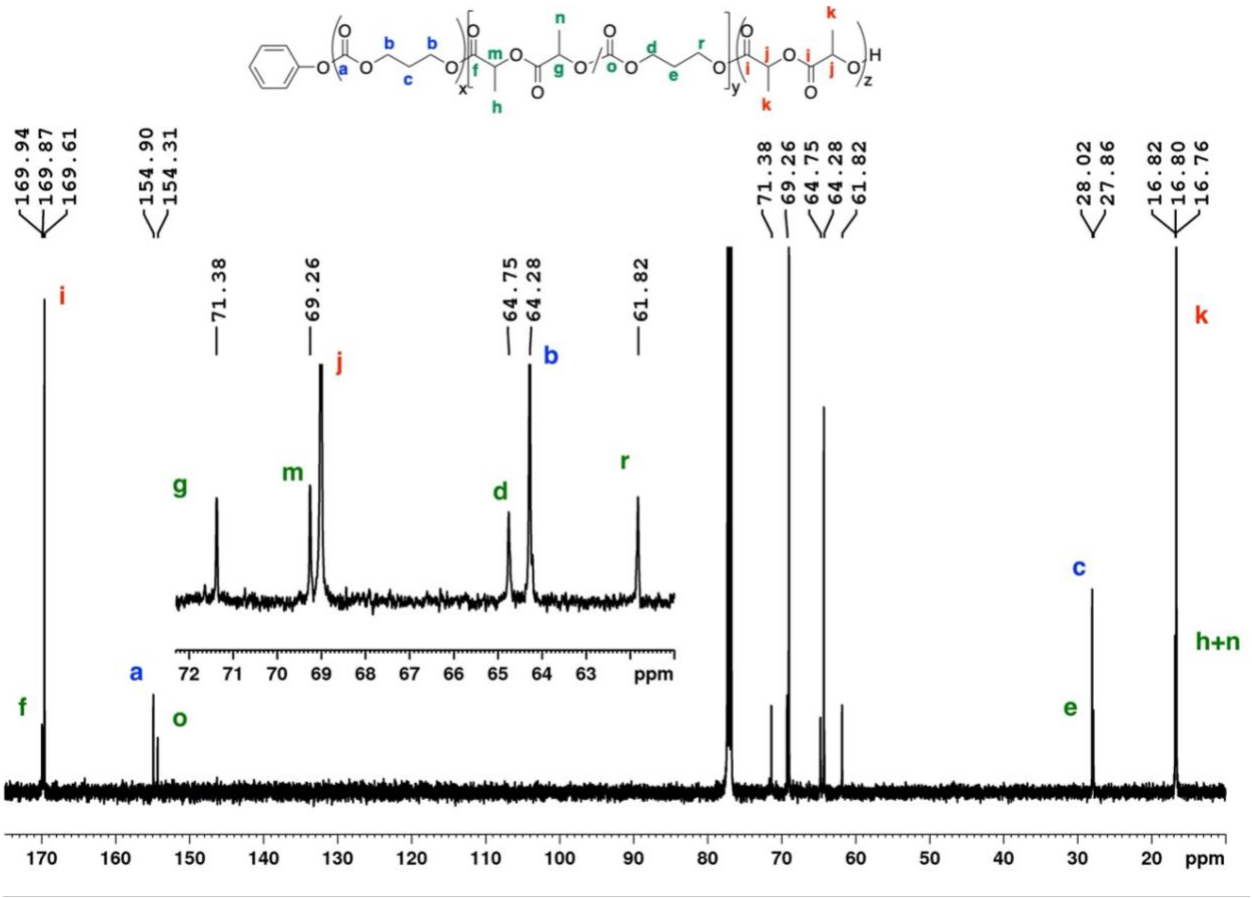

Figure A39. $^{13}C\{^{1}H\}$ NMR ($CDCl_3$, 125 MHz, 298 K) spectrum of 200 equivalents of LLA, 200 equivalents of TMC copolymerization (Table 2-2, entry 2).

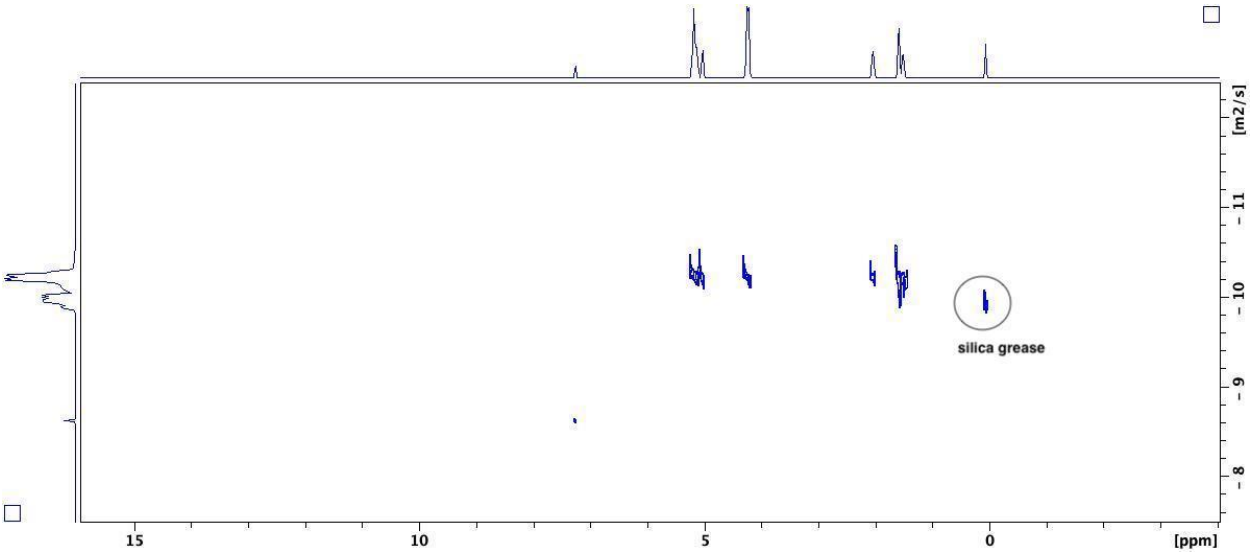

Figure A40. DOSY ($CDCl_3$, 500 MHz, 298 K) of PLLA-PTMC copolymer (Table 2-2, entry 1).

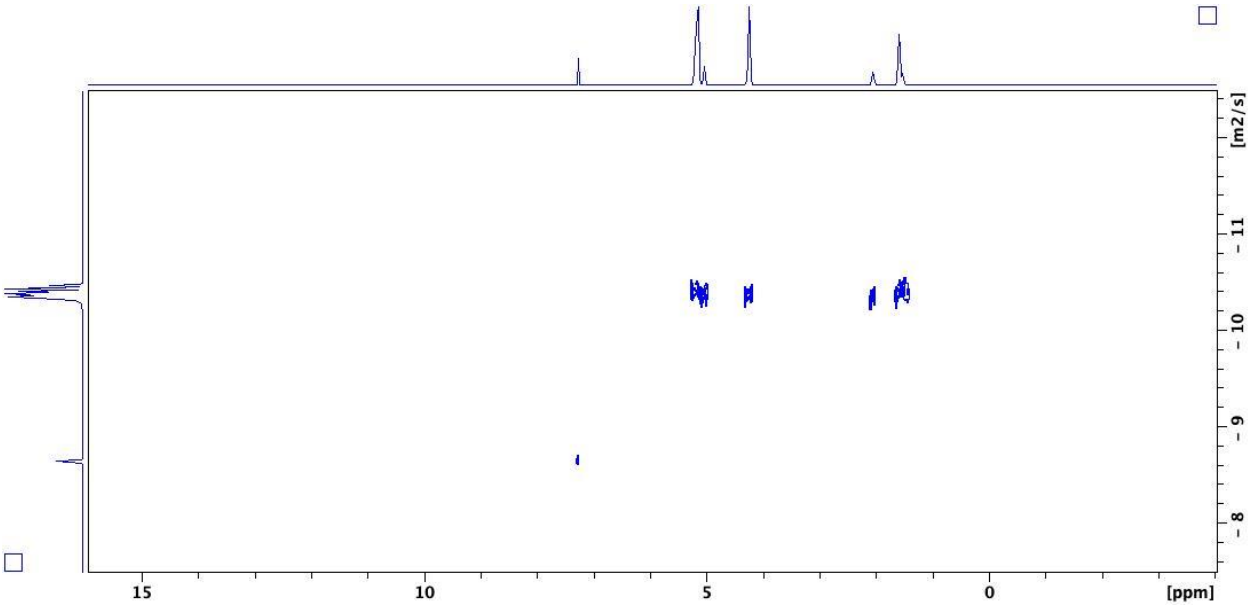

Figure A41. DOSY ($CDCl_3$, 500 MHz, 298 K) of PLLA-PTMC copolymer (Table 2-2, entry 2).

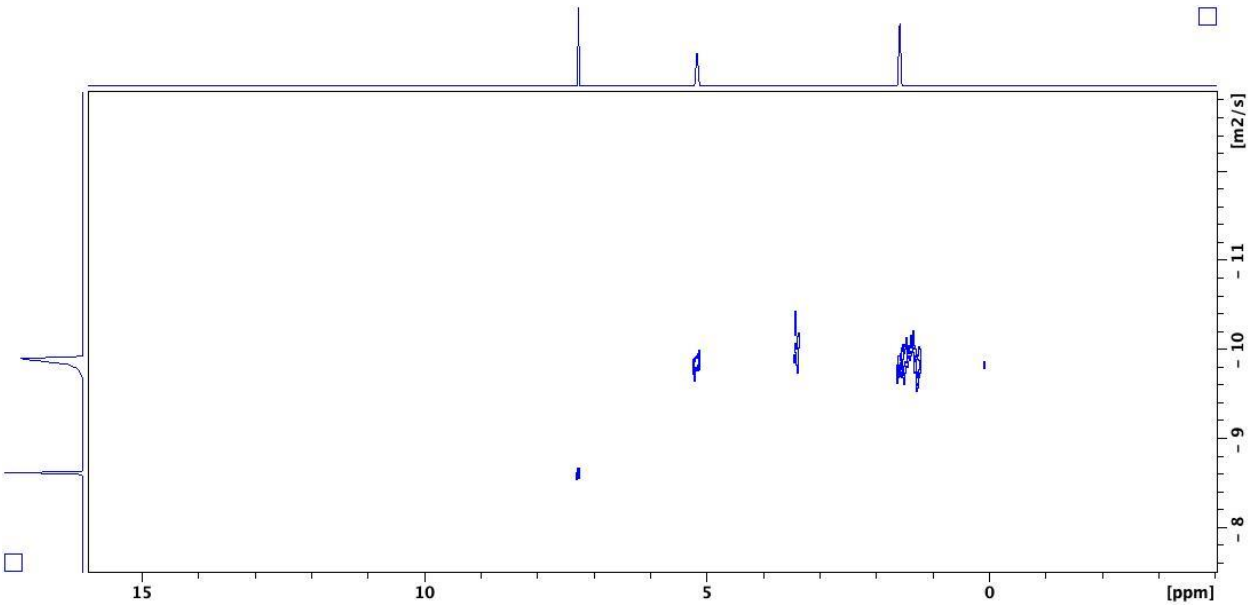

Figure A42. DOSY ($CDCl_3$, 500 MHz, 298 K) of PLLA-PCHO copolymer (Table 2-2, entry 3).

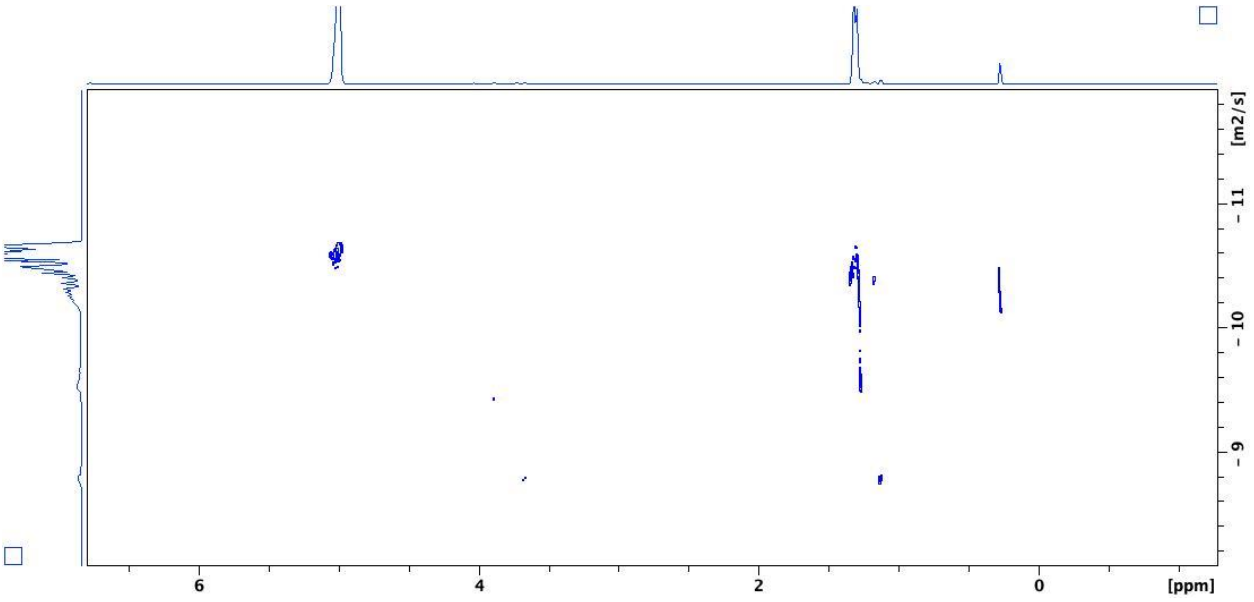

Figure A43. DOSY ($CDCl_3$, 500 MHz, 298 K) of PLLA before quenching with H_2O

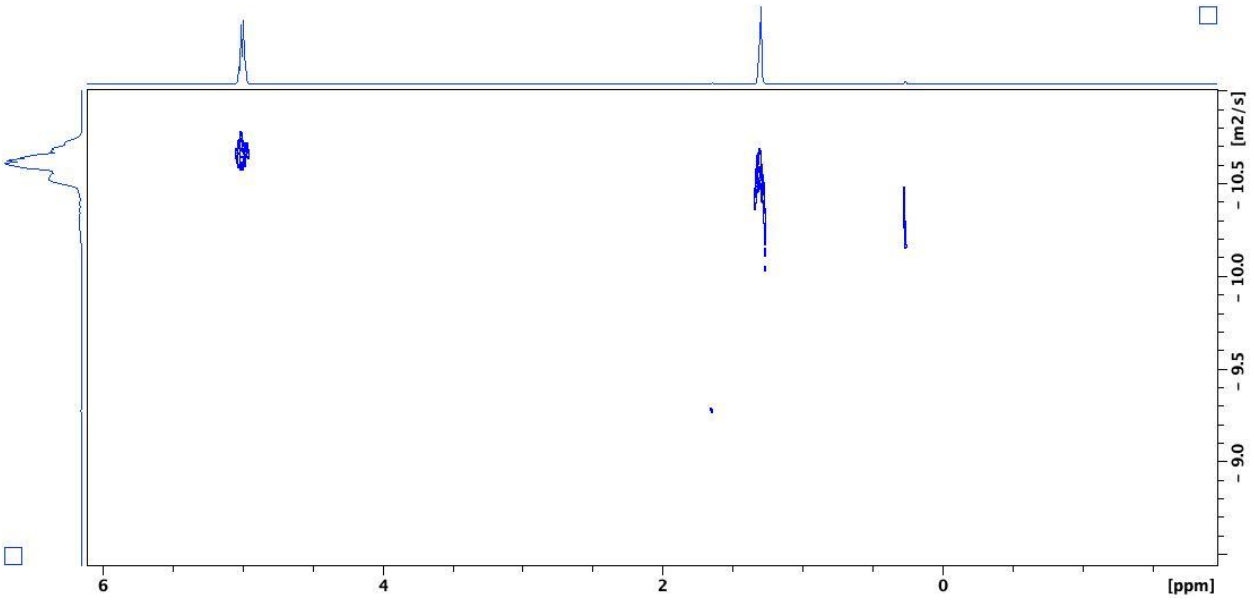

Figure A44. DOSY ($CDCl_3$, 500 MHz, 298 K) of PLLA after quenching with H_2O

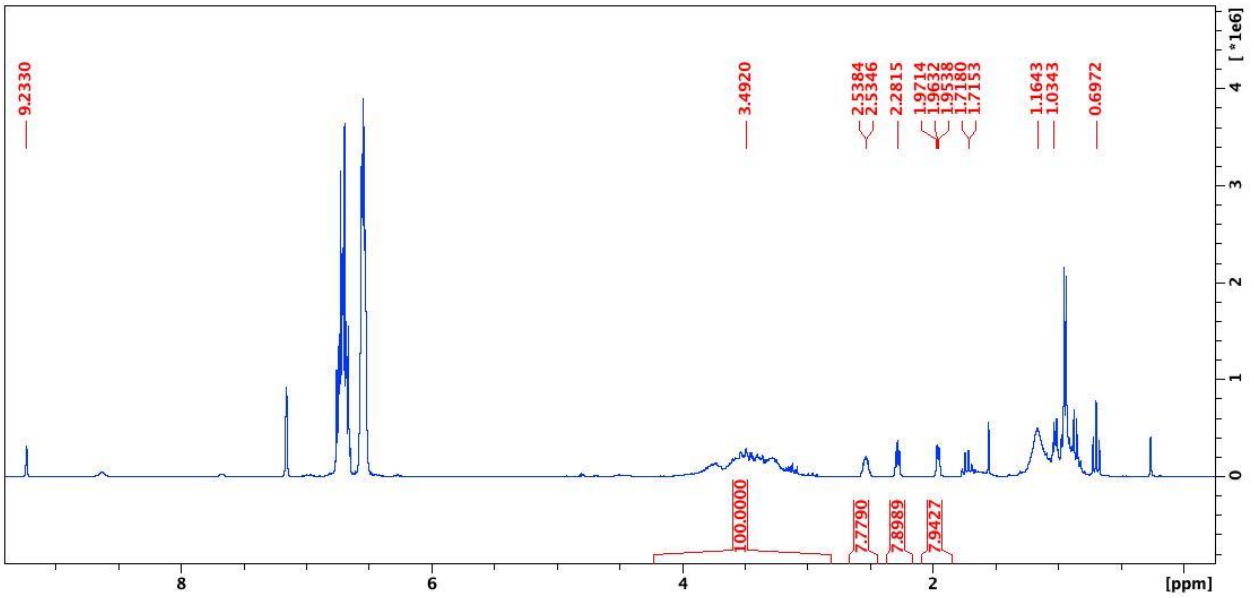

Figure A45. ^1H NMR (C_6D_6, 300 MHz, 298 K) spectrum of 200 equivalents of propylene oxide polymerization by $^{Ac}FcBAr^F$ at 298K after 2 hours. δ (ppm): 3.50 (br, 3H, OC*H*(CH_3)C*H*$_2$O, PPO), 2.57(m, 1H, OC*H*(CH_3)CH_2O, PO), 2.32(t, 1H, OCH(CH_3)C*H*$_2$O, PO), 2.00(m, 1H, OCH(CH_3)C*H*$_2$O, PO), 1.18 (br, 3H, OCH(C*H*$_3$)CH_2O, PPO), 0.97(d, 3H, OCH(C*H*$_3$)CH_2O, PO).

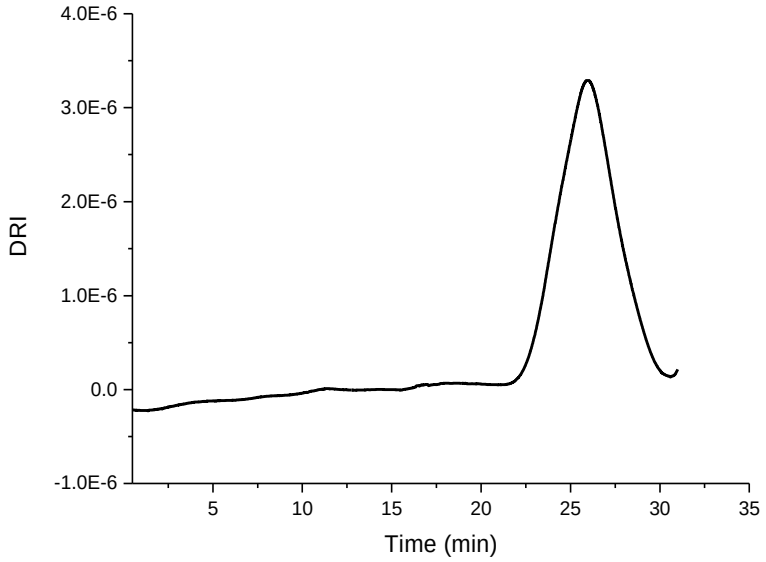

Figure A46. SEC trace for the reaction between 200 equivalents of LLA and $[(salfen)Y(OPh)]_2$ (Table 2-1, entry 1).

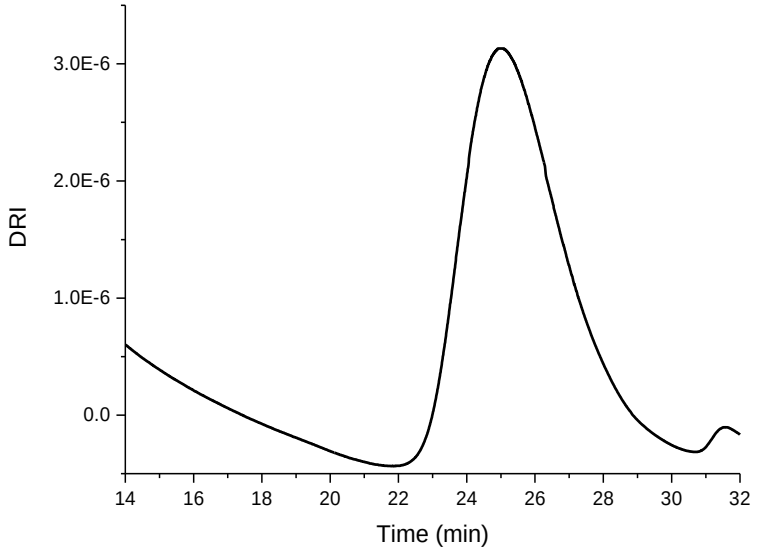

Figure A47. SEC trace for the reaction between 200 equivalents of LLA and *in situ* generated $[(salfen)Y(OPh)]_2^+$ (Table 2-1, entry 2).

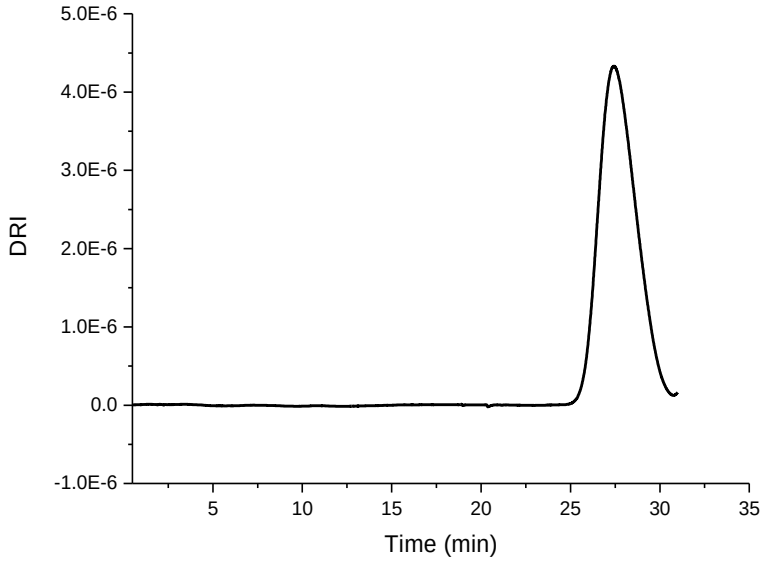

Figure A48. SEC trace for the reaction between 200 equivalents of LLA and *in situ* generated $[(salfen)Y(OPh)]_2^{2+}$ (Table 2-1, entry 3).

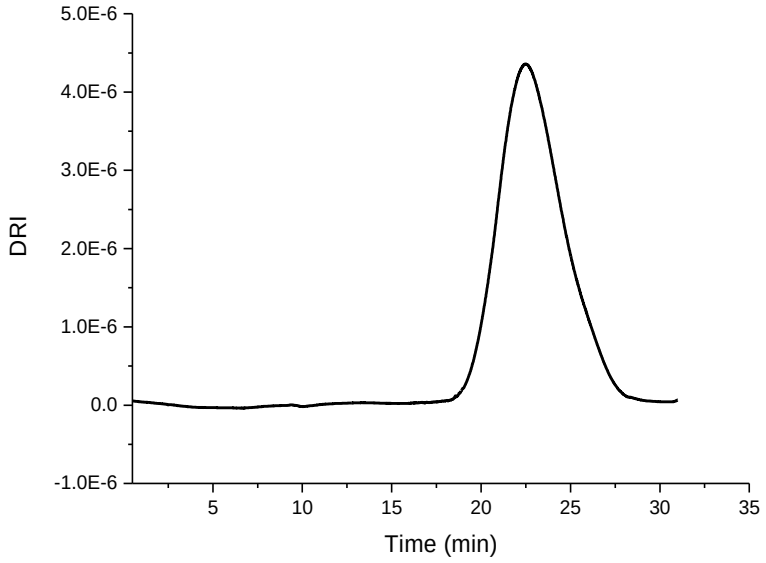

Figure A49. SEC trace for the reaction between 200 equivalents of CL and $[(salfen)Y(OPh)]_2$ (Table 2-1, entry 4).

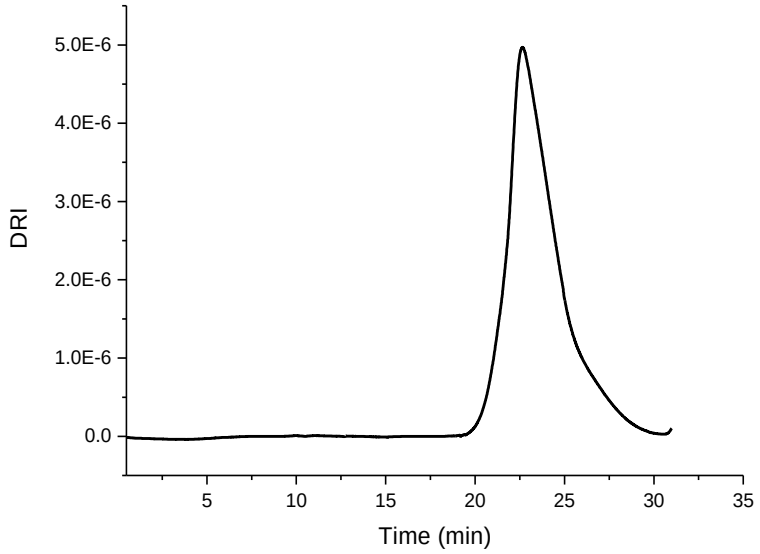

Figure A50. SEC trace for the reaction between 200 equivalents of VL and $[(salfen)Y(OPh)]_2$ (Table 2-1, entry 7).

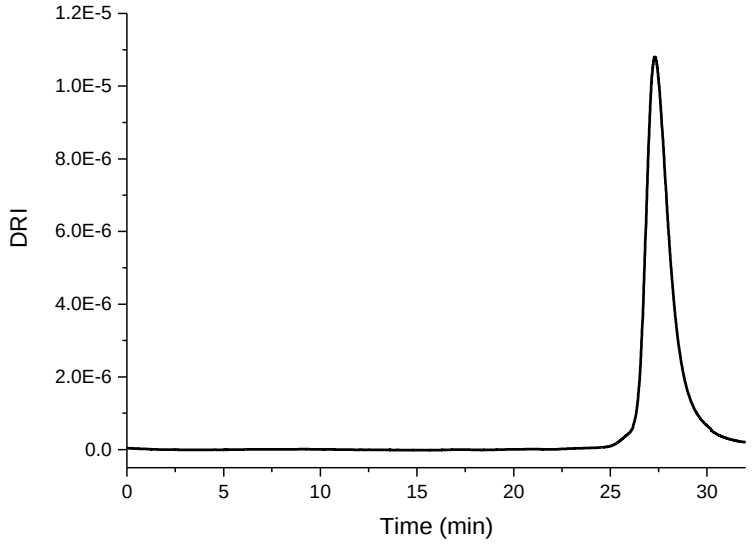

Figure A51. SEC trace for the reaction between 200 equivalents of VL and *in situ* generated $[(salfen)Y(OPh)]_2^+$ (Table 2-1, entry 8).

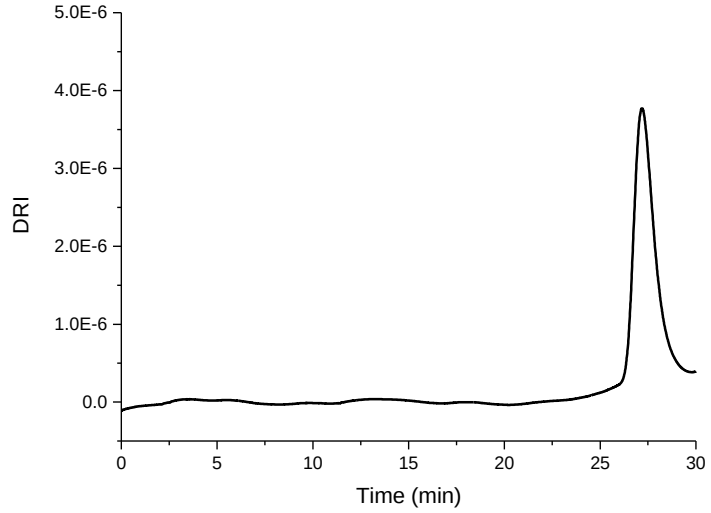

Figure A52. SEC trace for the reaction between 200 equivalents of VL and *in situ* generated $[(salfen)Y(OPh)]_2^{2+}$ (Table 2-1, entry 9).

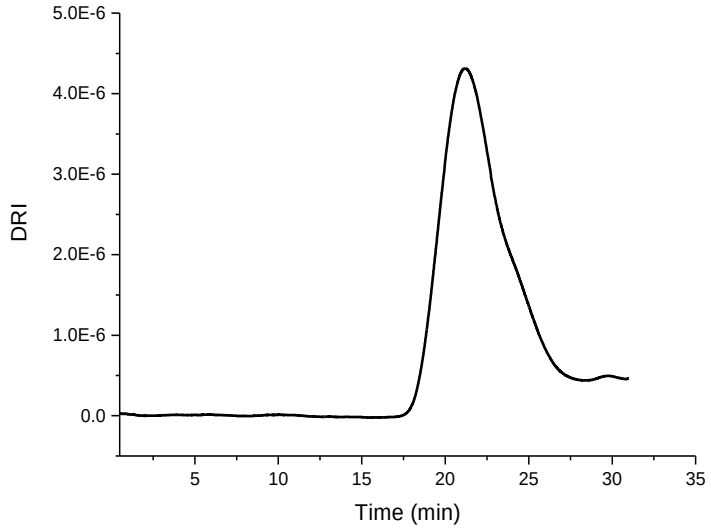

Figure A53. SEC trace for the reaction between 200 equivalents of TMC and $[(salfen)Y(OPh)]_2$ (Table 2-1, entry 10).

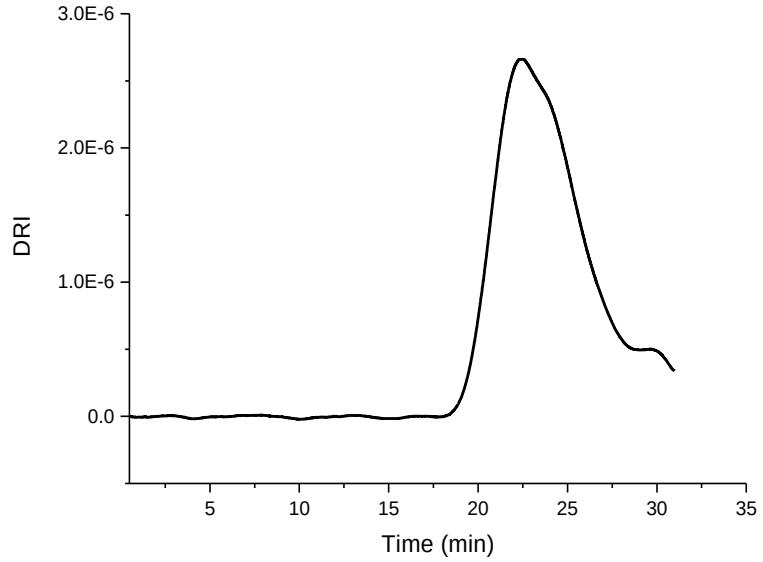

Figure A54. SEC trace for the reaction between 200 equivalents of TMC and *in situ* generated $[(salfen)Y(OPh)]_2^+$ (Table 2-1, entry 11).

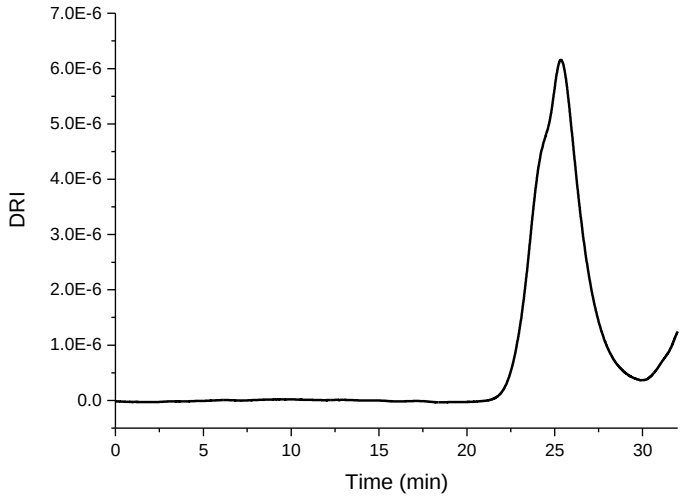

Figure A55. SEC trace for the reaction between 200 equivalents of TMC and *in situ* generated $[(salfen)Y(OPh)]_2^{2+}$ (Table 2-1, entry 12).

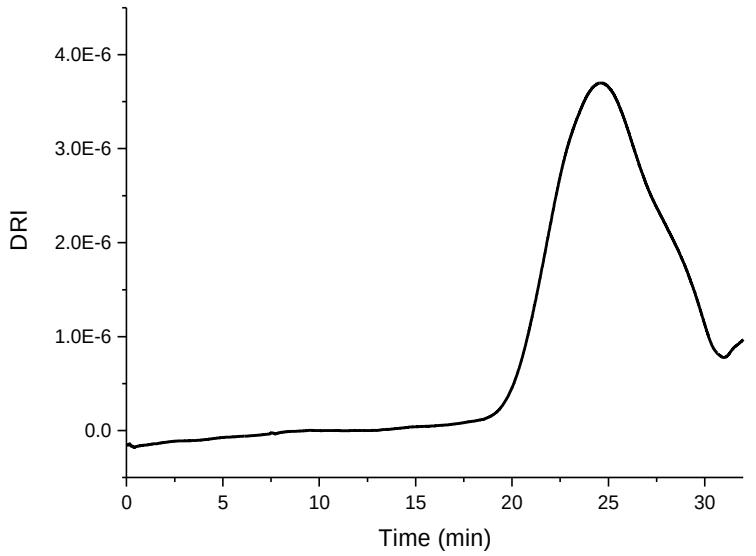

Figure A56. SEC trace for the reaction between 200 equivalents of CHO and *in situ* generated [(salfen)Y(OPh)]$_2^+$ (Table 2-1, entry 14).

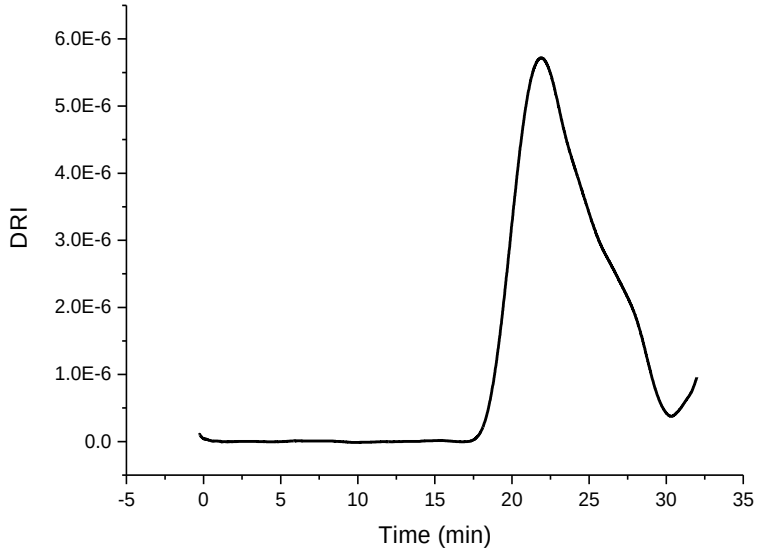

Figure A57. SEC trace for the reaction between 200 equivalents of CHO and *in situ* generated [(salfen)Y(OPh)]$_2^{2+}$ (Table 2-1, entry 15).

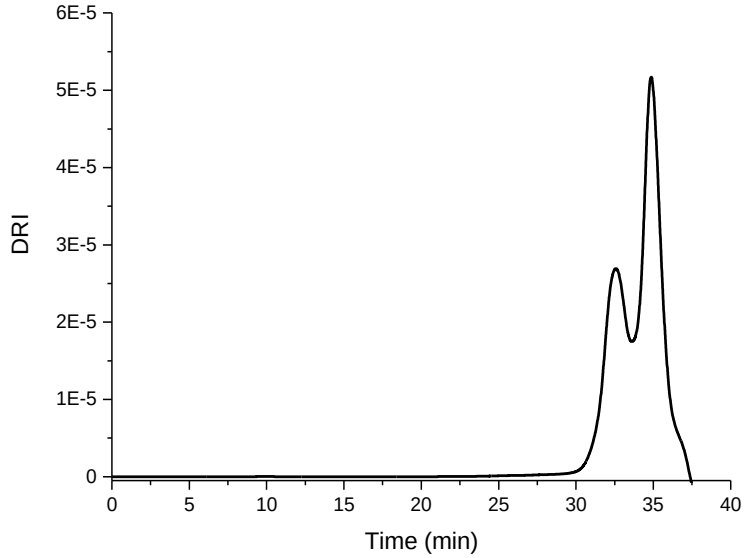

Figure A58. SEC trace for the reaction between 200 equivalents of PO and *in situ* generated [(salfen)Y(OPh)]$_2^+$ (Table 2-1, entry 17).

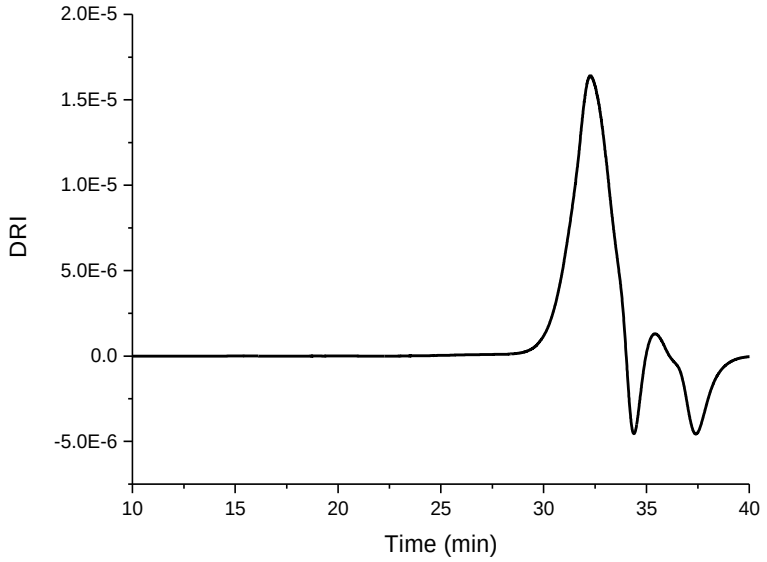

Figure A59. SEC trace for the reaction between 200 equivalents of PO and *in situ* generated [(salfen)Y(OPh)]$_2^{2+}$ (Table 2-1, entry 18).

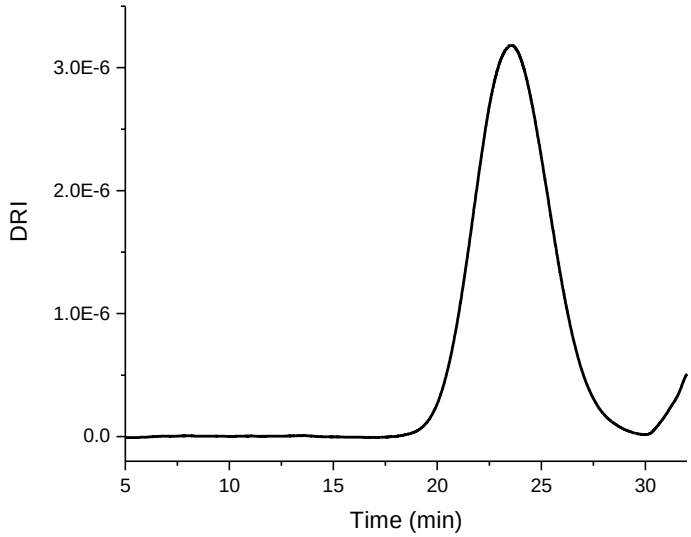

Figure A60. SEC trace for PLLA-PTMC copolymer (Table 2, entry 1).

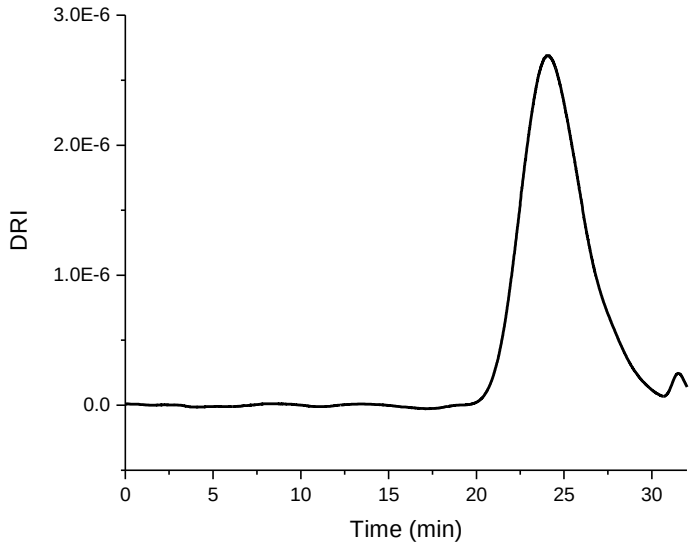

Figure A61. SEC trace for PLLA-PTMC copolymer (Table 2, entry 2).

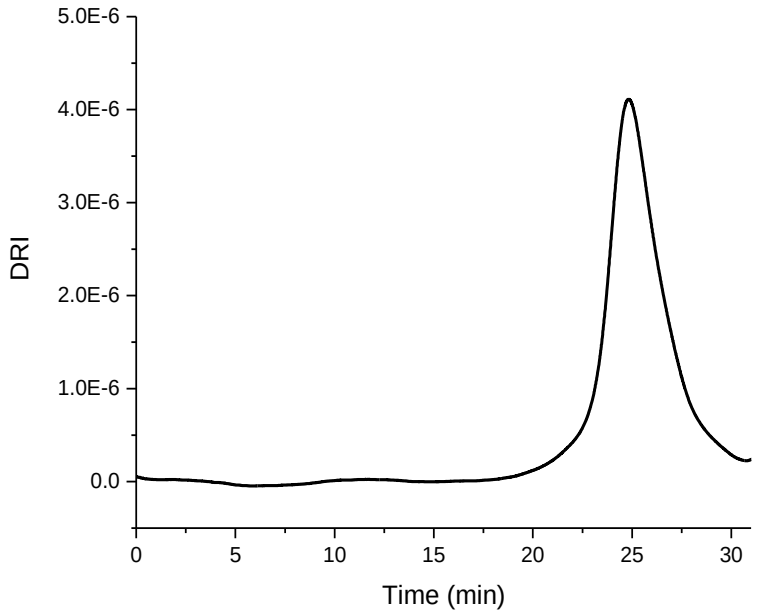

Figure A62. SEC trace for PLLA-PCHO copolymer (Table 2, entry 3).

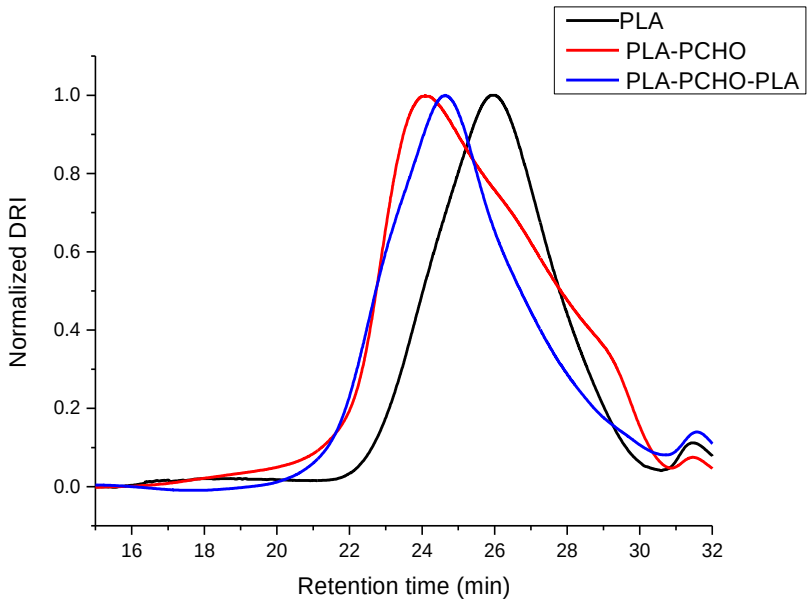

Figure A63. SEC traces corresponding to the stepwise preparation of PLLA-PCHO-PLLA (Table 2-2, entry 4).

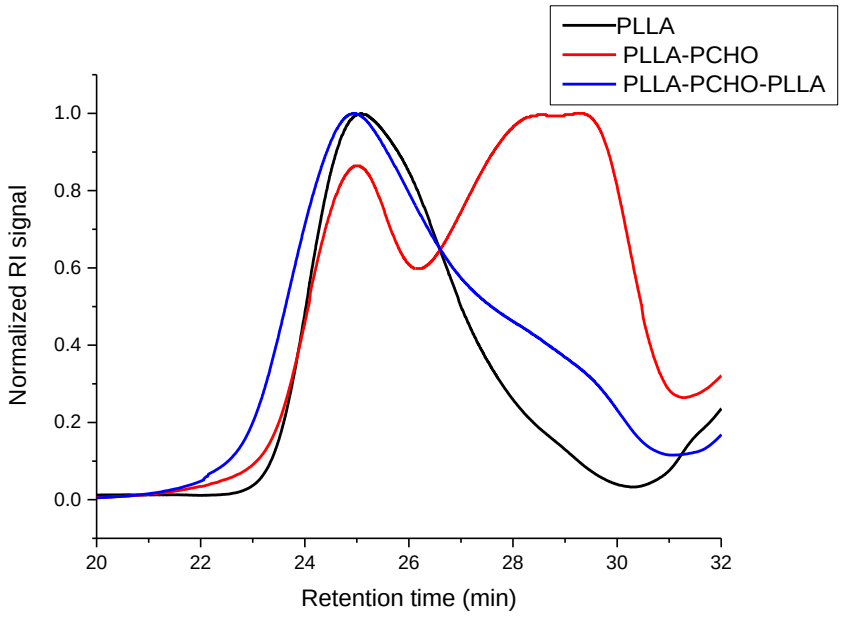

Figure A64. SEC traces corresponding to the stepwise preparation of PLLA-PCHO-PLLA (Table 2-2, entry 5).

Table A1. Replication of homopolymerization results

Entry	Monomer[b]	Cat.[c]	Time	Conv. (%)	$M_{n,calc}$[d] (kDa)	$M_{n,exp}$[e] (kDa)	Đ
1	LLA	red	0.6 h	92	13	17	1.26
2	LLA	ox^{+}	5 h	84	12	29	1.20
3	LLA	ox^{2+}	24 h	31	4.4	7.9	1.27
4	CL	red	21 h	81	8.3	83	1.59
5	CL	ox^{+}	24 h	11	N/A		
6	CL	ox^{2+}	24 h	0	N/A		
7	VL	red	10 h	82	N/A		
8	VL	ox^{+}	24 h	32	N/A		
9	VL	ox^{2+}	24 h	7	N/A		
10	TMC	red	25 h	99	10	118	1.50
11	TMC	ox^{+}	72 h	84	8.6	16	1.33
12	TMC	ox^{2+}	72 h	40	N/A		
13	CHO	red	24 h	0	N/A		
14	CHO	ox^{+}	5 min	99	9.7	27	2.5
15	CHO	ox^{2+}	5 min	99	9.7	60	3.5
16[f]	PO	red	24 h	0	N/A		
17[f]	PO	ox^{+}	48 h	25	N/A		
18[f]	PO	ox^{2+}	49 h	56	3.3	300	1.39

[a] All polymerization reactions were performed with 2.5 μmol precatalyst, 0.6 mL of C_6D_6 as the solvent, 200 equivalents of monomer, at ambient temperature unless otherwise mentioned; conversions were determined by ^{1}H NMR spectroscopy. [b] LLA stands for L-lactide, CL stands for ε-caprolactone, VL stands for δ-valerolactone, TMC stands for 1,3-trimethylene carbonate, CHO stands for cyclohexene oxide, and PO stands for propylene oxide. [c] "red" represents $[(salfen)Y(OPh)]_2$, "ox^{+}" represents *in situ* generated $[(salfen)Y(OPh)]_2^{+}$, and "ox^{2+}" represents *in situ* generated $[(salfen)Y(OPh)]_2^{2+}$. [d] $M_{n,calc}$ is calculated based on initiation from both phenoxide groups, $M_{n,calc} = M_{monomer} \times 100 \times$ conversion. [e] $M_{n,exp}$ were determined by SEC measurements. [f] Polymerization was conducted at 80 °C.

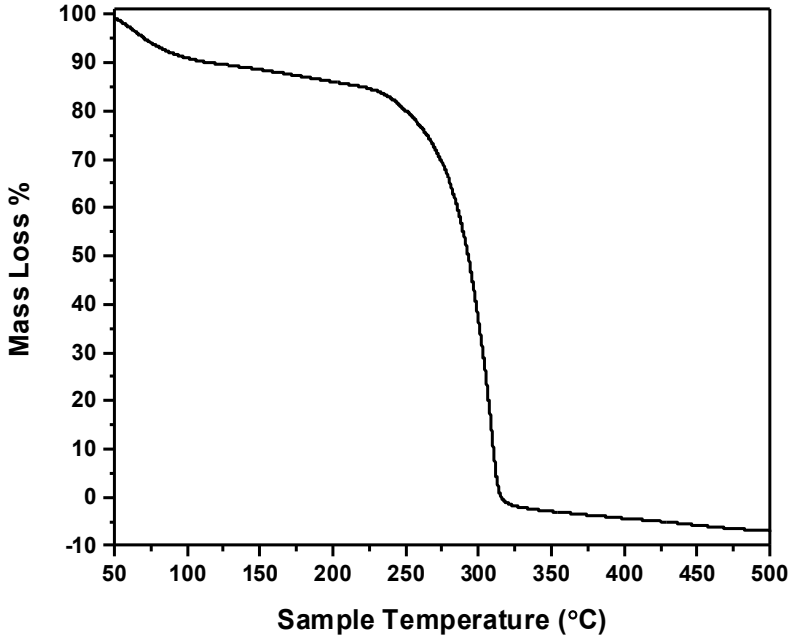

Figure A65. TGA trace for PLLA-PTMC copolymer (Table 2-2, entry 1)

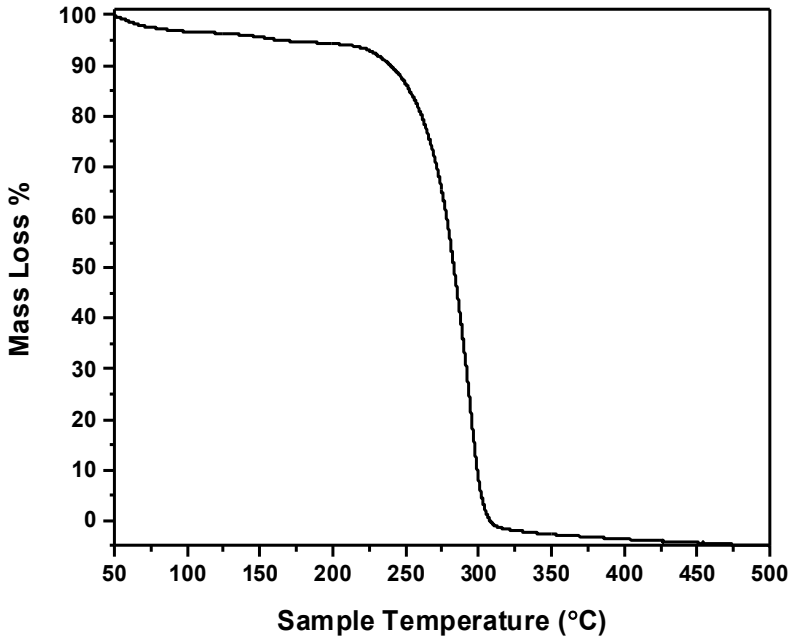

Figure A66. TGA trace for PLLA-PTMC copolymer (Table 2-2, entry 2).

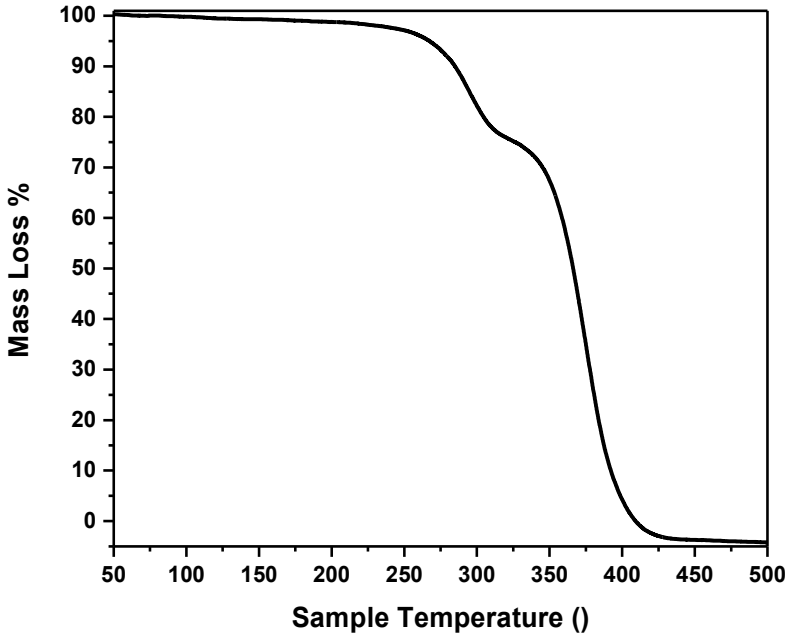

Figure A67. TGA trace for PLLA-PCHO copolymer (Table 2-2, entry 3).

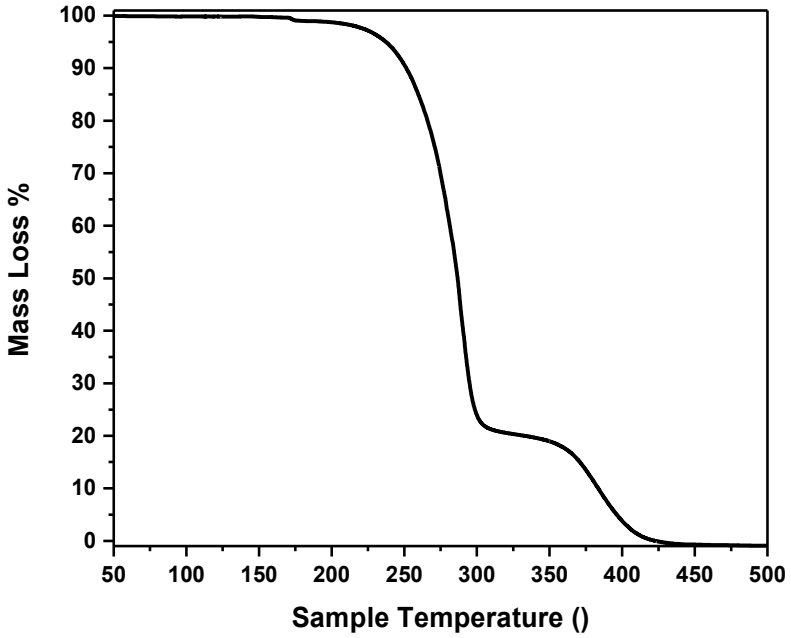

Figure A68. TGA trace for PLLA-PCHO-PLLA copolymer (Table 2-2, entry 4).

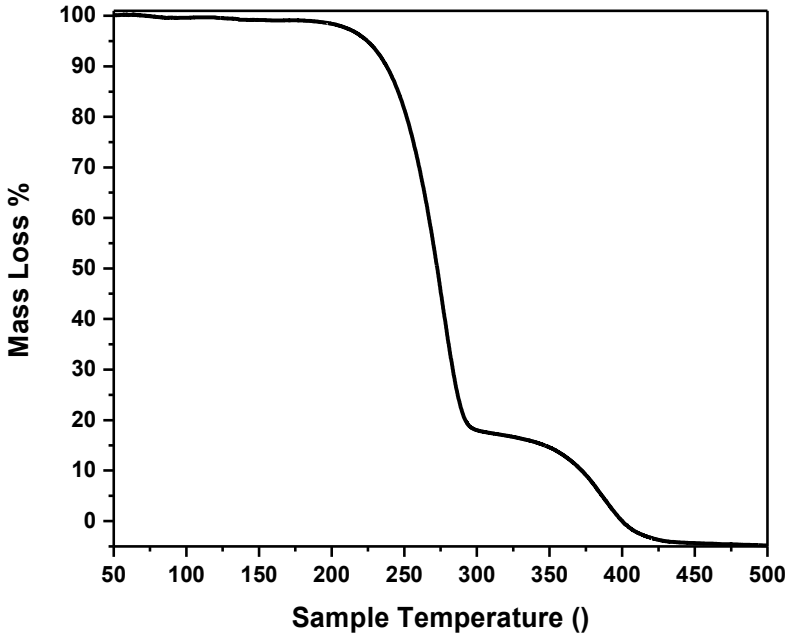

Figure A69. TGA trace for PLLA-PCHO-PLLA copolymer (Table 2-2, entry 5).

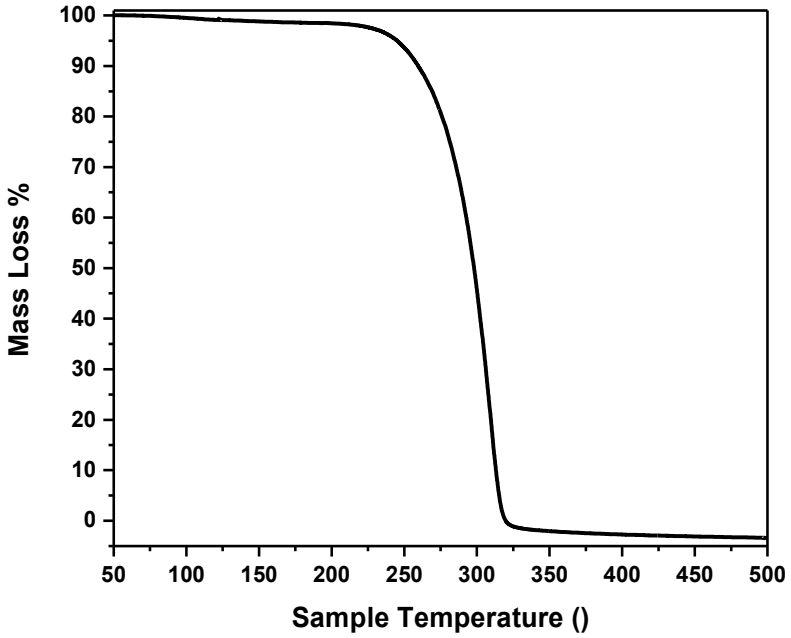

Figure A70. TGA trace for PLLA-PTMC copolymer (Table 2-2, entry 6).

X-ray data

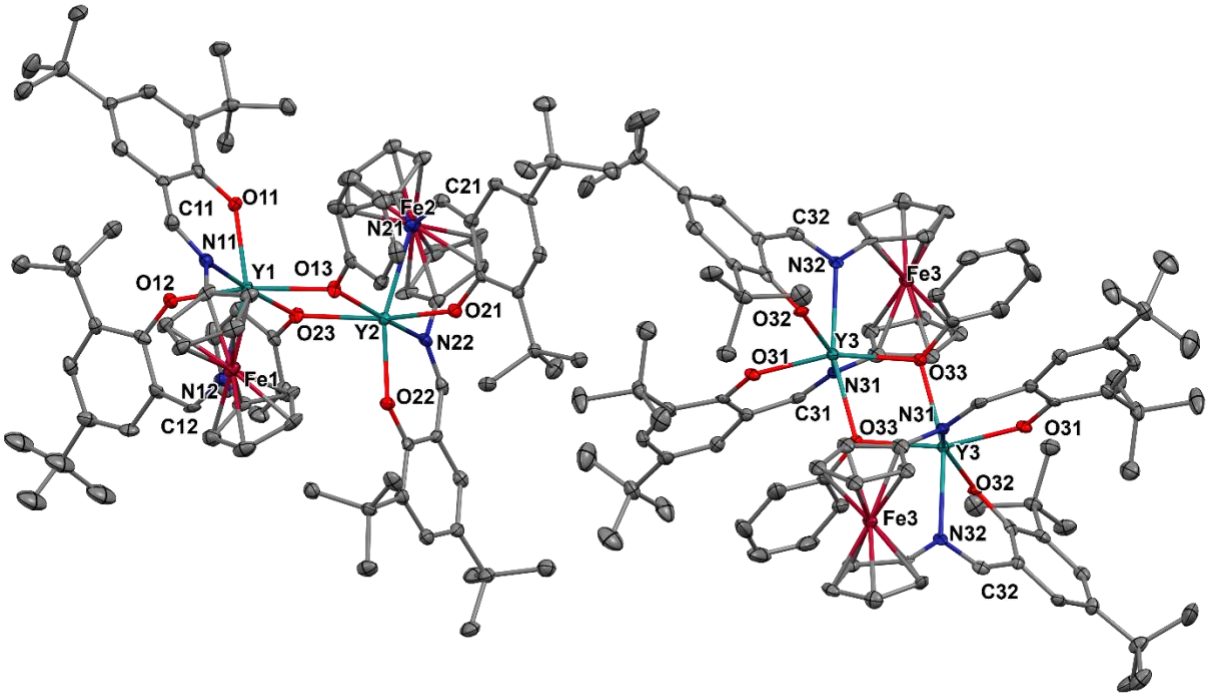

Figure A71. Thermal ellipsoid (50% probability) representation of the crystallographically independent molecules of [(salfen)Y(OPh)]$_2$ in the unit cell (CCDC# 2049815). Hydrogen atoms were omitted for clarity. Single crystals suitable for X-ray crystallography were grown from a hexanes solution. A total of 102675 reflections ($-17 \leq h \leq 17$, $-18 \leq k \leq 18$, $-39 \leq l \leq 39$) were collected at T = 100 K with $2\theta_{max} = 50.00°$, of which 23299 were unique. The residual peak and hole electron density were 1.62 and -0.83 eA^{-3}. The least-squares refinement converged normally with residuals of R_1 = 0.0550 and GOF = 0.965. Crystal and refinement data for [(salfen)Y(OPh)]$_2$: formula $C_{92}H_{110}Fe_2N_4O_6Y_2$, space group P-1, a = 14.8170(17), b = 15.3498(18), c = 33.240(4) Å; α = 84.575(2), β = 81.112(2), γ = 62.305(2)°; V = 6611.2(13) Å^3; Z = 3; λ = 0.71073 Å; μ = 1.678 mm^{-1}; d_{calc} = 1.249 g·cm^{-3}; F(000) = 2604, $R1$ = 0.1025 and $wR2$ = 0.1370 (based on all data, I > 2δ(I)).

2.6. References

(1) Allgeier, A. M.; Mirkin, C. A. Ligand Design for Electrochemically Controlling Stoichiometric and Catalytic Reactivity of Transition Metals. *Angew. Chem. Int. Ed.* **1998**, *37* (7), 894-908.

(2) Teator, A. J.; Lastovickova, D. N.; Bielawski, C. W. Switchable Polymerization Catalysts. *Chem. Rev.* **2016**, *116* (4), 1969-1992.

(3) Blanco, V.; Leigh, D. A.; Marcos, V. Artificial switchable catalysts. *Chem. Soc. Rev.* **2015**, *44* (15), 5341-5370, 10.1039/C5CS00096C.

(4) Chen, C. Redox-Controlled Polymerization and Copolymerization. *ACS Catal.* **2018**, *8* (6), 5506-5514.

(5) Wei, J.; Diaconescu, P. L. Redox-switchable Ring-opening Polymerization with Ferrocene Derivatives. *Acc. Chem. Res.* **2019**, *52* (2), 415-424.

(6) Gregson, C. K. A.; Gibson, V. C.; Long, N. J.; Marshall, E. L.; Oxford, P. J.; White, A. J. P. Redox Control within Single-Site Polymerization Catalysts. *J. Am. Chem. Soc.* **2006**, *128* (23), 7410-7411.

(7) Broderick, E. M.; Guo, N.; Wu, T.; Vogel, C. S.; Xu, C.; Sutter, J.; Miller, J. T.; Meyer, K.; Cantat, T.; Diaconescu, P. L. Redox control of a polymerization catalyst by changing the oxidation state of the metal center. *Chem. Commun.* **2011**, *47*, 9897-9899.

(8) Sauer, A.; Buffet, J.-C.; Spaniol, T. P.; Nagae, H.; Mashima, K.; Okuda, J. Switching the Lactide Polymerization Activity of a Cerium Complex by Redox Reactions. *ChemCatChem* **2013**, *5* (5), 1088-1091.

(9) Biernesser, A. B.; Li, B.; Byers, J. A. Redox-Controlled Polymerization of Lactide Catalyzed by Bis(imino)pyridine Iron Bis(alkoxide) Complexes. *J. Am. Chem. Soc.* **2013**, *135* (44), 16553-16560.

(10) Qi, M.; Dong, Q.; Wang, D.; Byers, J. A. Electrochemically switchable ring-opening polymerization of lactide and cyclohexene oxide. *J. Am. Chem. Soc.* **2018**, *140* (17), 5686-5690.

(11) Ortuño, M. A.; Dereli, B.; Chiaie, K. R. D.; Biernesser, A. B.; Qi, M.; Byers, J. A.; Cramer, C. J. The Role of Alkoxide Initiator, Spin State, and Oxidation State in Ring-Opening Polymerization of ε-Caprolactone Catalyzed by Iron Bis(imino)pyridine Complexes. *Inorg. Chem.* **2018**, *57* (4), 2064-2071.

(12) Delle Chiaie, K. R.; Biernesser, A. B.; Ortuño, M. A.; Dereli, B.; Iovan, D. A.; Wilding, M. J. T.; Li, B.; Cramer, C. J.; Byers, J. A. The role of ligand redox non-innocence in ring-opening polymerization reactions catalysed by bis(imino)pyridine iron alkoxide complexes. *Dalton Trans.* **2017**, *46* (38), 12971-12980, 10.1039/C7DT03067C.

(13) Biernesser, A. B.; Delle Chiaie, K. R.; Curley, J. B.; Byers, J. A. Block Copolymerization of Lactide and an Epoxide Facilitated by a Redox Switchable Iron-Based Catalyst. *Angew. Chem. Int. Ed.* **2016**, *55* (17), 5251–5254.

(14) Fang, Y.-Y.; Gong, W.-J.; Shang, X.-J.; Li, H.-X.; Gao, J.; Lang, J.-P. Synthesis and structure of a ferric complex of 2,6-di(1H-pyrazol-3-yl)pyridine and its excellent performance in the redox-controlled living ring-opening polymerization of ε-caprolactone. *Dalton Trans.* **2014**, *43* (22), 8282-8289, 10.1039/C4DT00475B.

(15) Xu, X.; Luo, G.; Hou, Z.; Diaconescu, P. L.; Luo, Y. Theoretical insight into the redox-switchable activity of group 4 metal complexes for the ring-opening polymerization of ε-caprolactone. *Inorg. Chem. Front.* **2020**, *7* (4), 961-971, 10.1039/C9QI01466G.

(16) Lai, A.; Hern, Z. C.; Diaconescu, P. L. Switchable Ring-Opening Polymerization by a Ferrocene Supported Aluminum Complex. *ChemCatChem* **2019**, *11* (16), 4210-4218.

(17) Lai, A.; Clifton, J.; Diaconescu, P. L.; Fey, N. Computational mapping of redox-switchable metal complexes based on ferrocene derivatives. *Chem. Commun.* **2019**, *55*, , 7021-7024 10.1039/C9CC01977D.

(18) Dai, R.; Diaconescu, P. L. Investigation of a Zirconium Compound for Redox Switchable Ring Opening Polymerization. *Dalton Trans.* **2019**, *48*, 2996-3002.

(19) Dai, R.; Lai, A.; Alexandrova, A. N.; Diaconescu, P. L. Geometry Change in a Series of Zirconium Compounds during Lactide Ring-Opening Polymerization. *Organometallics* **2018**, *37* (21), 4040-4047.

(20) Abubekerov, M.; Vlček, V.; Wei, J.; Miehlich, M. E.; Quan, S. M.; Meyer, K.; Neuhauser, D.; Diaconescu, P. L. Exploring Oxidation State-Dependent Selectivity in Polymerization of Cyclic Esters and Carbonates with Zinc(II) Complexes. *iScience* **2018**, *7*, 120-131.

(21) Wei, J.; Riffel, M. N.; Diaconescu, P. L. Redox Control of Aluminum Ring-Opening Polymerization: A Combined Experimental and DFT Investigation. *Macromolecules* **2017**, *50* (5), 1847-1861.

(22) Quan, S. M.; Wei, J.; Diaconescu, P. L. Mechanistic Studies of Redox-Switchable Copolymerization of Lactide and Cyclohexene Oxide by a Zirconium Complex. *Organometallics* **2017**, *36* (22), 4451-4457.

(23) Lowe, M. Y.; Shu, S.; Quan, S. M.; Diaconescu, P. L. Investigation of redox switchable titanium and zirconium catalysts for the ring opening polymerization of cyclic esters and epoxides. *Inorg. Chem. Front.* **2017**, *4*, 1798-1805, 10.1039/C7QI00227K.

(24) Quan, S. M.; Wang, X.; Zhang, R.; Diaconescu, P. L. Redox Switchable Copolymerization of Cyclic Esters and Epoxides by a Zirconium Complex. *Macromolecules* **2016**, *49* (18), 6768-6778.

(25) Wang, X.; Brosmer, J. L.; Thevenon, A.; Diaconescu, P. L. Highly Active Yttrium Catalysts for the Ring-Opening Polymerization of ε-Caprolactone and δ-Valerolactone. *Organometallics* **2015**, *34* (19), 4700–4706.

(26) Quan, S. M.; Diaconescu, P. L. High activity of an indium alkoxide complex toward ring opening polymerization of cyclic esters. *Chem. Commun.* **2015**, *51*, 9643 - 9646, 10.1039/C5CC01312G.

(27) Wang, X.; Thevenon, A.; Brosmer, J. L.; Yu, I.; Khan, S. I.; Mehrkhodavandi, P.; Diaconescu, P. L. Redox Control of Group 4 Metal Ring-Opening Polymerization Activity toward l-Lactide and ε-Caprolactone. *J. Am. Chem. Soc.* **2014**, *136* (32), 11264-11267.

(28) Zou, W.; Pang, W.; Chen, C. Redox control in palladium catalyzed norbornene and alkyne polymerization. *Inorg. Chem. Front.* **2017**, *4* (5), 795-800, 10.1039/C6QI00562D.

(29) Chen, M.; Yang, B.; Chen, C. Redox-Controlled Olefin (Co)Polymerization Catalyzed by Ferrocene-Bridged Phosphine-Sulfonate Palladium Complexes. *Angew. Chem. Int. Ed.* **2015**, *54* (51), 15520-15524.

(30) Yang, B.; Pang, W.; Chen, M. Redox Control in Olefin Polymerization Catalysis by Phosphine–Sulfonate Palladium and Nickel Complexes. *Eur. J. Inorg. Chem.* **2017**, *2017* (18), 2510-2514.

(31) Anderson, W. C.; Rhinehart, J. L.; Tennyson, A. G.; Long, B. K. Redox-Active Ligands: An Advanced Tool To Modulate Polyethylene Microstructure. *J. Am. Chem. Soc.* **2016**, *138* (3), 774-777.

(32) Anderson, W. C.; Long, B. K. Modulating Polyolefin Copolymer Composition via Redox-Active Olefin Polymerization Catalysts. *ACS Macro Lett.* **2016**, *5* (9), 1029-1033.

(33) Anderson, W. C.; Park, S. H.; Brown, L. A.; Kaiser, J. M.; Long, B. K. Accessing multiple polyethylene grades via a single redox-active olefin polymerization catalyst. *Inorg. Chem. Front.* **2017**, *4* (7), 1108-1112, 10.1039/C7QI00079K.

(34) Abubekerov, M.; Khan, S. I.; Diaconescu, P. L. Ferrocene-bis(phosphinimine) Nickel(II) and Palladium(II) Alkyl Complexes: Influence of the Fe–M (M = Ni and Pd) Interaction on Redox Activity and Olefin Coordination. *Organometallics* **2017**, *36* (22), 4394-4402.

(35) Abubekerov, M.; Shepard, S. M.; Diaconescu, P. L. Switchable Polymerization of Norbornene Derivatives by a Ferrocene-Palladium(II) Heteroscorpionate Complex. *Eur. J. Inorg. Chem.* **2016**, *2016* (15-16), 2634-2640.

(36) Abubekerov, M.; Diaconescu, P. L. Synthesis and Characterization of Ferrocene-Chelating Heteroscorpionate Complexes of Nickel(II) and Zinc(II). *Inorg. Chem.* **2015**, *54* (4), 1778–1784.

(37) Teator, A. J.; Bielawski, C. W. Remote control grubbs catalysts that modulate ring-opening metathesis polymerizations. *J. Polym. Sci. A Polym. Chem.* **2017**, *55* (18), 2949-2960.

(38) Lastovickova, D. N.; Teator, A. J.; Shao, H.; Liu, P.; Bielawski, C. W. A redox-switchable ring-closing metathesis catalyst. *Inorg. Chem. Front.* **2017**, *4* (9), 1525-1532, 10.1039/C7QI00018A.

(39) Lastovickova, D. N.; Shao, H.; Lu, G.; Liu, P.; Bielawski, C. W. A Ring-Opening Metathesis Polymerization Catalyst That Exhibits Redox-Switchable Monomer Selectivities. *Chem. Eur. J.* **2017**, *23* (25), 5994-6000.

(40) Varnado, C. D.; Jr; Rosen, E. L.; Collins, M. S.; Lynch, V. M.; Bielawski, C. W. Synthesis and study of olefin metathesis catalysts supported by redox-switchable

diaminocarbene[3]ferrocenophanes. *Dalton Trans.* **2013**, *42* (36), 13251-13264, 10.1039/C3DT51278A.

(41) Arumugam, K.; Varnado, C. D.; Sproules, S.; Lynch, V. M.; Bielawski, C. W. Redox-Switchable Ring-Closing Metathesis: Catalyst Design, Synthesis, and Study. *Chem. Eur. J.* **2013**, *19* (33), 10866-10875.

(42) Dadashi-Silab, S.; Lorandi, F.; Fantin, M.; Matyjaszewski, K. Redox-switchable atom transfer radical polymerization. *Chem. Commun.* **2019**, *55* (5), 612-615, 10.1039/C8CC09209E.

(43) Magenau, A. J. D.; Strandwitz, N. C.; Gennaro, A.; Matyjaszewski, K. Electrochemically Mediated Atom Transfer Radical Polymerization. *Science* **2011**, *332* (6025), 81-84.

(44) Leibfarth, F. A.; Mattson, K. M.; Fors, B. P.; Collins, H. A.; Hawker, C. J. External Regulation of Controlled Polymerizations. *Angew. Chem. Int. Ed.* **2013**, *52* (1), 199-210.

(45) Zhao, M.; Chen, C. Accessing Multiple Catalytically Active States in Redox-Controlled Olefin Polymerization. *ACS Catal.* **2017**, *7* (11), 7490-7494.

(46) Straube, A.; Coburger, P.; Dütsch, L.; Hey-Hawkins, E. Triple the fun: tris(ferrocenyl)arene-based gold(I) complexes for redox-switchable catalysis. *Chem. Sci.* **2020**, *11* (39), 10657-10668, 10.1039/D0SC03604H.

(47) Broderick, E. M.; Guo, N.; Vogel, C. S.; Xu, C.; Sutter, J.; Miller, J. T.; Meyer, K.; Mehrkhodavandi, P.; Diaconescu, P. L. Redox Control of a Ring-Opening Polymerization Catalyst. *J. Am. Chem. Soc.* **2011**, *133* (24), 9278–9281.

(48) Abubekerov, M.; Wei, J.; Swartz, K. R.; Xie, Z.; Pei, Q.; Diaconescu, P. L. Preparation of multiblock copolymers via step-wise addition of l-lactide and trimethylene carbonate. *Chem. Sci.* **2018**, *9* (8), 2168-2178, 10.1039/C7SC04507G.

(49) Brown, L. A.; Rhinehart, J. L.; Long, B. K. Effects of Ferrocenyl Proximity and Monomer Presence during Oxidation for the Redox-Switchable Polymerization of l-Lactide. *ACS Catal.* **2015**, *5* (10), 6057-6060.

(50) Atkinson, R. C. J.; Gerry, K.; Gibson, V. C.; Long, N. J.; Marshall, E. L.; West, L. J. Synthesis of 1,1‘-Ferrocenediyl Salicylaldimine Ligands and Their Application in Titanium-Initiated Lactide Polymerization. *Organometallics* **2006**, *26* (2), 316-320.

(51) Doerr, A. M.; Burroughs, J. M.; Legaux, N. M.; Long, B. K. Redox-switchable ring-opening polymerization by tridentate ONN-type titanium and zirconium catalysts. *Catal. Sci. Technol.* **2020**, *10* (19), 6501-6510, 10.1039/D0CY00642D.

(52) Stevels, W. M.; Ankoné, M. J. K.; Dijkstra, P. J.; Feijen, J. A Versatile and Highly Efficient Catalyst System for the Preparation of Polyesters Based on Lanthanide Tris(2,6-di-tert-butylphenolate)s and Various Alcohols. *Macromolecules* **1996**, *29* (9), 3332-3333.

(53) Simic, V.; Spassky, N.; Hubert-Pfalzgraf, L. G. Ring-Opening Polymerization of d,l-Lactide Using Rare-Earth μ-Oxo Isopropoxides as Initiator Systems. *Macromolecules* **1997**, *30* (23), 7338-7340.

(54) Ovitt, T. M.; Coates, G. W. Stereoselective Ring-Opening Polymerization of meso-Lactide: Synthesis of Syndiotactic Poly(lactic acid). *J. Am. Chem. Soc.* **1999**, *121* (16), 4072-4073.

(55) Bakewell, C.; Cao, T.-P.-A.; Long, N.; Le Goff, X. F.; Auffrant, A.; Williams, C. K. Yttrium Phosphasalen Initiators for rac-Lactide Polymerization: Excellent Rates and High Iso-Selectivities. *J. Am. Chem. Soc.* **2012**, *134* (51), 20577-20580.

(56) Lyubov, D. M.; Tolpygin, A. O.; Trifonov, A. A. Rare-earth metal complexes as catalysts for ring-opening polymerization of cyclic esters. *Coord. Chem. Rev.* **2019**, *392*, 83-145.

(57) Platel, R. H.; Hodgson, L. M.; White, A. J. P.; Williams, C. K. Synthesis and Characterization of a Series of Bis(oxo/thiophosphinic)diamido Yttrium Complexes and Their Application as Initiators for Lactide Ring-Opening Polymerization. *Organometallics* **2007**, *26* (20), 4955-4963.

(58) Platel, R. H.; White, A. J. P.; Williams, C. K. Bis(phosphinic)diamido Yttrium Amide, Alkoxide, and Aryloxide Complexes: An Evaluation of Lactide Ring-Opening Polymerization Initiator Efficiency. *Inorg. Chem.* **2011**, *50* (16), 7718-7728.

(59) Crockett, M. P.; Zhang, H.; Thomas, C. M.; Byers, J. A. Adding diffusion ordered NMR spectroscopy (DOSY) to the arsenal for characterizing paramagnetic complexes. *Chem. Commun.* **2019**, *55* (96), 14426-14429, 10.1039/C9CC08229H.

(60) Guerin, W.; Helou, M.; Slawinski, M.; Brusson, J.-M.; Guillaume, S. M.; Carpentier, J.-F. Macromolecular engineering via ring-opening polymerization (2): l-lactide/trimethylene carbonate copolymerization - kinetic and microstructural control via catalytic tuning. *Polym. Chem.* **2013**, *4* (13), 3686-3693, 10.1039/C3PY00397C.

(61) Simic, V.; Pensec, S.; Spassky, N. Synthesis and characterization of some block copolymers of lactides with cyclic monomers using yttrium alkoxide as initiator. *Macromol. Symp.* **2000**, *153* (1), 109-121.

(62) Shen, Y.; Shepard, S. M.; Reed, C. J.; Diaconescu, P. L. Zirconium Complexes Supported by a Ferrocene-Based Ligand as Redox Switches for Hydroamination Reactions. *Chem. Commun.* **2019**, *55*, 5587-5590.

(63) Pangborn, A. B.; Giardello, M. A.; Grubbs, R. H.; Rosen, R. K.; Timmers, F. J. Safe and Convenient Procedure for Solvent Purification. *Organometallics* **1996**, *15* (5), 1518-1520.

(64) Dhar, D.; Yee, G. M.; Spaeth, A. D.; Boyce, D. W.; Zhang, H.; Dereli, B.; Cramer, C. J.; Tolman, W. B. Perturbing the Copper(III)–Hydroxide Unit through Ligand Structural Variation. *J. Am. Chem. Soc.* **2016**, *138* (1), 356-368.

(65) Broderick, E. M.; Diaconescu, P. L. Cerium(IV) Catalysts for the Ring-Opening Polymerization of Lactide. *Inorg. Chem.* **2009**, *48*, 4701-4706.

(66) Dolomanov, O. V.; Bourhis, L. J.; Gildea, R. J.; Howard, J. A. K.; Puschmann, H. OLEX2: a complete structure solution, refinement and analysis program. *J. Appl. Crystallogr.* **2009**, *42* (2), 339-341.

Chapter 3: Ring opening polymerization of six-membered ring N-carboxyanhydride toward aromatic polyamide synthesis

3.1. Introduction

Aromatic polyamides are extra tough and flame-resistant materials that have a wide range of applications.[1-3] The introduction of alkyl groups to the nitrogen atoms in the backbone significantly expands the range of chemical variations that can be achieved in aromatic poly- and oligoamides, making them an important group of abiotic foldamers.[4-6] While para- and meta- subtrates have been investigated, examples of ortho-aromatic polyamides remained rare. Hamilton and coworkers reported that the presence of intramolecular hydrogen bonds in ortho- benzamide oligomers leads to a planar arrangement of substituents and promotes the formation of linear strand structures.[7] Alkylation of the nitrogen atom would disrupt these hydrogen bonds, allowing an increased chemical diversity and the possibility of tuning cis/trans isomerization based on steric and electronic interactions.

The synthesis of aromatic polyamides, however, is generally limited to polycondensation reactions that lead to polymers with low molecular weight and broad dispersity.[8, 9] In 2000, Yokozawa and coworkers reported a strategy that used a base to deactivate monomers and a reactive initiator to optimize the condensation reaction.[10-13] Similarly, in 2021, Kiblinger and coworkers reported another activation strategy that showed good control over the polycondensation reaction.[14] These methods were only effective for para- and meta-aromatic polyamides, while the synthesis of ortho-aromatic polyamides remains challenging (Scheme 3-1).[15]

Although the ring-opening polymerization of *N*-carboxyanhydrides (NCAs) has been investigated in polyamide synthesis as an alternative route to polycondensation reactions,[16-21] aromatic β-NCAs, such as isatoic anhydride and its derivatives, have not been employed before.

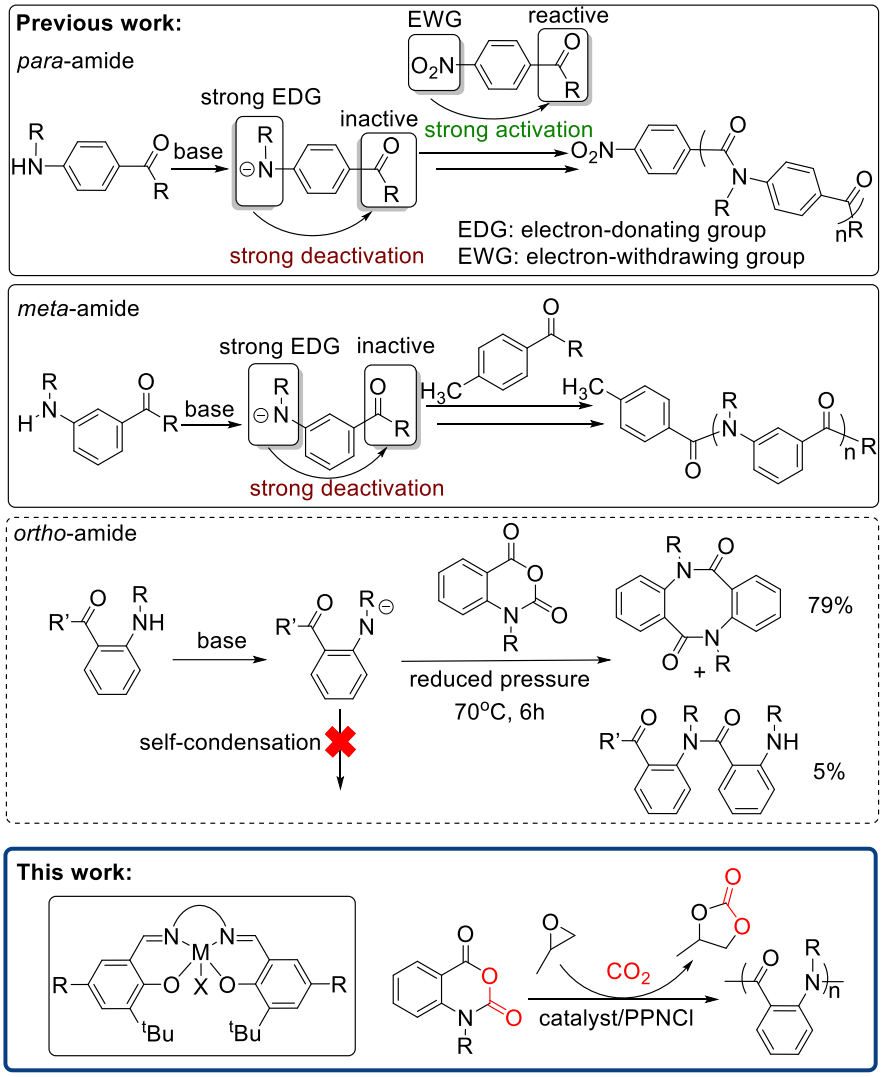

Scheme 3-1. Synthesis of aromatic polyamides. Chain-growth polymerization for the synthesis of para-[11] and meta-[12] aromatic polyamides was reported by Yokozawa and coworkers, but the same strategy does not apply to ortho-aromatic polyamides.[15]

Given our previous success with using metal complexes for the ring opening polymerization of cyclic esters and ethers,[22-37] we decided to apply similar systems to NCA polymerization. Herein, we report the successful ring-opening polymerization of aromatic β-NCAs using Schiff base metal compounds and PPNCl ($[PPN]^+$ = bis(triphenylphosphoranylidene)iminium). Such systems have

been previously exploited in the ring-opening copolymerization of epoxides and anhydrides,[38, 39] ring-opening copolymerization of epoxides and dihydrocoumarin,[40] as well as coupling reactions between CO_2 and epoxides.[41, 42] The homopolymerization of α-NCAs by salen complexes for polypeptide synthesis was also reported.[43]

3.2. Results and Discussion

Table 3-1. Ring-opening polymerization of 6-NCA-R[a].

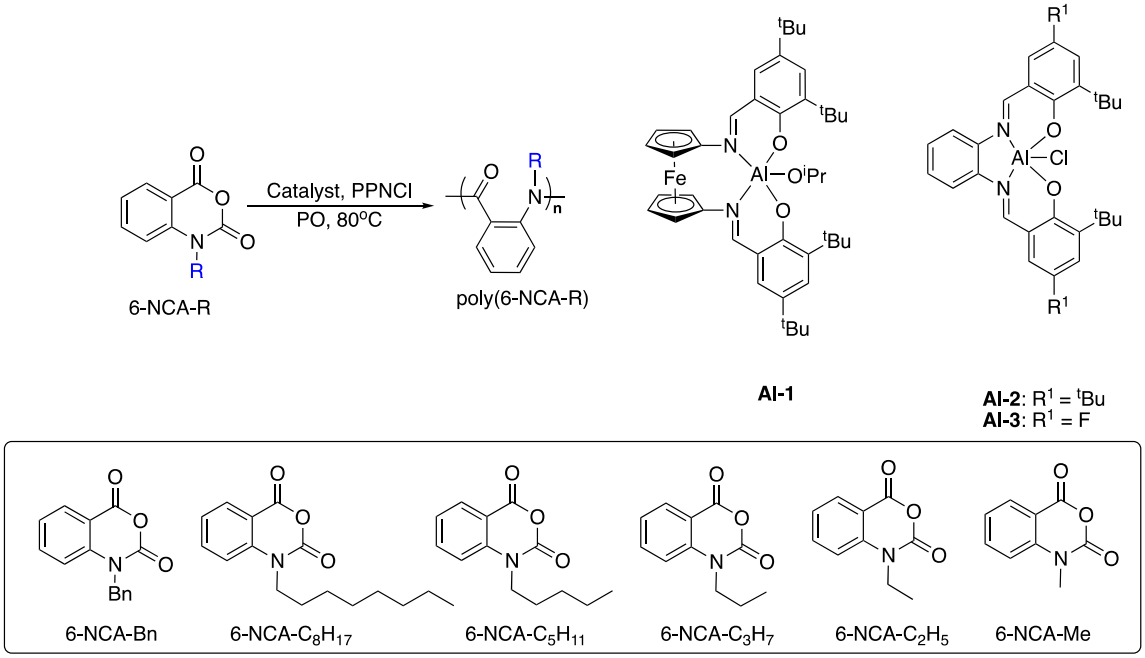

Entry	Catalyst	6-NCA-R	[cat] : [PPNCl] : [6-NCA-R]	Time	Polymer yield[b]	$M_{n,theo}$[c] (kDa)	$M_{n,SEC}$[d] (kDa)	$Đ$[d]
1	**Al-1**	6-NCA-Bn	1:2:50	2h	86%	--	--	--
2	**Al-1**	6-NCA-C_8H_{17}	1:2:50	2h	74%	8.7	38.1	1.33
3	**Al-2**	6-NCA-C_8H_{17}	1:2:50	2h	83%	9.6	25.3	1.33
4	**Al-2**	6-NCA-C_8H_{17}	0:1:50	4h	82%	9.5	43.2	1.31
5	**Al-2**	6-NCA-C_8H_{17}	1:0:50	24h	-	-	-	-
6[e]	**Al-2**	6-NCA-C_8H_{17}	1:1:50	2h	91%	10.5	97.0	1.39
7	**Al-2**	6-NCA-C_8H_{17}	1:1:50	2h	70%	8.8	25.9	1.38
8	**Al-2**	6-NCA-C_8H_{17}	1:5:50	2h	74%	8.6	18.5	1.23
9	**Al-3**	6-NCA-C_8H_{17}	1:1:50	22h	79%	9.1	28.0	1.33
10	**Al-2**	6-NCA-C_8H_{17}	1:2:25	1h	65%	3.8	20.8	1.21
11	**Al-2**	6-NCA-C_8H_{17}	1:2:100	4h	90%	20.8	32.2	1.35
12	**Al-2**	6-NCA-C_8H_{17}	1:2:200	7h	86%	39.8	44.5	1.41
13	**Al-2**	6-NCA-C_5H_{11}	1:2:50	2h	90%	8.5	19.3	1.21
14	**Al-2**	6-NCA-C_3H_7	1:2:50	2h	94%	7.8	25.6	1.12
15	**Al-2**	6-NCA-C_2H_5	1:2:50	2h	90%	6.6	22.6	1.12

16	**Al-2**	6-NCA-Me	1:2:50	2h	89%	--	--	--

[a] All polymerizations were carried out at 80 °C using 4 μmol precatalyst, 0.6 mL PO unless otherwise noted. [b] Polymer yields were determined gravimetrically. [c] $M_{n,\,theo}$ =([6-NCA-R]$_0$/[Cat]) × (MW of 6-NCA-R - MW of CO_2) × polymer yield. [d] M_n and $Đ$ were determined by SEC measurements. [e] Polymerization was carried out in THF with 100 equiv. of PO.

We started by adapting reaction conditions from reported five-membered ring NCA polymerizations[43] using a ferrocene-based aluminum complex.[24] An equivalent of (salfen)AlO^{i}Pr (**Al-1,** salfen = *N,N'*-bis(2,4-di-*tert*-butylphenoxy)-1,1′-ferrocenediimine), 2 equivalents of PPNCl, 50 equivalents of 6-NCA-Bn, and propylene oxide (PO) as the solvent were used (Table 3-1, entry 1). The reaction mixture was heated at 80 °C for 2 hours, resulting in the formation of an off-white precipitate. Notably, the resulting solid was only slightly soluble in trifluoroacetic acid (TFA), while being insoluble in solvents such as THF, methylene chloride, DMF, or DMSO. We speculated that the product obtained was a polymer, but our characterization was limited due to its low solubility. To address this issue, we attempted to increase the polymer solubility by using monomers with longer *N*-alkyl side chains. We synthesized 6-NCA-C_8H_{17}, an analogue with an *N*-octyl group, and used it as a monomer (Table 3-1, entry 2). Using the same conditions as described above, we obtained poly(6-NCA-C_8H_{17}) with a significantly improved solubility, allowing us to acquire its ^{1}H and ^{13}C NMR spectra in $CDCl_3$ (Figure 3-1C). The integration of peaks in the ^{1}H NMR spectrum is consistent with the structure of poly(6-NCA-C_8H_{17}).

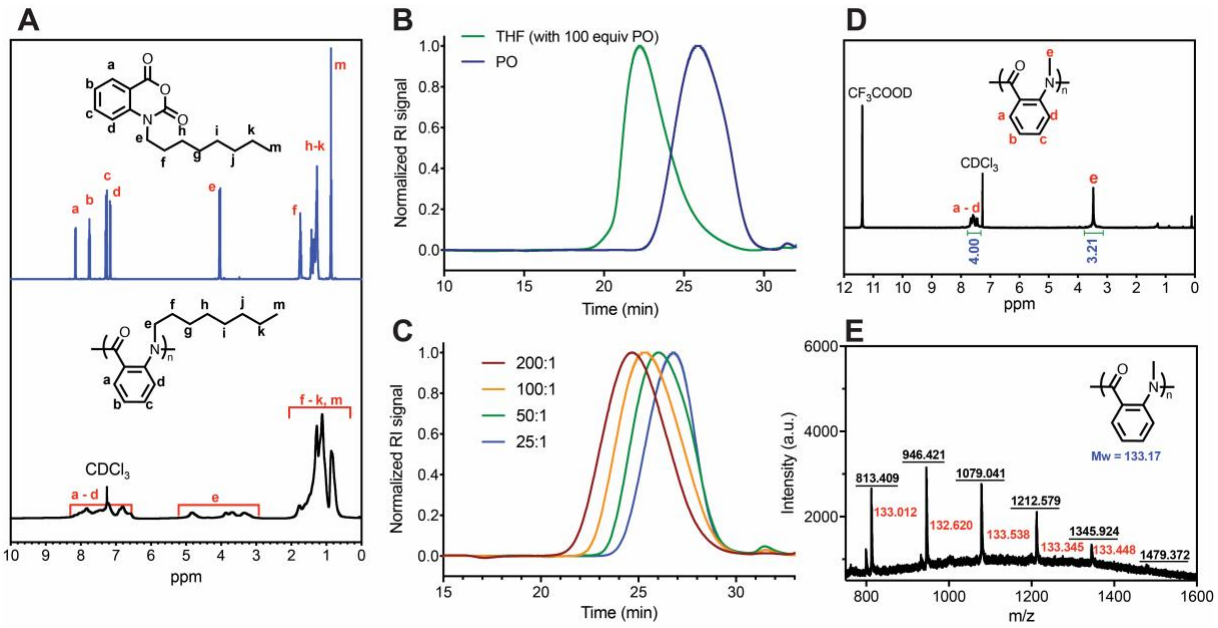

Figure 3-1. (A) ^{1}H NMR (500 MHz, 25 ˚C) spectra of 6-NCA-C_8H_{17} (top) and poly(6-NCA-C_8H_{17}) (bottom) in $CDCl_3$. (B) SEC traces of polymer obtained from using THF as the solvent with 100 equiv. of PO added (green) and using neat PO (blue, Table 3-1, entries 3, 6). (C) SEC traces of the polymers obtained with varying the [6-NCA-C_8H_{17}] : [cat] feed ratio (Table 3-1, entries 3, 10-12). (D) ^{1}H NMR (500 MHz, 25 ˚C) spectrum of poly(6-NCA-Me) (Table 3-1, entry 16) in $CDCl_3$: CF_3COOD = 5 : 1. (E) MALDI-TOF-MS of poly(6-NCA-Me) (Table 3-1, entry 16).

The polymer peaks in the ^{1}H NMR spectrum appeared broader compared to those of the corresponding NCA monomer, indicating the presence of both cis- and trans-isomers in the polymer backbone amide bonds (Figure 3-1A).[44, 45] Additionally, during the course of the 6-NCA-C_8H_{17} polymerization, the formation of propylene carbonate was observed when monitored by ^{1}H NMR spectroscopy. The formation of cyclic carbonate was also observed when the Schiff base metal compounds together with PPNCl and PO were employed in the 5-membered ring NCA polymerization.[43]

With the metal compounds bearing a ferrocene backbone, we also attempted the redox switchable copolymerization[22-37] of 6-NCA-C_8H_{17} and PO. We started with an equivalent of (salfen)AlO^iPr (**Al-1**), 2 equivalents of PPNCl, 50 equivalents of 6-NCA-C_8H_{17}, and propylene oxide (PO) as a solvent (the reduced **Al-1** does not polymerize epoxides). After heating at 80 °C for 0.5 hours, $^{Ac}FcBAr^F$ (^{Ac}Fc = acetylferrocene, BAr^F = tetrakis(3,5-bis(trifluoromethyl)phenyl) borate) was added to oxidize **Al-1** and initiate the polymerization of PO (Figure B24). Unfortunately, only the poly(6-NCA-C_8H_{17}) homopolymer was isolated. We also attempted to initiate the polymerization with the oxidized form of **Al-1**. However, upon the addition of the PPNCl cocatalyst, the decomposition of the oxidized aluminum compound was observed, as evidenced by the color change from dark red to orange and the formation of a black precipitate. The decomposition was attributed to the incompatibility between the ferrocenium backbone and the chloride anion.[53]

Given the lack of redox switchable copolymerization, we then turned to a simple salph (salph = *N,N'*-bis(3,5-di-*tert*-butylsalicylidene)-1,2-diaminobenzene) aluminum compound, (salph)AlCl (**Al-2)**, to study the role of the metal compound, PPNCl, and PO in 6-NCA-C_8H_{17} polymerization. **Al-2** demonstrated comparable activity to **Al-1**, and the resulting polymer had a molecular weight closer to the theoretical value (Table 3-1, entry 3). We first investigated the role of the PPNCl cocatalyst. In a control experiment using only **Al-2** without PPNCl, no polymerization was observed (Table 3-1, entry 5). However, when PPNCl was used alone without the aluminum compound, the polymerization still occurred at a slower rate, resulting in a higher polymer molecular weight compared to when the aluminum compound was present (Table 3-1, entry 4). As the amount of PPNCl increased from 1 to 2 and 5 equivalents, the polymer molecular weight decreased, and the molecular weight distribution became narrower (Table 3-1, entries 7, 8). These

findings suggest the importance of both the aluminum compound and the PPNCl cocatalyst in the polymerization process.

To investigate the effect of propylene oxide (PO) amount on initiation efficiency, we proceeded to conduct the polymerization using THF as the solvent. We added 100 equivalents of PO to initiate the polymerization and trap the CO_2 released. Interestingly, when the polymerization was performed in THF, the polymerization rate remained relatively unchanged, with a polymer yield of 91% after 2 hours (Table 3-1, entry 6). However, the polymer's molecular weight increased significantly from 25.9 kDa to 97.0 kDa, indicating a lower initiation efficiency. Both polymers, obtained from either using THF with 100 equiv. of PO or neat PO, exhibited unimodal size exclusion chromatography (SEC) traces. Specifically, the trace from neat PO displayed a shift towards a lower molecular weight (Figure 3-1B).

To further optimize the catalytic system and achieve better control over the polymerization process, we employed a fluorinated salph aluminum compound. Coates and coworkers reported that (salph-F)AlCl (**Al-3**) can effectively suppress side reactions in the copolymerization of propylene oxide and different cyclic anhydrides such as transesterification and epimerization.[54] However, in 6-NCA-C_8H_{17} polymerization, although **Al-3** was significantly slower than **Al-2**, no major difference was observed in the polymer molecular weight (Table 3-1, entry 7 vs. 9).

We also varied the monomer feed ratio (Table 3-1, entries 10-12). With a higher monomer feed ratio, the polymer molecular weight increased and was closer to the theoretical value, in agreement with a slow initiation of the polymerization process (Figure 3-1C).

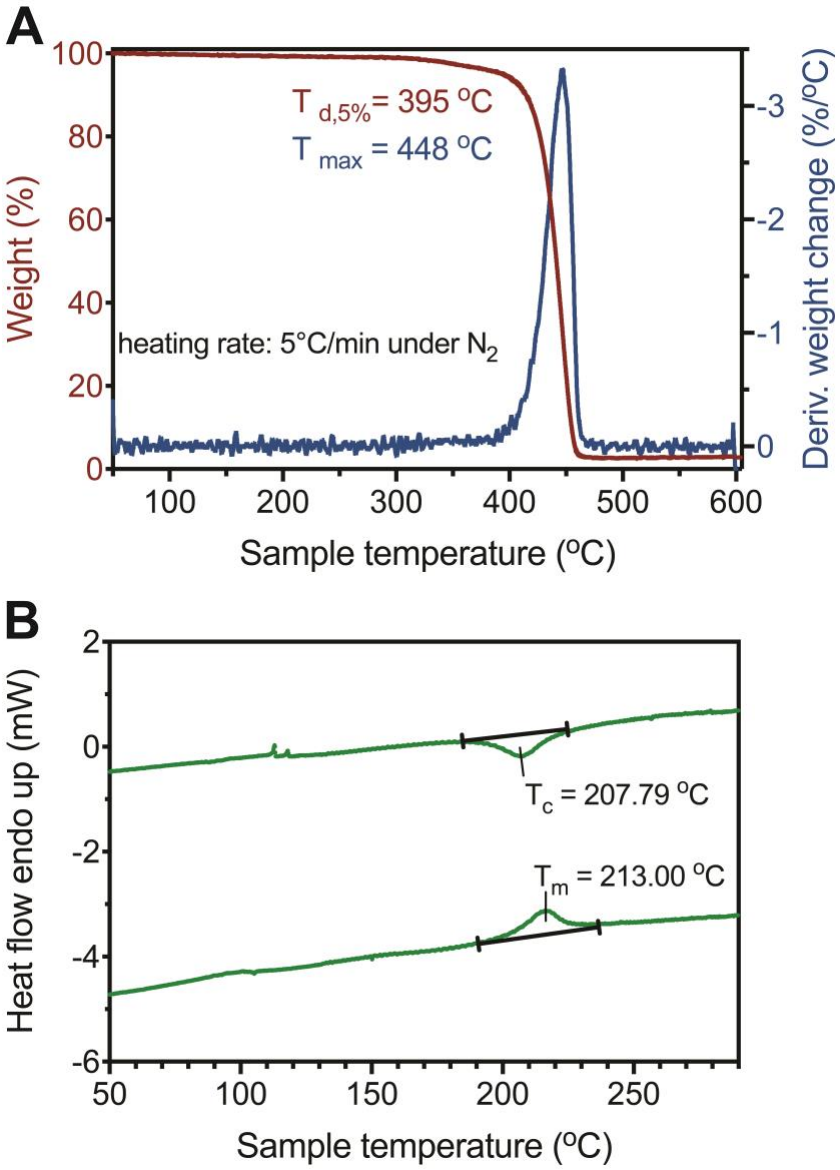

Figure 3-2. (A) Thermogravimetric analysis (TGA) and derivative thermogravimetry (DTG) curves of poly(6-NCA-C_8H_{17}). (B) Differential scanning calorimetry (DSC) curves of poly(6-NCA-C_8H_{17}) (Table 3-1, entry 3).

To investigate the influence of the *N*-alkyl side chain length on solubility and thermal properties, we varied the chain length (Table 3-1, entries 13-16). Previous studies have shown that *N*-alkylated poly(*p*-benzamide)s are only soluble in THF when the alkyl chain length is no shorter than heptyl.[55]

On the other hand, *N*-alkylated poly(*m*-benzamides) generally exhibit better solubility, with even the *N*-methyl polymer being soluble in THF.[56] In our current study, we focused on poly(6-NCA-R), which is *de facto* poly(*o*-benzamide). Interestingly, the solubility of poly(6-NCA-R) falls between its *para* and *meta* counterparts. We found that poly(6-NCA-R) with alkyl chains as short as an ethyl group was soluble in THF. Poly(6-NCA-Me) is soluble in TFA and only slightly soluble in methylene chloride. Therefore the ^{1}H NMR spectrum of poly(6-NCA-Me) was obtained in a $CF_3COOD/CDCl_3$ mixture (Figure 3-1D), which showed peak integrations matching the structure of an *N*-methyl aromatic polyamide. The polymer structure was further confirmed by the MALDI-TOF-MS (Figure 3-1E), in which the spacing between adjacent peaks was consistent with the molar mass of the *N*-methyl aromatic amide repeating unit.

The poly(6-NCA-R) polymers all demonstrated high thermal stability. For example, poly(6-NCA-C_8H_{17}) showed a $T_{d,5\%}$ (temperature at 5% weight loss) as high as 395 °C when heated at a scan rate of 5 °C/min under a nitrogen atmosphere (Figure 3-2A). This thermal stability is comparable to its para counterparts.[55] Differential scanning calorimetry analysis revealed a melting temperature T_m of 213 °C for poly(6-NCA-C_8H_{17}) (Figure 3-2B). However, at a scan rate of 10/min, T_g was too weak to be clearly identified. As the *N*-alkyl chain length decreases, the polymer's melting temperature increases. Poly(6-NCA-C_5H_{11}) showed a melting transition of 300 °C, while poly(6-NCA-C_3H_7) and poly(6-NCA-C_2H_5) showed no melting transitions within the temperature window of -50 °C to 300 °C. This observation indicates that the T_m of these polymers is close to T_d or that thermal decomposition occurs before melting.

3.3. Conclusions

In conclusion, we successfully developed a catalytic system consisting of a Schiff base metal compound, PPNCl, and propylene oxide for the polymerization of 6-NCA-R to *N*-alkylated ortho-aromatic polyamides. Through the investigation of each component's role in the catalytic system, we have achieved improved control over the polymerization process. Additionally, by varying the length of the *N*-alkyl chain, we were able to tune the polymer solubility and thermal properties. Overall, this study provides insight into the synthesis and characterization of *N*-alkylated ortho-aromatic polyamides, offering control over their solubility and thermal properties through rational design and optimization of the catalytic system and monomer structure. These findings open up new possibilities for the development of advanced polyamide materials with tailored properties for various applications.

3.4. Experimental Section

Materials and Methods

All experiments were performed under a dry nitrogen atmosphere in an MBraun glovebox or using standard Schlenk techniques. Solvents were purified with a two-state solid-state purification system by the method of Grubbs[57] and transferred into a glovebox without exposure to air. NMR solvents were purchased from Cambridge Isotope Laboratories, degassed, and stored over activated molecular sieves prior to use. Propylene oxide was dried over CaH_2 and distilled prior to used and stored in a glovebox. ^{1}H and ^{13}C NMR spectra were recorded on Bruker AV-300, Bruker AV-500, or Bruker DRX-500 spectrometers at room temperature. Chemical shifts are reported with respect to the residual solvent peaks. Molar masses of polymers were determined by size exclusion chromatography using a SEC-MALS instrument at UCLA. SEC-MALS uses a Shimazu Prominence-i LC 2030C 3D equipped with an autosampler, two MZ Analysentechnik MZ-Gel

SDplus LS 5 μm, 300 × 8 mm linear columns, a Wyatt DAWN HELEOS-II, and a Wyatt Optilab T-rEX. The column temperature was set at 40 °C. A flow rate of 0.70 mL/min was used and samples were dissolved in THF. The number average molar mass and molecular weight distribution values were determined using the dn/dc values which were calculated by 100% mass recovery method from the RI signal. Thermal gravimetric analysis (TGA) was performed using a PerkinElmer Pyris Diamond TG/DTA Instruments under nitrogen. The method used was to increase the temperature from 50 to 600 °C at 5 °C/min. Differential Scanning Calorimetry (DSC) was obtained using a PerkinElmer DSC model 8500 heat flow system with Intracooler II. The first heating scan was from 25°C to 300°C at 10 °C/min and the cooling scan was from 300°C to -50°C at 10 °C/min. The second heating scan was from -50°C to 300°C at 10 °C/min and the cooling scan was from 300°C to -50°C at 10 °C/min. The melting transition temperature (T_m), glass transition temperature (T_g) and crystallization temperature (T_c) were obtained from the second cycle after the thermal history was removed on the first heating scan. Ultraviolet-visible (UV-Vis) spectra were collected on an Agilent Cary 60 UV-Vis spectrophotometer. Isatoic anhydride and N-methylisatoic anhydride (6-NCA-Me) were purchased from TCI and used as received. Bis(triphenylphosphine)iminium chloride (PPNCl, 97%, Aldrich) was recrystallized by layering a saturated methylene chloride solution with diethyl ether. (salfen)AlO^iPr (**Al-1**),[24] (salph)AlCl (**Al-2**),[58] and (salph-F)AlCl (**Al-3**)[54] were synthesized following published procedures.

MALDI-TOF-MS

MALDI-TOF-MS analyses were performed on a Bruker UltraFlex mass spectrometer. Acquisition was performed using linear mode. Polymer sample was prepared at a concentration of 5mg/mL using a mixture solvent of TFA: acetonitrile = 1:9. Sinapinic acid was used as the matrix, and the

matrix solution was prepared at a concentration of 15 mg/mL using TA50 (50:50 [v/v] acetonitrile: 0.1% TFA in water) as the solvent. 5 μL of sample solution and 15 μL matrix solution were premixed and 2 μL were spotted on the MALDI plate.

Representative procedure for 6-NCA-R polymerization

The reaction was conducted under nitrogen in a 25 mL Schlenk tube equipped with a Teflon coated stir bar. In a glovebox, the metal compound (4 μmol) and PPNCl (1-5 equiv) were added into the Schlenk tube followed by propylene oxide (0.6 mL). 6-NCA-R was added last. The Schlenk tube was taken out of glovebox and placed in an oil bath with a preset temperature of 80 °C. The Schlenk tube was taken out of the oil bath after a designated period of time. The polymerization reaction was quenched by addition of MeOH. The precipitated polymer was redissolved in dichloromethane and precipitated from MeOH three times, dried *in vacuo* before being subjected to further characterization.

Procedure for attempted redox-switchable copolymerization of 6-NCA-R and PO

Starting with Al-1

The reaction was conducted under nitrogen in a J-young NMR tube, a capillary tube with C_6D_6 was placed in for NMR locking. In a glovebox, **Al-1** (2.9 mg, 4 μmol) and PPNCl (2.3 mg, 1 equiv.) were added into the J-young NMR tube followed by propylene oxide (0.6 mL). 6-NCA-C8H17 (55.1 mg, 0.2 mmol, 50 equiv.) was added last. The tube was taken out of glovebox and placed in an oil bath with a preset temperature of 80 °C. The J-young NMR tube was taken out of the oil bath after 30 minutes, and transferred back into the glovebox. A 0.04 M stock solution of $^{Ac}FcBAr^F$ (^{Ac}Fc = acetylferrocene, BAr^F = tetrakis(3,5-bis(trifluoromethyl)phenyl) borate) in

difluorobenzene (0.1 mL, 4μmol, 1 equiv.) was added. The reaction was left at room temperature for 24 hours before being quenched by addition of MeOH. The reaction was monitored by ^{1}H NMR (Figure B24). The precipitated polymer was redissolved in dichloromethane and precipitated from MeOH three times, dried *in vacuo* before being subjected to further characterization.

Starting with oxidized Al-1 ([(salfen)AlO^{i}Pr][BAr^{F}])

The reaction was conducted under nitrogen in a J-young NMR tube. In a glovebox, **Al-1** (2.9 mg, 4 μmol) and a 0.04 M stock solution of ^{Ac}FcBAr^{F} in difluorobenzene (0.1 mL, 4μmol, 1 equiv.) was added into the J-young NMR tube generate the oxidized **Al-1** *in situ*. 0.6 mL PO was added followed by PPNCl (2.3 mg, 1 equiv.). Upon the addition of PPNCl, the dark red solution turned orange immediately along with the formation of a black precipitate.

Synthesis of 6-NCA-R

1-octyl-2H-benzo[d][1,3]oxazine-2,4(1H)-dione (6-NCA-C$_8$H$_{17}$)

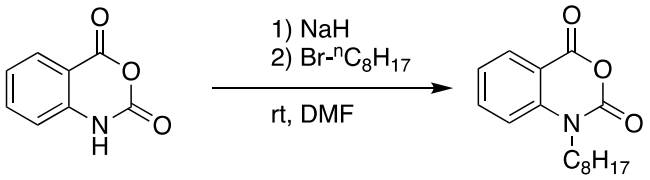

6-NCA-C$_8$H$_{17}$ was synthesized following a modified published procedure.[59] The synthesis was carried out under a nitrogen atmosphere. Isatoic anhydride (1.63 g, 10 mmol, 1 equiv) and 15 mL of a freshly distilled DMF were added to a 100 mL round bottom flask, then 90% NaH (0.4 g, 15 mmol, 1.5 equiv) was added slowly to the reaction mixture. After 1 h, 1-bromooctane (2.32 g,12 mmol, 1.2 equiv) was added to the reaction mixture, and the reaction was stirred under nitrogen for 12 hours. After completion, the reaction mixture was added dropwise into 500 mL of ice water

to afford a solid precipitate. After filtration, the filter cake was washed with water. The solid was collected and recrystallized from diethyl ether to form white needle-shaped crystals (yield: 2.0 g, 80%). This compound was reported previously.[59] **^{1}H NMR** (500 MHz, 298 K, $CDCl_3$) δ (ppm): 8.15 (d, *J* = 7.7 Hz, 1H, Ar*H*), 7.75 (t, *J* = 8.2 Hz, 1H, Ar*H*), 7.36 (t, *J* = 7.9 Hz, 1H, Ar*H*), 7.16 (d, *J* = 8.5 Hz, 1H, Ar*H*), 4.04 (m, 2H, NC*H*$_2$$(CH_2)_6CH_3$), 1.74 (m, 2*H* , -C*H*$_2$$(CH_2)_5CH_3$), 1.55–1.32 (m, 10H, -C*H*$_2$$(CH_2)_4CH_3$, -C*H*$_2$$(CH_2)_3CH_3$, -C*H*$_2$$(CH_2)_2CH_3$, -C*H*$_2$$CH_2CH_3$, -C*H*$_2$$CH_3$), 0.96 (t, *J* = 6.8 Hz, 3H, -C*H*$_3$). **^{13}C NMR** (125 MHz, 298 K, $CDCl_3$) δ (ppm): 158.6 (Ar*C*OO), 147.7(ArN*C*OO), 141.4(Ar*C*), 137.2(Ar*C*), 130.9(Ar*C*), 123.8(Ar*C*), 113.9(Ar*C*), 111.8(Ar*C*), 45.0(N*C*$H_2$$(CH_2)_6CH_3$), 31.7(NCH$_2$*C*H$_2$$(CH_2)_5CH_3$), 29.2(N$(CH_2)_2$*C*H$_2$$(CH_2)_4CH_3$), 29.1(N$(CH_2)_3$*C*H$_2$$(CH_2)_3CH_3$), 26.8(N$(CH_2)_4$*C*H$_2$$(CH_2)_2CH_3$), 26.6(N$(CH_2)_5$*C*H$_2CH_2CH_3$), 22.6(N$(CH_2)_6$*C*H$_2CH_3$), 14.0(N$(CH_2)_7CH_3$).

1-pentyl-2H-benzo[d][1,3]oxazine-2,4(1H)-dione (6-NCA-C_5H_{11})

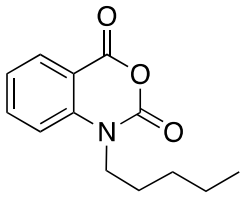

6-NCA-C_5H_{11}

6-NCA-C_5H_{11} was prepared using the same procedure as 6-NCA-C_8H_{17}. White needle-shaped crystals were obtained with a yield of 1.63 g (70%). This compound was reported previously.[60] **^{1}H NMR** (500 MHz, 298 K, $CDCl_3$) δ (ppm): 8.11 (d, *J* = 7.7 Hz, 1H, Ar*H*), 7.73 (t, *J* = 8.2 Hz, 1H, Ar*H*), 7.25 (t, *J* = 7.9 Hz, 1H, Ar*H*), 7.14 (d, *J* = 8.5 Hz, 1H, Ar*H*), 4.01 (m, 2H, NC*H*$_2$$(CH_2)_3CH_3$), 1.72 (m, 2*H*, -C*H*$_2$$(CH_2)_3CH_3$), 1.42–1.31 (m, 4H, -C*H*$_2$$CH_2CH_3$, -C*H*$_2$$CH_3$), 0.88 (t, *J* = 6.8 Hz, 3H, -C*H*$_3$). **^{13}C NMR** (125 MHz, 298 K, $CDCl_3$) δ (ppm): 158.6 (Ar*C*OO), 147.7(ArN*C*OO),

141.4(Ar*C*), 137.3(Ar*C*), 130.9(Ar*C*), 123.8(Ar*C*), 113.9(Ar*C*), 111.8(Ar*C*), 45.0(N*C*H_2(CH_2)$_3$$CH_3$), 28.7(N$CH_2$*C*$H_2$($CH_2$)$_2$$CH_3$), 26.6 (N($CH_2$)$_2$*C*$H_2$$CH_2$$CH_3$), 22.3 (N($CH_2$)$_3$*C*$H_2$$CH_3$), 13.9(N($CH_2$)$_4$*C*$H_3$).

1-propyl-2H-benzo[d][1,3]oxazine-2,4(1H)-dione (6-NCA-C_3H_7)

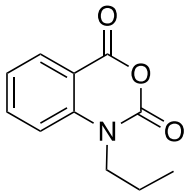

6-NCA-C_3H_7

6-NCA-C_3H_7 was prepared using the same procedure as 6-NCA-C_8H_{17}. White needle-shaped crystals were obtained with a yield of 1.47 g (72%). This compound was reported previously.[60] **^{1}H NMR** (500 MHz, 298 K, $CDCl_3$) δ (ppm): 8.11 (d, *J* = 7.7 Hz, 1H, Ar*H*), 7.75 (t, J=8.2 Hz, 1H, Ar*H*), 7.26 (t, *J* = 7.9 Hz, 1H, Ar*H*), 7.17 (d, *J* = 8.5 Hz, 1H, Ar*H*), 4.00 (m, 2H, NC*H*$_2$$CH_2$$CH_3$), 1.77 (m, 2*H*, -C*H*$_2$$CH_3$), 1.02(t, *J* = 6.8 Hz, 3H, -C*H*$_3$). **^{13}C NMR** (125 MHz, 298 K, $CDCl_3$) δ (ppm): 158.6 (Ar*C*OO), 147.7(ArN*C*OO), 141.4(Ar*C*), 137.3(Ar*C*), 130.9(Ar*C*), 123.9(Ar*C*), 113.9(Ar*C*), 111.7(Ar*C*), 46.4(N*C*$H_2$$CH_2$$CH_3$), 20.2(N$CH_2$*C*$H_2$$CH_3$), 11.0(N($CH_2$)$_2$$CH_3$).

1-ethyl-2H-benzo[d][1,3]oxazine-2,4(1H)-dione (6-NCA-C_2H_5)

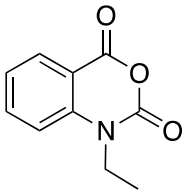

6-NCA-C_2H_5

6-NCA-C_2H_5 was prepared using the same procedure as 6-NCA-C_8H_{17}. White needle-shaped crystals were obtained with a yield of 1.33 g (70%). This compound was reported previously.[60] **^{1}H NMR** (500 MHz, 298 K, $CDCl_3$) δ (ppm): 8.13 (d, J = 7.7 Hz, 1H, Ar*H*), 7.76 (t, J=8.2 Hz, 1H, Ar*H*), 7.27 (t, J = 7.9 Hz, 1H, Ar*H*), 7.20 (d, J = 8.5 Hz, 1H, Ar*H*), 4.12 (m, 2H, NC*H*$_2$$CH_3$), 1.36 (t, J = 6.8 Hz, 3H, NCH_2C*H*$_3$). **^{13}C NMR** (125 MHz, 298 K, $CDCl_3$) δ (ppm): 158.6 (Ar*C*OO), 147.5(ArN*C*OO), 141.1(Ar*C*), 137.4(Ar*C*), 130.9(Ar*C*), 123.9(Ar*C*), 113.8(Ar*C*), 111.8(Ar*C*), 40.1(NCH_2CH_3), 12.1(NCH_2CH_3)

Table B-1. Solubility of poly(6-NCA-R) in organic solvents.

	Hexanes	**Et_2O**	**THF**	**CH_2Cl_2**	**MeOH**	**DMF**
Poly(6-NCA-Me)	-	-	-	+	-	-
Poly(6-NCA-C_2H_5)	-	-	++	++	-	++
Poly(6-NCA-C_3H_7)	-	-	++	++	-	++
Poly(6-NCA-C_5H_{11})	-	-	++	++	-	++
Poly(6-NCA-C_8H_{17})	-	-	++	++	-	+

++: soluble at room temperature, +: soluble when heated, -: insoluble

3.5. Appendix B

NMR spectra

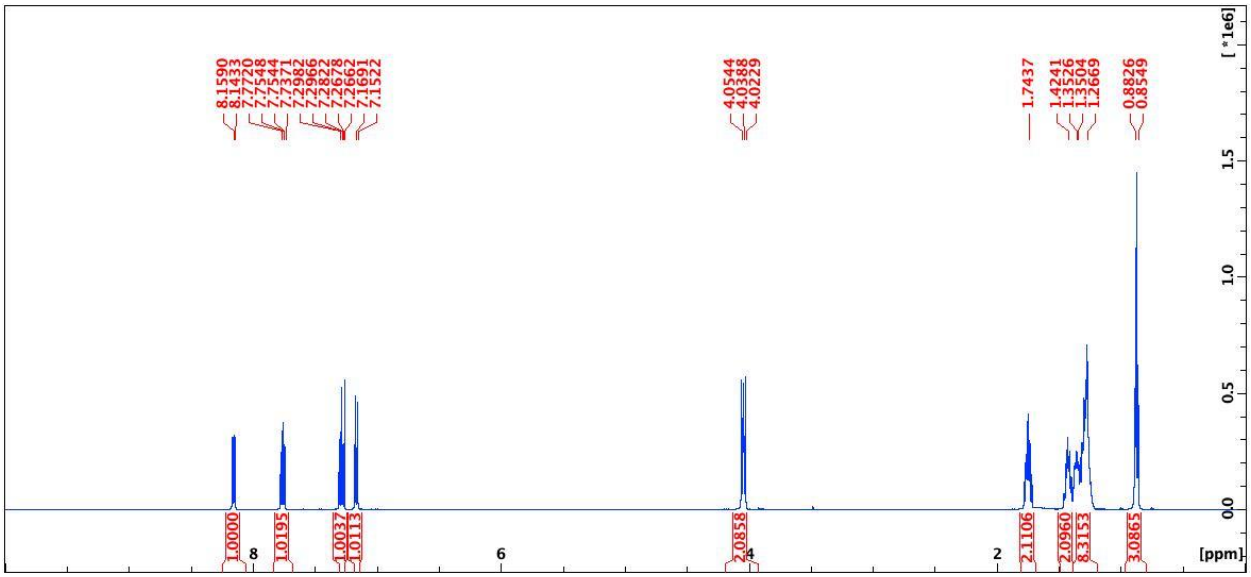

Figure B1. ^{1}H NMR spectrum (500 MHz, 298 K, $CDCl_3$) of 6-NCA-C_8H_{17}.

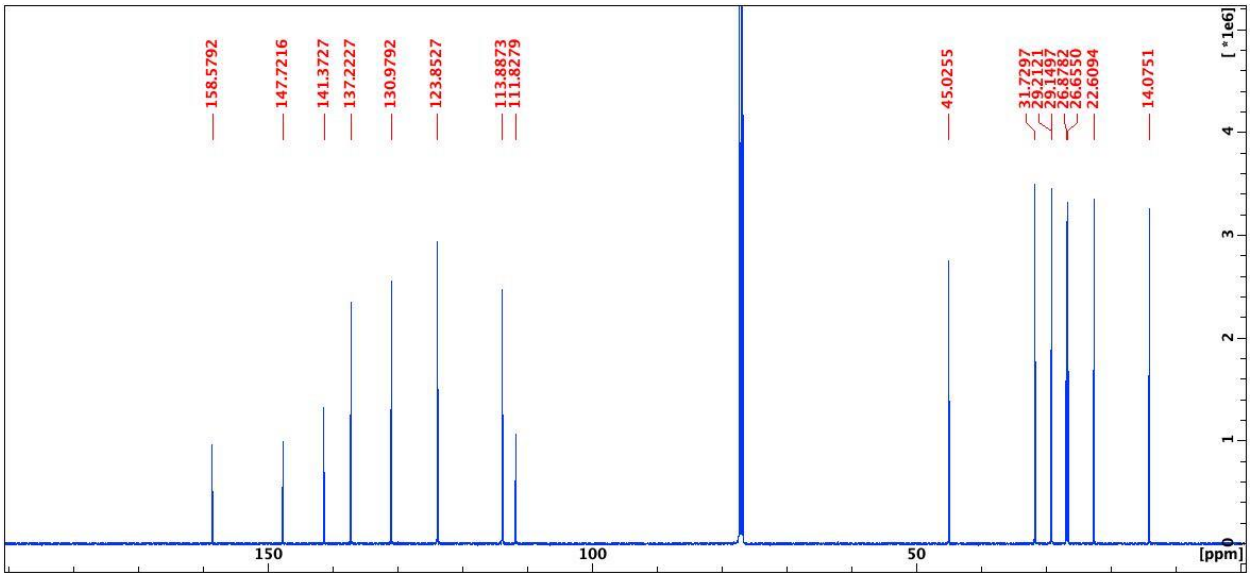

Figure B2. $^{13}C\{^{1}H\}$ NMR spectrum (125 MHz, 298 K, $CDCl_3$) of 6-NCA-C_8H_{17}.

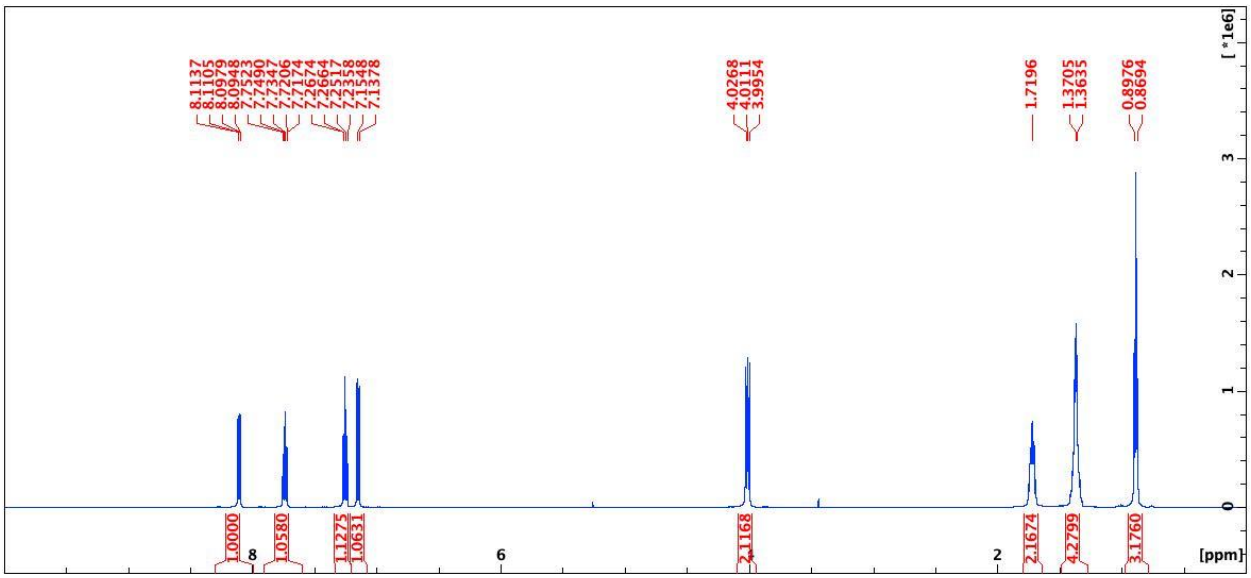

Figure B3. ^{1}H NMR spectrum (500 MHz, 298 K, $CDCl_3$) of 6-NCA-C_5H_{11}.

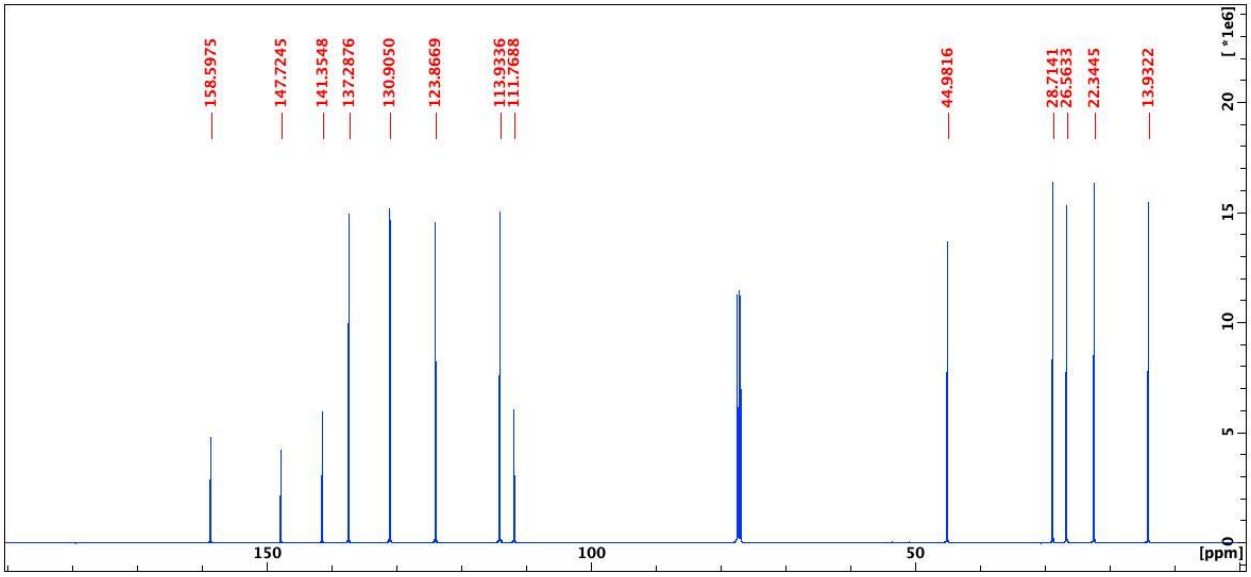

Figure B4. $^{13}C\{^{1}H\}$ NMR spectrum (125 MHz, 298 K, $CDCl_3$) of 6-NCA-C_5H_{11}.

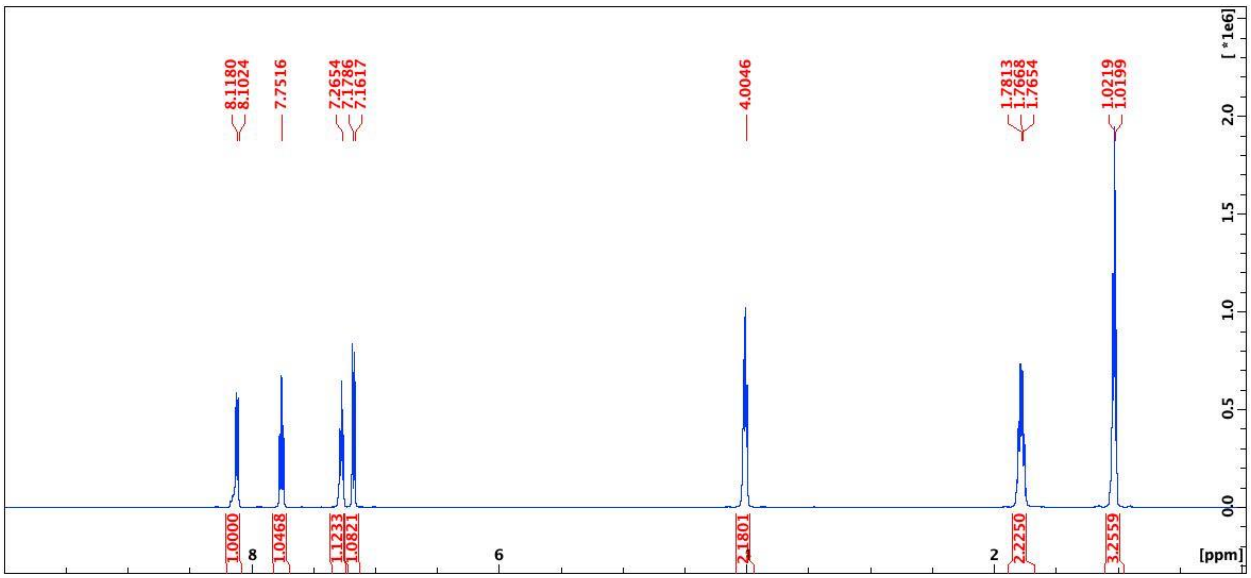

Figure B5. ^{1}H NMR spectrum (500 MHz, 298 K, $CDCl_3$) of 6-NCA-C_3H_7.

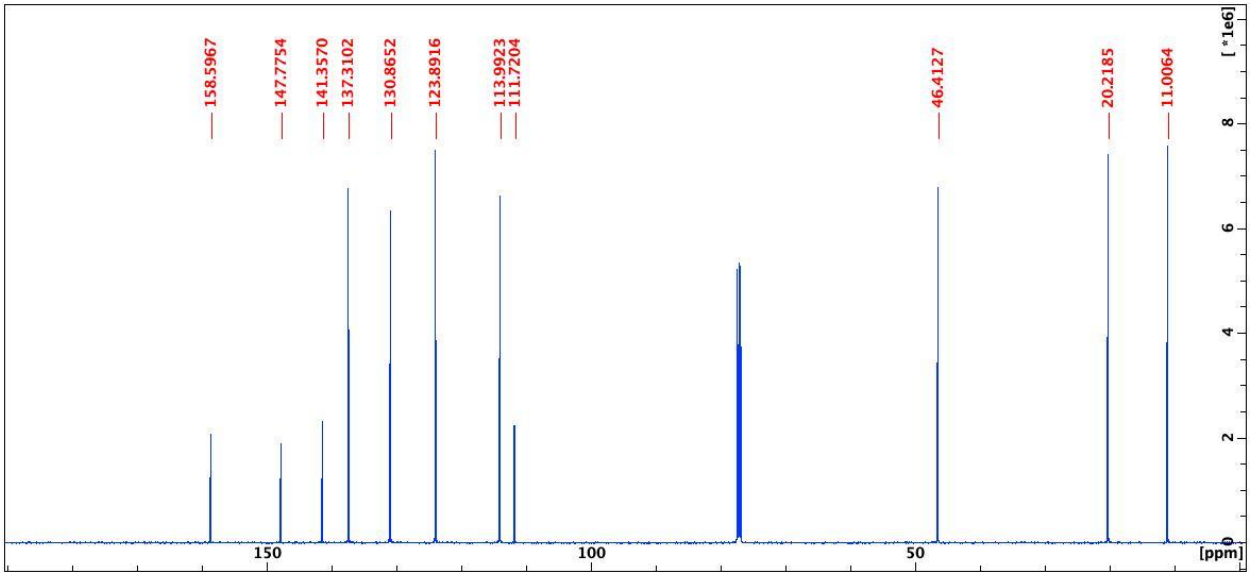

Figure B6. $^{13}C\{^{1}H\}$ NMR spectrum (125 MHz, 298 K, $CDCl_3$) of 6-NCA-C_3H_7.

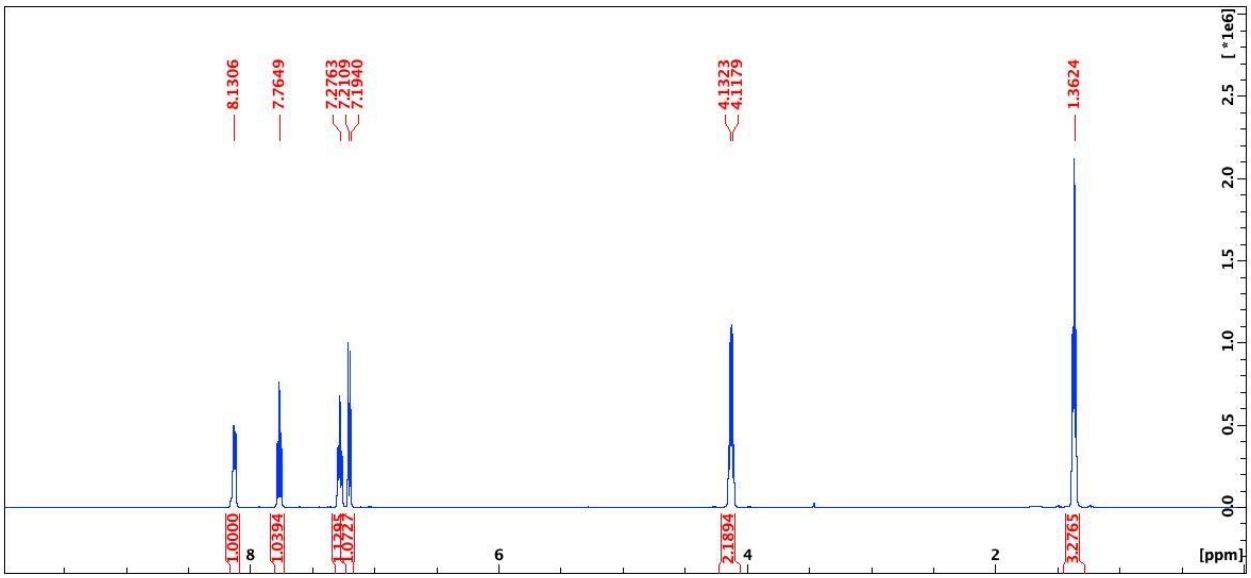

Figure B7. ^{1}H NMR spectrum (500 MHz, 298 K, $CDCl_3$) of 6-NCA-C_2H_5.

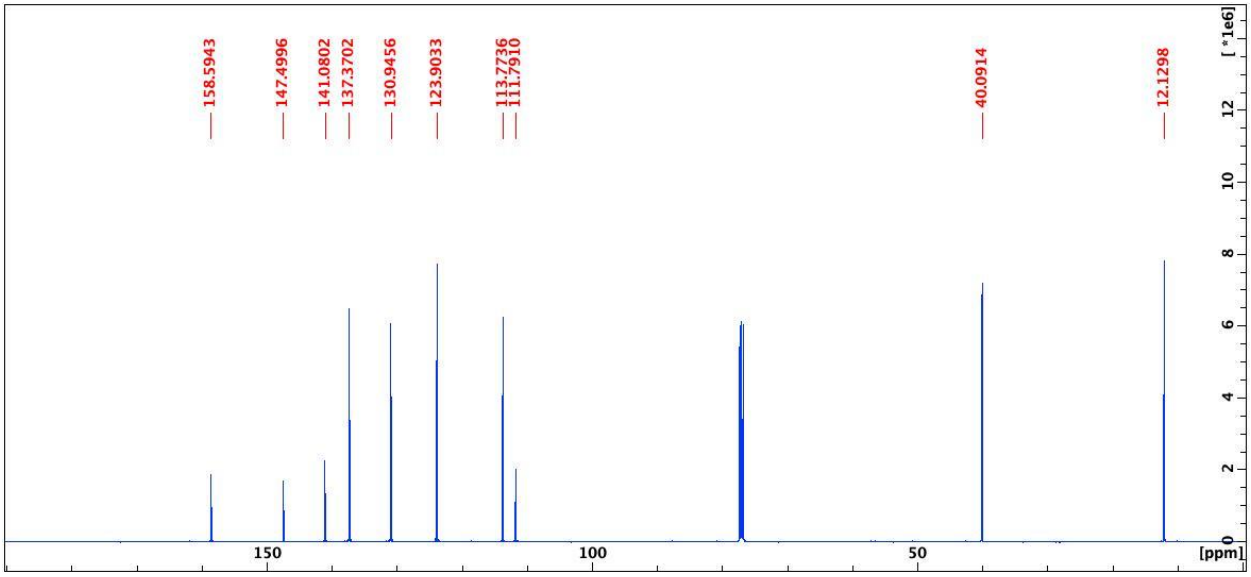

Figure B8. $^{13}C\{^{1}H\}$ NMR spectrum (125 MHz, 298 K, $CDCl_3$) of 6-NCA-C_2H_5.

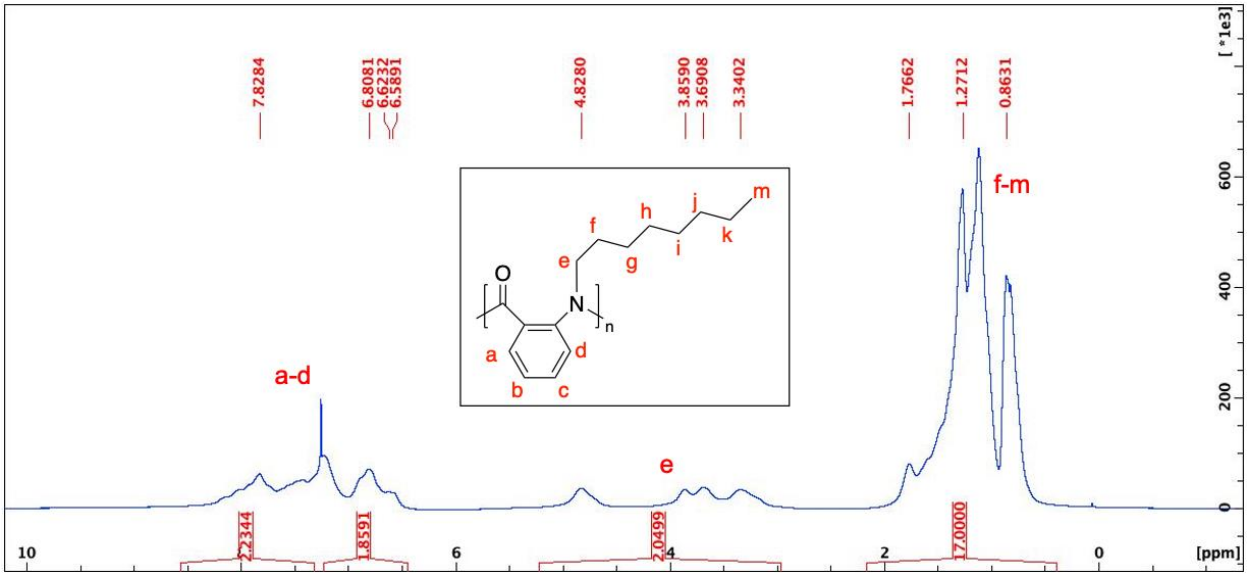

Figure B9. ^{1}H NMR spectrum (500 MHz, 298 K, $CDCl_3$) of poly(6-NCA-C_8H_{17}) (Table 3-1, entry 7).

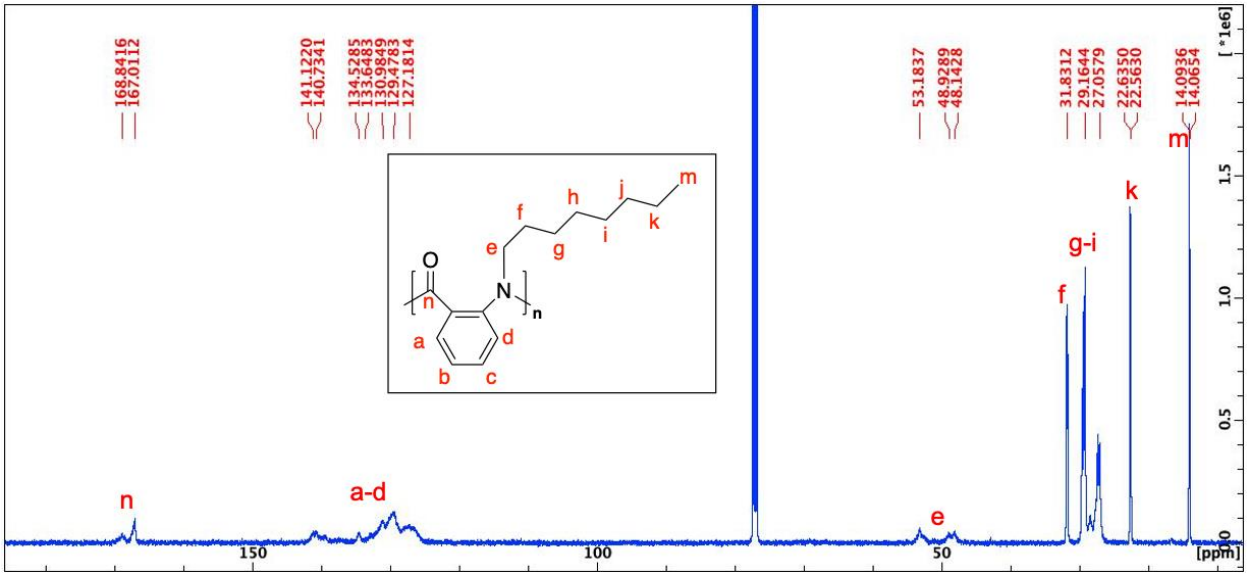

Figure B10. $^{13}C\{^{1}H\}$ NMR spectrum (125 MHz, 298 K, $CDCl_3$) of poly (6-NCA-C_8H_{17}) (Table 3-1, entry 7).

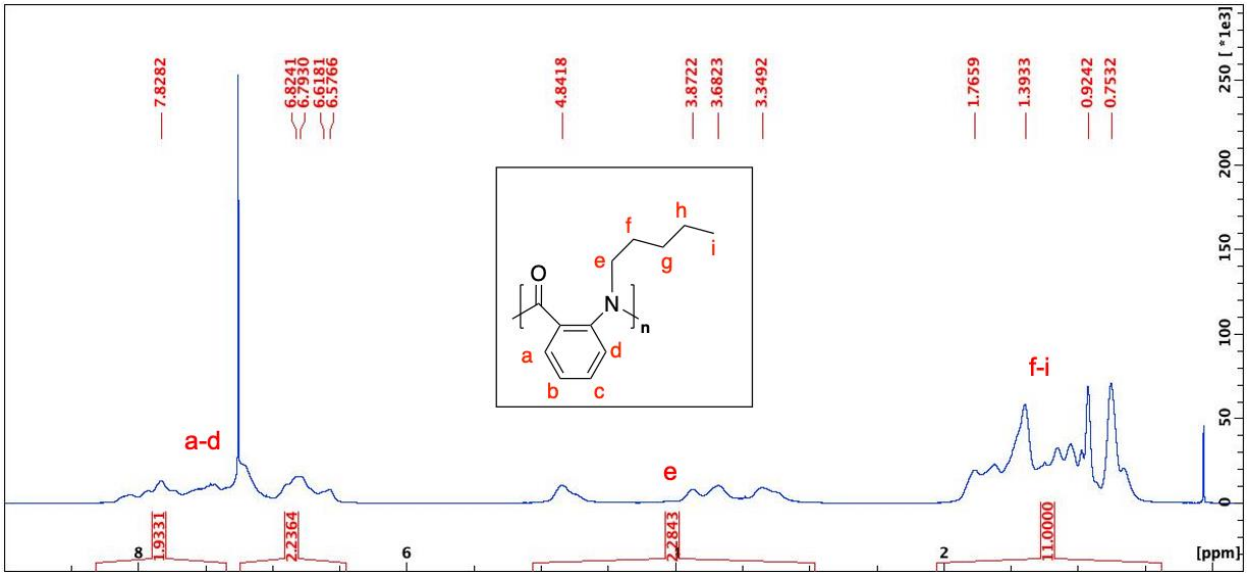

Figure B11. ^{1}H NMR spectrum (500 MHz, 298 K, $CDCl_3$) of poly (6-NCA-C_5H_{11}) (Table 3-1, entry 17).

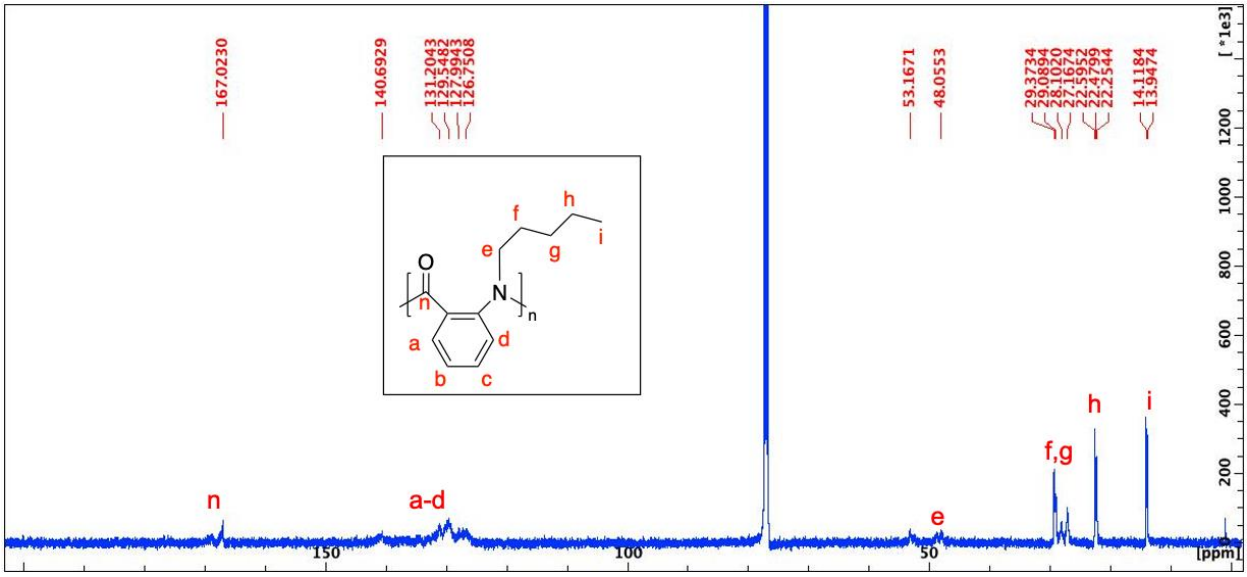

Figure B12. $^{13}C\{^{1}H\}$ NMR spectrum (125 MHz, 298 K, $CDCl_3$) of poly (6-NCA-C_5H_{11}) (Table 3-1, entry 17).

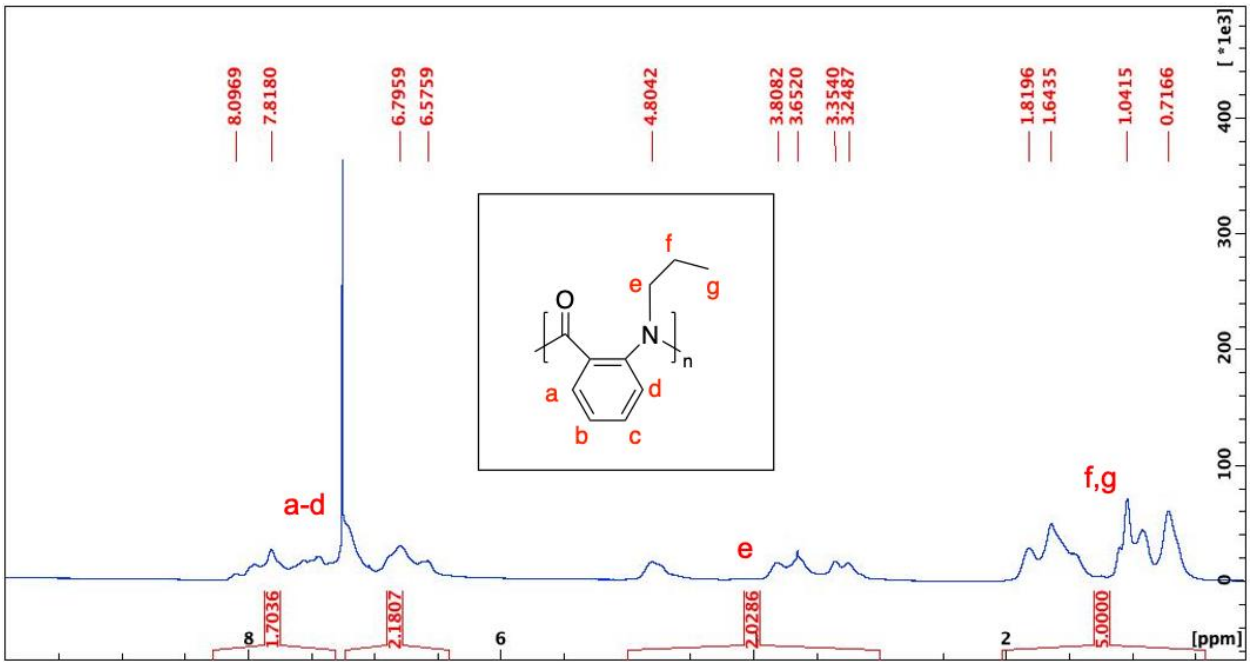

Figure B13. ^{1}H NMR spectrum (500 MHz, 298 K, $CDCl_3$) of poly (6-NCA-C_3H_7) (Table 3-1, entry 18).

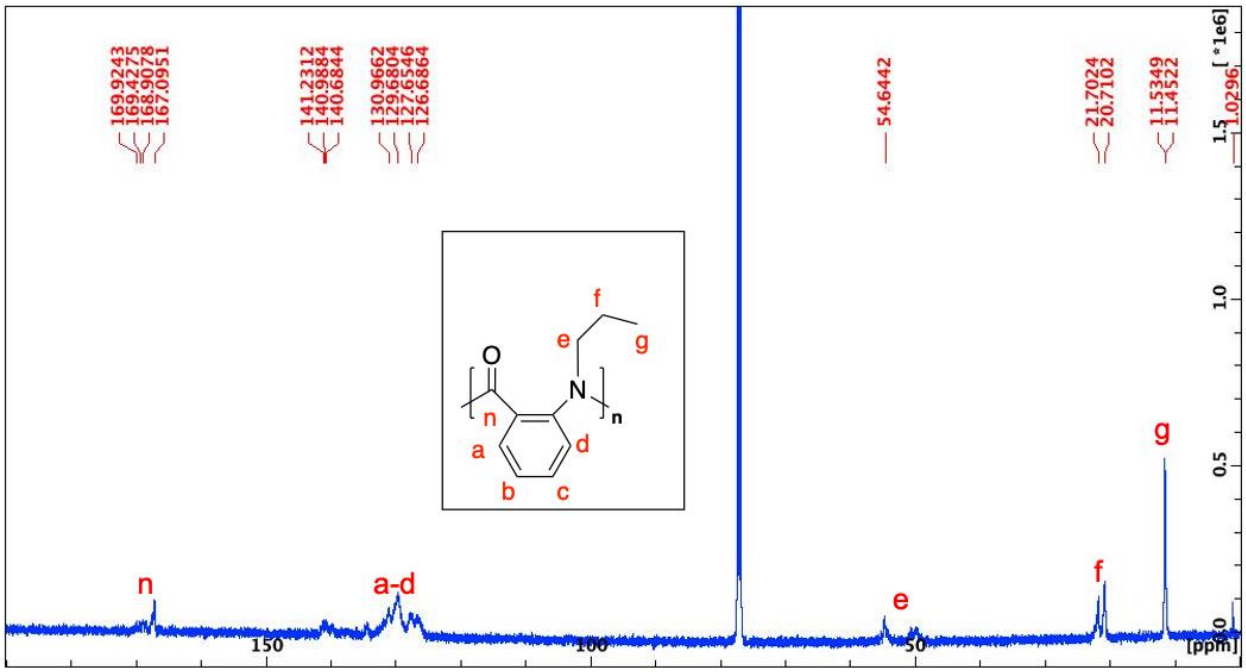

Figure B14. $^{13}C\{^{1}H\}$ NMR spectrum (125 MHz, 298 K, $CDCl_3$) of poly (6-NCA-C_3H_7) (Table 3-1, entry 18).

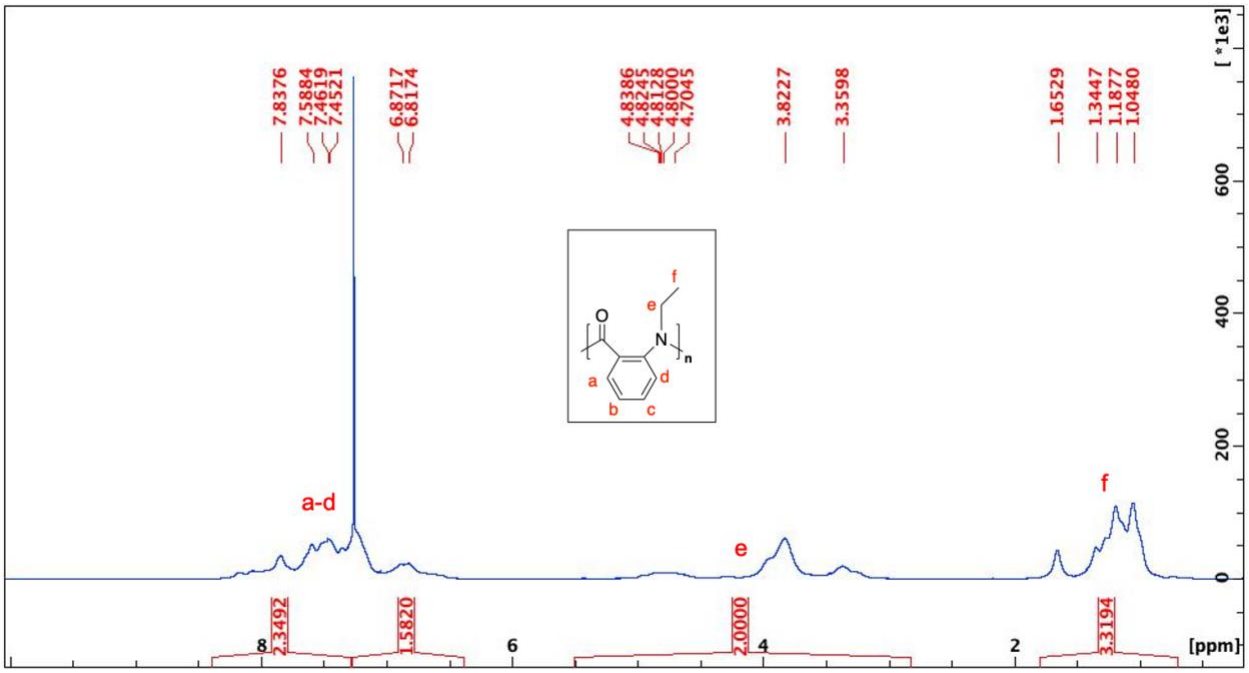

Figure B15. ^{1}H NMR spectrum (500 MHz, 298 K, $CDCl_3$) of poly (6-NCA-C_2H_5) (Table 3-1, entry 19).

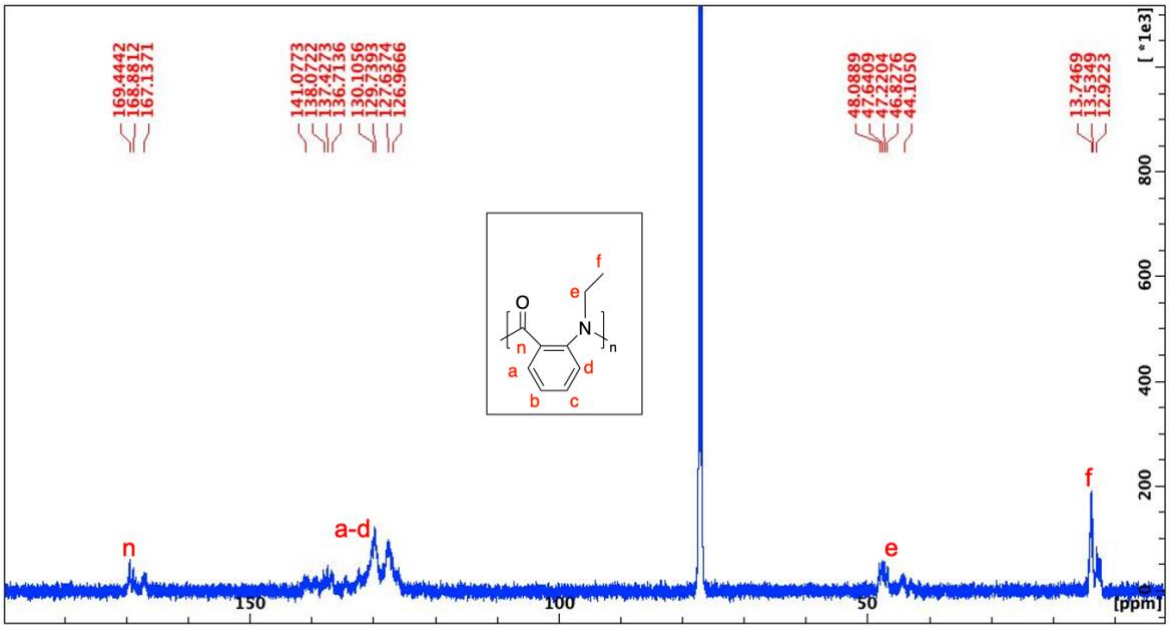

Figure B16. $^{13}C\{^{1}H\}$ NMR spectrum (125 MHz, 298 K, $CDCl_3$) of poly (6-NCA-C_2H_5) (Table 3-1, entry 19).

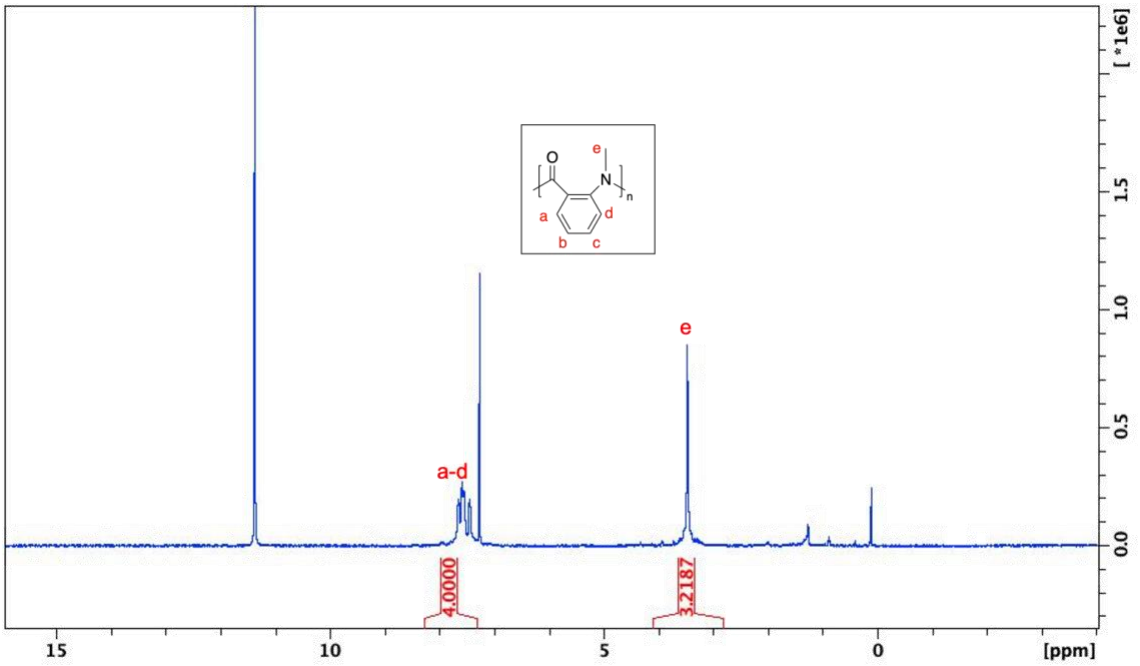

Figure B17. ^{1}H NMR spectrum (500 MHz, 298 K, CF_3COOD: $CDCl_3$ = 1:5) of poly (6-NCA-Me) (Table 3-1, entry 20).

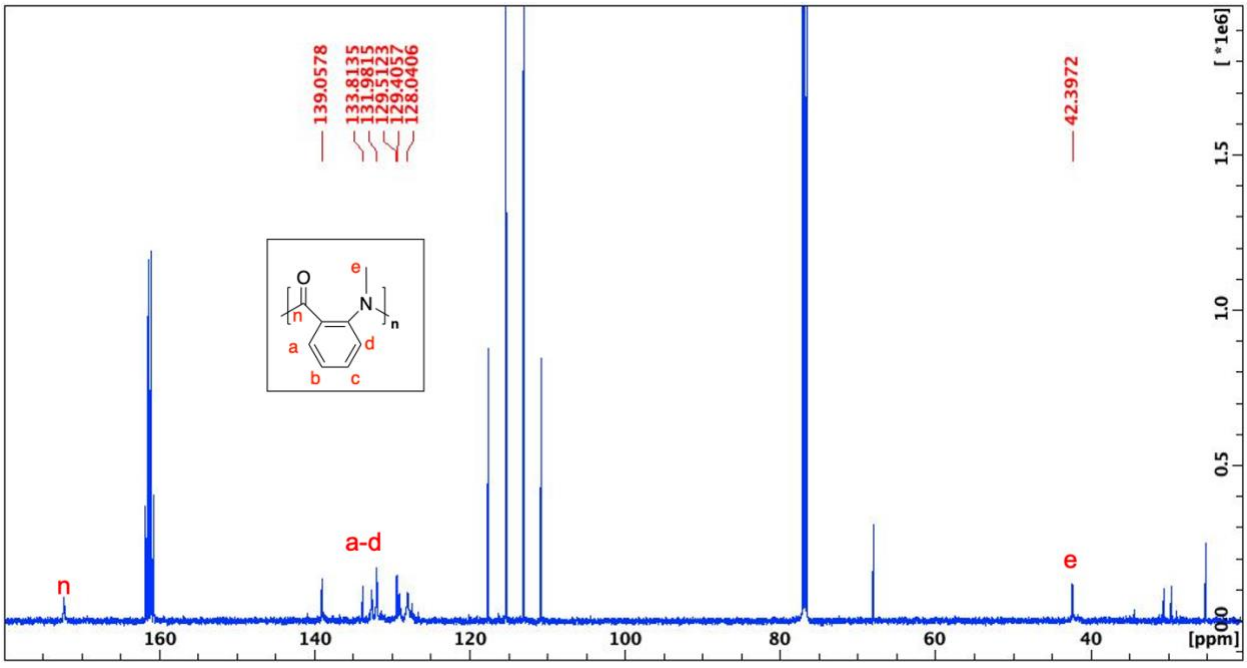

Figure B18. $^{13}C\{^{1}H\}$ NMR spectrum (125 MHz, 298 K, CF_3COOD: $CDCl_3$ = 1:5) of poly (6-NCA-Me) (Table 3-1, entry 20).

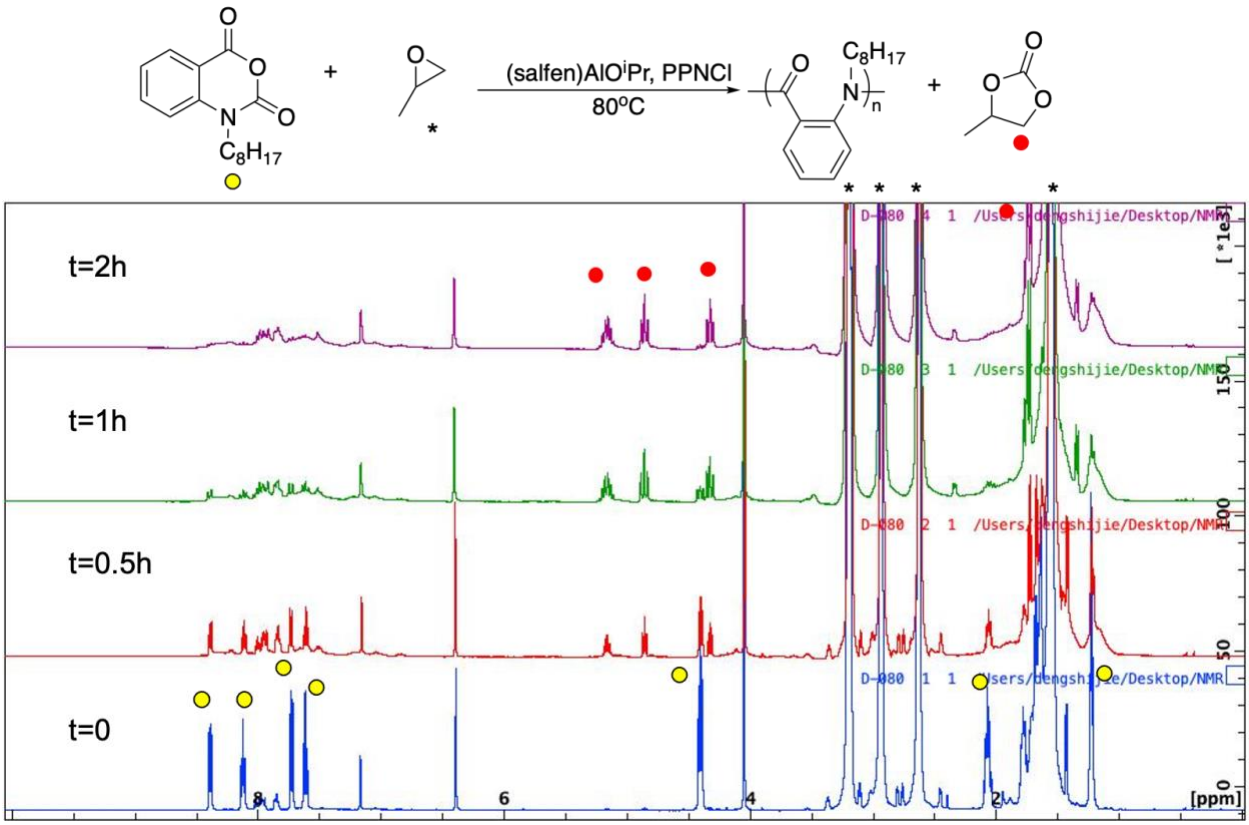

Figure B19. Polymerization progress as monitored by ^{1}H NMR spectroscopy (500 MHz, 298 K, C_6D_6); 1,3,5-trimethoxybeneze (TMB) was used as an internal standard. **Al-1** : PPNCl : 6-NCA-C_8H_{17} : TMB = 1 : 2 : 50 : 25; 0.6 mL PO was used as a solvent. The polymerization reaction was carried out in a J-young NMR tube, a flame-sealed capillary tube with C_6D_6 was placed in for locking. The reaction was heated to 80 °C.

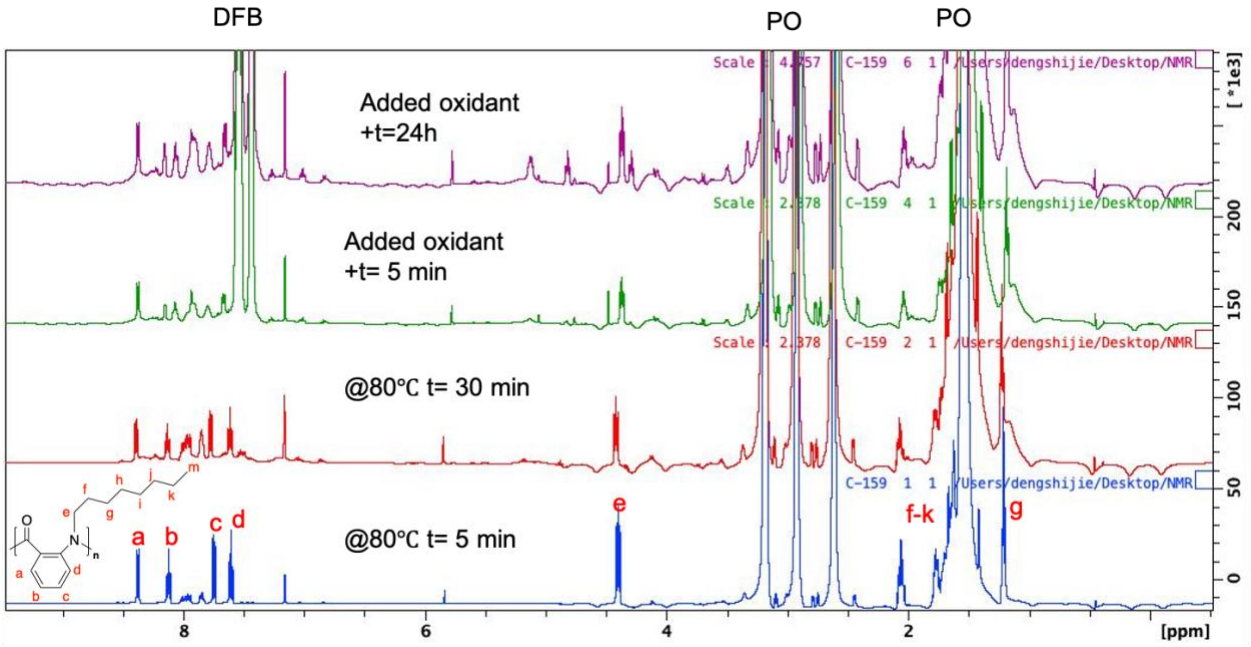

Figure B20. Polymerization progress was monitored by ^{1}H NMR spectroscopy (500 MHz, 298 K, C_6D_6); **Al-1** : PPNCl : 6-NCA-C_8H_{17} = 1 : 2 : 50; 0.6 mL PO was used as a solvent. The polymerization reaction was carried out in a J-young NMR tube, a flame-sealed capillary tube with C_6D_6 was placed in for locking. The reaction was heated to 80 °C. The spectra were taken after heating at 80 °C for 5 minutes (blue) and for 30 minutes (red) respectively. The J-young NMR tube was then transferred into glovebox to add 1 equivalent of ^{Ac}FcBAr^{F}. Two additional spectra were taken after the reaction was left at room temperature for 5 minutes (green) and 24 hours (purple).

SEC traces

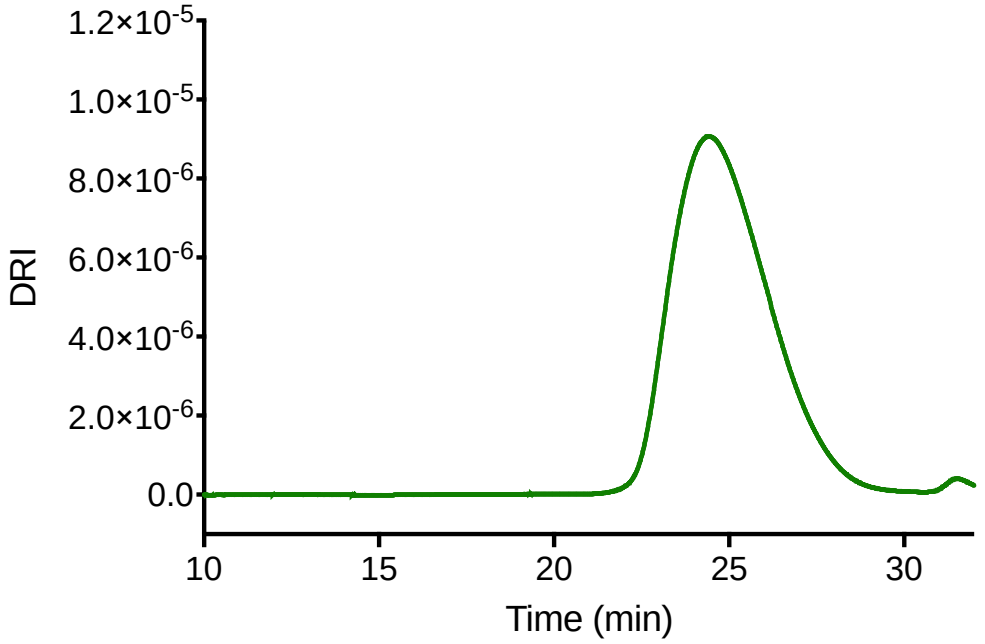

Figure B21. SEC trace of poly (6-NCA-C_8H_{17}) (Table 3-1, entry 2).

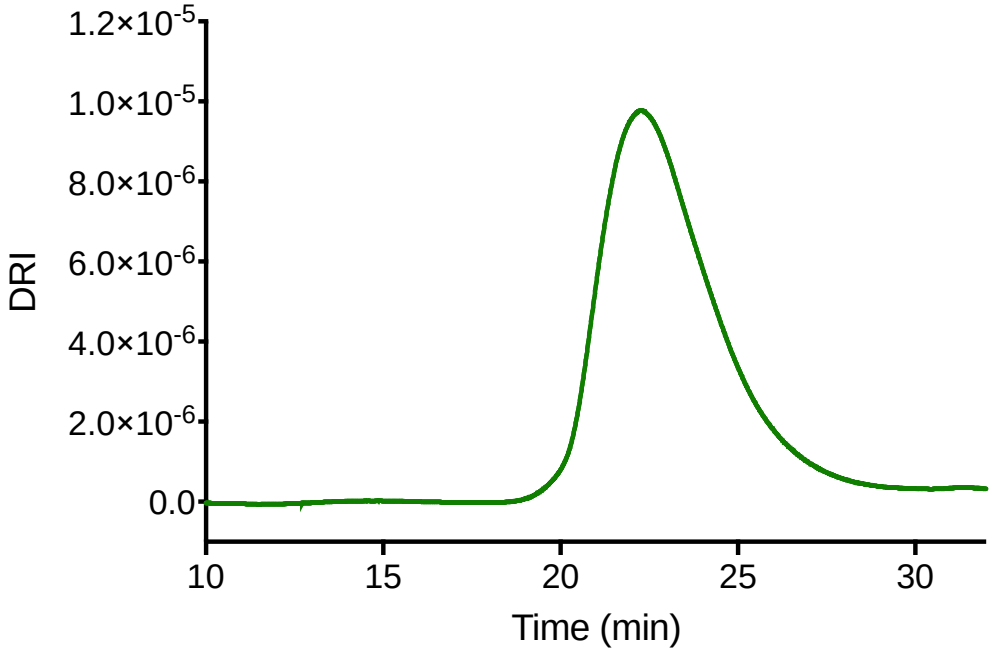

Figure B22. SEC trace of poly (6-NCA-C_8H_{17}) (Table 3-1, entry 7).

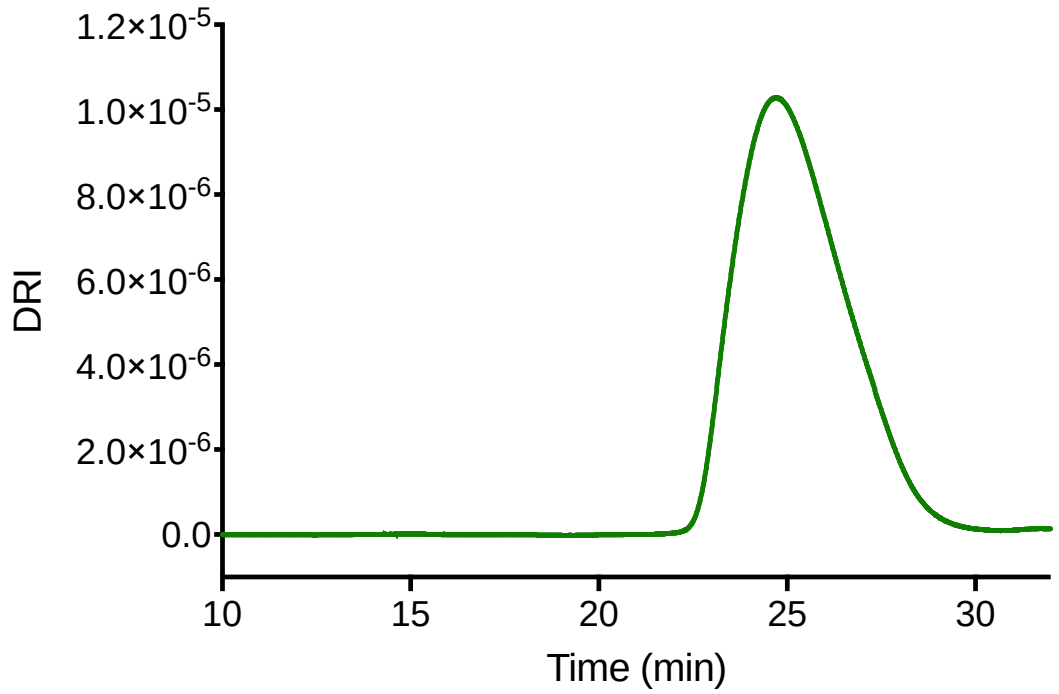

Figure B23. SEC trace of poly (6-NCA-C_8H_{17}) (Table 3-1, entry 8).

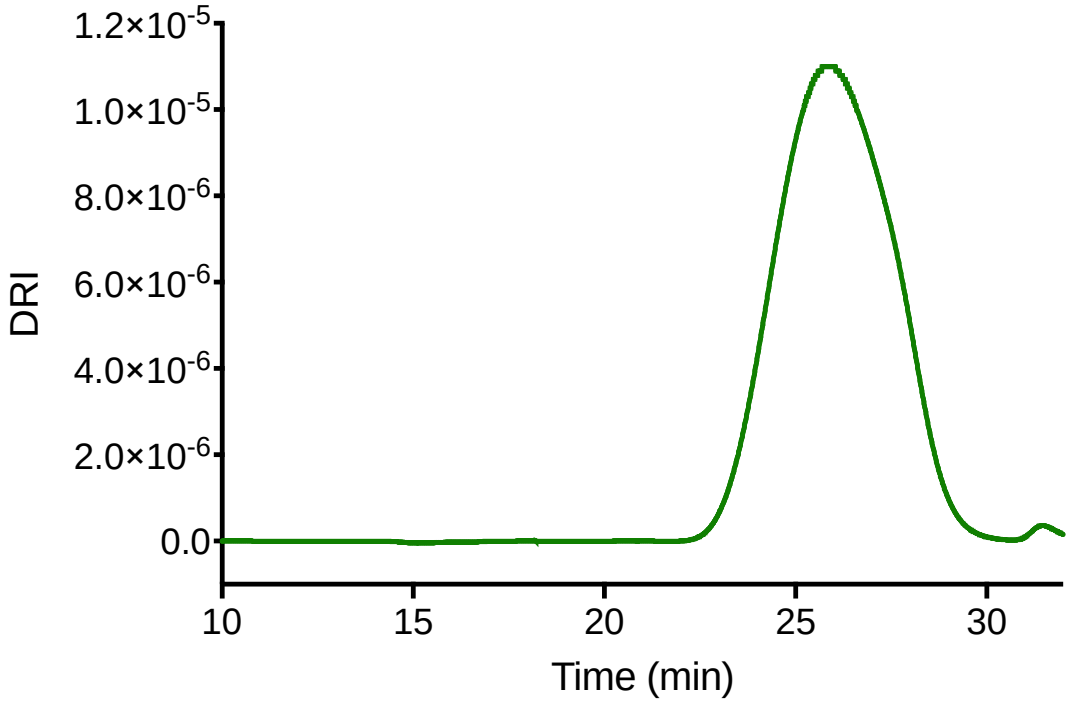

Figure B24. SEC trace of poly (6-NCA-C_8H_{17}) (Table 3-1, entry 10).

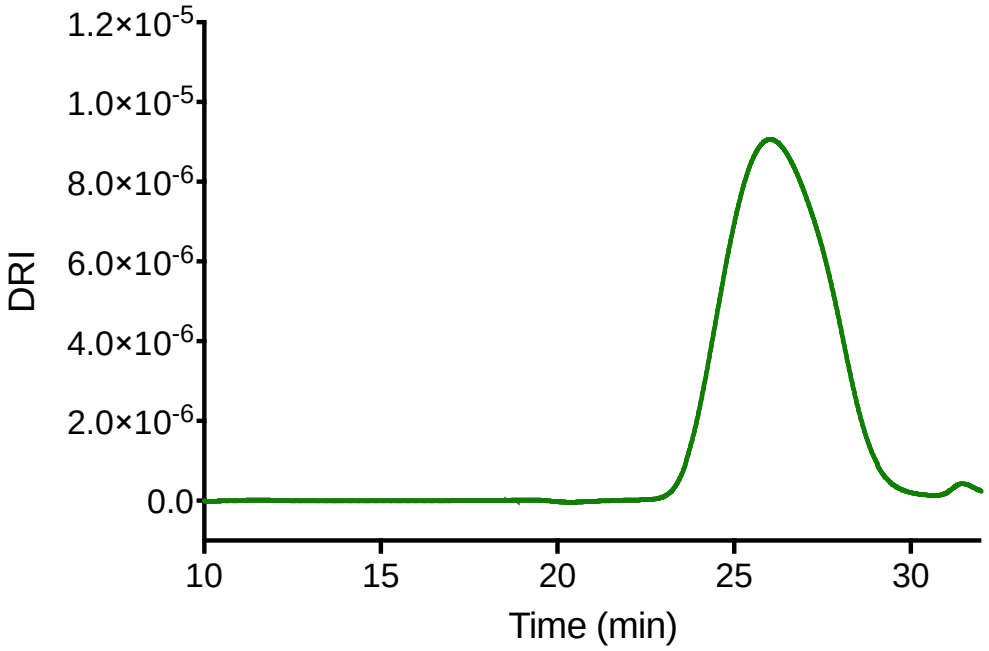

Figure B25. SEC trace of poly (6-NCA-C_8H_{17}) (Table 3-1, entry 11).

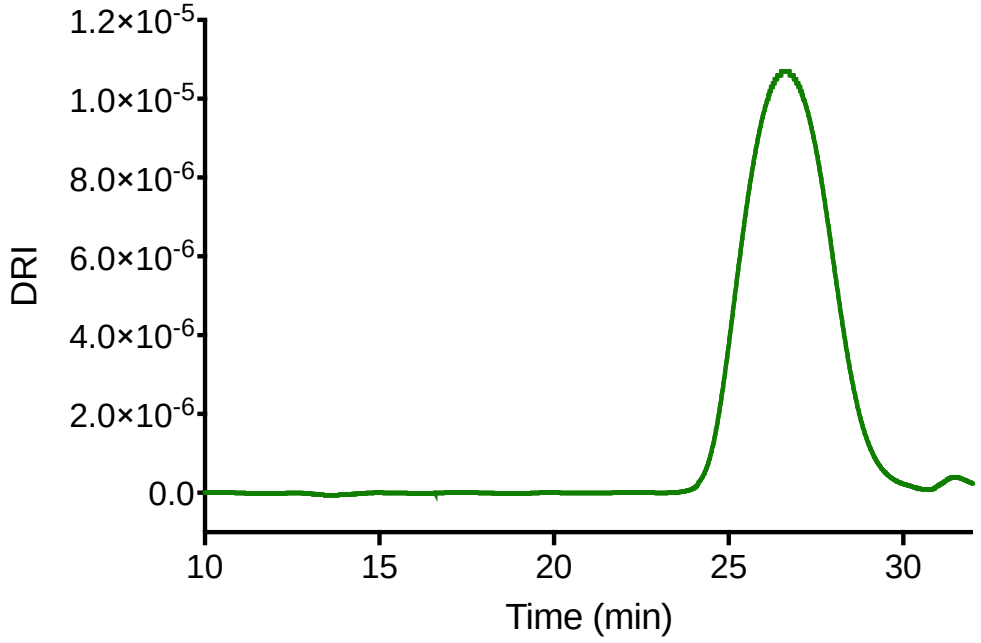

Figure B26. SEC trace of poly (6-NCA-C_8H_{17}) (Table 3-1, entry 12).

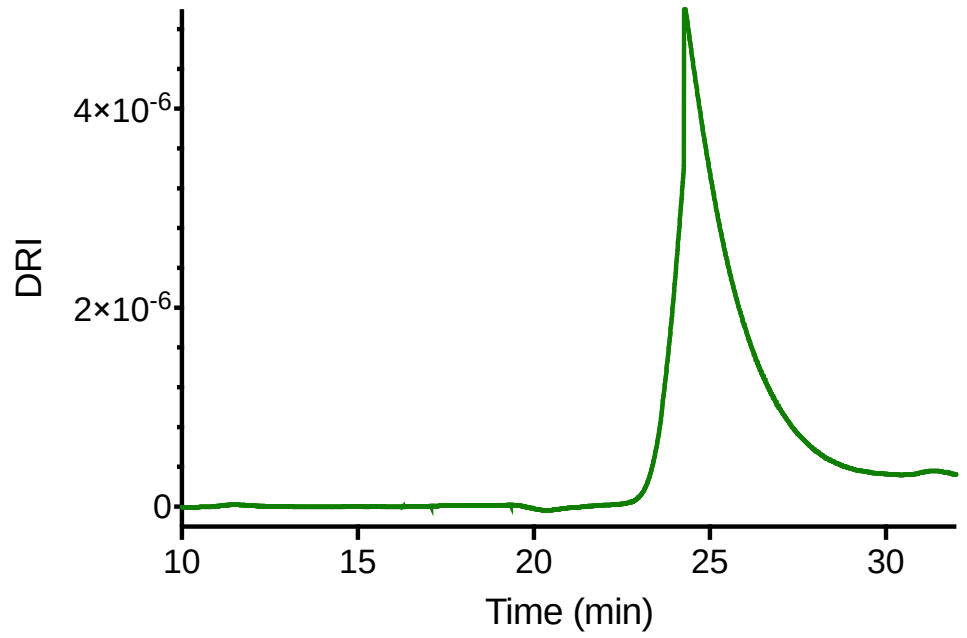

Figure B27. SEC trace of poly (6-NCA-C_8H_{17}) (Table 3-1, entry 13).

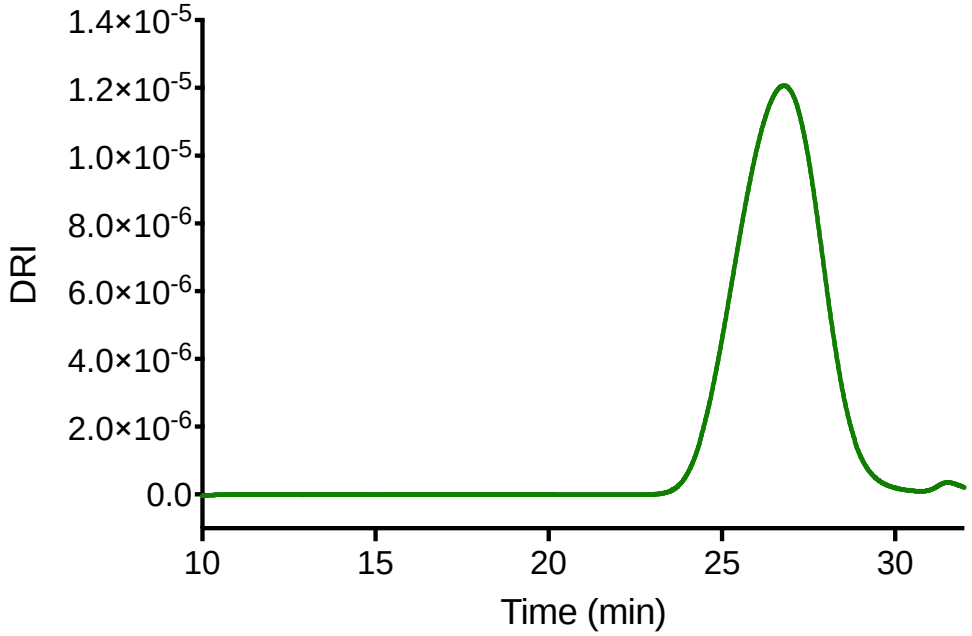

Figure B28. SEC trace of poly (6-NCA-C_8H_{17}) (Table 3-1, entry 14).

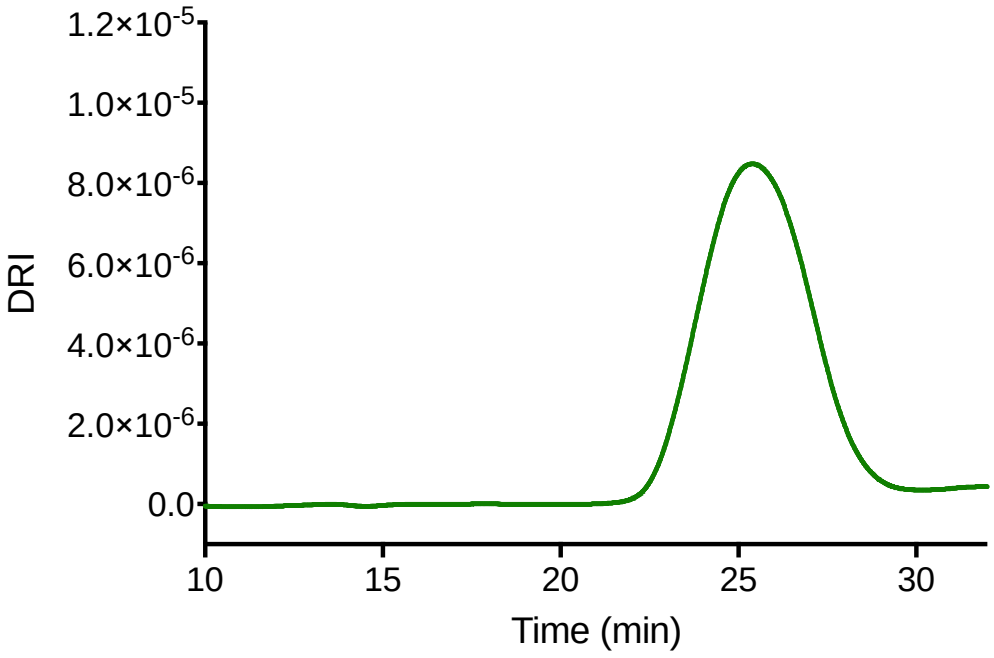

Figure B29. SEC trace of poly (6-NCA-C_8H_{17}) (Table 3-1, entry 15).

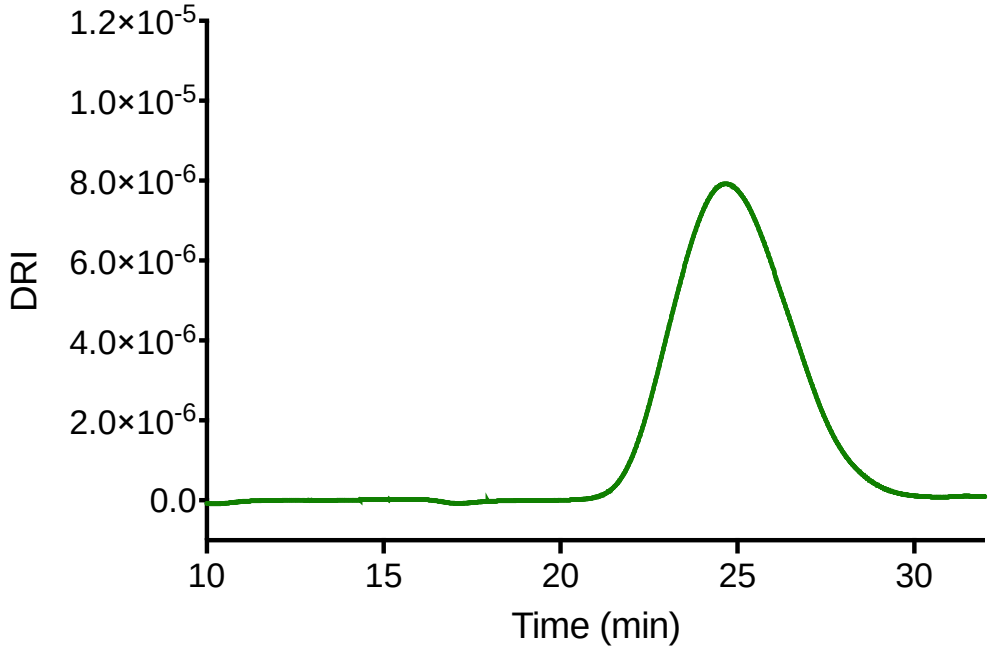

Figure B30. SEC trace of poly (6-NCA-C_8H_{17}) (Table 3-1, entry 16).

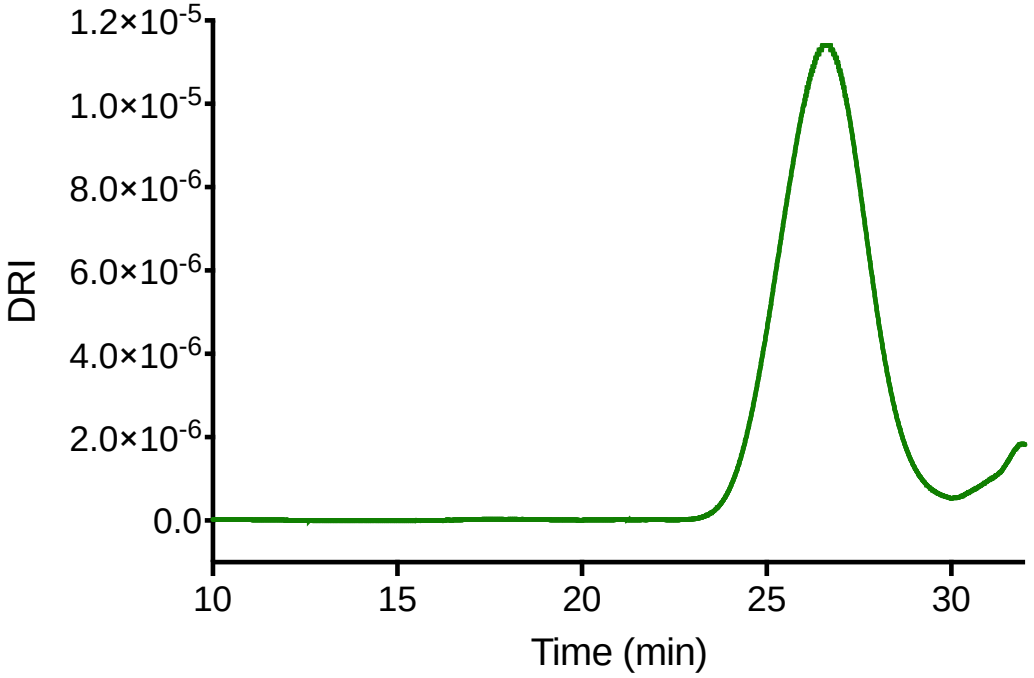

Figure B31. SEC trace of poly (6-NCA-C_5H_{11}) (Table 3-1, entry 17).

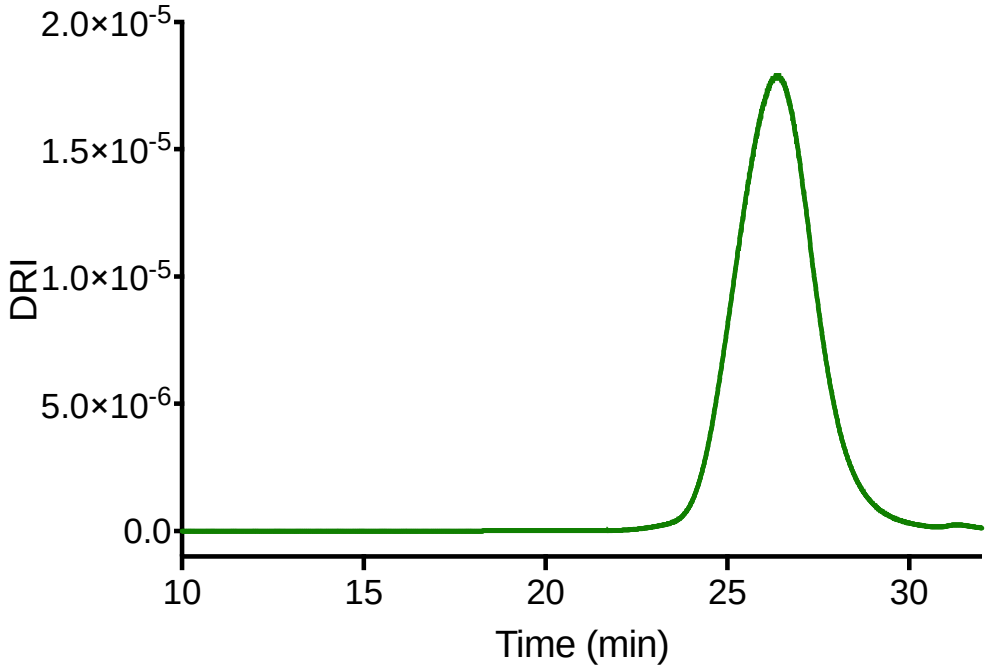

Figure B32. SEC trace of poly (6-NCA-C_3H_7) (Table 3-1, entry 18).

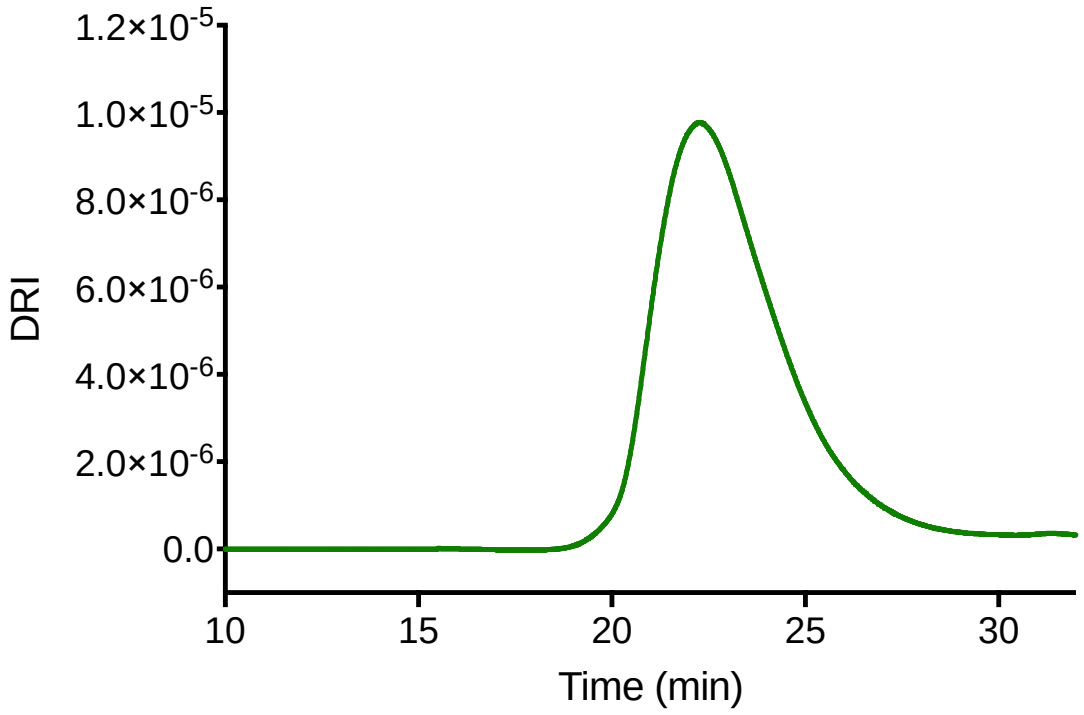

Figure B33. SEC trace of poly (6-NCA-C_2H_5) (Table 3-1, entry 19).

TGA traces

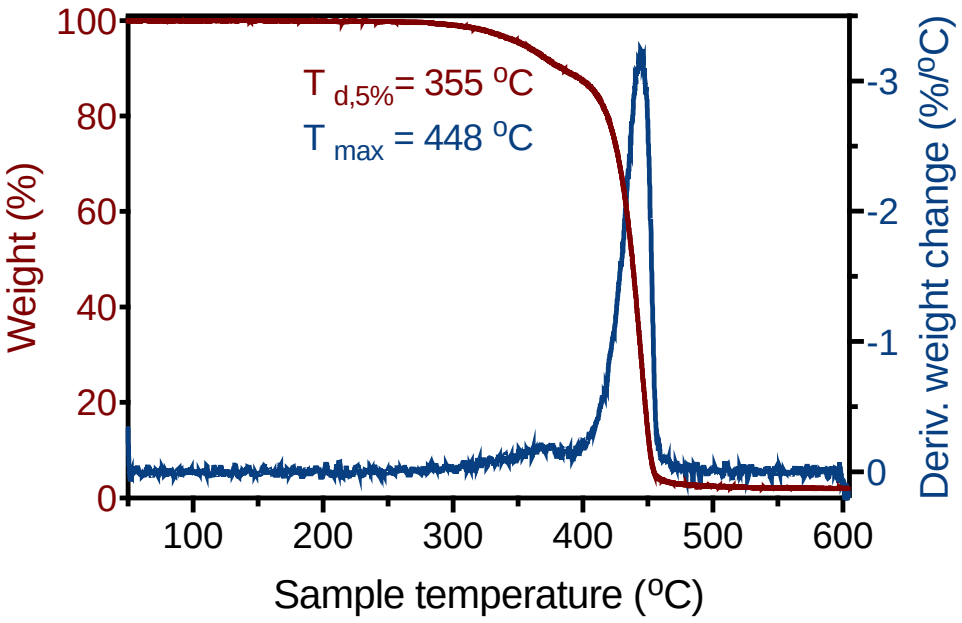

Figure B34. TGA and DTG curves of poly(6-NCA-C_5H_{11}) (Table 3-1, entry 17).

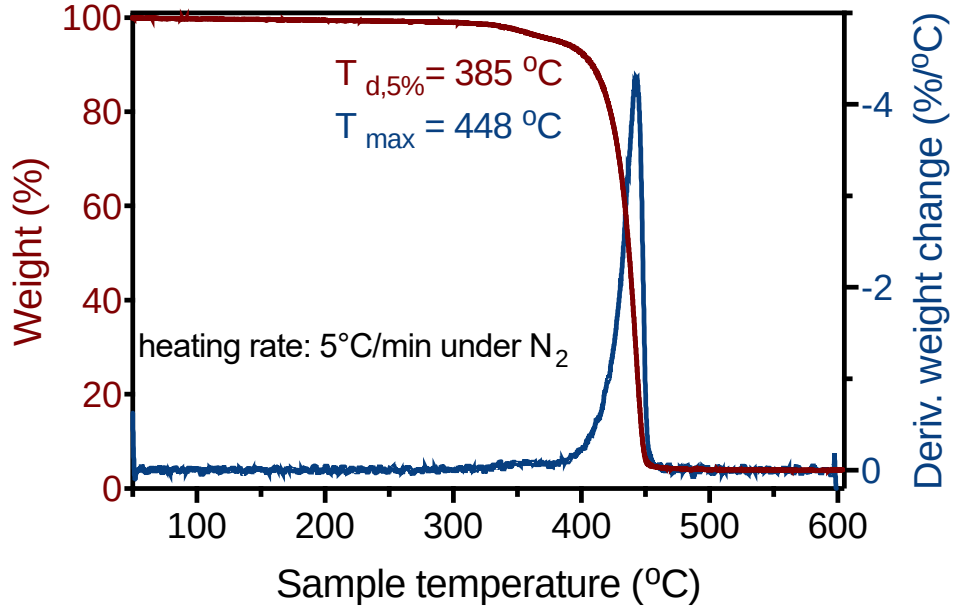

Figure B35. TGA and DTG curves of poly(6-NCA-C_3H_7) (Table 3-1, entry 18).

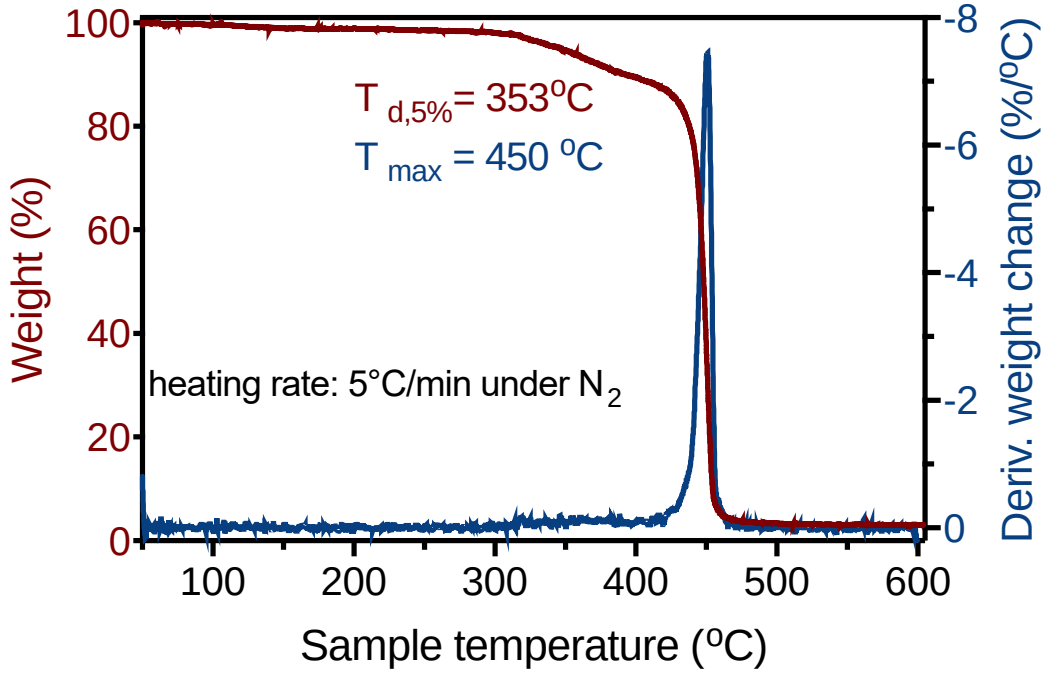

Figure B36. TGA and DTG curves of poly(6-NCA-C_2H_5) (Table 3-1, entry 19).

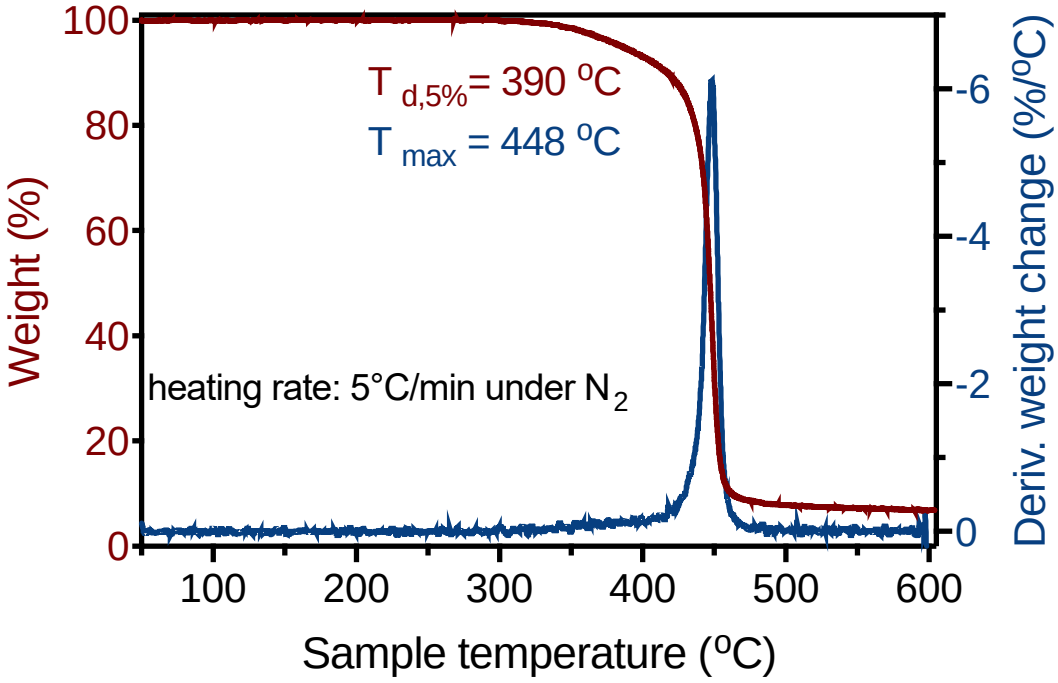

Figure B37. TGA and DTG curves of poly(6-NCA-Me) (Table 3-1, entry 20).

DSC traces

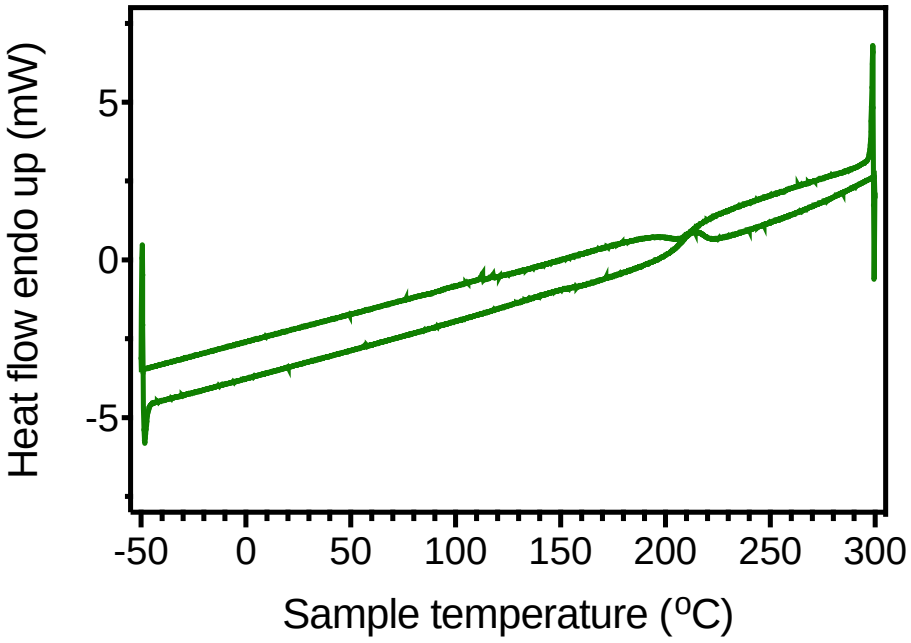

Figure B38. DSC trace of poly(6-NCA-C_8H_{17}) (Table 3-1, entry 7).

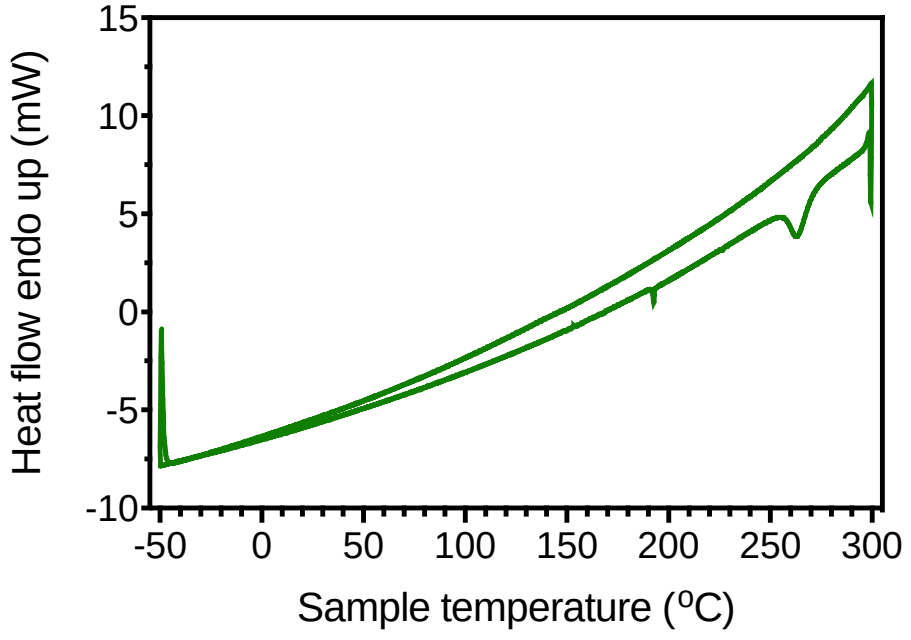

Figure B39. DSC trace of poly(6-NCA-C_5H_{11}) (Table 3-1, entry 17).

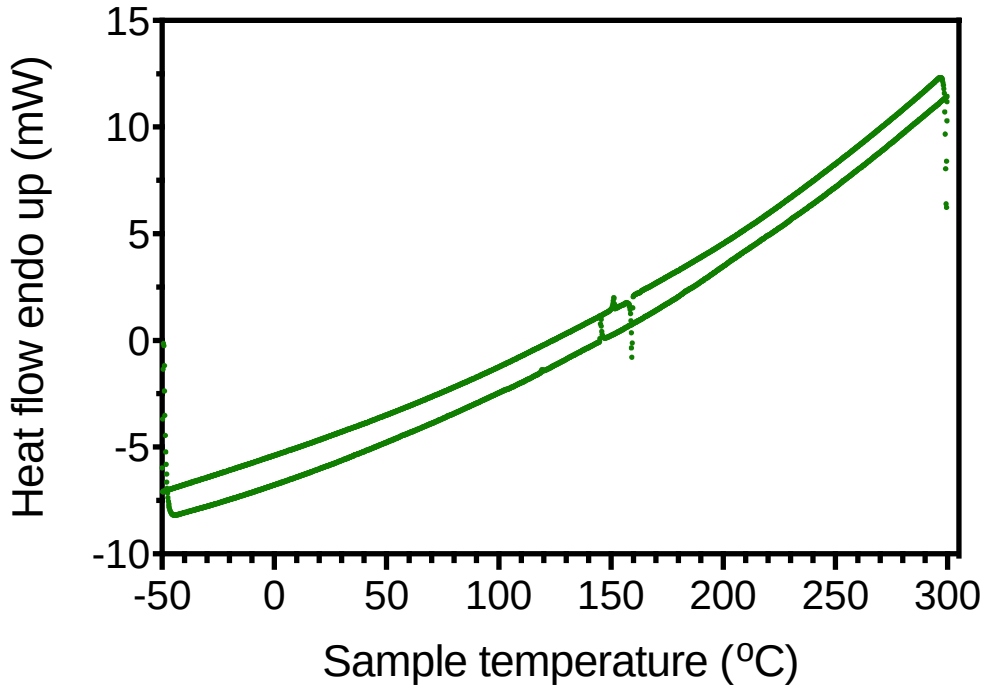

Figure B40. DSC trace of poly(6-NCA-C_3H_7) (Table 3-1, entry 18).

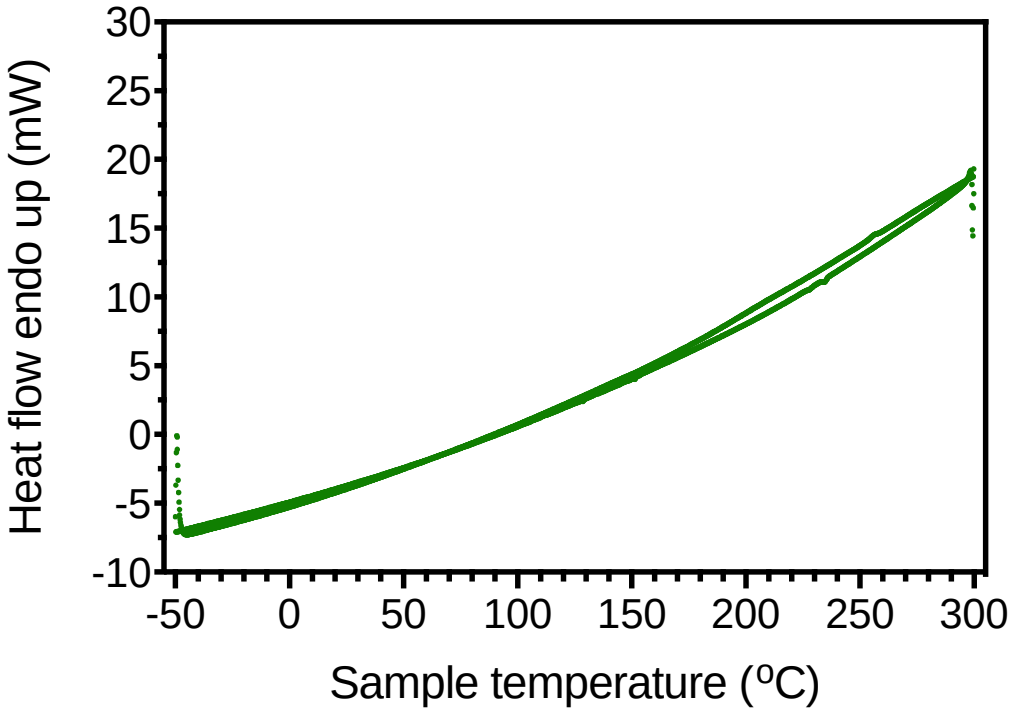

Figure B41. DSC trace of poly(6-NCA-C_2H_5) (Table 3-1, entry 19).

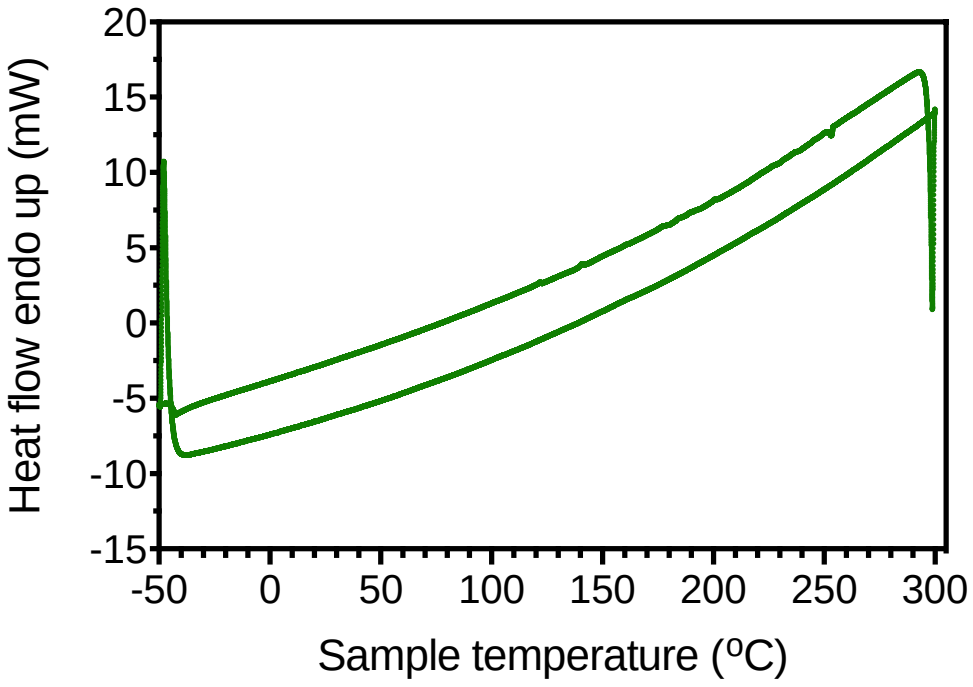

Figure B42. DSC trace of poly(6-NCA-Me) (Table 3-1, entry 1).

3.6. References

(1) Yang, B.; Wang, L.; Zhang, M.; Luo, J.; Lu, Z.; Ding, X. Fabrication, Applications, and Prospects of Aramid Nanofiber. *Adv. Funct. Mater.* **2020**, *30* (22), 2000186.

(2) Sobiech, T. A.; Zhong, Y.; Gong, B. Cavity-containing aromatic oligoamide foldamers and macrocycles: progress and future perspectives. *Org. Biomol. Chem.* **2022**, *20* (35), 6962-6978, 10.1039/D2OB01467J.

(3) Coste, M.; Suárez-Picado, E.; Ulrich, S. Hierarchical self-assembly of aromatic peptide conjugates into supramolecular polymers: it takes two to tango. *Chem. Sci.* **2022**, *13* (4), 909-933, 10.1039/D1SC05589E.

(4) Akhdar, A.; Gautier, A.; Hjelmgaard, T.; Faure, S. N-Alkylated Aromatic Poly- and Oligoamides. *ChemPlusChem* **2021**, *86* (2), 298-312.

(5) Zhang, D.-W.; Zhao, X.; Hou, J.-L.; Li, Z.-T. Aromatic Amide Foldamers: Structures, Properties, and Functions. *Chem. Rev.* **2012**, *112* (10), 5271-5316.

(6) Li, Z.; Cai, B.; Yang, W.; Chen, C.-L. Hierarchical Nanomaterials Assembled from Peptoids and Other Sequence-Defined Synthetic Polymers. *Chem. Rev.* **2021**, *121* (22), 14031-14087.

(7) Hamuro, Y.; Geib, S. J.; Hamilton, A. D. Oligoanthranilamides. Non-Peptide Subunits That Show Formation of Specific Secondary Structure. *J. Am. Chem. Soc.* **1996**, *118* (32), 7529-7541.

(8) Reese, C. J.; Qi, Y.; Abele, D. T.; Shlafstein, M. D.; Dickhudt, R. J.; Guan, X.; Wagner, M. J.; Liu, X.; Boyes, S. G. Aromatic Polyamide Brushes for High Young's Modulus Surfaces by Surface-Initiated Chain-Growth Condensation Polymerization. *Macromolecules* **2022**, *55* (6), 2051-2066.

(9) Alizadeh, M.; Kilbinger, A. F. M. Synthesis of Telechelic Poly(p-benzamide)s. *Macromolecules* **2018**, *51* (11), 4363-4369.

(10) Yokozawa, T.; Asai, T.; Sugi, R.; Ishigooka, S.; Hiraoka, S. Chain-Growth Polycondensation for Nonbiological Polyamides of Defined Architecture. *J. Am. Chem. Soc.* **2000**, *122* (34), 8313-8314.

(11) Yokozawa, T.; Ogawa, M.; Sekino, A.; Sugi, R.; Yokoyama, A. Chain-Growth Polycondensation for Well-Defined Aramide. Synthesis of Unprecedented Block Copolymer Containing Aramide with Low Polydispersity. *J. Am. Chem. Soc.* **2002**, *124* (51), 15158-15159.

(12) Sugi, R.; Yokoyama, A.; Furuyama, T.; Uchiyama, M.; Yokozawa, T. Inductive Effect-Assisted Chain-Growth Polycondensation. Synthetic Development from para- to meta-Substituted Aromatic Polyamides with Low Polydispersities. *J. Am. Chem. Soc.* **2005**, *127* (29), 10172-10173.

(13) Yokozawa, T.; Ohta, Y. Transformation of Step-Growth Polymerization into Living Chain-Growth Polymerization. *Chem. Rev.* **2016**, *116* (4), 1950-1968.

(14) Pal, S.; Nguyen, D. P. T.; Molliet, A.; Alizadeh, M.; Crochet, A.; Ortuso, R. D.; Petri-Fink, A.; Kilbinger, A. F. M. A versatile living polymerization method for aromatic amides. *Nat. Chem.* **2021**, *13* (7), 705-713.

(15) Yokoyama, A.; Karasawa, M.; Taniguchi, M.; Yokozawa, T. Successive Formation of Two Amide Linkages between Two Benzene Rings. *Chem. Lett.* **2013**, *42* (6), 641-642.

(16) Rasines Mazo, A.; Allison-Logan, S.; Karimi, F.; Chan, N. J.-A.; Qiu, W.; Duan, W.; O'Brien-Simpson, N. M.; Qiao, G. G. Ring opening polymerization of α-amino acids: advances in synthesis, architecture and applications of polypeptides and their hybrids. *Chem. Soc. Rev.* **2020**, *49* (14), 4737-4834, 10.1039/C9CS00738E.

(17) Cheng, J.; Deming, T. J. Synthesis and Conformational Analysis of Optically Active Poly(β-peptides). *Macromolecules* **2001**, *34* (15), 5169-5174.

(18) Thompson, M. S.; Johnson, S. A.; Gonsales, S. A.; Brown, G. M.; Kristufek, S. L.; Byers, J. A. Adding Polypeptides to the Toolbox for Redox-Switchable Polymerization and Copolymerization Catalysis. *Macromolecules* **2023**, *56* (8), 3024-3035.

(19) Chen, C.; Fu, H.; Baumgartner, R.; Song, Z.; Lin, Y.; Cheng, J. Proximity-Induced Cooperative Polymerization in "Hinged" Helical Polypeptides. *J. Am. Chem. Soc.* **2019**, *141* (22), 8680-8683.

(20) Grazon, C.; Salas-Ambrosio, P.; Ibarboure, E.; Buol, A.; Garanger, E.; Grinstaff, M. W.; Lecommandoux, S.; Bonduelle, C. Aqueous Ring-Opening Polymerization-Induced Self-Assembly (ROPISA) of N-Carboxyanhydrides. *Angew. Chem. Int. Ed.* **2020**, *59* (2), 622-626.

(21) Deming, T. J. Facile synthesis of block copolypeptides of defined architecture. *Nature* **1997**, *390* (6658), 386-389.

(22) Deng, S.; Diaconescu, P. L. A switchable dimeric yttrium complex and its three catalytic states in ring opening polymerization. *Inorg. Chem. Front.* **2021**, *8* (8), 2088-2096, 10.1039/D0QI01479F.

(23) Wei, J.; Diaconescu, P. L. Redox-switchable Ring-opening Polymerization with Ferrocene Derivatives. *Acc. Chem. Res.* **2019**, *52* (2), 415-424.

(24) Lai, A.; Hern, Z. C.; Diaconescu, P. L. Switchable Ring-Opening Polymerization by a Ferrocene Supported Aluminum Complex. *ChemCatChem* **2019**, *11* (16), 4210-4218.

(25) Dai, R.; Diaconescu, P. L. Investigation of a Zirconium Compound for Redox Switchable Ring Opening Polymerization. *Dalton Trans.* **2019**, *48*, 2996-3002.

(26) Dai, R.; Lai, A.; Alexandrova, A. N.; Diaconescu, P. L. Geometry Change in a Series of Zirconium Compounds during Lactide Ring-Opening Polymerization. *Organometallics* **2018**, *37* (21), 4040-4047.

(27) Abubekerov, M.; Wei, J.; Swartz, K. R.; Xie, Z.; Pei, Q.; Diaconescu, P. L. Preparation of multiblock copolymers via step-wise addition of l-lactide and trimethylene carbonate. *Chem. Sci.* **2018**, *9* (8), 2168-2178, 10.1039/C7SC04507G.

(28) Abubekerov, M.; Vlček, V.; Wei, J.; Miehlich, M. E.; Quan, S. M.; Meyer, K.; Neuhauser, D.; Diaconescu, P. L. Exploring Oxidation State-Dependent Selectivity in Polymerization of Cyclic Esters and Carbonates with Zinc(II) Complexes. *iScience* **2018**, *7*, 120-131.

(29) Wei, J.; Riffel, M. N.; Diaconescu, P. L. Redox Control of Aluminum Ring-Opening Polymerization: A Combined Experimental and DFT Investigation. *Macromolecules* **2017**, *50* (5), 1847-1861.

(30) Quan, S. M.; Wei, J.; Diaconescu, P. L. Mechanistic Studies of Redox-Switchable Copolymerization of Lactide and Cyclohexene Oxide by a Zirconium Complex. *Organometallics* **2017**, *36* (22), 4451-4457.

(31) Lowe, M. Y.; Shu, S.; Quan, S. M.; Diaconescu, P. L. Investigation of redox switchable titanium and zirconium catalysts for the ring opening polymerization of cyclic esters and epoxides. *Inorg. Chem. Front.* **2017**, *4*, 1798-1805, 10.1039/C7QI00227K.

(32) Quan, S. M.; Wang, X.; Zhang, R.; Diaconescu, P. L. Redox Switchable Copolymerization of Cyclic Esters and Epoxides by a Zirconium Complex. *Macromolecules* **2016**, *49* (18), 6768-6778.

(33) Wang, X.; Brosmer, J. L.; Thevenon, A.; Diaconescu, P. L. Highly Active Yttrium Catalysts for the Ring-Opening Polymerization of ε-Caprolactone and δ-Valerolactone. *Organometallics* **2015**, *34* (19), 4700–4706.

(34) Quan, S. M.; Diaconescu, P. L. High activity of an indium alkoxide complex toward ring opening polymerization of cyclic esters. *Chem. Commun.* **2015**, *51*, 9643 - 9646, 10.1039/C5CC01312G.

(35) Qi, M.; Zhang, H.; Dong, Q.; Li, J.; Musgrave, R. A.; Zhao, Y.; Dulock, N.; Wang, D.; Byers, J. A. Electrochemically switchable polymerization from surface-anchored molecular catalysts. *Chem. Sci.* **2021**, *12*, 9042-9052, 10.1039/D1SC02163J.

(36) Ortuño, M. A.; Dereli, B.; Chiaie, K. R. D.; Biernesser, A. B.; Qi, M.; Byers, J. A.; Cramer, C. J. The Role of Alkoxide Initiator, Spin State, and Oxidation State in Ring-Opening Polymerization of ε-Caprolactone Catalyzed by Iron Bis(imino)pyridine Complexes. *Inorg. Chem.* **2018**, *57* (4), 2064-2071.

(37) Delle Chiaie, K. R.; Biernesser, A. B.; Ortuño, M. A.; Dereli, B.; Iovan, D. A.; Wilding, M. J. T.; Li, B.; Cramer, C. J.; Byers, J. A. The role of ligand redox non-innocence in ring-opening polymerization reactions catalysed by bis(imino)pyridine iron alkoxide complexes. *Dalton Trans.* **2017**, *46* (38), 12971-12980, 10.1039/C7DT03067C.

(38) Longo, J. M.; Sanford, M. J.; Coates, G. W. Ring-Opening Copolymerization of Epoxides and Cyclic Anhydrides with Discrete Metal Complexes: Structure–Property Relationships. *Chem. Rev.* **2016**, *116* (24), 15167-15197.

(39) Fieser, M. E.; Sanford, M. J.; Mitchell, L. A.; Dunbar, C. R.; Mandal, M.; Van Zee, N. J.; Urness, D. M.; Cramer, C. J.; Coates, G. W.; Tolman, W. B. Mechanistic Insights into the Alternating Copolymerization of Epoxides and Cyclic Anhydrides Using a (Salph)AlCl and Iminium Salt Catalytic System. *J. Am. Chem. Soc.* **2017**, *139* (42), 15222-15231.

(40) Van Zee, N. J.; Coates, G. W. Alternating copolymerization of dihydrocoumarin and epoxides catalyzed by chromium salen complexes: a new route to functional polyesters. *Chem. Commun.* **2014**, *50* (48), 6322-6325, 10.1039/C4CC01566E.

(41) Darensbourg, D. J.; Mackiewicz, R. M.; Phelps, A. L.; Billodeaux, D. R. Copolymerization of CO2 and Epoxides Catalyzed by Metal Salen Complexes. *Acc. Chem. Res.* **2004**, *37* (11), 836-844.

(42) Lu, X.-B.; Shi, L.; Wang, Y.-M.; Zhang, R.; Zhang, Y.-J.; Peng, X.-J.; Zhang, Z.-C.; Li, B. Design of Highly Active Binary Catalyst Systems for CO2/Epoxide Copolymerization: Polymer Selectivity, Enantioselectivity, and Stereochemistry Control. *J. Am. Chem. Soc.* **2006**, *128* (5), 1664-1674.

(43) Raman, S. K.; Brulé, E.; Tschan, M. J. L.; Thomas, C. M. Tandem catalysis: a new approach to polypeptides and cyclic carbonates. *Chem. Commun.* **2014**, *50* (89), 13773-13776, 10.1039/C4CC05730A.

(44) Sui, Q.; Borchardt, D.; Rabenstein, D. L. Kinetics and Equilibria of Cis/Trans Isomerization of Backbone Amide Bonds in Peptoids. *J. Am. Chem. Soc.* **2007**, *129* (39), 12042-12048.

(45) Tojo, Y.; Urushibara, K.; Yamamoto, S.; Mori, H.; Masu, H.; Kudo, M.; Hirano, T.; Azumaya, I.; Kagechika, H.; Tanatani, A. Conformational Properties of Aromatic Oligoamides Bearing Pyrrole Rings. *J. Org. Chem.* **2018**, *83* (8), 4606-4617.

(46) Shepard, S. M.; Diaconescu, P. L. Redox-Switchable Hydroelementation of a Cobalt Complex Supported by a Ferrocene-Based Ligand. *Organometallics* **2016**, *35* (15), 2446–2453.

(47) Stößer, T.; Williams, C. K. Selective Polymerization Catalysis from Monomer Mixtures: Using a Commercial Cr-Salen Catalyst To Access ABA Block Polyesters. *Angew. Chem. Int. Ed.* **2018**, *57* (21), 6337-6341.

(48) Van Zee, N. J.; Coates, G. W. Alternating copolymerization of propylene oxide with biorenewable terpene-based cyclic anhydrides: a sustainable route to aliphatic polyesters with high glass transition temperatures. *Angew. Chem. Int. Ed.* **2015**, *127* (9), 2703-2706.

(49) Liu, Y.; Guo, J.-Z.; Lu, H.-W.; Wang, H.-B.; Lu, X.-B. Making various degradable polymers from epoxides using a versatile dinuclear chromium catalyst. *Macromolecules* **2018**, *51* (3), 771-778.

(50) Lu, X.-B.; Darensbourg, D. J. Cobalt catalysts for the coupling of CO2 and epoxides to provide polycarbonates and cyclic carbonates. *Chem. Soc. Rev.* **2012**, *41* (4), 1462-1484, 10.1039/C1CS15142H.

(51) Liu, Y.; Zhou, H.; Guo, J. Z.; Ren, W. M.; Lu, X. B. Completely recyclable monomers and polycarbonate: approach to sustainable polymers. *Angew. Chem. Int. Ed.* **2017**, *56* (17), 4862-4866.

(52) Luinstra, G. A.; Haas, G. R.; Molnar, F.; Bernhart, V.; Eberhardt, R.; Rieger, B. On the Formation of Aliphatic Polycarbonates from Epoxides with Chromium(III) and Aluminum(III) Metal–Salen Complexes. *Chem. Eur. J.* **2005**, *11* (21), 6298-6314.

(53) Cuartero, M.; Acres, R. G.; Bradley, J.; Jarolimova, Z.; Wang, L.; Bakker, E.; Crespo, G. A.; De Marco, R. Electrochemical mechanism of ferrocene-based redox molecules in thin film membrane electrodes. *Electrochim. Acta* **2017**, *238*, 357-367.

(54) Van Zee, N. J.; Sanford, M. J.; Coates, G. W. Electronic Effects of Aluminum Complexes in the Copolymerization of Propylene Oxide with Tricyclic Anhydrides: Access to Well-Defined, Functionalizable Aliphatic Polyesters. *J. Am. Chem. Soc.* **2016**, *138* (8), 2755-2761.

(55) Shibasaki, Y.; Abe, Y.; Sato, N.; Fujimori, A.; Oishi, Y. Direct condensation polymerization of N-alkylated p-aminobenzoic acid and packing of rigid-rod main chains with flexible side chains. *Polym. J.* **2010**, *42* (1), 72-80.

(56) Ohishi, T.; Sugi, R.; Yokoyama, A.; Yokozawa, T. A variety of poly(m-benzamide)s with low polydispersities from inductive effect-assisted chain-growth polycondensation. *J. Polym. Sci., Part A: Polym. Chem.* **2006**, *44* (17), 4990-5003.

(57) Pangborn, A. B.; Giardello, M. A.; Grubbs, R. H.; Rosen, R. K.; Timmers, F. J. Safe and Convenient Procedure for Solvent Purification. *Organometallics* **1996**, *15* (5), 1518-1520.

(58) Rutherford, D.; Atwood, D. A. Five-Coordinate Aluminum Amides. *Organometallics* **1996**, *15* (21), 4417-4422.

(59) Yang, G.; Cheng, C.; Xu, G.-B.; Tang, L.; Chua, K.-L.; Yang, Y.-Y. Synthesis and antibiofilm evaluation of 3-hydroxy-2, 3-dihydroquinazolin-4 (1H)-one derivatives against opportunistic pathogen Acinetobacter baumannii. *Bioorganic & Medicinal Chemistry* **2020**, *28* (16), 115606.

(60) Wube, A. A.; Bucar, F.; Hochfellner, C.; Blunder, M.; Bauer, R.; Hüfner, A. Synthesis of N-substituted 2-[(1E)-alkenyl]-4-(1H)-quinolone derivatives as antimycobacterial agents against non-tubercular mycobacteria. *European journal of medicinal chemistry* **2011**, *46* (6), 2091-2101.

Chapter 4: PLA-PEG-PLA block copolymer synthesis and its shear viscosity study

4.1. Introduction

In the hydraulic fracturing process, turbulent fluid flow introduces frictional drag, causing energy dissipation. This necessitates additional energy input to maintain desired flow rates, as compared to laminar flow. To address this issue and save energy, drag reducing agents are commonly employed. Among them are water-soluble polymers with ultra-high molecular weight such as poly(ethylene glycol) (PEG), polyacrylamide (PAM),[1] and certain natural polymers like xanthan and cellulose derivatives. However, these covalently linked ultra-long polymers suffer from irreversible shear degradation. A study by Horn and Merrill indicated that high-molecular-weight polymers are more prone to degradation than lower-molecular-weight ones.[2]

As an alternative to covalently linked ultra-high molecular weight polymers, associative polymers that aggregate through hydrophobic interactions have gained attention.[3] Examples include hydrophobically modified PEG[4-6] and PAM[7-12] with hydrophobic units distributed randomly or in block-like arrangements. Telechelic polymers, featuring hydrophilic middle blocks and hydrophobic end blocks, exhibit self-assembly into flower-shaped micelles interconnected by hydrophilic chains. One such instance is PLA-PEG-PLA. Notably eco-friendly and sustainable, PLA-PEG-PLA could serve as a substitute for ultra-high molecular weight PAM and derivatives, given that its degradation products are environmentally benign.

Since Ikada and coworkers' pioneering work in 1987 on PLLA and PDLA stereocomplex,[13] numerous studies have demonstrated the enhanced thermomechanical properties resulting from stereocomplexation between PLLA and PDLA.[14] PLA and PEO copolymers stereocomplexation has been explored in hydrogel[15-18] and micelle [19-22] formations for drug delivery. However, to the best of our knowledge, their application as drag reducers remains unexplored. Herein, we propose

that PLLA-PEG-PLLA/PDLA-PEG-PDLA stereocomplex, when in aqueous solution, can form bridged micelles that, under moderate shear rates, stretch into a loosely associative polymer network. This network could offer better friction-reducing performance than isolated polymer chains.[23-25] Under higher shear rates, the polymer network could reversibly dissociate to prevent chain scission at covalent bonds (Figure 4-1).

In this report, we synthesized a series of PLLA-PEG-PLLA/PDLA-PEG-PDLA amphiphilic triblock copolymers and investigated how the length of the hydrophilic/hydrophobic blocks as well as stereocomplexation between the PLLA and PDLA influence the rheology properties the polymer solution in brine.

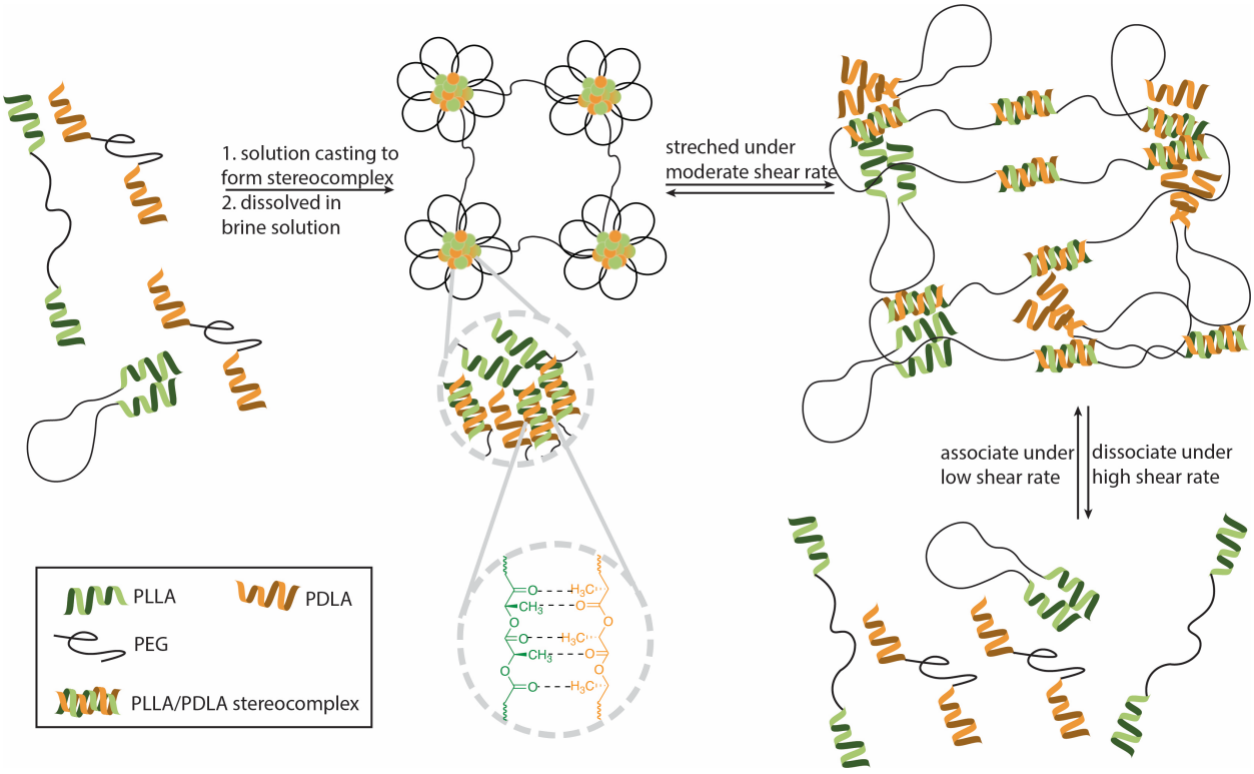

Figure 4-1. Enhanced drag-reducing performance by stereocomplexation between PLLA-PEG-PLLA and PDLA-PEG-PDLA.

4.2. Results and Discussion

Table 4-1. Synthesis of PLA-PEG-PLA triblock copolymer

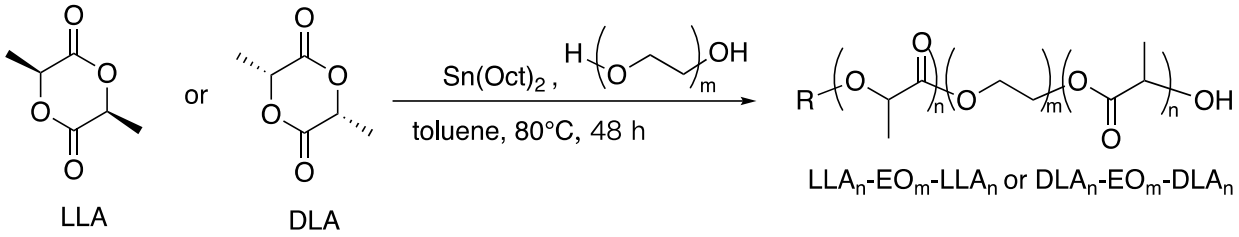

Entry	Polymer formula[a]	PEG[b]	LLA[b]	Solubility[c]
1	LLA_8-EO_{100}-LLA_8	80 mg	40 mg	soluble
2	LLA_6-EO_{458}-LLA_6	400 mg	40 mg	soluble
3	LLA_{17}-EO_{458}-LLA_{17}	400 mg	65 mg	Partially soluble
4	DLA_{17}-EO_{458}-DLA_{17}	400 mg	65 mg	Partially soluble
5	LLA_{24}-EO_{458}-LLA_{24}	400 mg	85 mg	Partially soluble
6	DLA_{24}-EO_{458}-DLA_{24}	400 mg	65 mg	Partially soluble
7	LLA_{27}-EO_{458}-LLA_{27}	400 mg	95 mg	Partially soluble
8	DLA_{27}-EO_{458}-DLA_{27}	400 mg	95 mg	Partially soluble

[a] Polymer formulas were determined by ^{1}H NMR spectra. [b] Amounts of PEG and lactide used to synthesize corresponding PLA-PEG-PLA copolymers. [c] Solubility was determined by dissolving 1 mg of polymer into 1 mL of American Petroleum Institute (API) brine (aqueous 8 wt % sodium chloride and 2 wt % calcium chloride).

A series of PLA-PEG-PLA triblock copolymer were synthesized using $Sn(Oct)_2$ as the catalyst and toluene as the solvent (Table 4-1). Dihydroxy-terminated PEGs were used as the macro-initiators to initiate the ring-opening polymerization of D- or L-lactide. The molecular weight and molecualr weight distribution of triblock copolymers were characterized by SEC (Figure 2, a). The PEG20K macro-initiator was calibrated by SEC to be HO-EO_{458}-OH. Additionally, the polymer structure was characterized by ^1H NMR spectroscopy. The peaks at 5.15 ppm and 1.58 ppm are attributed to the methine and methyl protons in the PLA block, while the peak at 3.64 ppm is attributed to the methylene protons in the PEG block (Figure 4-2, b).

We used solution casting method to prepare the stereocomplex. Equal amount of PLLA-PEG-PLLA and PDLA-PEG-PDLA in DCM solution were mixed and stirred at room temperature. Subsequenlty, the solvent was allowed to slowly evaperate, resulting in the formation of a solid form stereocomplex (Figure 4-3, c). The polymer solubility in API brine was then tested. When the PLA block is as short as 8 lactic acid repeating units, the PLA-PEG-PLA triblock copolymer is soluble in API brine at a concentration of 1 mg/mL. However, when the PLA is longer, e.g. as long as 17 lactic acid repeating units, the PLA-PEG-PLA became partially soluble in the brine solution (Figure 4-2, d).

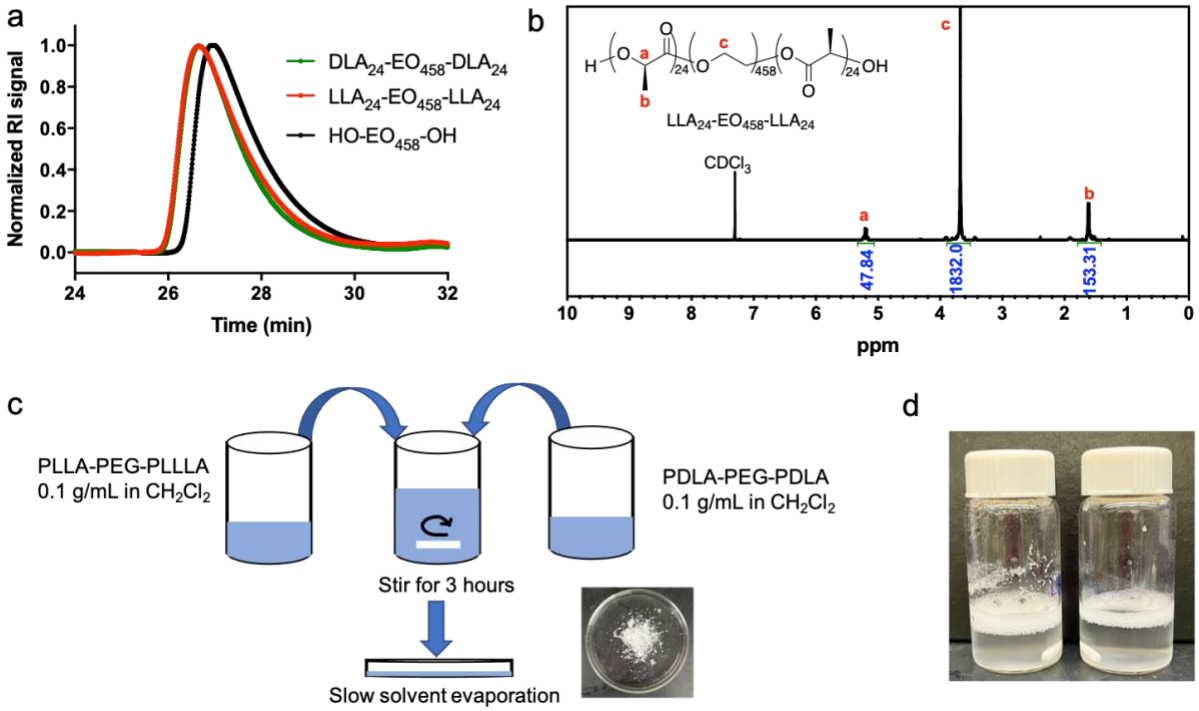

Figure 4-2. a. SEC traces of the macroinitiator HO-EO_{458}-OH, LLA_{24}-EO_{458}-LLA_{24} (Table 4-1, entry 5), and DLA_{24}-EO_{458}-DLA_{24}(Table 4-1, entry 6). b. ^{1}H NMR spectrum of LLA_{24}-EO_{458}-LLA_{24} (Table 4-1, entry 5) c. PLA-PEG-PLA stereocomplex preparation by solution casting. d. LA_{17}-EO_{458}-LA_{17} stereocomplex (left) and LLA_{17}-EO_{458}-LLA_{17} (right) in API brine solution at a concentration of 1 mg/mL.

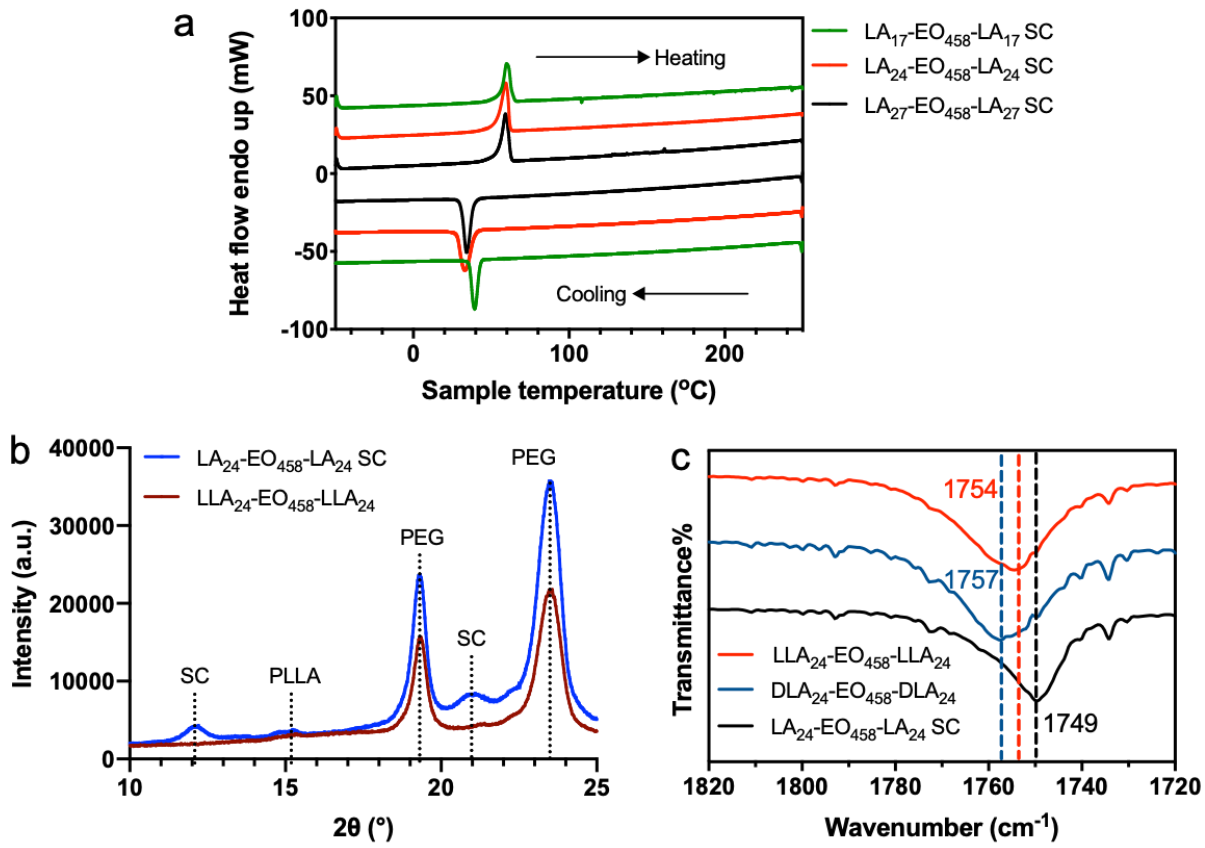

Figure 4-3. a. DSC traces of PLA-PEG-PLA stereocomplex samples. b. XRD analysis of LLA_{24}-EO_{458}-LLA_{24} and LA_{24}-EO_{458}-LA_{24} stereocomplex, c. FT-IR spectra of PLA-PEG-PLA samples.

DSC has been widely used to characterize the stereocomplexation because the formation of the stereocomplex would lead to the increase of the melting temperature of the PLA block from 180 °C to 230 °C.[26] To confirm the formation of the stereocomplex between PLLA-PEG-PLLA and PDLA-PEG-PDLA, we first did the differential scanning calorimetry (DSC) on our polymer samples (Figure 4-3, a). However, due to the short PLA chain length in the triblock copolymer and good miscibility between PLA block and PEG block, no PLA melting peak was observed. We then conducted X-ray diffraction analysis (XRD) to characterize the formation of stereocomplex. As reported by Ikada and coworkers,[13, 27] enantiomerically pure PLA homocrystallite would show 2θ

peak at 15°, 16°, 18.5°, and 22.5°, while sterecomplex would show peaks at 12°, 21°, and 24°. For the LA_{24}-EO_{458}-LA_{24} sterecomplex sample, we observed peaks at at 12°, 21° that were not present for LLA_{24}-EO_{458}-LLA_{24} (Figure 3, b) supporting the formation of the stereocomplex. Similar XRD spectra were obtained for LA_{17}-EO_{458}-LA_{17} and LA_{27}-EO_{458}-LA_{27} stereocomplexes

We also performed Fourier-transform infrared spectroscopy (FT-IR) analysis to confirm the formation of the stereocomplex. Previous reports indicate that in enantiomerically pure PLA the carbonyl C=O stretching wavenumber is at 1754 cm^{-1} while in sterecomplex, a red shift to 1749 cm^{-1} occurs due to the CH3···O=C interaction between PLLA and PDLA.[28] In our case, the C=O stretching bands were observed at 1754 cm^{-1} for LLA_{24}-EO_{458}-LLA_{24} and 1757 cm^{-1} for DLA_{24}-EO_{458}-DLA_{24}, respectively. For the LA_{24}-EO_{458}-LA_{24} sterecomplex sample, a C=O stretching of 1749 cm^{-1} was observed, which is in accordance with the formation of the stereocomplex (Figure 4-3, c). Similar red shift of the C=O stretching band was observed for LA_{17}-EO_{458}-LA_{17} LA_{27}-EO_{458}-LA_{27} stereocomplexes (Figure C18 and C19).

With the PLA-PEG-PLA copolymers in hand, we then proceeded to test the rheology properties of these polymers in API brine. Our initial attempt was to assess the impact of PEG middle block chain length by comparing LLA_8-EO_{100}-LLA_8 and LLA_6-EO_{458}-LLA_6. Despite having similar PLA end block lengths, LLA_6-EO_{458}-LLA_6 showed higher shear viscosity, indicating that longer PEG middle block can enhance the shear viscosity of the copolymer in solution. Among the partially soluble polymers, LLA_{27}-EO_{458}-LLA_{27} showed higher shear viscosity than LLA_{17}-EO_{458}-LLA_{17} and LLA_{24}-EO_{458}-LLA_{24} at 1 mg/mL concentration. However, the stereocomplex showed no enhancement for all three copolymers (Figure 4-4, a). PAM at 1.2 mg/mL was used as a benchmark to evaluate the performance of these copolymers. In comparison, the shear viscosity of PLA-PEG-PLA copolymers at 1 mg/mL concentration were generally much lower than that of the

PAM. Even though the copolymers were partially soluble even at 1 mg/mL, we still did shear viscosity measurements at increased concentrations.

At a concentration of 2 mg/mL, both LA_{17}-EO_{458}-LA_{17} and LA_{24}-EO_{458}-LA_{24} stereocomplexes displayed significantly improved shear viscosity compared to their L-lactide counterparts. Remarkably, these stereocomplexes even exhibited shear viscosities surpassing those of the PAM standard at shear rates lower than 100 s^{-1} (Figure 4-4, b). At 4 mg/mL, LLA_{24}-EO_{458}-LLA_{24} and LA_{24}-EO_{458}-LA_{24} stereocomplex showed the best shear viscosity among all the polymers with LA_{24}-EO_{458}-LA_{24} stereocomplex demonstrating the highest performance (Figure 4-4, c). When the concentration was further increased to 8 mg/mL, LA_{24}-EO_{458}-LA_{24} stereocomplex still displayed the highest shear viscosity, but the disparity among different copolymers is diminishing (Figure 4-4, d).

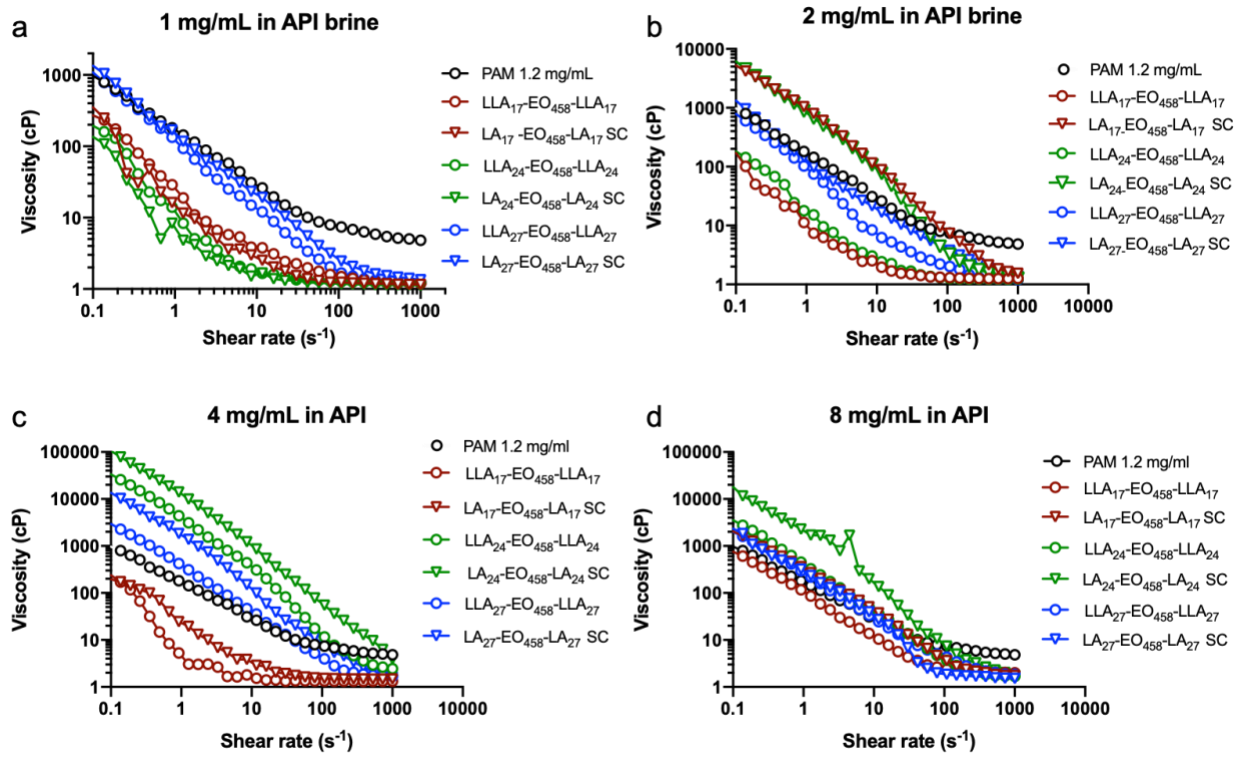

Figure 4-4. Shear viscosity measurements of PLA-PEG-PLA in brine solution samples in at different concentrations: 1 mg/mL (a), 2 mg/mL (b), 4 mg/mL (c), 8 mg/mL (d).

To understand the mechanism behind the enhanced shear viscosity of the PLA-PEG-PLA stereocomplexes, we conducted ^{1}H diffusion-ordered NMR spectroscopy (DOSY) experiments to investigate the self-assembled structure of the copolymers in API brine. 2 mg/mL PLA-PEG-PLA polymer solutions were prepared using deuterated API brine solution. In the ^{1}H NMR dimension, the peak attributed to hydrophilic PEG block can be observed, while the signal corresponding to the hydrophobic PLA block was not detected. In general, the stereocomplexes have smaller diffusion coefficient than their L-lactide counterparts. Interesting, LLA_{24}-EO_{458}-LLA_{24} and LA_{24}-EO_{458}-LA_{24} sterecomplex have the highest diffusion coefficients (Figure 4-5).

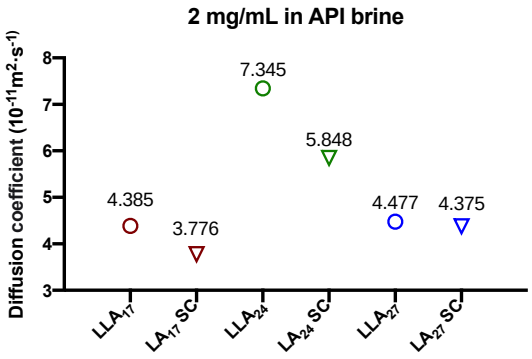

Figure 4-5. Diffusion coefficient obtained by DOSY experiments in deuterated API brine solution at 2 mg/mL. LLA_{17}-EO_{458}-LLA_{17} (red circle), LA_{17}-EO_{458}-LA_{17} sterecomplex (red triangle), LLA_{24}-EO_{458}-LLA_{24}(green circle), LA_{24}-EO_{458}-LA_{24} sterecomplex (green triangle), LLA_{27}-EO_{458}-LLA_{27}(blue circle), LA_{27}-EO_{458}-LA_{27} sterecomplex (blue triangle).

4.3. **Conclusions**

In summary, we synthesized a series of PLA-PEG-PLA copolymers with varying PLA and PEG block lengths. The polymer structures were characterized using ^{1}H NMR spectroscopy and GPC. Stereocomplexes were prepared for LA_{17}-EO_{458}-LA_{17}, LA_{24}-EO_{458}-LA_{24}, and LA_{27}-EO_{458}-LA_{27}. The formation of the stereocomplexes was confirmed through FT-IR spectroscopy and XRD analysis. Rheology measurements demonstrated that the formation of the stereocomplexes enhanced the shear viscosity of the polymer solutions in API brine, with LA_{24}-EO_{458}-LA_{24} stereocomplex showing the best performance. This makes it the most promising candidate for future drag reduction applications. Additionally, DOSY experiments were conducted to characterize the self-assembled structures of the copolymer solutions in API brine.

4.4. Experimental Section

Materials and methods:

L-lactide, D-lactide, dihydroxy PEG, and $Sn(Oct)_2$ were purchased from Fisher chemical. L-lactide, D-lactide were recrystallized from Ethyl acetate twice and toluene once before use. PEG was purified via azeotropic distillation with toluene. $Sn(Oct)_2$ was used as received. 1H and 13C NMR spectra were recorded on Bruker AV-300, Bruker AV-500, or Bruker DRX-500 spectrometers at room temperature. Chemical shifts are reported with respect to the residual solvent peaks. Molar masses of polymers were determined by size exclusion chromatography using a SEC-MALS instrument at UCLA. SEC-MALS uses a Shimazu Prominence-i LC 2030C 3D equipped with an autosampler, two MZ Analysentechnik MZ-Gel SDplus LS 5 μm, 300 × 8 mm linear columns, a Wyatt DAWN HELEOS-II, and a Wyatt Optilab T-rEX. The column temperature was set at 40 ^{o}C. A flow rate of 0.70 mL/min was used and samples were dissolved in THF. The number average molar mass and molecular weight distribution values were determined using the dn/dc values which were calculated by 100% mass recovery method from the RI signal. Differential Scanning Calorimetry (DSC) was obtained using a PerkinElmer DSC model 8500 heat flow system with Intracooler II. The first heating scan was from 25°C to 300°C at 10 °C/min and the cooling scan was from 300°C to -50°C at 10 °C/min. The second heating scan was from -50°C to 300°C at 10 °C/min and the cooling scan was from 300°C to -50°C at 10 °C/min. The melting transition temperature (Tm) were obtained from the second cycle after the thermal history was removed on the first heating scan. Attenuated total reflection Fourier transform infrared (ATR - FTIR) spectroscopy was performed on Agilent Cary 600 series FTIR microscope equipped with a universal ATR assembly. Viscosity versus shear rate measurements were assessed by rheology experiments (Anton Paar MCR 302) using a cone and plate geometry (50 mm diameter, 2° cone angle). Samples were dissolved in the indicated brine to a final concentration of 1.2 mg/mL and

transferred to the rheometer within an hour. A solvent trap was installed during measurements to minimize solvent evaporation, and the temperature was set to 25°C for measurements. Samples were allowed to equilibrate (2 minutes) and pre-sheared by subjecting them to an oscillatory strain with strain amplitude (γ) of 0.5% and angular frequency (ω) of 1 rad s^{-1} for ~2 minutes. Samples were then subject to increasing shear rates from either 0.1 or 1 rad s^{-1} up to 1,000 rad s^{-1} over 20 steps at 30 second intervals and viscosity was recorded. X-ray diffraction (XRD) patterns of the films were recorded by X-ray diffractometer (PANalytical) with Cu kα radiation at a scan rate of 4 ^{o}/min.

Synthesis of PLA-PEG-PLA

PLLA-PEG-PLLA and PDLA-PEG-PDLA were prepared through ring-opening polymerization using dihydroxy-terminated PEG as a macroinitiator and $Sn(Oct)_2$ as a catalyst. Under nitrogen atmosphere, to a Schlenk flask added purified L-lactide, anhydrous toluene, PEG initiator, and catalyst. The bottle was tightly sealed, transferred outside the glovebox, and placed in an oil bath at 90 °C for 24 hours. Subsequently, the mixture was cooled and dissolved in dichloromethane, followed by precipitation in cold ether. The precipitated polymer was washed with ether and dried uder vacuum for 24 hours before further characterization. The synthesis of PDLA-b-PEG-b-PDLA samples followed the same procedure, except that D-lactide was used instead of L-lactide.

Preparation of PLLA-PEG-PLLA/PDLA-PEG-PDLA stereocomplex

The PLLA-PEG-PLLA and PDLA-PEG-PDLA block copolymers were dissolved separately in dichloromethane at a concentration of 0.10 g/mL. After that, equal amounts of each polymer solution were mixed together under vigorous stirring for a duration of 3 hours. The resulting

mixture was then poured into a petri dish, allowing the solvent to evaporate slowly at room temperature. Finally, the blends were dried under vacuum before being used.

4.5. Appendix C

NMR spectra

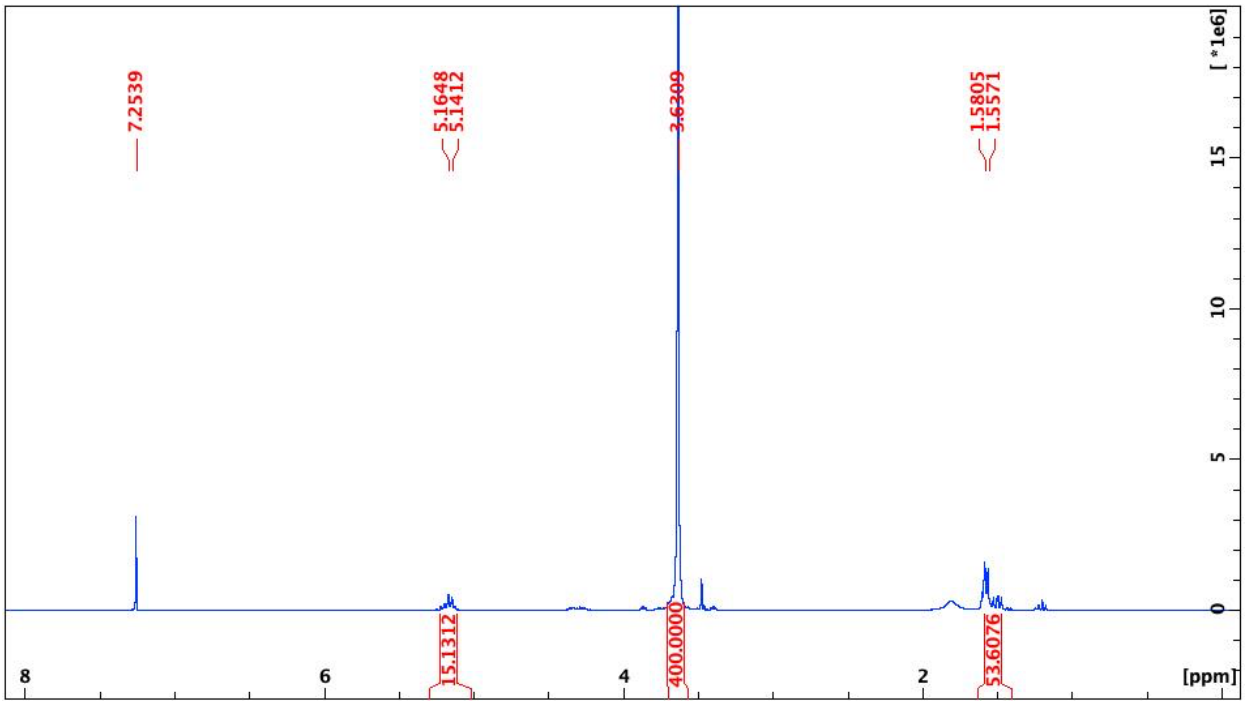

Figure C1. ^{1}H NMR spectrum ($CDCl_3$, 500 MHz, 298 K) of LLA_8-EO_{100}-LLA_8 (Table 4-1, entry 1).

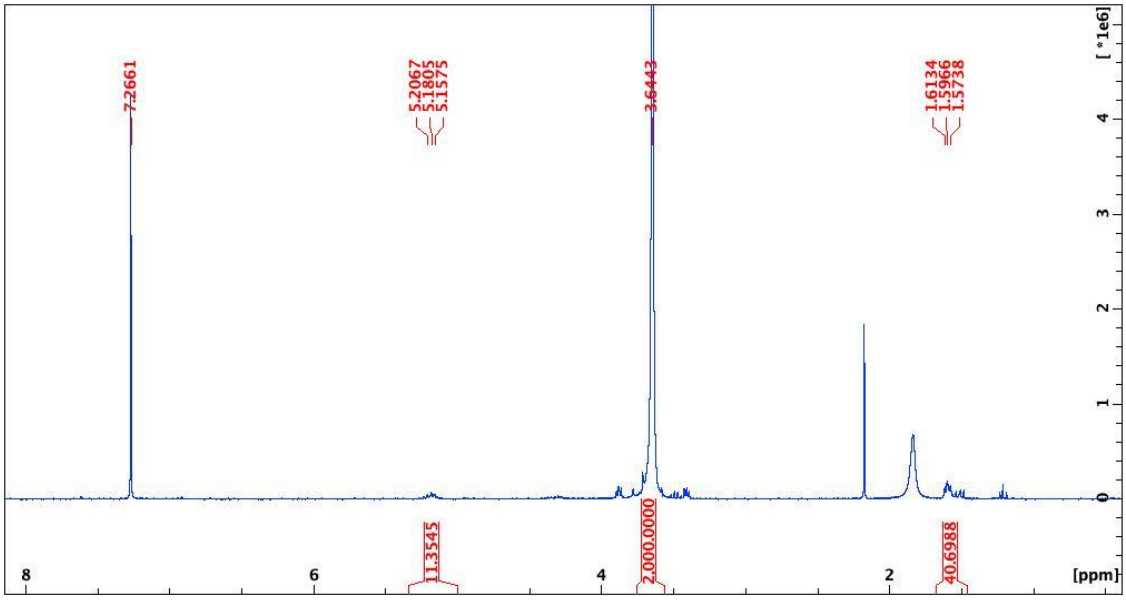

Figure C2. ^{1}H NMR spectrum ($CDCl_3$, 500 MHz, 298 K) of LLA_6-EO_{458}-LLA_6 (Table 4-1, entry 2).

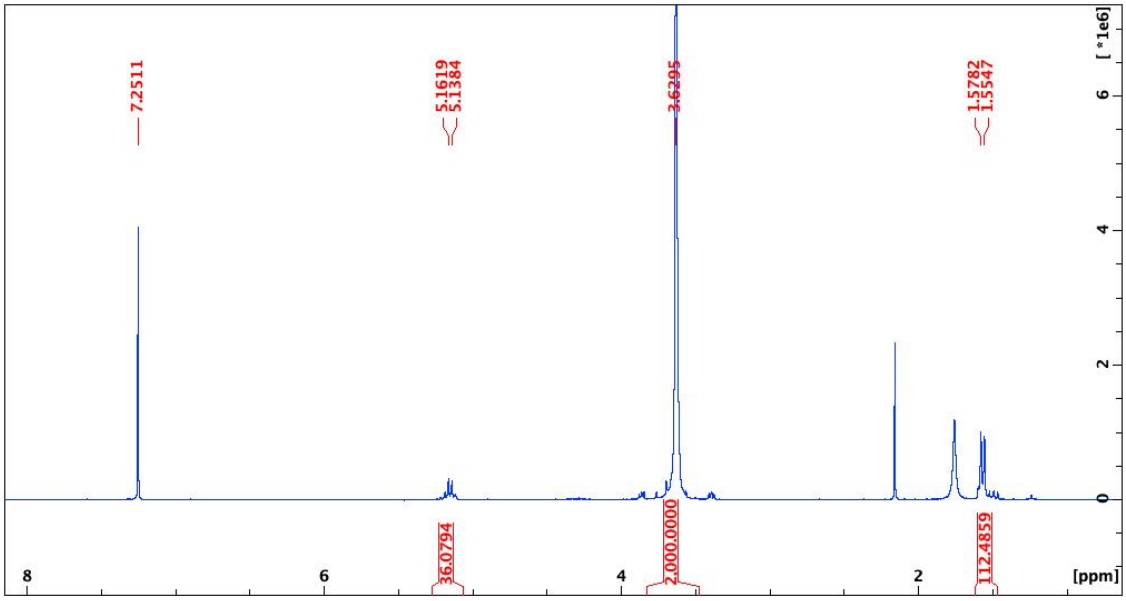

Figure C3. ^{1}H NMR spectrum ($CDCl_3$, 500 MHz, 298 K) of LLA_{17}-EO_{458}-LLA_{17} (Table 4-1, entry 3).

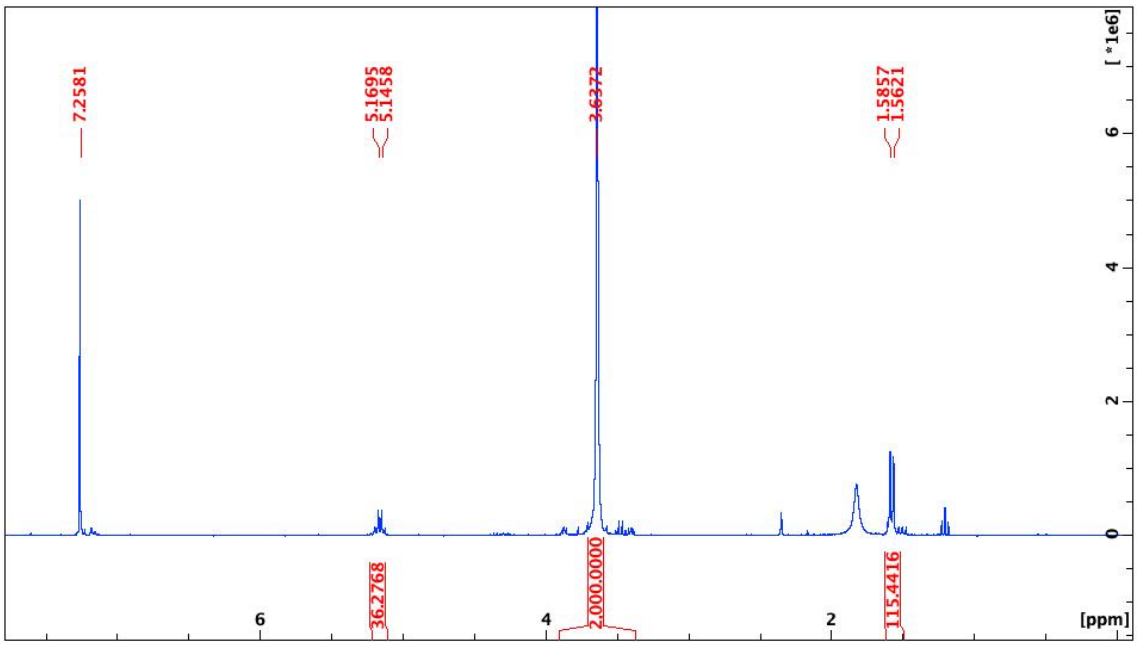

Figure C4. ^{1}H NMR spectrum ($CDCl_3$, 500 MHz, 298 K) of DLA_{17}-EO_{458}-DLA_{17} (Table 4-1, entry 4).

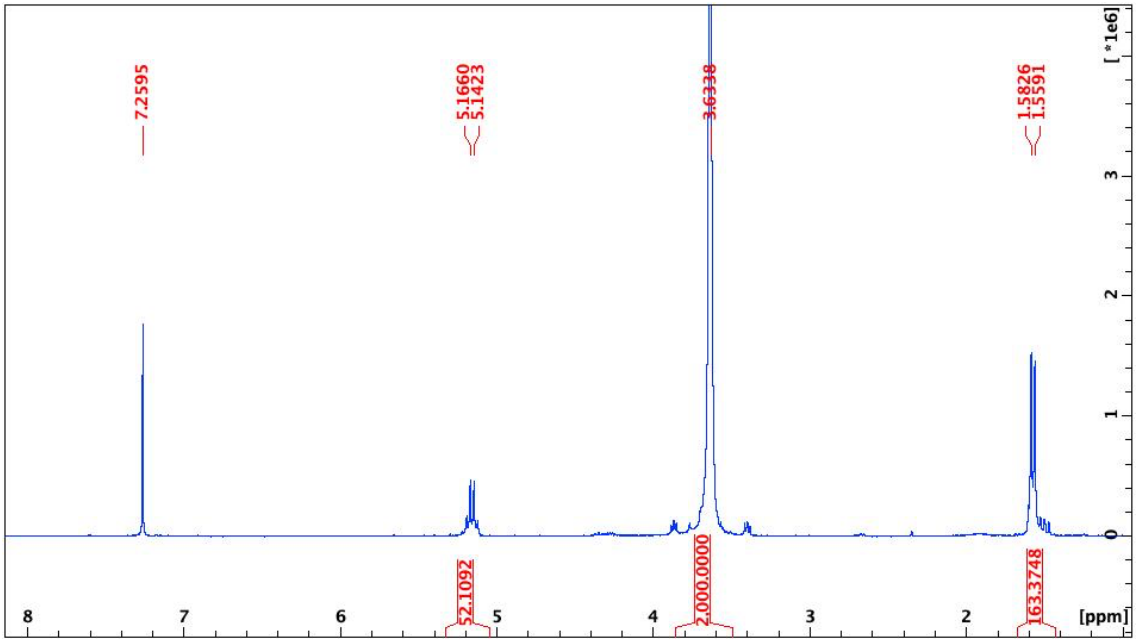

Figure C5. ^{1}H NMR spectrum ($CDCl_3$, 500 MHz, 298 K) of LLA_{24}-EO_{458}-LLA_{24} (Table 4-1, entry 5).

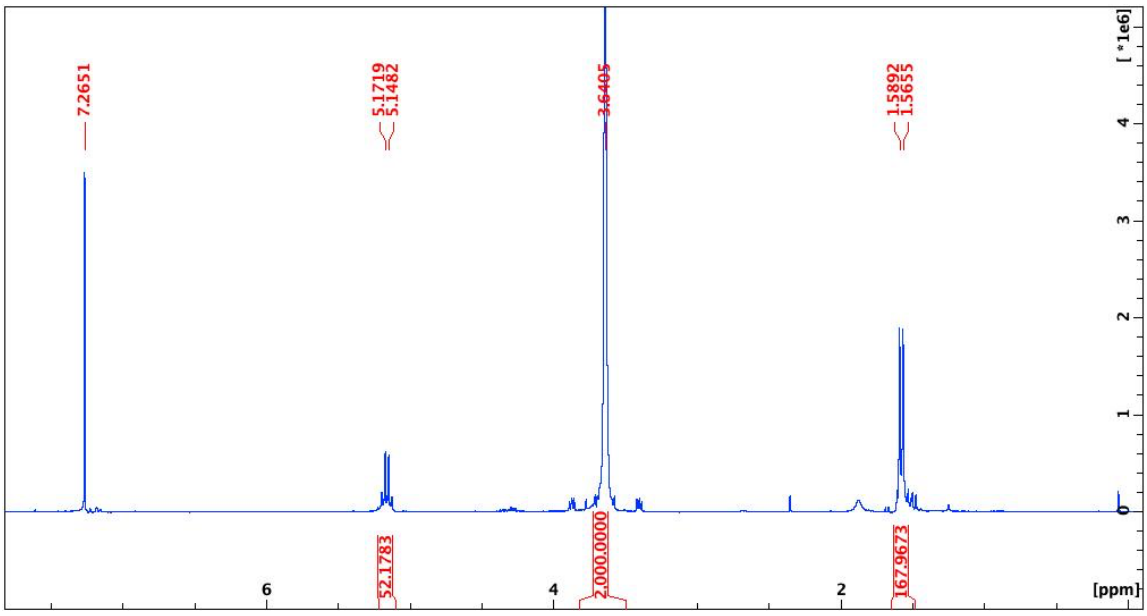

Figure C6. ^{1}H NMR spectrum ($CDCl_3$, 500 MHz, 298 K) of DLA_{24}-EO_{458}-DLA_{24} (Table 4-1, entry 6).

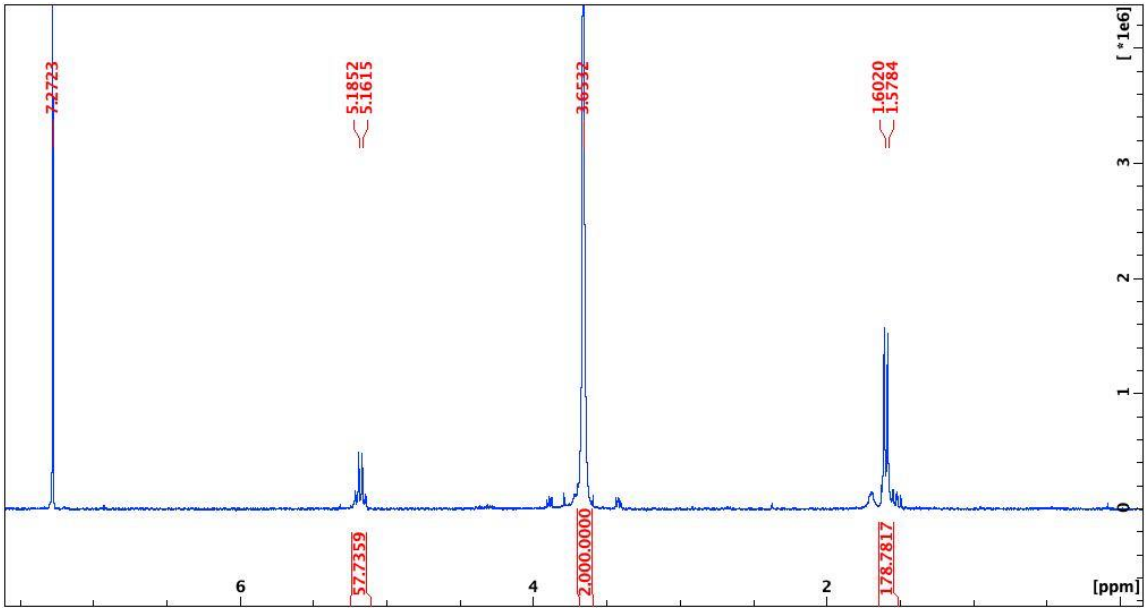

Figure C7. ^{1}H NMR spectrum ($CDCl_3$, 500 MHz, 298 K) of LLA_{27}-EO_{458}-LLA_{27} (Table 4-1, entry 7).

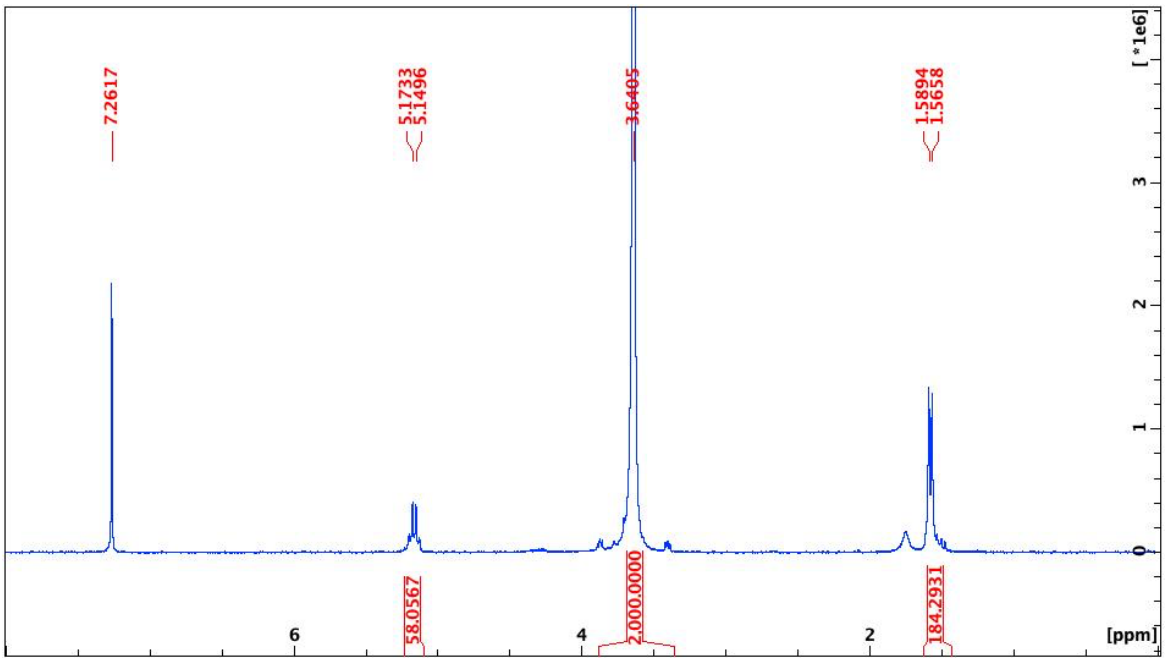

Figure C8. ^{1}H NMR spectrum ($CDCl_3$, 500 MHz, 298 K) of DLA_{27}-EO_{458}-DLA_{27} (Table 4-1, entry 8).

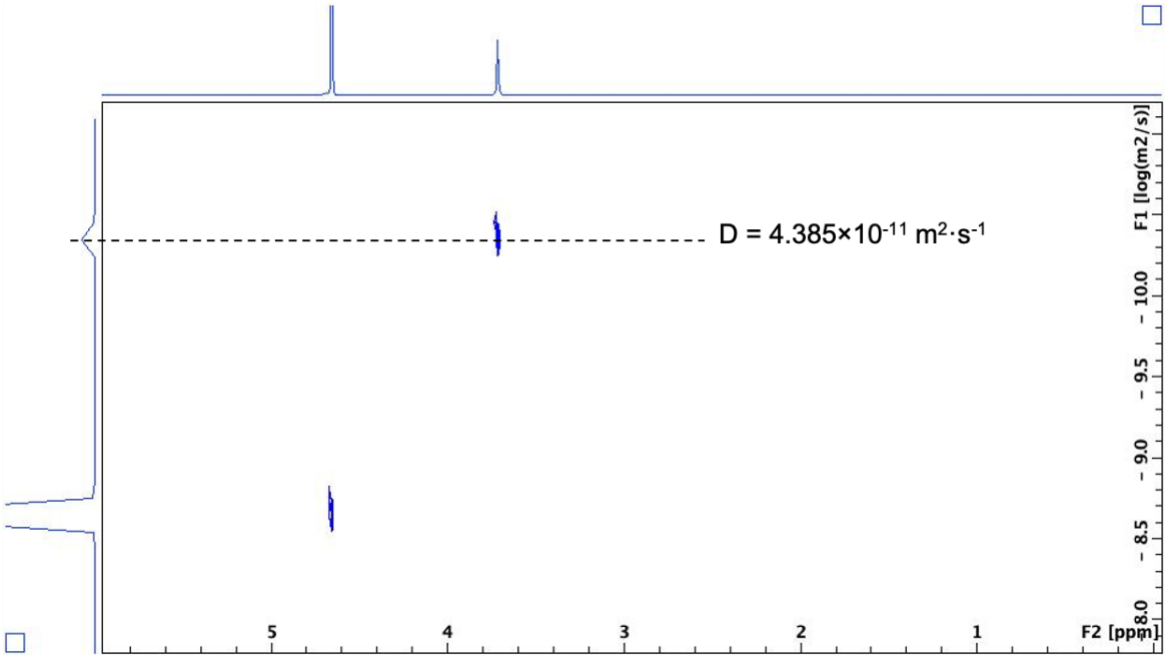

Figure C9. DOSY NMR spectrum (D_2O with 8 wt.% NaCl and 2 wt.% $CaCl_2$, 500 MHz, 298 K) of LLA_{17}-EO_{458}-LLA_{17}.

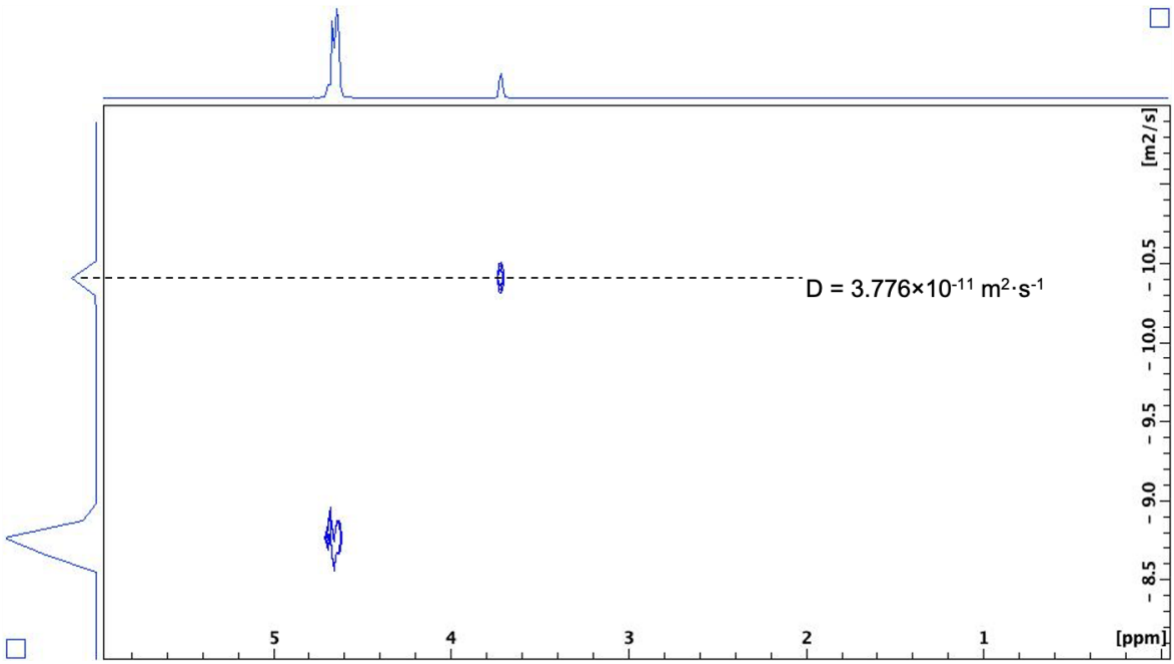

Figure C10. DOSY NMR spectrum (D_2O with 8 wt.% NaCl and 2 wt.% $CaCl_2$, 500 MHz, 298 K) of LA_{17}-EO_{458}-LA_{17} stereocomplex.

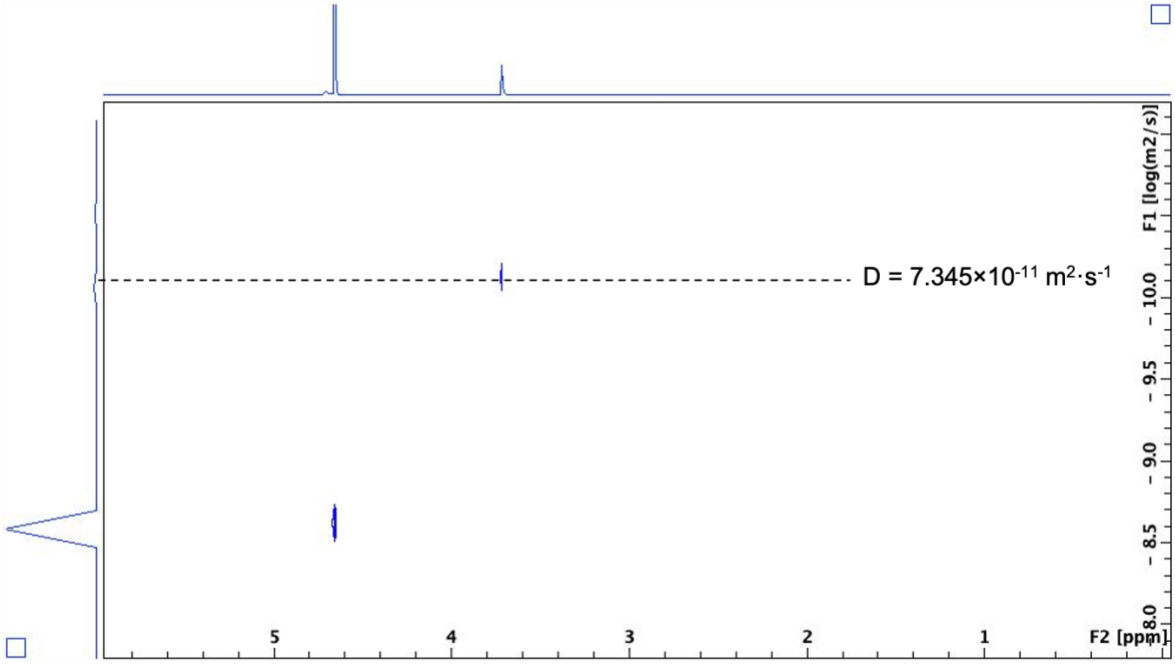

Figure C11. DOSY NMR spectrum (D_2O with 8 wt.% NaCl and 2 wt.% $CaCl_2$, 500 MHz, 298 K) of LLA_{24}-EO_{458}-LLA_{24}.

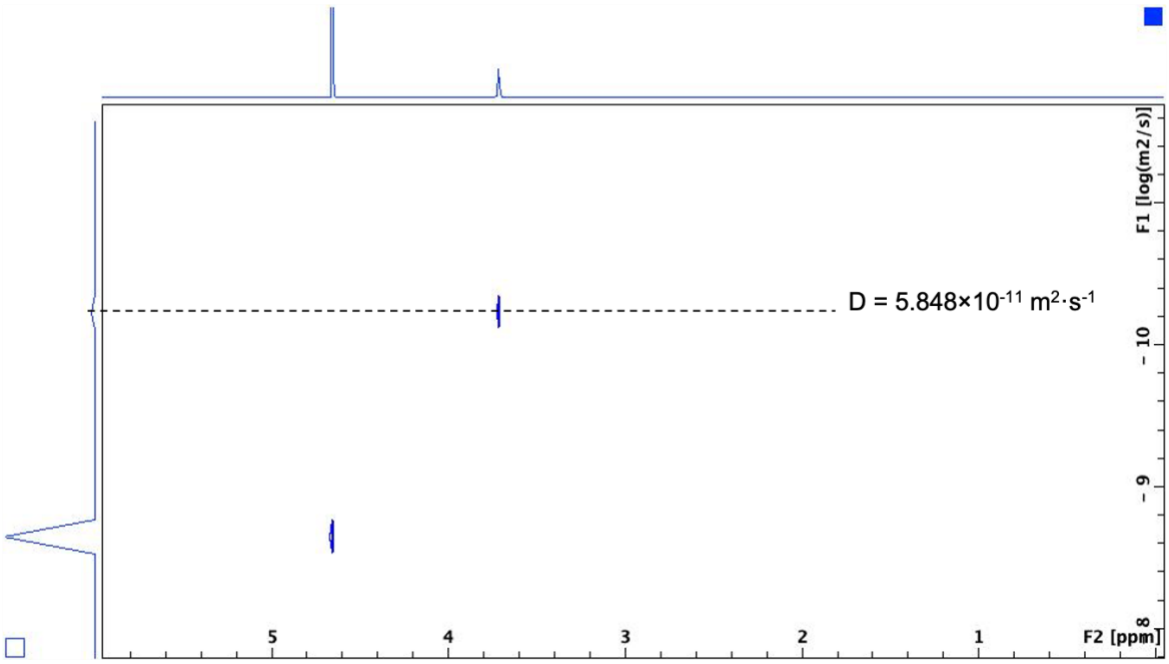

Figure C12. DOSY NMR spectrum (D_2O with 8 wt.% NaCl and 2 wt.% $CaCl_2$, 500 MHz, 298 K) of LA_{24}-EO_{458}-LA_{24} stereocomplex.

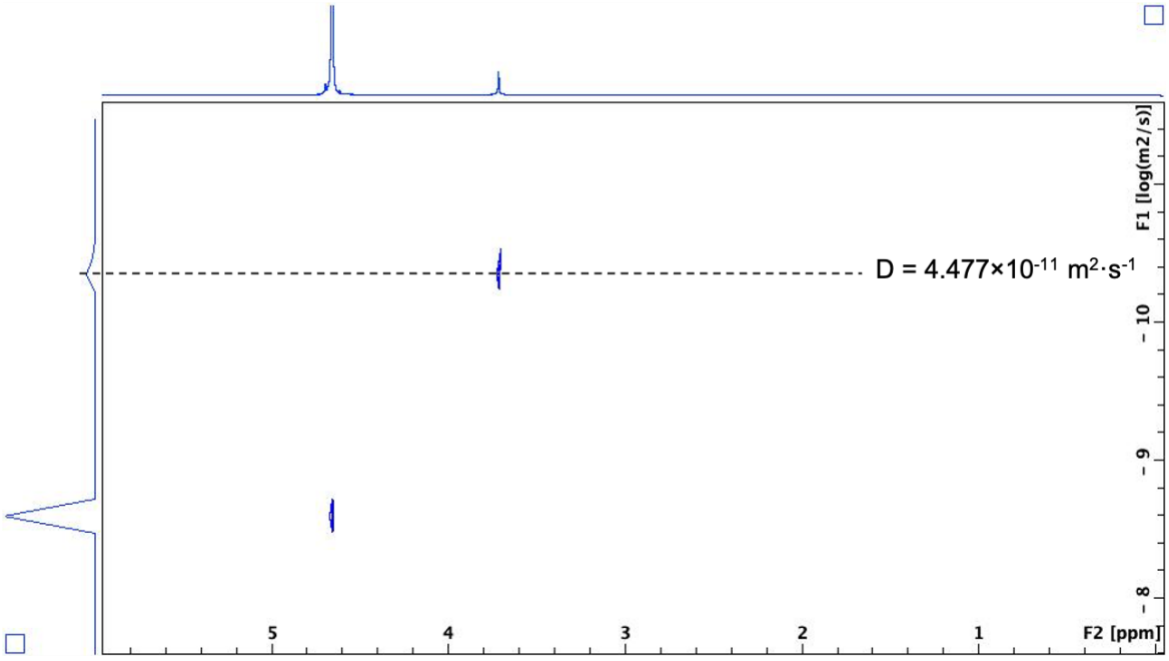

Figure C13. DOSY NMR spectrum (D_2O with 8 wt.% NaCl and 2 wt.% $CaCl_2$, 500 MHz, 298 K) of LLA_{27}-EO_{458}-LLA_{27}.

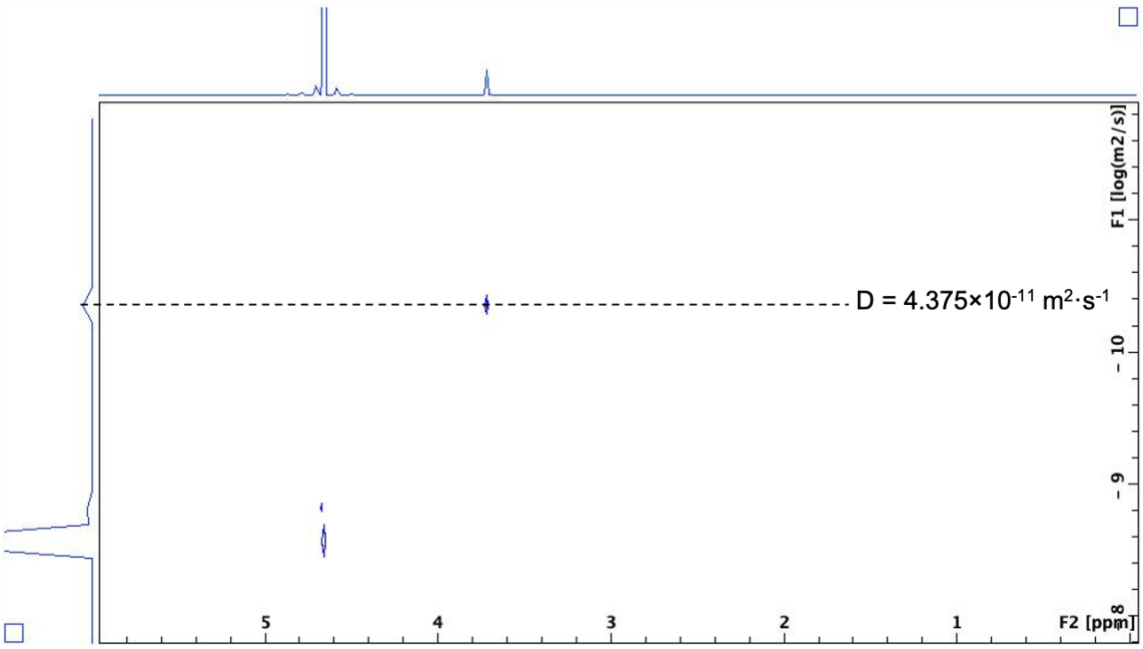

Figure C14. DOSY NMR spectrum (D_2O with 8 wt.% NaCl and 2 wt.% $CaCl_2$, 500 MHz, 298 K) of LA_{27}-EO_{458}-LA_{27} stereocomplex.

SEC traces

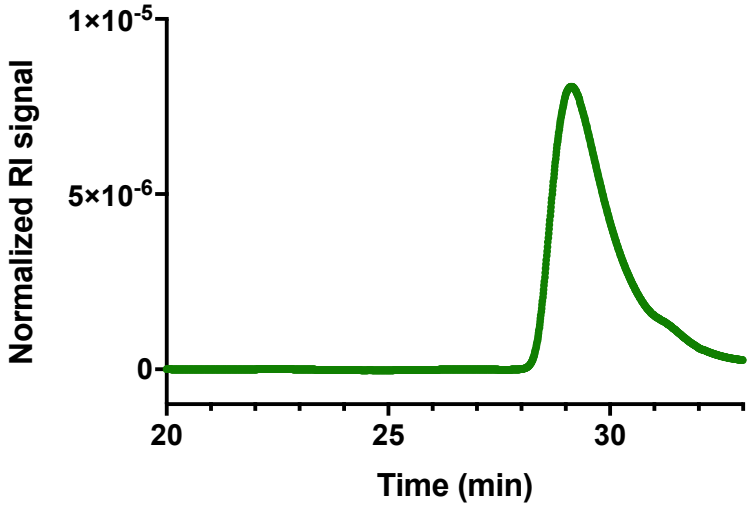

Figure C15. SEC trace of LLA_8-EO_{100}-LLA_8 (Table 4-1, entry 1)

FT-IR Spectra

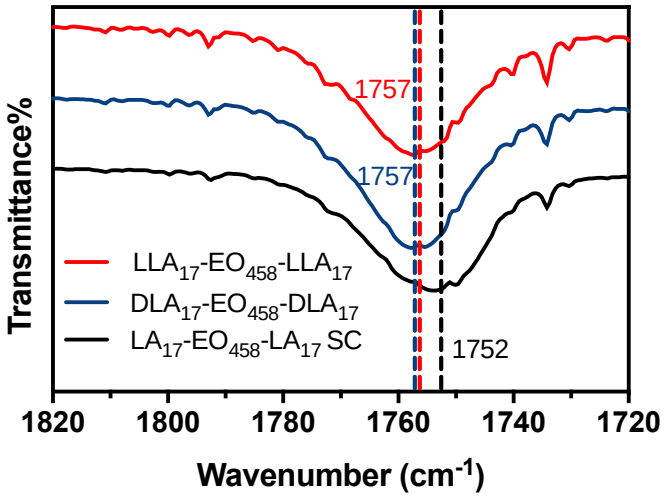

Figure C16. FT-IR spectra of LLA_{17}-EO_{458}-LLA_{17}, DLA_{17}-EO_{458}-DLA_{17}, and LA_{17}-EO_{458}-LA_{17} stereocomplex.

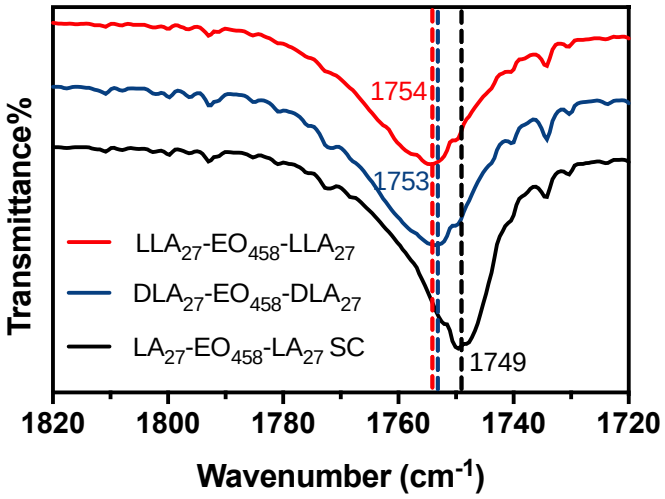

Figure C17. FT-IR spectra of LLA_{27}-EO_{458}-LLA_{27}, DLA_{27}-EO_{458}-DLA_{27}, and LA_{27}-EO_{458}-LA_{27} stereocomplex.

XRD Spectra

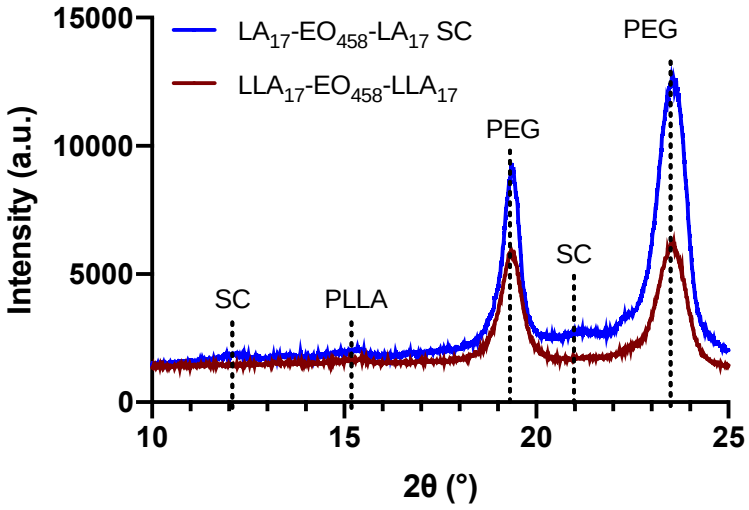

Figure C18. XRD spectra of LLA_{17}-EO_{458}-LLA_{17} and LA_{17}-EO_{458}-LA_{17} stereocomplex.

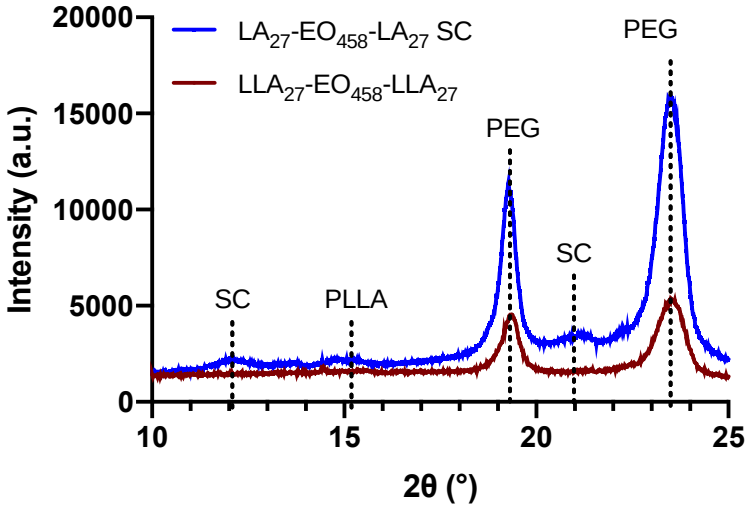

Figure C19. FT-IR spectra of LLA_{27}-EO_{458}-LLA_{27} and LA_{27}-EO_{458}-LA_{27} stereocomplex.

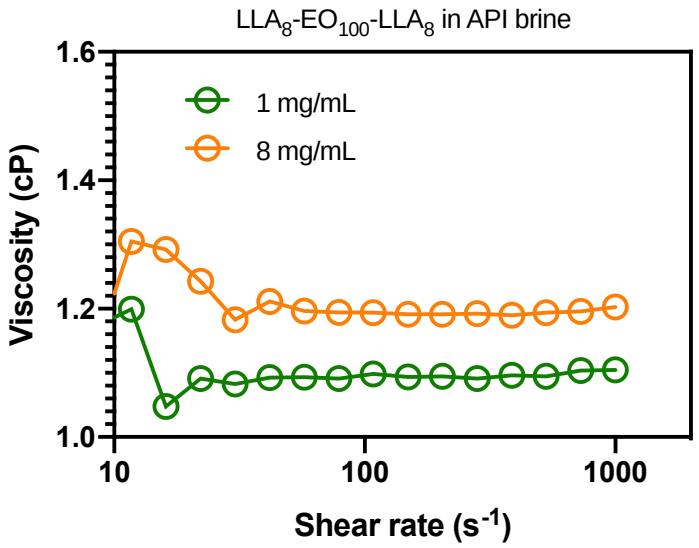

Figure C20. Shear viscosity measurements of LLA_8-EO_{100}-LLA_8 at 1 mg/mL (green) and 8 mg/mL (orange) concentration.

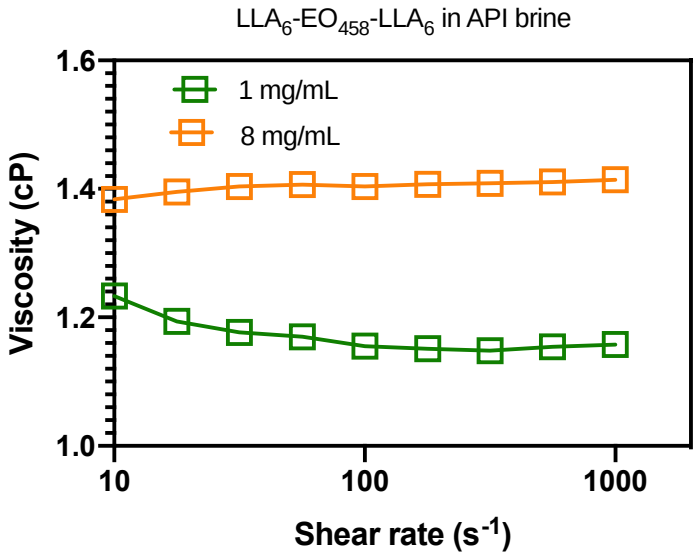

Figure C21. Shear viscosity measurements of LLA_6-EO_{458}-LLA_6 at 1 mg/mL (green) and 8 mg/mL (orange) concentration.

4.6. References

(1) Virk, P. S. Drag reduction fundamentals. *AIChE Journal* **1975**, *21* (4), 625-656.

(2) Horn, A. F.; Merrill, E. W. Midpoint scission of macromolecules in dilute solution in turbulent flow. *Nature* **1984**, *312* (5990), 140-141.

(3) Annable, T.; Buscall, R.; Ettelaie, R.; Whittlestone, D. The rheology of solutions of associating polymers: Comparison of experimental behavior with transient network theory. *Journal of Rheology* **1993**, *37* (4), 695-726.

(4) Xu, B.; Li, L.; Zhang, K.; Macdonald, P. M.; Winnik, M. A.; Jenkins, R.; Bassett, D.; Wolf, D.; Nuyken, O. Synthesis and Characterization of Comb Associative Polymers Based on Poly(ethylene oxide). *Langmuir* **1997**, *13* (26), 6896-6902.

(5) Alami, E.; Almgren, M.; Brown, W.; François, J. Aggregation of Hydrophobically End-Capped Poly(ethylene oxide) in Aqueous Solutions. Fluorescence and Light-Scattering Studies. *Macromolecules* **1996**, *29* (6), 2229-2243.

(6) Maechling-Strasser, C.; Clouet, F.; Francois, J. Hydrophobically end-capped polyethylene-oxide urethanes: 2. Modelling their association in water. *Polymer* **1992**, *33* (5), 1021-1025.

(7) Yahaya, G.; Ahdab, A.; Ali, S.; Abu-Sharkh, B.; Hamad, E. Solution behavior of hydrophobically associating water-soluble block copolymers of acrylamide and N-benzylacrylamide. *Polymer* **2001**, *42* (8), 3363-3372.

(8) Wever, D.; Picchioni, F.; Broekhuis, A. Polymers for enhanced oil recovery: a paradigm for structure–property relationship in aqueous solution. *Progress in polymer science* **2011**, *36* (11), 1558-1628.

(9) Volpert, E.; Selb, J.; Candau, F. Influence of the Hydrophobe Structure on Composition, Microstructure, and Rheology in Associating Polyacrylamides Prepared by Micellar Copolymerization. *Macromolecules* **1996**, *29* (5), 1452-1463.

(10) Chang, Y.; McCormick, C. L. Water-soluble copolymers. 49. Effect of the distribution of the hydrophobic cationic monomer dimethyldodecyl(2-acrylamidoethyl)ammonium bromide on the solution behavior of associating acrylamide copolymers. *Macromolecules* **1993**, *26* (22), 6121-6126.

(11) Hwang, F. S.; Hogen-Esch, T. E. Effects of Water-Soluble Spacers on the Hydrophobic Association of Fluorocarbon-Modified Poly(acrylamide). *Macromolecules* **1995**, *28* (9), 3328-3335.

(12) Castelletto, V.; Hamley, I. W.; Xue, W.; Sommer, C.; Pedersen, J. S.; Olmsted, P. D. Rheological and Structural Characterization of Hydrophobically Modified Polyacrylamide Solutions in the Semidilute Regime. *Macromolecules* **2004**, *37* (4), 1492-1501.

(13) Ikada, Y.; Jamshidi, K.; Tsuji, H.; Hyon, S. H. Stereocomplex formation between enantiomeric poly(lactides). *Macromolecules* **1987**, *20* (4), 904-906.

(14) Tsuji, H. Poly(lactide) Stereocomplexes: Formation, Structure, Properties, Degradation, and Applications. *Macromolecular Bioscience* **2005**, *5* (7), 569-597.

(15) Sheldon, R. A. Characteristic features and biotechnological applications of cross-linked enzyme aggregates (CLEAs). *Appl. Microbiol. Biotechnol.* **2011**, *92* (3), 467-477.

(16) Li, S.; Vert, M. Synthesis, Characterization, and Stereocomplex-Induced Gelation of Block Copolymers Prepared by Ring-Opening Polymerization of l(d)-Lactide in the Presence of Poly(ethylene glycol). *Macromolecules* **2003**, *36* (21), 8008-8014.

(17) Li, F.; Li, S.; Vert, M. Synthesis and Rheological Properties of Polylactide/Poly(ethylene glycol) Multiblock Copolymers. *Macromolecular Bioscience* **2005**, *5* (11), 1125-1131.

(18) Li, S.; El Ghzaoui, A.; Dewinck, E. Rheology and Drug Release Properties of Bioresorbable Hydrogels Prepared from Polylactide/Poly(ethylene glycol) Block Copolymers. *Macromolecular Symposia* **2005**, *222* (1), 23-36.

(19) Feng, C.; Piao, M.; Li, D. Stereocomplex-reinforced PEGylated polylactide micelle for optimized drug delivery. *Polymers* **2016**, *8* (4), 165.

(20) Chen, L.; Xie, Z.; Hu, J.; Chen, X.; Jing, X. Enantiomeric PLA–PEG block copolymers and their stereocomplex micelles used as rifampin delivery. *Journal of Nanoparticle Research* **2007**, *9* (5), 777-785.

(21) Kang, N.; Perron, M.-È.; Prud'homme, R. E.; Zhang, Y.; Gaucher, G.; Leroux, J.-C. Stereocomplex Block Copolymer Micelles: Core−Shell Nanostructures with Enhanced Stability. *Nano Letters* **2005**, *5* (2), 315-319.

(22) Xie, W.; Jiang, C.; Yu, X.; Shi, X.; Wang, S.; Sun, Y.; Yin, M.; Wu, D. Stereocomplex-Induced Self-Assembly of PLLA-PEG-PLLA and PDLA-PEG-PDLA Triblock Copolymers in an Aqueous System. *ACS Applied Polymer Materials* **2021**, *3* (12), 6078-6089.

(23) Wei, M.-H.; Li, B.; David, R. L. A.; Jones, S. C.; Sarohia, V.; Schmitigal, J. A.; Kornfield, J. A. Megasupramolecules for safer, cleaner fuel by end association of long telechelic polymers. *Science* **2015**, *350* (6256), 72-75.

(24) Toms, B. A. Some observations on the flow of linear polymersolutions through straight tubes at large Reynolds numbers. In *Proc. 1st Intl Congr. Rheol.*, 1949; Vol. 2, pp 135-141.

(25) Owolabi, B. E.; Dennis, D. J. C.; Poole, R. J. Turbulent drag reduction by polymer additives in parallel-shear flows. *Journal of Fluid Mechanics* **2017**, *827*, R4.

(26) Tsuji, H.; Hyon, S. H.; Ikada, Y. Stereocomplex formation between enantiomeric poly(lactic acid)s. 4. Differential scanning calorimetric studies on precipitates from mixed solutions of poly(D-lactic acid) and poly(L-lactic acid). *Macromolecules* **1991**, *24* (20), 5657-5662.

(27) Zhang, J.; Tashiro, K.; Tsuji, H.; Domb, A. J. Investigation of phase transitional behavior of poly (L-lactide)/poly (D-lactide) blend used to prepare the highly-oriented stereocomplex. *Macromolecules* **2007**, *40* (4), 1049-1054.

(28) Zhang, J.; Sato, H.; Tsuji, H.; Noda, I.; Ozaki, Y. Infrared Spectroscopic Study of CH3···OC Interaction during Poly(l-lactide)/Poly(d-lactide) Stereocomplex Formation. *Macromolecules* **2005**, *38* (5), 1822-1828.

Chapter 5: Synthesis of mono-substituted ferrocene-based yttrium compounds

5.1. Introduction

Redox-switchable catalysis enables different catalytic pathways using a single precatalyst. In reduced and oxidized states, the catalyst can catalyze different types of reactions or exhibit varying reactivity toward the same reaction, thus allowing precise control over the reaction process. Yttrium compounds have been extensively investigated as catalysts for ring-opening polymerization.[1] However, yttrium compounds have been underexplored in redox-switchable catalysis. Our group has reported two redox-switchable yttrium compounds with a ferrocene backbone that can serve as a redox handle.[2, 3] Nonetheless, the impact of the position and proximity of the redox handle on reactivity and switchability still lacks investigation.

Herein, we present the synthesis and characterization of a tridentate yttrium compound with a pendant ferrocene moiety. Chemical redox experiments were also conducted to confirm the compound's switchability.

5.2. Results and Discussion

$(Fc^{ONO})YBn(THF)_2$ (Fc^{ONO}= 6,6'-((ferrocenylazanediyl)bis(methylene))bis(2,4-di-*tert*-butylphenoxide) was synthesized by reaction between $H_2(Fc^{ONO})$ and $Y(Bn)_3(THF)_3$. The $(Fc^{ONO})Y(OPh)(THF)_2$ (Fc^{ONO}= 6,6'-((ferrocenylazanediyl)bis(methylene))bis(2,4-di-*tert*-butylphenoxide) can be generated in situ by adding one equivalent of 2,6-dimethylphenol into $(Fc^{ONO})YBn(THF)_2$ (Figure 5-1). The redox swithcability of was confirmed by chemical redox experiments. As monitored by ^1H NMR spectroscopy, after the addition of the oxidant $^{Fc}AcBAr^F$, the peaks of $(Fc^{ONO})Y(OPh)(THF)_2$ were shifted and broadened due to the paramagnetic nature of

the oxidized compound. Upon the addition of the reductant, $CoCp_2$, the peaks of $(Fc^{ONO})Y(OPh)(THF)_2$ reappeared indicating that the compound can be reversibly oxidized and reduced back.

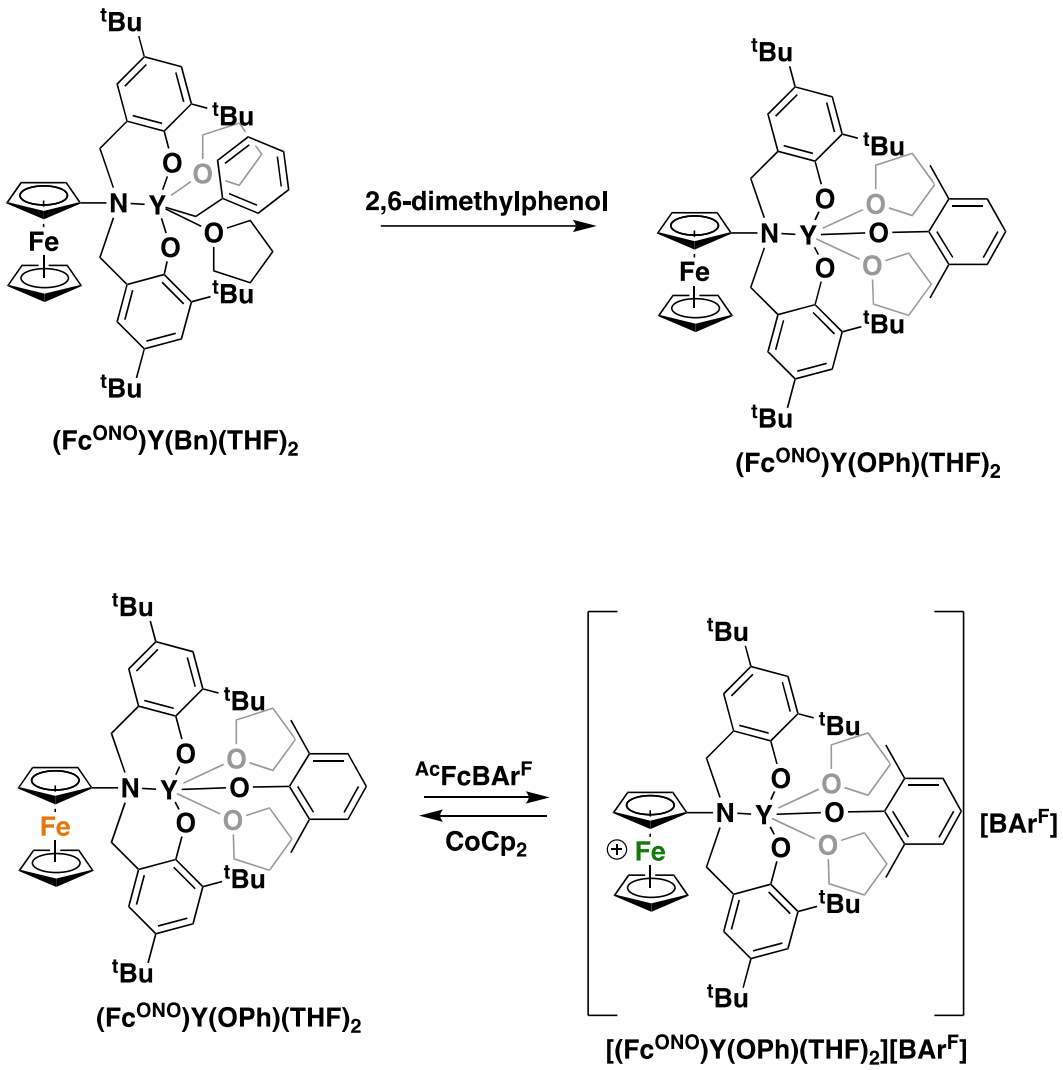

Figure 5-1. *In situ* generation of $(Fc^{ONO})YOPh(THF)_2$ and its chemical redox switch.

5.3. Conclusions

Tridentate yttrium compounds with a pendant ferrocene moiety were synthesized. The chemical redox experiment of the yttrium phenoxide compound was performed to confirm the redox switchability.

5.4. Experimental Section

$H_2(Fc^{ONO})$[4] and $Y(Bn)_3(THF)_3$[5] were synthesized according to published procedures.

Synthesis of $(Fc^{ONO})YBn(THF)_2$

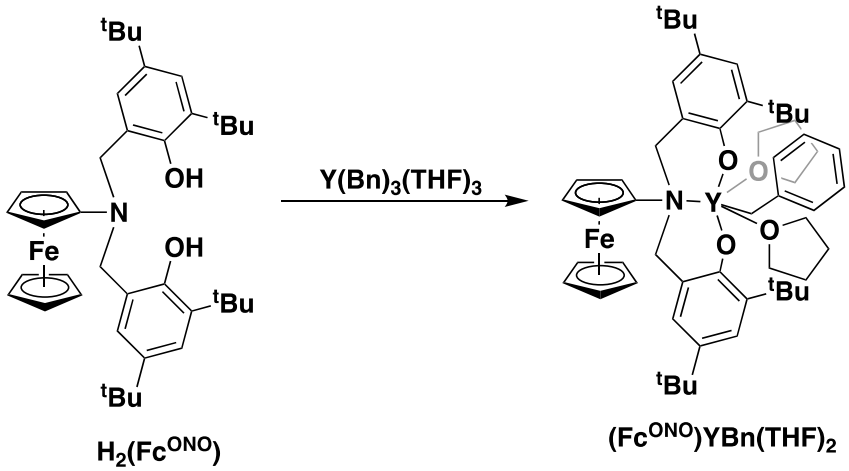

In a glovebox under nitrogen atmosphere, $H_2(Fc^{ONO})$ proligand (120 mg, 0.188 mmol, 1 equiv) and $Y(Bn)_3(THF)_3$ (109 mg, 0.189 mmol, 1 equiv) were dissolved in toluene respectively. The proligand solution was added dropwise into the $Y(Bn)_3(THF)_3$ solution. The reaction mixture was stirred at room temperature for one hour and then the volatile was removed under vacuum. The resulting yellow oil was washed with cold hexanes to give a yellow powder (114 mg, 70%).

***In situ* generation of (Fc^{ONO})YOPh(THF)$_2$ and its chemical redox experiment**

In a J-young NMR tube, 2,6-dimethylphenol (1.7 mg, 0.0138 mmol, 1 equiv) was added into (Fc^{ONO})YBn(THF)$_2$ (12 mg, 0.0138 mmol, 1 equiv) to generate (Fc^{ONO})YOPh(THF)$_2$ in situ. Then ^{Ac}FcBAr^F (^{Ac}Fc = acetylferrocene, BAr^F = tetrakis(3,5-bis(trifluoromethyl)-phenyl)borate) (15.1 mg, 0.0138 mmol, 1 equiv) and $CoCp_2$ (2.6 mg 0.0138 mmol, 1 equiv) were added respectively to oxidize and reduce back (Fc^{ONO})YBn(THF)$_2$. ^{1}H NMR spectroscopy was used to monitor the reaction at each step.

5.5. Appendix D

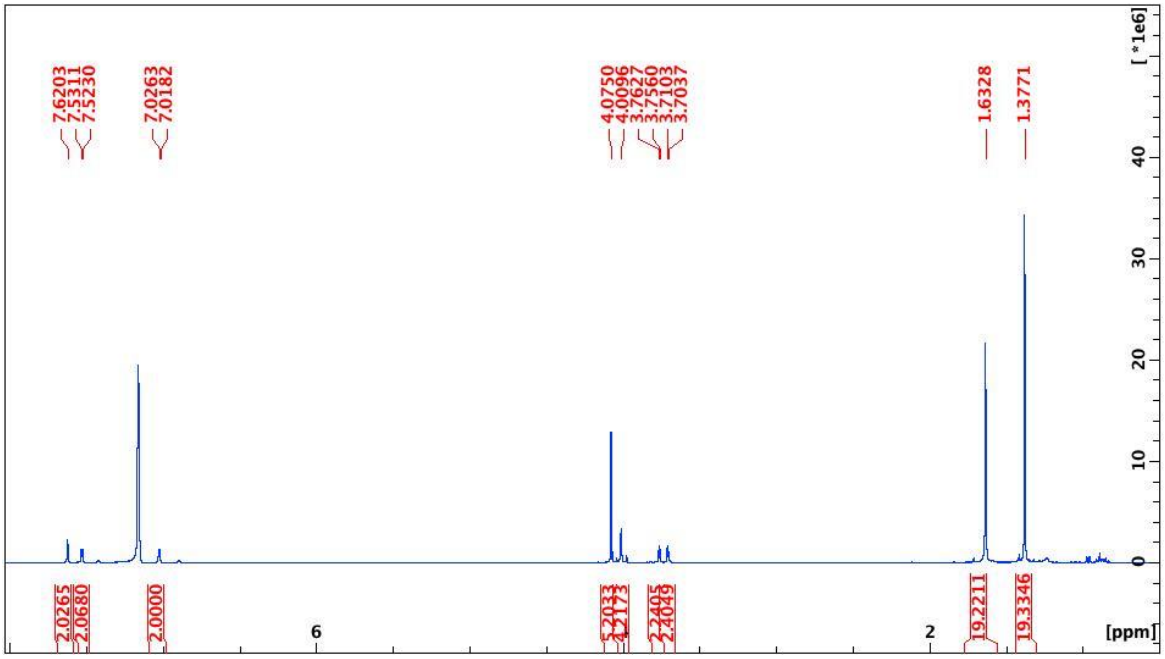

Figure D1. ^{1}H NMR spectrum (C_6D_6, 500 MHz, 298 K) of H_2(Fc^{ONO}). δ (ppm): 7.62 (d, 2H, ArO*H*), 7.53 (d, 2H, Ar*H*), 7.02 (d, 2H, Ar*H*), 4.08 (s, 5H, C_5H_5), 4.0 1(s, 4H, C_5H_4), 3.76 (t, 2H, NCH_2), 3.71 (t, 2H,NCH_2), 1.63 (s, 18H, C(CH_3)$_3$), 1.38 (s, 18H, C(CH_3)$_3$).

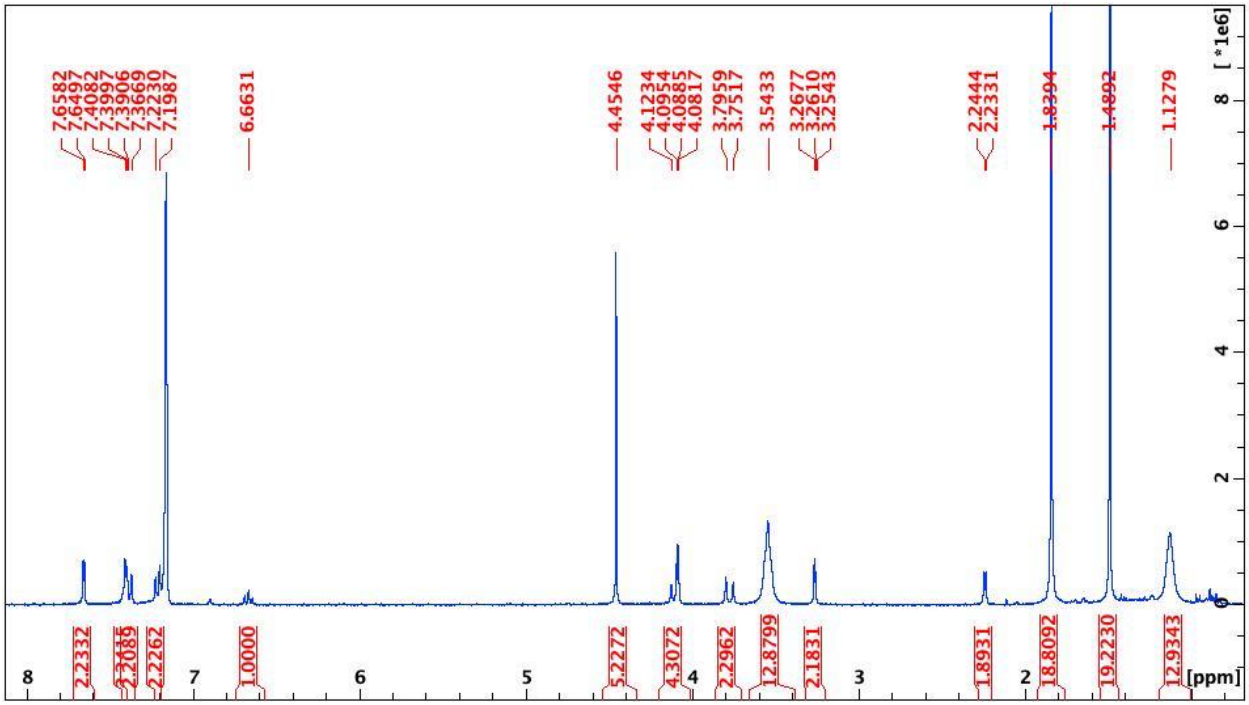

Figure D2. ^{1}H NMR spectrum (C_6D_6, 500 MHz, 298 K) of (Fc^{ONO})YBn(THF)$_2$. δ (ppm): 7.66 (d, 2H, Ar*H*), 7.40 (d, 2H, Ar*H*), 7.38 (d, 2H, Ar*H*), 7.22 (d, 2H, Ar*H*), 6.66 (t, 1H, Ar*H*), 4.45 (s, 5H, C_5H_5), 4.12 (d, 2H, NCH_2), 4.08 (t, 2H, C_5H_4), 3.78 (d, 2H, NCH_2), 3.54 (br, 8H, THF), 3.26 (t, 2H, C_5H_4), 2.24 (d, 2H,CH_2Ar), 1.84 (s, 18H, C(CH_3)$_3$), 1.49 (s, 18H, C(CH_3)$_3$), 1.13 (br, 8H, THF).

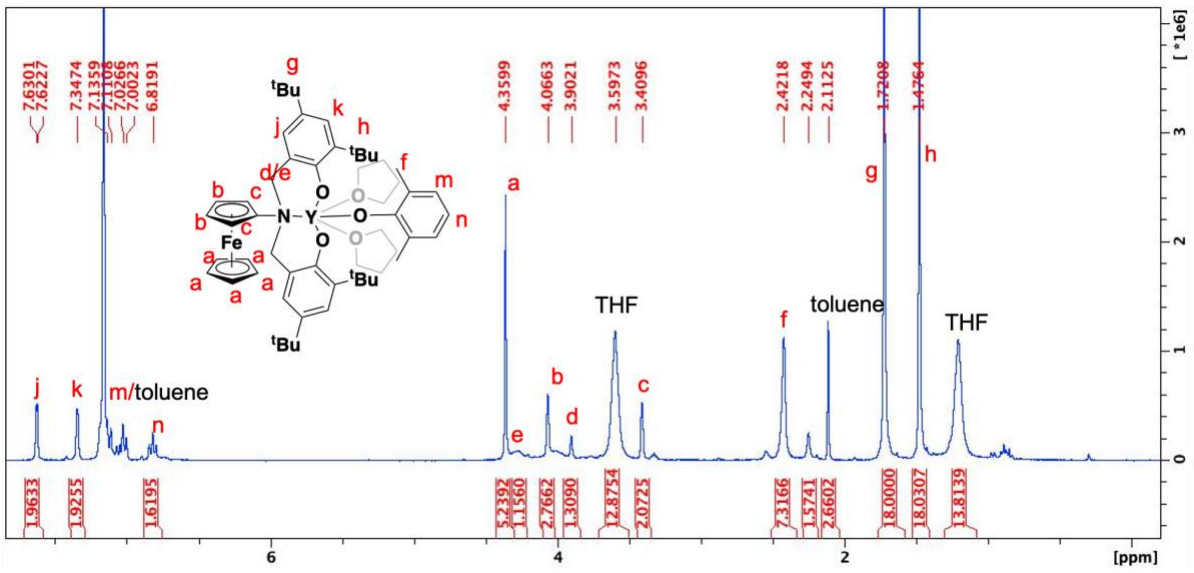

Figure D3. ^{1}H NMR spectrum (C_6D_6, 500 MHz, 298 K) of (Fc^{ONO})YOPh(THF)$_2$. δ (ppm): 7.63 (d, 2H, Ar*H*), 7.35 (d, 2H, Ar*H*), 7.02 (d, 2H, Ar*H*), 6.82 (d, 1H, Ar*H*), 4.36 (s, 5H, C_5H_5), 4.28 (d, 2H, NCH_2), 4.07 (t, 2H, C_5H_4), 3.90 (d, 2H, NCH_2), 3.60 (br, 8H, THF), 3.41 (t, 2H, C_5H_4), 2.42 (t, 6H, ArCH_3), 1.72 (s, 18H, C(CH_3)$_3$), 1.48 (s, 18H, C(CH_3)$_3$), 1.19 (br, 8H, THF).

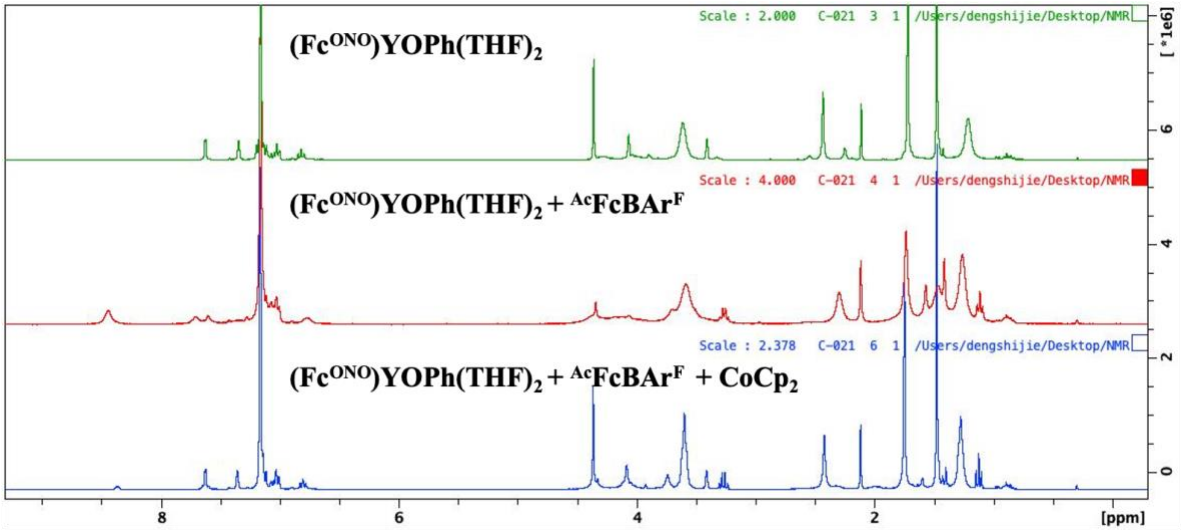

Figure D4. ^{1}H NMR spectrum (C_6D_6, 500 MHz, 298 K) of chemical redox of *in situ* generated (Fc^{ONO})YOPh(THF)$_2$.

5.6. References

(1) Carpentier, J.-F. Rare-earth complexes supported by tripodal tetradentate bis (phenolate) ligands: a privileged class of catalysts for ring-opening polymerization of cyclic esters. *Organometallics* **2015**, *34* (17), 4175-4189.

(2) Broderick, E. M.; Guo, N.; Vogel, C. S.; Xu, C. L.; Sutter, J.; Miller, J. T.; Meyer, K.; Mehrkhodavandi, P.; Diaconescu, P. L. Redox control of a ring-opening polymerization catalyst. *J. Am. Chem. Soc.* **2011**, *133* (24), 9278-9281.

(3) Deng, S.; Diaconescu, P. L. A switchable dimeric yttrium complex and its three catalytic states in ring opening polymerization. *Inorganic Chemistry Frontiers* **2021**, *8* (8), 2088-2096, 10.1039/D0QI01479F.

(4) Gao, J. *Synthesis of Yttrium and Aluminum Complexes Supported by a Mono-Substituted Ferrocene Ligand*; University of California, Los Angeles, 2015.

(5) Huang, W.; Upton, B. M.; Khan, S. I.; Diaconescu, P. L. Synthesis and Characterization of Paramagnetic Lanthanide Benzyl Complexes. *Organometallics* **2013**, *32* (5), 1379-1386.